Role of hepatic p38δ MAPK in liver metabolism

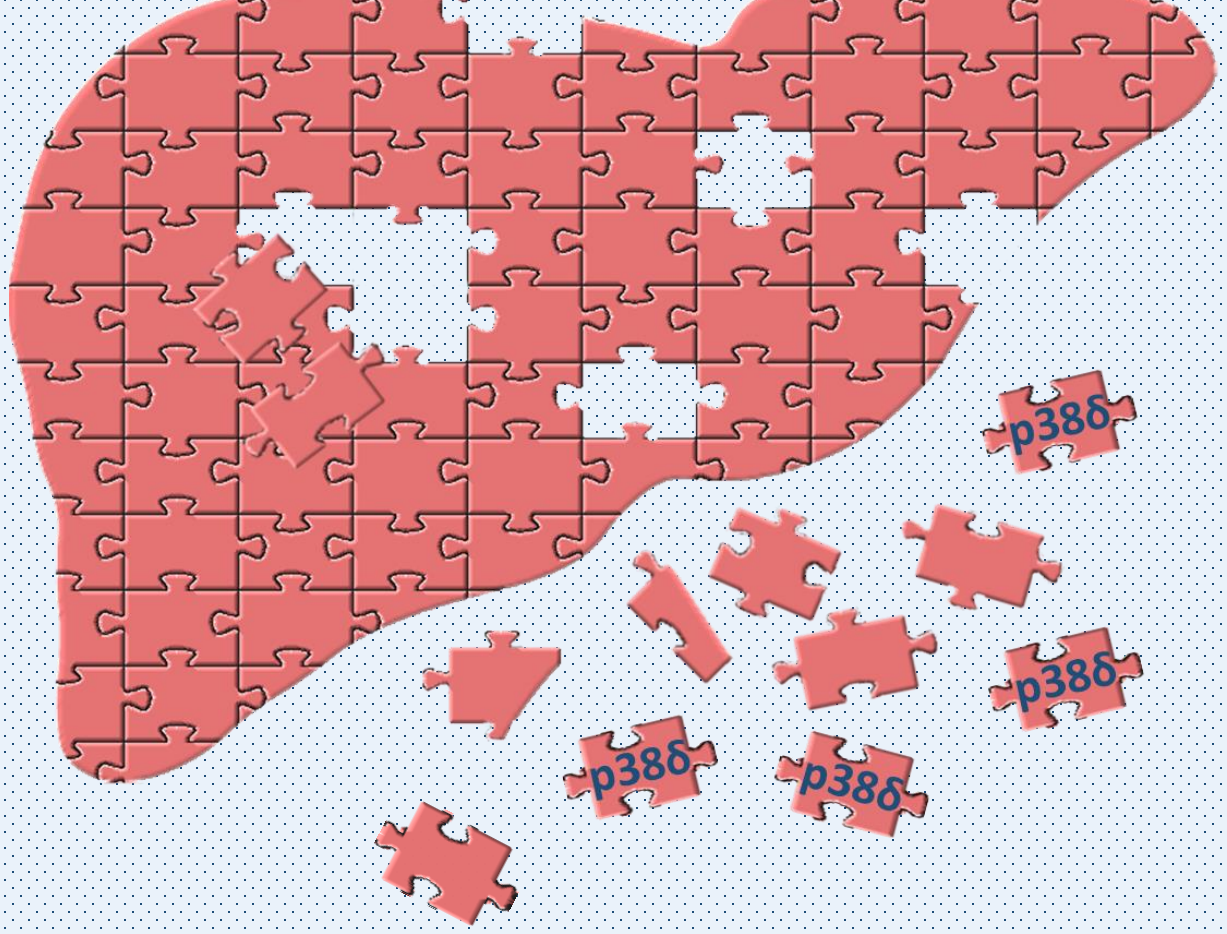

María del Valle Montalvo Romeral

Programa de Doctorado de Biociencias Moleculares

Departamento de Biología Molecular

Universidad Autónoma de Madrid

Madrid, 2019

Universidad Autónoma de Madrid

Facultad de Ciencias

Departamento de Biología Molecular

Role of hepatic p38δ MAPK in liver metabolism

María del Valle Montalvo Romeral

Licenciada en Biología

Madrid, 2019

Director Tesis: Guadalupe Sabio Buzo

Co-director Tesis: Antonia Tomás Loba

UNIVERSIDAD AUTONOMA DE MADRID

Dra. Guadalupe Sabio Buzo, jefa del grupo: Papel de las quinasas activadas por el estrés en el desarrollo de enfermedades cardiovasculares, diabetes y cáncer; del área de Fisiopatología del Miocardio, Centro Nacional de Investigaciones Cardiovasculares (CNIC)-Carlos III, **como Directora**

Dra. Antonia Tomás Loba, investigadora postdoctoral del área de Fisiopatología del Miocardio, Centro Nacional de Investigaciones Cardiovasculares (CNIC)-Carlos III, **como co-Directora**

Dra. Cristina Murgas Montesinos, profesora titular del departamento de Biología Molecular de la Universidad Autónoma de Madrid, **como tutora**

CERTIFICAN

Que la Tesis Doctoral titulada: **Role of hepatic p38δ MAPK in liver metabolism** ha sido realizada en el Centro Nacional de Investigaciones Cardiovasculares y tutelada por el Departamento de Biología Molecular de la Universidad Autónoma de Madrid.

El trabajo realizado por Doña María del Valle Montalvo Romeral reúne todas las condiciones requeridas por la legislación vigente, así como la originalidad y calidad científica para poder ser presentada y defendida ante el Tribunal Calificador con el fin de optar al grado de Doctor.

Y para que conste se extiende el presente certificado

Madrid, 11 de Marzo 2019

V°B° Directora	V°B° Co-Directora	V°B° Tutora
Dra. Guadalupe Sabio Buzo	Dra. Antonia Tomás Loba	Dra. Cristina Murga Montesinos

Yale University

March 19, 2019

Dear Sir or Madam:

I support the Doctoral Thesis of María del Valle Montalvo Romeral entitled ¨Role of hepatic p38δ MAPK in liver metabolism¨ and I believe this research study on stress kinase signaling is a breakthrough in metabolism.

She described that this kinase is a central metabolic regulator, not only in the liver, but also controlling whole-body homeostasis. The hepatic p38δ MAPK is mainly involved in the regulation of glucose metabolism and normoglycemia, but it also seems to have a main role in hepatic lipid metabolism.

María del Valle´s Doctoral Thesis represents a visionary contribution to the field, and I am pleased to offer my strong support for her graduation and her application for the International PhD.

Sincerely,

Gerald I. Shulman, M.D., Ph.D.
George R. Cowgill Professor of Physiological Chemistry
Professor of Medicine and Cellular & Molecular Physiology
Director, Yale Mouse Metabolic Phenotyping Center
Co-Director, Yale Diabetes Research Center

Unité de Biologie Fonctionnelle & Adaptative
Functional and Adaptive Biology
Université Paris Diderot-Paris 7, CNRS UMR 8251

Team C_2OFFEE:
Central COntrol of Feeding behaviour and Energy Expenditure

Paris, March 19th, 2019

Object: Letter of support for Miss María del Valle Montalvo Romeral

To whom it may concern

It is my great pleasure to provide my full support to the Doctoral work of Ms. María del Valle Montalvo Romeral entitled ¨Role of hepatic p38δ MAPK in liver metabolism¨. This is an impressive body of work that will undoubtedly have long-lasting impact in the field. In this work Ms. María del Valle Montalvo Romeral highlighted a crucial role for the the hepatic p38δ MAPK as a main metabolic regulator. This work has opened new avenue for the treatment of diabetes and liver dyslipidemia by a providing a new promising target.

During her PhD, María del Valle did a short stay in my lab for 6 weeks, performing hyperinsulinemic-euglycemic clamp in the hepatic specific p38δ knockout mice. These technics are complex and required both delicacy, technical skills and conceptual abstraction. During that short stay I could witness the rare quality of Ms. María del Valle Montalvo Romeral at several levels. Scientifically and technically she completed her task with very little supervision and with impressive ease, she sorted and analyzed the data in a very efficient way and could extract the physiological concepts that her data were supporting. In addition, Ms. María del Valle was also a great citizen in the lab with evident social skills and could interact at scientific level with virtually everyone in my lab.

She has done an exceptional work during her PhD and even her stay in my lab was brief she has earned my highest recommendation. I am pleased to offer my enthusiastic support for her graduation and her application to the International PhD.

Sincerely,

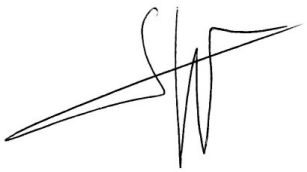

Serge Luquet, PhD
Unité "Biologie Fonctionnelle & Adaptative" (BFA)/Unit of Functional and Adaptive Biology (BFA)
Université Paris Diderot-Paris 7, CNRS UMR 8251
Team: C_2OFFEE Central COntrol of Feeding behaviour and Energy Expenditure
4 rue Marie-Andrée Lagroua Weill-Hallé
Bâtiment Buffon, 5ème étage, pièce 512A
Case courrier 7126
75205 Paris Cedex 13, France
Tel : +33 1 57 27 77 93
Fax :+33 1 57 27 77 96
http://www.bfa.univ-paris-diderot.fr/spip.php?rubrique81

This PhD Thesis has been carried out by María del Valle Montalvo Romeral at the ¨Stress Kinases in Diabetes, Cancer and Cardiovascular Disease¨ laboratory from the Myocardial Pathophysiology Area at Centro Nacional de Investigaciones Cardiovasculares Carlos III (CNIC-Carlos III) in Madrid, under the supervision of Dra. Guadalupe Sabio Buzo and Dra. Antonia Tomás Loba.

The support received from the following Grants and Fellowships has permitted to develop this PhD work:

-Programa de ayudas predoctorales FPI, del Ministerio de Economía, Industria y Competitividad del 2014 (BES-2014-069332).

-Quinasas del estrés en el cáncer y las enfermedades metabólicas. Principal Investigador: Guadalupe Sabio. SAF2013-43506-R. Ministerio de Economía, Industria y Competitividad 2014-2016

-Programa de ayudas a la movilidad predoctoral para la realización de estancias breves en centros de I+D 2017 (EEBB-I-18-12998).

-The company of Biologist. Travelling fellowship grant (JCSTF-170505)

A mis padres,

porque ellos son el mejor ejemplo de lucha a seguir

Summary

Summary

Hepatic metabolism is a complex regulatory network which controls whole body homeostasis. Therefore, it is crucial to deeply understand its function, to better comprehend human physiology and to uncover novel targets and effective clinical approaches to treat metabolic diseases that are reaching pandemic proportions such as type 2 diabetes (T2D) and non-alcoholic fatty liver disease (NAFLD).

Contrary to the role of c-Jun NH2-terminal kinases (JNK) in hepatocytes, the role of the p38 mitogen-activated protein kinases (MAPK), other stress kinases, and particularly, the role of the p38δ MAPK isoform in hepatocytes is unknown. Interestingly, the expression of p38δ MAPK is increased in livers from obese patients with NAFLD, suggesting that this kinase might play an important function in liver metabolism. Therefore, the main purpose of this thesis was to clarify the function of the hepatic p38δ MAPK in liver metabolism, its repercussion in whole body homeostasis and its function in obesity, to open new avenues for this kinase as a putative target in obesity-related T2D and NAFLD.

We demonstrated that p38δ is a key regulator of glucose metabolism and it is essential to keep normoglycemia. Particularly, we found that p38δ controls glycogen metabolism and glycolysis, through phosphorylation of glycogen synthase 2 (GYS2) and 6-phosphofructo-2-kinase/fructose-2,6-bisphosphatase 3 (PFKFB3) respectively. We showed that mice lacking p38δ in hepatocytes ($Alb^{p38\delta KO}$) presented decreased glycogenesis, hepatic glycogen storage and consequently, reduced blood glucose levels. This protected against high fat diet (HFD)-induced hyperglycemia and promoted mild hypoglycemia in chow diet (CD)-fed mice. Moreover, HFD-fed $Alb^{p38\delta KO}$ mice showed reduced glycolysis, which may impair the hepatic *de novo* lipogenesis (DNL), the subsequent intrahepatic lipid accumulation and therefore, protect against NAFLD and insulin resistance development.

Additionally, p38δ might control lipid metabolism, regulating peroxisome-proliferator-activated receptor α (PPARα) pathway and hepatokine fibroblast growth factor 21 (FGF21) plasma levels. Moreover, p38δ might regulate different lipid oxidation pathways. Lastly, p38δ might also have a main function in the hepatic metabolism of long-chain acyl CoAs (LCCoA) and diacylglycerides (DAG).

Summarizing, this Thesis work firstly defines the function of the hepatic p38δ MAPK, identifying substrates for this kinase; giving therefore new insights into the complex stress kinases network. Secondly, this thesis reveals that p38δ MAPK is a central metabolic regulator, mainly controlling glucose but also lipid metabolism. Lastly, p38δ MAPK might be a target to treat T2D and NAFLD, because the lack of p38δ MAPK in hepatocytes protects against hyperglycemia, insulin resistance and NAFLD.

Resumen

El metabolismo hepático es una compleja red reguladora que controla la homeostasis de todo el organismo. Es por tanto crucial entender completamente su función, para comprender mejor los mecanismos que gobiernan la fisiología humana. De esta manera, se podrán encontrar nuevas dianas y tratamientos efectivos para enfermedades metabólicas complejas, como la diabetes tipo 2 (DT2) y la enfermedad del hígado graso no alcohólico (EHGNA), las cuales están alcanzando proporciones pandémicas en la actualidad. Mientras que el papel de las quinasas de estrés c-Jun NH2-terminal (JNK) en hepatocitos se ha estudiado en profundidad, poco se sabe de la función de las quinasas activadas por mitógenos (MAPK), p38, y en particular, se desconoce la función de la p38δ en hepatocitos. El hecho de que su expresión esté aumentada en los hígados de pacientes obesos con EHGNA, sugiere que p38δ podría desempeñar una función principal en el metabolismo hepático. Por lo tanto, el objetivo principal de esta tesis ha sido entender la función de la p38δ hepática en el metabolismo del hígado, así como su repercusión en la homeostasis global del organismo. También se ha explorado su función en obesidad, abriendo así la posibilidad de poder ser considerada como una diana terapéutica en el tratamiento de la DT2 y la EHGNA asociadas a la obesidad. En esta tesis demostramos que la p38δ hepática es un regulador clave del metabolismo de la glucosa, siendo esencial para mantener la normoglucemia. Particularmente, p38δ controla el metabolismo del glucógeno y la glucólisis hepática, mediante la fosforilación de la proteína glucógeno sintasa 2 (GYS2) y de la 6-fosfofructo-2-quinasa/fructosa-2,6-bifosfatasa 3 (PFKFB3) respectivamente. Así los ratones que carecen de p38δ en hepatocitos ($Alb^{p38\delta KO}$), tienen reducida la glucogénesis, bajo contenido de glucógeno hepático y en consecuencia menores niveles de glucosa en sangre. Esta limitada capacidad de almacenaje de glucógeno protege frente a hiperglucemia cuando los ratones son alimentados con una dieta alta en grasa, pero produce una ligera hipoglucemia cuando tienen una dieta normal. Además, los ratones $Alb^{p38\delta KO}$ alimentados con dieta alta en grasa tienen reducida la glucólisis, reduciendo así la síntesis *de novo* (DNL) y la acumulación hepática de lípidos; estando por tanto protegidos frente al desarrollo de la EHGNA y de resistencia a insulina. Adicionalmente, p38δ podría tener un papel importante en el metabolismo lipídico del hígado, regulando la vía de los receptores activados por el proliferador del peroxisoma α (PPARα) y los niveles del factor de crecimiento fibroblástico 21 (FGF21) en plasma. Además, p38δ parece controlar varias vías de oxidación lipídica. Por último, nuestros datos indican que p38δ tendría un papel en el metabolismo hepático de los acil-coenzima A de cadena larga (LCCoA) y de los diacilglicéridos (DAG). Resumiendo, esta Tesis por primera vez define la función de p38δ en hepatocitos, identificando nuevos substratos para esta quinasa. En segundo lugar, esta Tesis revela que p38δ es un regulador metabólico importante, controlando principalmente el metabolismo glucídico, pero teniendo también una función clara en el metabolismo lipídico. Por último, hemos visto que p38δ puede ser una nueva diana terapéutica el tratamiento de la diabetes tipo 2 y el EHGNA asociados a la obesidad, ya que la deleción de p38δ en hepatocitos protege frente a hiperglucemia, resistencia a insulina y EHGNA.

A

AA	Amino acids
AAV	Adeno-associated virus
AcAc	Acetoacetate
ACAD	acyl-CoA dehydrogenases
ACC	Acetyl CoA carboxylase
acetyl-CoA	Acetyl coenzyme A
ACL	ATP-citrate lyase
ACOT	Acyl-CoA thioesterases
ACOX	Acyl-coenzyme A oxidase
ACS	Acyl-CoA synthetases
AGE	Advanced glycation end products
Alb^{cre}	Mice expressing CRE recombinase protein in hepatocytes
$Alb^{p38\delta KO}$	Mice lacking p38δ in hepatocytes
$Alb^{p38\delta/FGF21KO}$	Mice lacking p38δ and FGF21 in hepatocytes
AMPK	AMP-activated protein kinase
ASM	Acid-soluble metabolites

B

BMI	Body mass index

C

CE	Cholesterol ester
C/EBPalpha	CCAAT-enhancer-binding protein alpha
CD	Chow diet
ChREBP	Carbohydrate-responsive element-binding protein
CIDE-A/B	Cell death-inducing DNA fragmentation factor A (DFFA)-like effector A/B
CK2	Protein kinase casein 2
CoA	Coenzyme A
CREB	c-AMP response element binding

CS	Citrate synthase
CVD	Cardiovascular diseases
CYP	Cytochrome P450

D

DAG	Diacylglycerol
2DG	2-deoxy-*d*-(1-^{14}C)-glucose
D_2O	Heavy water
DHAP	Dihydroxyacetone phosphate
DNL	*de novo* lipogenesis

E

ECM	Extracellular matrix
EE	Energy expenditure
EGP	Endogenous glucose appearance
EHGNA	Hígado graso no alcohólico
ETS	Electron transfer system
ER	Endoplasmic reticulum
ERK	Extracellular signal-regulated kinases

F

FA	Fatty acid(s)
FABPs	Fatty acid binding proteins
FAO	Fatty acid oxidation
FATPs	Fatty acid binding transport proteins
FAS	Fatty acid synthase
FBPase	Fructose 1,6 bisphosphatase
FC	Free cholesterol
FDR	False discovery rate
FFA	Free fatty acids
FGF21	Fibroblast growth factor 21

FoxO	Forkhead box O
F-1,6-bisP	Fructose-1,6-biphosphate
Fru-2,6-P_2	Fructose-2,6-biphosphate
F6P	Fructose-6-phosphate

G

GCK	Glucokinase
GC-MS	Gas chromatography-mass spectrometry
GIR	Glucose infusion rate
GK	Glucokinase
GKRP	Glucokinase regulatory protein
GLUT2	Glucose transporter type 2
GNG	Gluconeogenesis
GPAT	Glycerol-3-phosphate acyltransferase
GP	Glycogen phosphorylase
GPDH	Glycerol 3-phosphate dehydrogenase
GSD0	Glycogen storage disease 0
GSK3	Glycogen synthase kinase 3
GTT	Glucose tolerance test
GYS	Glycogen synthase
G6P	Glucose-6-phosphate
G6Pase	Glucose-6-phosphatase
G3P	Glycerol-3-phosphate

H

hAAT	Human alpha1-antitrypsin
HCC	Hepatocellular carcinoma
HCR	Apolipoprotein E locus control region
HFD	High fat diet
HGP	Hepatic glucose production

HMGCS	3-hydroxymethylglutaryl-CoA synthase
3HB	β-hydroxybutyrate

I

ITT	Insulin tolerance test
IRS	Insulin receptor substrate

J

JNK	c-Jun NH2-terminal kinase

K

KC	Kupffer cells
KG	Ketogenesis

L

LCCoA	Long-chain CoA
LCFA	Long chain fatty acids
LC-MS/MS	Liquid chromatography-mass spectrometry
LDH	Lactate dehydrogenase
LPA	Lysophosphatidic acid
LPL	Lipoprotein lipase
LXR	Liver X receptors

M

MAPKK	Mitogen-activated protein kinase kinase (MKK, MEK or MAP2K)
MAPKKK	Mitogen-activated protein kinase kinase kinase (MAP3K or MEKK)
MCD	Methionine-coline deficient diet
MCFA	Medium chain fatty acids
MDH	Malate dehydrogenase
MK	MAPK-activated protein kinases
MKP	MAPK phosphatases
mtGPAT	mitochondrial acyl-CoA: glycerol-sn-3-phosphate acyltransferase

mTORC1	mammalian target of rapamycin complex 1
MTP	Mitochondrial trifunctional protein

N

NADP(H)	Nicotinamide adenine dinucleotide phosphate
NAFLD	Non-alcoholic fatty liver disease
NASH	Non-alcoholic steatohepatitis
NF-κB	Nuclear factor κB
NKT	Natural killers T
Nox4	NADP(H) oxidase homologue 4
NPC	Non-parenchymal cells

O

OAA	Oxaloacetate
OXPHOS	Oxidative phosphorylation

P

PAS	Periodic acid–Schiff
PC	Pyruvate carboxylase
PDH	Pyruvate dehydrogenase complex
PDK	Phosphoinositide-dependent kinase-1
PEPCK	Phosphoenolpyruvate carboxylase
PFK	Phosphofructokinase
PFKFB/PFK2	6-phosphofructo-2-kinase/fructose-2,6-bisphosphatase
PFKFB3	6-phosphofructo-2-kinase/fructose-2,6-bisphosphatase 3
PGC-1α	Peroxisome proliferator-activated receptor gamma coactivator 1 alpha
PINTA	Positional isotopomer NMR tracer analysis
PK	Pyruvate kinase
PKA	Protein kinase A
PKC	Protein kinase C
PKD1	Protein kinase D1

PLIN	Perilipin
PPAR	Peroxisome-proliferator-activated receptor
PP1	Protein phosphatase-1
PUFA	Polyunsaturated fatty acids

R

Rd	Glucose disappearance (peripheral glucose uptake)
RQ	Respiratory quotient
ROS	Reactive oxygen species

S

SAPK	Stress-activated kinases
SCFA	Short chain fatty acids
SLC27	Solute carrier protein family 27
SREBP-1c	Sterol regulatory element-binding protein-1c

T

TCA	Tricarboxilic acid cycle
TG or TAG	Triacylglycerols/Triacylglycerides
TNF	Tumor necrosis factor
TZD	Thiazodilinione
T2D	Type 2 diabetes

U

UPR	Unfolded protein response

V

VLDL	Very low-density lipoprotein

W

WAT	White adipose tissue

X

Xbp1s	X-box binding protein 1

Introduction

1. Metabolism and obesity

Metabolism is a compendium of interrelated processes whose main function is to supply the required fuel to every cell of our body, to stay alive, to grow, and to reproduce. Metabolism is a complex network, adjustable, which is strictly regulated by different signals. Nutrition is the base of metabolism. There are three primary sources of energy that the human body can use. These include sugars, proteins, and fats. Each cell type uses different substrates and the type of substrate can change according to the physiological situation of the cell, such as fed and fasting states. Cells transform the potential chemical energy of food into useful one, ATP. There are two mechanisms of ATP synthesis: 1) Oxidative phosphorylation (OXPHOS), the process by which ATP is synthesized from ADP and inorganic phosphate (Pi) that takes place in the mitochondria; and 2) Substrate-level phosphorylation, in which ATP is synthesized through the transfer of high-energy phosphoryl groups to ADP from high-energy compounds. This occurs in both, the cytoplasm during glycolysis and in the mitochondria during the tricarboxylic acid (TCA) cycle, also called Krebs cycle.

To fully understand metabolism is essential to have a deeper knowledge of metabolic disorders such as obesity and its related-chronic comorbidities such as T2D, cardiovascular diseases (CVD) and cancer; to open new perspective in their treatments.

Obesity and overweight are defined as an abnormal fat accumulation along the body, due to a chronic imbalance between energy intake and energy expenditure (EE). The usual parameter to classify obesity is the body mass index (BMI), which establishes overweighed a person with a BMI≥25, while a person with a BMI≥30 is considered obese. Nowadays, obesity is considered a serious health problem because it affects more than 600 million people worldwide (WHO, 16 February 2018) mainly in middle-income countries of Eastern Europe, Latin America and Asia (Verma and Hussain, 2017). Moreover, in 2015, nearly 30 % more people worldwide died from being obese than in 1990 (Collaborators et al., 2017) and in 2014, the global economic impact of obesity was estimated to be $2.0 trillion (Tremmel et al., 2017). Therefore, to find new treatments to overcome obesity and its related-worldwide epidemic diseases is currently a challenge.

2. Obesity and type 2 diabetes

One of the main obesity-related comorbidity is T2D (Verma and Hussain, 2017), which is characterized by high blood glucose levels (hyperglycemia, fasting blood glucose >125 mg/dL and 2 hours postprandial blood glucose >180 mg/dL) (Mouri MI, 2019), and insulin resistance (ADA, 2013). T2D has also reached epidemic proportion due to obesity escalation. It is estimated that about 90% of T2D is attributed to excess body weight (Hossain et al., 2007). In 2015, 415 million adult people (20-79 years) were diabetic, and forecast point out that in 2040 this disease will affect 642 million people (IDF, 2017). In addition, T2D is a main driver of the two leading cause of death: ischemic heart disease or stroke (Gu et al., 1999) and cancer development (Ohkuma et al., 2018), being hepatocellular carcinoma (HCC) one of the most related cancer (Wainwright et al., 2017).

Genetics factors can contribute to develop obesity and T2D, although known related genes can only predict 15% of T2D and 5% of obesity (Eckel et al., 2011, Felber and Golay, 2002). The main factors involve in the development of T2D in obese individuals are proinflammatory cytokines, insulin resistance, β cell dysfunction and disturbed fatty acid metabolism (Eckel et al., 2011, Felber and Golay, 2002). Particularly, in obesity, insulin resistance and in consequence high insulin levels (hyperinsulinemia) are the first step to develop T2D. Insulin resistance is mainly produced by a permanent elevation of plasma free fatty acids (FFA) (Eckel et al., 2011), which increase fatty acids (FA) cell uptake and mitochondrial β-oxidation. The high mitochondrial activity blocks cell glucose metabolism by substrate competition, intracellular signaling, intermediates accumulation, enzyme regulation and gene transcription (Lois and Kumar, 2009), promoting high blood glucose levels. This glucotoxicity also contributes to impair insulin sensitivity; mainly, through protein and lipid glycation and subsequent advanced glycation end products (AGE) formation, which promote pancreatic β cell secretory dysfunction (Coughlan et al., 2011). β cell failure is also enhanced by the increased production of reactive oxygen species (ROS), as consequence of the high mitochondrial β-oxidation activity, which causes oxidative and cellular damage (Chang-Chen et al., 2008). Therefore, β cell dysfunction is the second hit that occurs in the development of T2D and that also contributes to hyperglycemia (Verma and Hussain, 2017). Moreover, other less common factors such as: Impaired tissue perfusion, sleep disturbances, androgen dysfunction, altered vitamin D levels and gastrointestinal stress can also drive T2D in obesity (Verma and Hussain, 2017).

Therefore, there are 3 main considered hypotheses to explain obesity-T2D relation (Chadt et al., 2000):

1. The inflammation hypothesis which assumes that obesity is a chronic inflammatory condition as a consequence of the macrophages infiltration in the white adipose tissue (WAT), which produces changes in insulin sensitivity and pancreatic β cells function.

2. The adipose tissue expandability hypothesis which proposes that the ectopic lipid accumulation, mainly in liver and skeletal muscle, due to the limited WAT storage capacity, exerts cytotoxic effects in peripheral cells, impairing their function, survival and regeneration.

3. The adipokine hypothesis which postulates that insulin resistance and pancreatic β cell failure is the consequence of the dysfunction in the secretion of endocrine factors from WAT.

In these 3 hypotheses, it is clear that the inflammation and expandability of the WAT are crucial in the connection among obesity and T2D. But, it is important to consider that WAT is also an important metabolic and endocrine tissue (Coelho et al., 2013); therefore, it is crucial to maintain a correct WAT balance to keep a healthy status. In fact, deficiency of this tissue (lipodystrophy) also predisposes to insulin resistance, T2D and hepatic steatosis (Stefan et al., 2017).

3. The liver

The liver is a central metabolic regulator which governs body energy metabolism. Liver functions involve carbohydrates, lipids and proteins metabolism, detoxification, coagulation, and immune response.

There are four major liver cell types, among them, the hepatocytes, which constitute around 70% of the total liver cell population, are primarily engaged in the basic functions of the liver. The other 3 types are the non-parenchymal cells (NPC), which are the hepatic stellate cells, the Kupffer cells, and the liver sinusoidal endothelial cells (Racanelli and Rehermann, 2006). While Kupffer cells (KC) serve as immune sentinels, hepatic stellate cells play central roles in vitamin A and lipid storage (Racanelli and Rehermann, 2006, Winau et al., 2008); and liver sinusoidal endothelial cells, which comprise the largest part (50%) of liver NPCs, separate the underlying hepatocytes from the sinusoidal lumen (Ding et al., 2016).

The liver plays a central role maintaining blood glucose homeostasis. In the postprandial state, insulin is secreted from pancreatic β cells and promotes glucose condensation into glycogen (glycogenesis), which is one of the two main forms of long-term energy reserves in humans. Although glucose can be also converted into FA or amino acids (AA), which will be metabolize to provide energy or use to synthesize proteins, glucose, and/or other bioactive molecules. Insulin also promotes DNL, when FA are esterified with glycerol-3-phosphate (G3P), to generate triacylglycerols (TG) or converted into ceramides or cholesterol. TG are stored in lipid droplets in hepatocytes or secreted into the circulation as very low-density lipoprotein (VLDL) particles, to extrahepatic tissues utilization.

After fasting, glucagon is secreted from pancreatic α cells and drives hepatic glucose production (HGP), from glycogen breakdown (glycogenolysis) as well as by *de novo* glucose synthesis from available precursors (Gluconeogenesis (GNG)) (Sharabi et al., 2015). Moreover, FA are oxidized to generate fuel and/or to generate ketone bodies (ketogenesis (KG)), which are used in other tissues, like brain, for getting energy.

As main metabolic tissue, the liver is deeply affected in obesity, basically because of the ectopically FFA accumulation that promotes the synthesis and intracellular storage of lipids into hepatocytes. This triggers the development of NAFLD, also known as hepatic steatosis (defined by hepatic TG droplets >5%) (Szczepaniak et al., 2005). Obesity is the most common associated condition to develop hepatic steatosis (Angulo, 2002); but also hepatic steatosis is associated with T2D, because up to 70% of T2D patients have NAFLD (Williamson et al., 2011). Moreover, a major concern of NAFLD is that can lead to worse pathologies, such as non-alcoholic steatohepatitis (NASH), fibrosis, cirrhosis or even HCC, constituting a high burden for public health (Nassir et al., 2015, Cohen et al., 2011).

3.1. From insulin resistance to NAFLD. Involved mechanisms. Fatty acid uptake, transport and *de novo* lipogenesis

NAFLD affects up to one-third of the population (Firneisz, 2014) and it is one of the most important chronic liver disorders worldwide (Ratziu et al., 2015). Its pathophysiology is not fully understood, although there is a growing body of evidence suggesting that lipid compartmentalization in hepatocytes and in particular the type or "quality" as opposed to the "quantity" of lipids accumulated may play a central role in the risk for progressive disease (McClain et al., 2007). Furthermore, differences in lipid vesicles size are associated to different etiologies. Histologically, microvesicular steatosis is characterized by distended hepatocytes with foamy appearing cytoplasm and small lipid vesicles (<1μm in diameter), where the nucleus is typically centrally located; whereas in macrovesicular steatosis the nucleus is displaced peripherally (Tandra et al., 2011). Microvesicles are usually related to severe dysfunction while macrovesicles are more related to an uptake/secretion imbalance; although, mixed forms can be frequently observed (Thoolen et al., 2010). On the contrary, less is known about differences in the lipid droplets distribution. However, lipid droplet proteins distribution seems to be dependent on the lipid droplet size (Straub et al., 2008). The increase of some lipid droplets proteins such as perilipin (PLIN), mainly PLIN-2, and the non-perilipin proteins, cell death-inducing DNA fragmentation factor A (DFFA)-like effector (CIDE-A and CIDE-C), promote hepatic steatosis (Carr and Ahima, 2016).

Liver FA come from cytoplasmic triacylglycerol stores, from TG of lipoprotein (remnants chylomicrons) directly taken up by the liver and broken by lipoprotein lipase (LPL), from the adipose tissue release or from DNL. Whereas short-($<C_6$) and medium- chain (C_6-C_{12}) -chain FA (SCFA and MCFA respectively) enter into hepatocyte independently of transport proteins; long-chain FA (LCFA) (C_{13}-C_{20}) need fatty acid binding transport proteins (FATP), also known as solute carrier protein family 27 (SLC27), particularly FATP2, 4 and 5; or enter through the fatty acid translocase (CD36) or using caveolins. Similarly, most commonly, only long- and very long-chain FA are transported by fatty acid binding protein (FABP), specifically the liver isoform (L-FABP or FABP1).

FA need to be activated by acyl-CoA synthetases (ACS) to form acyl-CoA. Whereas, LCFA-CoA are formed in the cytosol and must be transferred to the interior of the mitochondria via the carnitine shuttle; SCFA and MCFA, at least those of carbon atom number up to C8, are in the inner mitochondrial membrane in the non-esterified form and are activated to their CoA-derivatives in the mitochondrial matrix (Schonfeld and Wojtczak, 2016). FA transport proteins are also involved in the NAFLD pathophysiology, because for example FATP5 or FABP1 silencing reverses NAFLD in mice (Doege et al., 2008, Mukai et al., 2017). However, the binding of free LCFA or LCFA-CoA esters to fatty acid binding proteins also minimizes their toxic effects (Atshaves et al., 2010).

Activated FA bind to FABP acting as transcription factor (Furuhashi and Hotamisligil, 2008), they are oxidized (reviewed later) or used for lipid synthesis. In the DNL, acetyl coenzyme A (acetyl-CoA), which can come from lipid oxidation or from glucose hydrolyzation, is condensed with oxaloacetate (OAA) by citrate synthase (CS) to form citrate which should be oxidized in the citric acid cycle. But, when there are nutrients excess, citrate is transported to the cytosol to generate acetyl-CoA by ATP-citrate lyase (ACL), which is converted to malonyl-CoA by acetyl CoA carboxylase (ACC) and subsequently to palmitic acid by fatty acid synthase (FAS), a fully saturated 16-carbon FA ($C_{16:0}$). Palmitic acid is further elongated and desaturated to generate the diverse spectrum of saturated and unsaturated FA synthesized by mammalian cell (except α-linolenic acid and linoleic acid which need to be obtained from the diet). FA are esterified with glycerol 3-phosphate by glycerol-3-phosphate acyltransferase (GPAT), to generate TAG. However, intermediates of this pathway can be converted into different phosphoglycerides, including phosphatidylcholine, which build the major structural components of biological membranes or with cholesterol to produce cholesterol esters. These lipids are stored in lipid droplets and membrane structures, or secreted into the circulation as VLDL particles. Transient inhibition of both ACC1 and ACC2 in the liver decreases levels of hepatic malonyl-CoA and lipogenesis, increases β-oxidation, and protects against hepatic steatosis (Savage et al., 2006). Mice with liver-specific deletion of FAS are relatively normal (Chakravarthy et al., 2005), suggesting that fatty acid uptake is sufficient to maintain normal hepatic lipid content in the absence of liver FAS. Another class of lipids that are important for membrane function are sterols, mainly cholesterol and cholesteryl-esters (CEs). Cholesterol is synthesized from acetyl-CoA via the mevalonate

pathway. Other lipids that are generated from FA are the sphingolipids (such as ceramides), phosphoinositides and eicosanoids.

Under normal conditions, the contribution of DNL to TG and VLDL synthesis is low in humans (<5% in the postabsorptive state) (Donnelly et al., 2005) and excessive carbohydrates in the liver are first converted into glycogen. However, conditions such as ingestion of a high-carbohydrate diet, hyperglycemia and hyperinsulinemia, are associated with a shift in cellular metabolism from lipid oxidation to lipid synthesis and the excessive carbohydrates are also converted into FA via lipogenesis using the acetyl-CoA generated from glycolysis-driven pyruvate. Therefore, DNL is increased paradoxically, because there is a selective resistance to insulin in the liver (Brown and Goldstein, 2008). This means that HGP is not inhibited, because there is insulin-resistance in one transcriptional program (FoxO1-mediated GNG); but DNL is still increased (Brown and Goldstein, 2008), because there is insulin sensitivity in the lipogenesis-mediated program. This suggests that the insulin signaling pathway must bifurcate at some point. It has been proposed that the paradoxical increase in DNL is mediated by 2 transcription factors which are activated by glucose: 1) the activation of the carbohydrate-responsive element-binding protein (ChREBP), which not only controls glycolysis, but also regulates lipogenic genes expression and 2) the high insulin levels promote lipogenesis through the stimulation of the transcription factor sterol regulatory element-binding protein-1c (SREBP-1c), which increases the expression of lipogenic genes (ACC or FAS) (Horton et al., 2002) and liver X receptors (LXR) (Chen et al., 2004, Grefhorst et al., 2002, Mitro et al., 2007). Evidence for this branch point also points out to the mammalian target of rapamycin complex 1 (mTORC1), which is required for lipid synthesis, but it does not for GNG inhibition (Li et al., 2010). Moreover, NAD(P)H oxidase homologue 4 (Nox4) has been proposed as other factor involved in the selective insulin resistance (Wu and Williams, 2012). The third transcription factor that has been involved is the PPAR-γ, whose expression increase in response to insulin and also during hepatic steatosis (Zhang et al., 2006). The molecular mechanisms that controls PPARγ is unknown; however, it has been postulated that PPARγ activates ¨adipocyte specific lipogenic genes¨ in the hepatocytes (Yu et al., 2003). Therefore, DNL plays a central role in the development of NAFLD, being the second source of liver TG (26%). Additionally, insulin resistance also promotes VLDL secretion reduction; and the intrahepatic increase of FA and particularly malonyl-CoA which inhibits carnitine palmitoyltransferase 1 (CPT-1) and promote the inhibition of FA β-oxidation. All this also contribute moderately to increase intrahepatic lipid levels (Lewis et al., 2002). However, the first source of TG is the fat lipolysis (56% of liver TG), which increases in insulin resistance and the subsequent increased plasma FFA and FA re-esterification to TG in hepatocytes. Lastly, dietary fats can also contribute to NAFLD although in a lesser way (only 14%) (Hazlehurst et al., 2016, Bhatt and Smith, 2015). The relative contribution of the 3

pathways in human has been reported by Donelly et al. (Donnelly et al., 2005). Moreover, it is also important to considerer that even in the absence of insulin resistance the increased flux of FFA to the liver is sufficient to promote NAFLD (Komatsu et al., 2008, Bandsma et al., 2008), due to an over storage of unmetabolized energy in hepatocytes, which exceeds the energy combustion capability of the lipid oxidation system. The majority of hepatic lipids in NAFLD are stored in the form of TG (Browning and Horton, 2004), although other lipid metabolites such as DAG, free cholesterol (FC), cholesterol ester (CE), ceramide, or phospholipids are also accumulated in the liver promoting hepatic steatosis (Cheung and Sanyal, 2008).

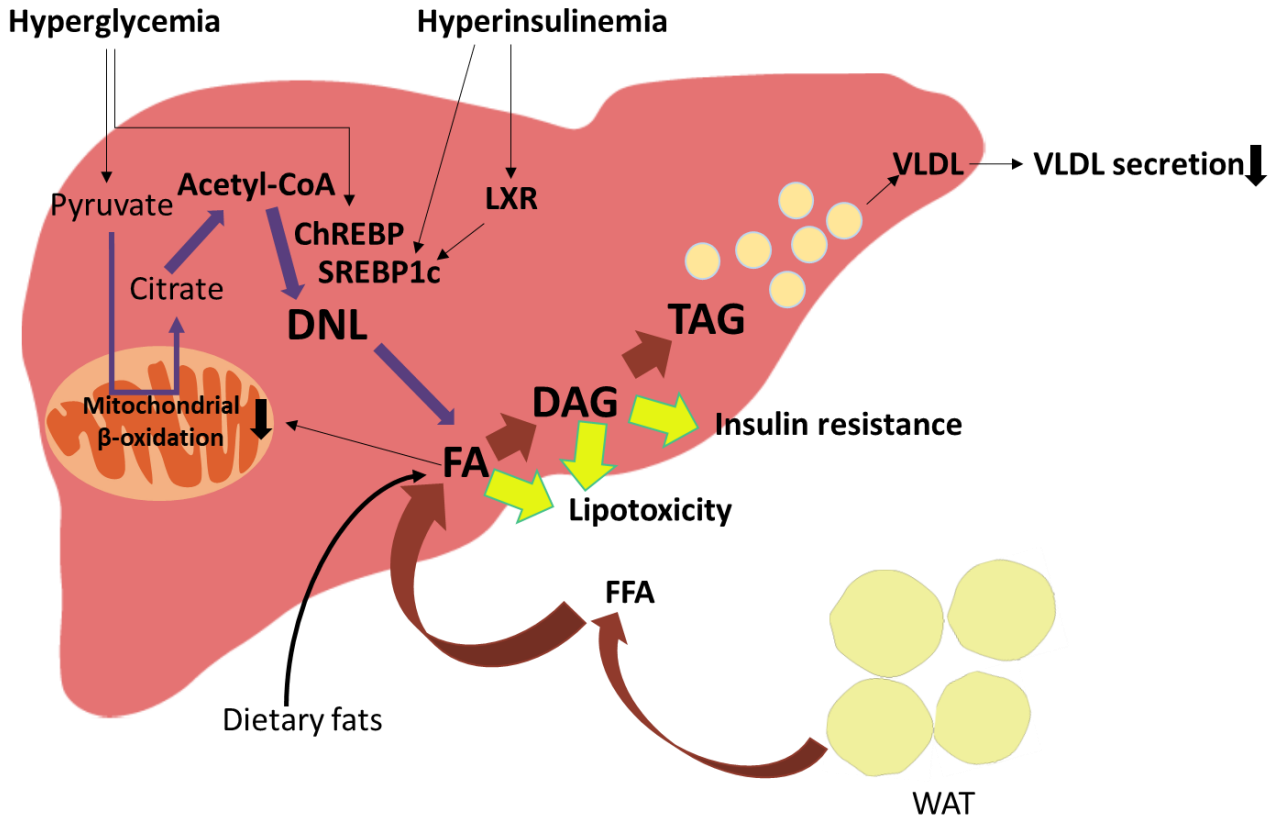

Scheme 1. Mechanisms that contribute to NAFLD in T2D

Triglycerides (TG) are produced from fatty acids (FA) re-esterification due to increased plasma FFA from fat lipolysis (56%) or from diet (14%). The rest of TG (26%) are produced from *de novo* lipogenesis (DNL), as consequence of hyperglycemia, hyperinsulinemia and mitochondrial β-oxidation impairment due to high FA and malonyl-CoA levels which inhibits CPT-1. This drives carbohydrate flux through DNL (pyruvate-citrate and acetyl-CoA). Moreover, the reduction in the very low-density lipoprotein (VLDL) secretion also contributes to intrahepatic lipid accumulation.

Hypersinsulinemia and selective insulin resistance only in the insulin-mediated gluconeogenic inhibition, promote DNL, through LXR and SREBP1c transcription factors activation. Moreover, high blood glucose levels increase ChREBP levels which also increases lipogenic genes expression.

Diacylglyerides (DAG) are main lipids driving insulin resistance, and together with FA are the main lipids that lead cellular lipotoxicity.

3.2. Progression from NAFLD to NASH, Cirrhosis and HCC. Involved mechanisms

Only 23% of hepatic steatosis progress into steatohepatitis (NASH) (Wong et al., 2010). NASH is characterized by liver inflammation. Although several hypotheses have been proposed to explain the progression from NAFLD to NASH; it is thought that requires two events (this is called the two hits hypothesis): 1) lipid accumulation; 2) liver injury, fibrosis and inflammation (Day and James, 1998). However recently, the multiple hits hypothesis has been extended; pointing out that hepatic steatosis is a consequence of insulin resistance together with several distinct injurious mechanisms instead of a two hits phenomenon (Cortez-Pinto et al., 2006, Tilg and Moschen, 2010) (Yilmaz, 2012a).

Several factors have been related with the progression to NASH: lipid peroxidation due to oxidative stress (high ROS levels (Garcia-Monzon et al., 2000) promoted by the release of inflammatory mediators (du Plessis et al., 2015) and by the impairment of mitochondrial β-oxidation capacity, which the consequent increase in peroxisomal β-oxidation and ω-microsomal oxidation (Wei et al., 2008, Browning and Horton, 2004). Additionally, lipotoxicity can directly promotes mitochondrial deregulation (Caldwell et al., 2004) (Sunny et al., 2011, Alkhouri et al., 2009), lysosomal permeabilization, and consequently apoptosis (Alkhouri et al., 2009, Feldstein et al., 2003). Finally decrease in the lipid removal cycle due to autophagy impairment (Singh et al., 2009, Czaja, 2016), endoplasmic reticulum (ER) stress and dysregulation of the unfolded protein response (UPR) (Cusi, 2009, Alkhouri et al., 2009), gut microbiota (Yilmaz, 2012b) and some genetic and epigenetics factors can promote NASH (Buzzetti et al., 2016).

NASH could progress to cirrhosis. Cirrhosis is described as the presence of scared tissue in the liver, which usually happens when hepatocytes activate the lipoapoptosis pathway (programed cell death) a key driving force of fibrosis progression. This consists in the activation of myofibroblasts, hepatic stellate cells, macrophages, cholangiocytes and components of the extracellular matrix (ECM) which are major fibrogenic effectors (Schuppan et al., 2018). Particularly, resident liver macrophages, called KC ($F4/80^+$ and $CD68^+$), which consist around the 10% of total liver population, have a central role by recruiting inflammatory immune cells and secreting pro-inflamatory cytokines, such as tumor necrosis factor (TNF)-α (Sica et al., 2014). Hepatic stellate cells are activated as consequence of lipid peroxidation (Ghatak et al., 2011). Moreover, oxidative stress

also promotes cytokine and Fas ligand induction (Angulo and Lindor, 2002), which also contribute to cirrhosis. Additionally, Fas system has been also related with the progression to HCC (Hammam et al., 2012). HCC usually appears when there is excessive ROS accumulation, which promotes DNA damage, DNA repair systems inhibition and leads inflammatory cells infiltration, which impairs antioxidant systems and increases hepatocytes proliferation (Villanueva et al., 2007, Makridakis and Vlahou, 2010, Friedman, 2008, Hammel et al., 2001).

3.3. Liver lipotoxicity and insulin resistance

NAFLD has a complex pathophysiology, which is not still well defined. TG liver accumulation has been defined as main defect in NAFLD (Donnelly et al., 2005, Ginsberg, 2006, Puri et al., 2007); however, some study propose that hepatic TG are not the effectors of cellular toxicity in NAFLD, but rather a defense mechanism to avoid free fatty acid accumulation, which are important mediator of cellular lipotoxicity (Yamaguchi et al., 2007, Listenberger et al., 2003). Conversely, cholesterol and sphingolipid species (such as ceramides) seem to play an important role promoting cellular toxicity (Ginsberg, 2006, Alkhouri et al., 2009). Actually, FA and cholesterol, especially when accumulated in the mitochondria, are considered the "aggressive" lipids triggering mitochondrial dysfunction secondary to ROS overproduction and lipid peroxidation. They also lead TNFα-mediated liver inflammation (mainly polyunsaturated FA (PUFA)), and finally, cell death pathways activation (Mari et al., 2006, Cheung and Sanyal, 2008). Additionally, lipidomic analyses have showed increased DAG and free cholesterol, and decreased phosphatidylcholine content in hepatic steatosis (Puri et al., 2007). Therefore, although there is still controversy regarding the type of lipids, fatty acid composition and the induction of insulin resistance and it requires further investigations; it seems that TG, neither cholesterol esters, are sufficient to promote insulin resistance (Matsuzaka and Shimano, 2011) (Monetti et al., 2007, Minehira et al., 2008). However DAG, ceramides and saturated FA are more closely related to insulin resistance development (Matsuzaka and Shimano, 2011, Samuel et al., 2010, Samuel and Shulman, 2012, Farese et al., 2012, Chavez and Summers, 2012) (Nagle et al., 2009, Samuel et al., 2010, Birkenfeld and Shulman, 2014). However, DAG role has been debated, because some mice models show high levels of DAG without insulin resistance (Minehira et al., 2008, Monetti et al., 2007). This controversy can be explained by a specific compartmentalization pattern of DAG, because only the DAG increase in hepatic plasma-membrane fractions and not in lipid-droplet associated ER have been related with insulin resistance (Cantley et al., 2013). Additionally, glycerolipid intermediates, such as lysophosphatidic acid (LPA) and phosphatidic acid have been also involved with fatty liver and phosphatidic acid has been also related with insulin signaling impairment (McIntyre et al., 2003, Wang et al., 2006, Matsuzaka and Shimano, 2011).

Supporting the role of lipid metabolism and NAFLD in the development of insulin resistance, some studies that target proteins related with lipid metabolism shown ameliorated hepatic steatosis and whole-body insulin resistance; although; the fact that adiposity also drives insulin resistance is a factor to consider in all these studies. For instance: 1) Decreased microsomal triglyceride transfer protein (MTTP*)* expression, which promote a reduction in the export of VLDL and consequently fatty liver is also accompanied by systemic insulin resistance (Shindo et al., 2010). 2) The reduction in hepatic steatosis in mice lacking hepatic fatty acid transporter protein 2 (FATP2) is associated with a protection against systemic insulin resistance (Falcon et al., 2010). 3) Liver constitutively activation of carnitine palmitoyl transferase 1α (Cpt1α) and consequently increase of fatty acid oxidation also protect against NAFLD and systemic insulin resistance (Orellana-Gavalda et al., 2011). By other hand, the controversy between the relation of hepatic steatosis and insulin resistance is due to some studies such as: in humans, mutations in *APOB, ATGL, CGI58* or *PNPLA3* genes produce hepatic steatosis without insulin resistance (Romeo et al., 2008, Hooper et al., 2011, Tanoli et al., 2004), NAFLD can occur in people without metabolic syndrome and in mice insulin sensitivity can be improved independently of hepatic steatosis (Monsenego et al., 2012). Moreover, glycogen storage disease type 1A and citrin deficiency, which enhance DNL, cause massive hepatic steatosis in the absence of obesity or insulin resistance (Birkenfeld and Shulman, 2014, Komatsu et al., 2008).

However, it is quite stablished that exists a vicious cycle between insulin resistance and NAFLD (Gruben et al., 2014). We have previously described how insulin resistance drives NAFLD; but, hepatic steatosis and lipotoxicity can also drive insulin resistance (Samuel and Shulman, 2012) through diacylglycerol-mediated activation of PKCε and insulin receptor kinase activity inhibition (Jornayvaz and Shulman, 2012, Petersen et al., 2016b, Lyu, 2018), ceramide mediated increases in protein phosphatase 2A and increased sequestration of Akt2 by PKCζ (Petersen and Shulman, 2017) and activation of the next 2 inflammatory pathways: The Nuclear factor κB (NF-κB) (Shoelson et al., 2003, Shi et al., 2006) and the c-Jun NH2-terminal kinase (JNK) pathways (Shoelson et al., 2006). NF-κB activation induced by IKK mediated phosphorylation and degradation of the NF-κB inhibitor, IκBα, promotes the transcription of pro-inflammatory genes (Shoelson et al., 2006, Tak and Firestein, 2001). Moreover, IKK2 can directly inhibit insulin signaling, through serine phosphorylation instead of tyrosine phosphorylation of the insulin receptor substrate (IRS)-1 (Aguirre et al., 2002, Gao et al., 2002). The second pathway involved, JNK, plays a central role in insulin resistance development (Shoelson et al., 2006, Hotamisligil, 2006, White, 2003, Weston and Davis, 2007), and it is activated by inflammation (proinflammatory cytokines, such as TNFα) and by high saturated FA (Jaeschke and Davis, 2007, Kant et al., 2013). It has been proposed that JNK can drive insulin resistance through 4 mechanisms: 1) in the liver, through negative regulation of PPARα and Fgf21; moreover, 2) in insulin target cells, through direct serine/threonine phosphorylation of IRS-1 and 2

(Ser307); 3) inducting macrophage M1 gene-expression and 4) inhibiting the pituitary thyroid axis in the case of JNK1 and 2, but not for JNK3 (Solinas and Becattini, 2017).

Lastly, inflammatory cells, particularly neutrophils and hepatic natural killers T (NKT) are also involved in the insulin resistance development. Whereas HFD fed mice with decreased neutrophils amount in liver are protected against systemic insulin resistance (Talukdar et al., 2012); NKT liver reduction is related with hepatic inflammation and insulin resistance (Hua et al., 2010, Martin-Murphy et al., 2014). Moreover, it seems KC are also involved, although their role is contradictory. On the one hand, activated KC inhibit insulin signaling through pro-inflammatory cytokines secretion (Huang et al., 2010, Henkel et al., 2011). But on the other hand, several works propose that KC improve insulin resistance. Therefore, it is possible that their role depends on their activation and inflammatory status (Papackova et al., 2012, Clementi et al., 2009).

4. Hepatic metabolism

4.1. Fatty acid oxidation. Role of the mitochondria and peroxisome

Hepatocytes are enriched in mitochondria, a central integratory organelle, harboring around 800 per cell (Nassir and Ibdah, 2014). Mitochondria is the main organelle involved in the lipid oxidation and the most effective pathway to get energy in the form of adenosine triphosphate (ATP) through OXPHOS during fast states. Mitochondria is also the main organelle that produces ROS (Caldwell et al., 2004), because around 1-5% of O_2 during respiration is not fully reduced to water.

Once LCFA are converted into acyl-CoA, they enter to the mitochondria through carnitine palmitoyl transferase (CPT)-1 and 2 proteins for β-oxidation, generating acetyl-CoA. These reactions are catalyzed by carbon length–specific acyl-CoA dehydrogenases (ACAD) and by the mitochondrial trifunctional protein (MTP). Additionally, acyl-

CoA can be also hydrolyzed by acyl-CoA thioesterases (ACOT), generating FA plus CoA, which have emerged as important lipid metabolism modulators (Tillander et al., 2017). It is important to consider that acetyl-CoA can be also produced from carbohydrates, as previously was mentioned, and proteins. Next, acetyl-CoA is oxidized in the Krebs cycle in the mitochondrial matrix. During this process NADH and $FADH_2$ are produced and electrons are transferred to O_2 through the electron transfer system (ETS), forming H_2O. The Krebs cycle is also an important source for precursors of many other molecules, such as OAA.

The ETS is in the inner mitochondrial membrane and belongs to the OXPHOS, where finally ATP is gotten by the ATPase (complex V) action. The ETS is formed by four protein complexes: NADH dehydrogenase (complex I), succinate dehydrogenase or succinate-CoQ reductase (complex II), cytochrome c oxidoreductase (complex III),

and cytochrome c oxidase (complex IV). Electron transport between the complexes occurs through other mobile electron carriers, ubiquinone or coenzyme Q (CoQ) and cytochrome c. Particularly, NADH enters to the ETC via complex I, and $FADH_2$ through complex II (succinate dehydrogenase or succinate-CoQ reductase) or other deshydrogenases such as electron-transfering flavoprotein (ETF) dehydrogenase. Electrons are then passed to CoQ and posteriorly to complex III, cytochrome C and complex IV, which donors them to oxygen (Acin-Perez and Enriquez, 2014).

Additionally, during fasting, KG from fatty acid oxidation-derived acetyl-CoA can also take place in the mitochondrial matrix. KG generates β-hydroxybutyrate, acetoacetate, and acetone which are exported into the circulation and provide metabolic fuels for extrahepatic tissues. KG rates are usually proportional to total lipid oxidation. The main and first enzyme involved is the 3-hydroxymethylglutaryl-CoA synthase (HMGCS)-2 (Puchalska and Crawford, 2017).

Mitochondria plays a main function in lipid oxidation, but it has also an important role in cell bioenergetics due to the proper functionality of mitochondrial shuttles is crucial for the regulation of metabolic processes. The electrons of NADH produced in the cytoplasm during glycolysis must be transported into the mitochondria for conversion to ATP by the electron transport pathway and NAD^+ must be regenerated. Because the NADH itself cannot cross the mitochondrial membrane, one important function of shuttle mechanisms is the transport of reducing equivalents across the mitochondrial membrane. Two of these mechanisms are: 1) the Glycerophosphate shuttle and 1) the Malate-Aspartate shuttle. 1) The glycolytic intermediate dihydroxyacetone phosphate (DHAP) can be converted to G3P by glycerol-3-phosphate dehydrogenase; this process also results in conversion of NADH to NAD. G3P can then be converted back to DHAP by flavoprotein dehydrogenase; this second enzyme is a FAD-dependent enzyme located in the mitochondrial inner membrane. Similar to the complex II of the electron transport chain, flavoprotein dehydrogenase donates electrons directly to Coenzyme Q without pumping protons and producing a maximum of 2 ATP. This shuttle is irreversible. 2) Regarding to the second shuttle: OAA in the cytoplasm is converted to malate by malate dehydrogenase (MDH), oxidizing NADH to NAD. The malate enters the mitochondria using an exchanger protein that must also transport α-ketoglutarate in the opposite direction. The malate is then oxidized to OAA by the mitochondrial MDH, resulting in formation of NADH, which can then enter the electron transport pathway. Return of the OAA to the cytoplasm requires a separate transporter, which exchanges aspartate for glutamate. This separate exchanger is necessary to allow net movement of electrons from one side of the membrane to the other. This process allows the synthesis of three ATP. The malate-aspartate shuttle is reversible; during GNG, parts of this shuttle act as one method for releasing OAA (in the form of malate) into the cytoplasm for the later reactions of the gluconeogenic pathway.

Since mitochondria has a limited capacity to β-oxidize lipids, alternative lipid oxidation pathways are also available. Particularly, peroxisomes (β-oxidation), but also smooth ER (ω-oxidation) can oxidize lipids. Peroxisomal oxidation is a four-step pathway that consists the normal route of metabolism of very long-chain fatty acyl-CoA esters (>C_{20}), branched FA, as well as prostaglandins and leukotrienes (Demarquoy and Le Borgne, 2015). Electrons from FADH2 and NADH are transferred directly to oxygen, but in this case generating hydrogen peroxide (H_2O_2), one of the main oxidative stress mediators. However, peroxisomes are uniquely provided with the enzyme catalase and other powerful anti-oxidant mechanisms to eliminate the excessive ROS (Schrader and Fahimi, 2006). Peroxisomes are only able to chain-shorten their substrates, and for fully oxidation to CO2 and H2O, peroxisomal β-oxidation products must be shuttled to mitochondria (Demarquoy and Le Borgne, 2015). In order to keep peroxisomal β-oxidation ongoing, it is crucial that NADH is reoxidized to NAD+. This process is thought to rely on a redox shuttle mechanism that involves mitochondria (Fransen et al., 2017).

Peroxisomal enzymes deficiency is also an important cause of microvesicular steatosis and steatohepatitis. For example, acyl-coenzyme A oxidase (ACOX) deficiency, the first enzyme involved in the peroxisomal β-oxidation, leads to very LCFA and dicarboxylic acids oxidation disruption, promoting extensive microvesicular steatosis and steatohepatitis (Fan et al., 1998).

Regarding to ω-oxidation, cytochrome P450 (CYP) enzymes are also involved in fatty acid oxidation. Their hepatic activity and expression are reported to be increased in patients with NASH. This is because these enzymes can be major producers of ROS because of a weak affinity to oxygen, leading to the release of species such as superoxide anion radical, hydroxyl radicals, and hydrogen peroxide (Basaranoglu et al., 2013).

The nuclear hormone PPARα is the master regulator of fatty acid metabolism and KG; increasing β-oxidation in mitochondria, peroxisomes and ER in the liver during fasting states (Evans et al., 2004, Pyper et al., 2010). But, it is also involved in the fatty acid uptake, intrahepatic transport and in lipogenesis pathway. Therefore, PPARα is a key factor that control the adaptation between fast and fed states, depending on its regulation by different kinases such us proteins such us (PK)-A, C, mitogen-activated protein kinases (MAPK) and mTORC1 (Pawlak et al., 2015). Actually, PPARα deletion decreases hepatic fatty acid β-oxidation in fasted state and exacerbates fasting-induced hepatic steatosis, hypoglycemia, hypoketonemia, and hypothermia (Kersten et al., 1999, Leone et al., 1999). Most of the studies point out that some of these PPARα effects are mediated by the FGF21 (Inagaki et al., 2007, Badman et al., 2007, Lundasen et al., 2007) , which is usually upregulated during ketosis and fasting Badman et al., 2007. Fgf21 plays a key role in insulin sensitivity (Holland et al., 2013, Camporez et al., 2013), glycemia (Jing Xu, 2009, Kharitonenkov et al., 2005), and obesity (Kharitonenkov et al., 2005, Coskun et al., 2008). FGF21 stimulates fatty acid oxidation and KG (Badman et al., 2007, Badman et al., 2009) and inhibits

lipogenesis in hepatocytes in culture (Zhang et al., 2011). Additionally, Vernia et al. demonstrated that the activation of JNK, during fed state, which has been implicated in hepatic steatosis and insulin resistance (Davis, 2000, Sabio and Davis, 2010), inhibits PPARα activation, decreasing FGF21 expression (Vernia et al., 2014). FGF21 has emerged as a promising therapeutic agent for the treatment of obesity and T2D (Jimenez et al., 2018) and it has been related with the protection against hepatic steatosis and insulin resistance, by suppressing liver glucose production and increasing glycogen content (Xu et al., 2009a, Berglund et al., 2009, Xu et al., 2009b).

4.2. Glucose metabolism

4.2.1 Glycolysis

In hepatocytes, glucose entry into cells is driven by the concentration gradient between the blood and the hepatocytes, through the glucose transporter type 2 (GLUT2) and independently of insulin signaling (Thorens and Mueckler, 2010). The catabolism of glucose into pyruvate is termed glycolysis and it is considered as a major pathway in eliciting ATP, but also NADH and $FADH_2$ which is used by OXPHOS. Glycolysis is mainly control at the level of three irreversible reactions: hexokinase IV, phosphofructokinase-1 (PFK-1) and pyruvate kinase (PK) (Berg JM, 2002). Once glucose is inside the hepatocytes, it is phosphorylated to glucose-6-phosphate (G6P) by the liver glucokinase (GCK) (hexokinase IV). Therefore, GCK promotes glycolysis and inhibits HGP. Contrary to other GCK, the liver isoform is not inhibited by its product, G6P; but it is inhibited by the glucokinase regulatory protein (GKRP) (van Schaftingen et al., 1997). At low glucose concentrations, GK is sequestered in the nucleus through its binding with GKRP, but when the glucose concentration increases, GK dissociates from GKRP and is transported into the cytoplasm to facilitate the uptake of glucose and its conversion into glycogen (6). GCK activity is lower in diabetic rats, and the specific restoration of GCK expression decreases HGP and hyperglycemia in these rats (Torres et al., 2009). Conversely, hepatocyte-specific deletion of GCK results in mild (Torres et al., 2009) hyperglycemia and hyperinsulinemia (Postic et al., 1999).

In the next step, G6P is catabolized into pyruvate in ten-step. PFK-1 is other key enzyme, converting fructose-6-phosphate (F6P) into fructose-1,6-biphosphate (F-1,6-bisP). F-1,6-bisP can follow glycolysis or can be transformed into DHAP, an important cell intermediate for cell bioenergetic (previously described).

PFK-1 is inhibited by its product F-1,6-bisP and by ATP, phosphoenolpyruvate and citrate, which generally indicate a sign of energy abundance. Reciprocally, it is allosterically activated by ADP or AMP. However, fructose 2,6-bisphosphate (Fru-2,6-P_2) is the most potent positive allosteric effector of PFK, enhancing glycolysis. The production of this substrate is controlled by 6-phosphofructo-2-kinase/fructose-2,6-bisphosphatase (PFKFB or PFK2) enzymes, mainly by PFKFB3, which converts F6P into Fru-2,6-P_2 (Bolanos, 2013). PFK-2 are bifunctional

proteins, with a terminus that serves as a kinase domain (for PFK-2), driving glycolysis; while the other acts as a phosphatase domain (FBPase-2), driving GNG (Hasemann et al., 1996). PFKFB3 is ubiquitous expressed; however, PFKFB1, is the main liver isoform and it is activated by insulin, which activates a protein phosphatase which dephosphorylates the PFK-2 complex, promoting glycolysis and inhibiting GNG (Kurland et al., 1992). In contrast, glucagon increases FBPase-2 activity, through a cAMP signal cascade and in turn, protein kinase A (PKA) phosphorylates Ser32, inactivating the bifunctional ability of the enzyme to act as a kinase and stabilizes the phosphatase activity. Therefore, glucagon decreases glycolysis and stimulates the GNG pathway (Nishimura et al., 1994).

In the last step, PK catalyzes the formation of one molecule of pyruvate and one molecule of ATP. The most significant PK activator is F-1,6-bisP, but also insulin-mediated dephosphorylation increase its activity. By contrast, PK activity is allosterically inhibited by ATP, acetyl-CoA, and LCCFA. Additionally, alanine and PKA following a glucagon-mediated increase in intracellular cAMP during fasting also inhibit its activity. Under aerobic conditions, pyruvate is transported to the mitochondria and converted to acetyl-CoA for its respiration through Krebs cycle. Under anaerobic conditions, pyruvate is converted into lactate by lactate dehydrogenase (LDH), which allows to regenerate the NAD^+ necessary for ATP production.

4.2.1 Glycogen metabolism

4.2.2.1 *Glycogenesis*

In the liver, the excess of carbohydrates during fed status is storage as glycogen, during glycogenesis. The main involved enzyme is the glycogen synthase (GYS) and in the liver, particularly the isoenzyme 2 (GYS2), whose expression is almost limited only to this tissue (Browner et al., 1989, Nuttall et al., 1994). GYS2 has a cytosolic distribution in the absence of glucose and goes to the hepatocyte cortex upon glucose (Fernandez-Novell et al., 1997, Garcia-Rocha et al., 2001, Fernandez-Novell et al., 2002), opposite to muscle GYS (GYS1), which is ubiquitously expressed. Moreover, it seems GYS2 has a greater role in overall glucose disposal and insulin sensitivity because mice with a disruption of the *GYS1* gene showed improved glucose tolerance (Pederson et al., 2005a, Pederson et al., 2005b). In the liver, periportal and perivenous hepatocytes have significantly differences in the glycogen metabolism (Bartels et al., 1987) and moreover, glycogen particles are often reported to be close to ER (Cardell et al., 1985).

In glycogenesis, firstly, G6P is converted to glucose-1-phosphate by phosphoglucomutase, and later to UDP-glucose by UDP-glucose phosphorylase (Roach, 2002). In glycogenesis, it is necessary an initiation step whereby

glycogenin self-glucosylates to form an oligosaccharide first chain (Krisman and Barengo, 1975, Pitcher et al., 1987, Lomako et al., 1988). After this, via its extreme C-terminus, glycogenin can interact directly with GYS2, which is responsible for the formation of the large majority of the α-1,4-glycosidic linkages of glycogen, also using UDP-glucose as the glucosyl donor. Finally, the α -1,6-glycosidic branchpoints are formed by the action of the branching enzyme.

GYS2 activation after feeding, occurs after its dephosphorylation, by protein phosphatase-1 (PP1) (Bollen et al., 1998). Actually, dephosphorylation of glycogen synthase, and other glycogen-metabolizing enzymes, is thought to be mediated by members of a family of glycogen-associated PP1 composed of a catalytic subunit (PP1c) bound to a glycogen-targeting subunit (Bollen, 2001, Ceulemans and Bollen, 2004); particularly in liver the G_L subunit, coded by the *PPP1R3B* gene (Doherty et al., 1995, Moorhead et al., 1995) (PP1-G_L). It has been described that the covalent modification of GYS, namely O-linked attachment of N -acetylglucosamine, makes the enzyme less sensitive to activation by phosphatases (Parker et al., 2003). G6P, formed by glucose phosphorylation, is the main allosterically regulator of GYS2 (von Wilamowitz-Moellendorff et al., 2013), producing a conformational rearrangement that converts GYS2 into a better substrate for protein phosphatases (Carabaza et al., 1992, Ferrer et al., 2003). Moreover, contrary to GYS1, which is mainly regulated by insulin-stimulated import of the sugar by the GLUT-4 transporter; GYS2 regulation depends more of the glucose-phosphorylating capacity of the cell (Azpiazu et al., 2000). Therefore, the hepatic glycogen deposition is also controlled by GK and GKRP coefficients, which regulate G6P levels (de la Iglesia et al., 2000, Petersen et al., 2017).

On the contrary, GYS2 is inhibited during fasting. GYS2 is inactivated by glycogen synthase kinase 3 (GSK3) phosphorylation, particularly in the liver by the α isoform (MacAulay et al., 2007). GSK3 is a downstream target of AKT/PI3K and therefore of insulin signaling. Thus, upon insulin or feeding AKT is activated, leading to the phosphorylation and inhibition of GSK3, in the liver particularly, GSK3α N-terminal phosphorylation in Ser21; then resulting in the activation of GYS2 (MacAulay et al., 2007). When GSK3 is active, it recognizes the sequence -SXXXpS- in GYS (Fiol et al., 1987) and phosphorylate C-terminal GYS at multiple sites (Ser641, Ser645, Ser649 and Ser653) inhibiting its activity in muscle (Mora et al., 2005, Jensen et al., 2012) and also in the liver (Coghlan et al., 2000, Cline et al., 2002). However, GSK3 need prior phosphorylation of GYS2 by protein kinase casein 2 (CK2) at Ser656 (Zhang et al., 1993). Moreover, it has been suggested that GSK3 is not the only kinase which phosphorylates the residues between Ser641 and Ser653 (Roach, 2002, Ferrer et al., 2003) and there is a study against the role of GSK3 in the regulation of the GYS2, because the mutation of GYS2 residues phosphorylated

by GSK3, did not affect the overall enzyme activity. However, the mutation of serine 7 to alanine, a site that is recognized by PKA and AMPK (Bultot et al., 2012, Ros et al., 2009) inhibiting GYS2 and it is dephosphorylated by insulin, leads to increase the GYS2 activity. Therefore, this indicates that Ser7 is a key regulator site of GYS2 (Ros et al., 2009, Ros et al., 2010). Actually, adenoviral overexpression of GYS2 with a Ser7 Ala mutation displayed increased levels of liver glycogen under both fasting and fed conditions (Ros et al., 2010).

4.2.2.2 *Glycogenolysis*

Glycogen is degraded in a process called glycogenolysis. The main involved enzyme is the glycogen phosphorylase (GP), which catalyzes the reaction of the removal of a glucose residue from the non-reducing end of a glycogen chain, leading to the generation of glucose 1-phosphate. Then, phosphoglucomutase converts glucose 1-phosphate into G6P, which can be incorporated into glycolysis or further converted into glucose by glucose 6-phosphatase, depending on the energy status of the organism.

Liver GP is activated through phosphorylation at serine 14 by phosphorylase kinase (PK) upon cAMP–PKA signaling, stimulated by glucagon during nutritional deprivation or adrenergic stimulation. On the contrary, insulin promotes the activation of PP1, which dephosphorylates and inactivates glycogen phosphorylase, at the same time that activates GYS2 and promote glycogen synthesis (Han et al., 2016). Moreover, it has been proposed that glucose allosterically binds and stabilizes GP, which stabilizes a conformation that enables dephosphorylation and inactivation of the enzyme in its inactive conformation; relieving the inhibition that GP exerts on the hepatic glycogen-associated form of PP1 (PP1-G_L), previously described, allowing PP1 to dephosphorylate and hence activate GYS2 (Kelsall et al., 2007). Therefore, elevated intracellular glucose levels can also stimulate GYS2 by a mechanism involving the liver-specific glycogen targeting subunit, G_L (Agius, 2010) (Han et al., 2016).

4.2.1 Gluconeogenesis

The liver is the main tissue involved in glucose homeostasis and particularly, the liver is responsible of keeping constant blood glucose levels. During fasting, the liver produces 85% of glucose and the rest is produced by kidneys (DeFronzo, 2004, Ekberg et al., 1999). Whereas glycogenolysis is the main contributor to HGP during short-term fasting periods (until 24h), with highest contribution to HGP upon around 8 fasting hours (Perry et al., 2018); there is a relative increase in the contribution from GNG, to HGP when glycogen stores are progressively depleted (Hellerstein et al., 1997, Chung et al., 2015, Southampton-University, 2017) contributing more than 90% of GNG after 48h of fasting (Hellerstein et al., 1997, Chung et al., 2015). However it has been

shown that GNG is also activated upon approximately 8 fasting hours, contributing 64% to HGP during the first 22 fasting hours (Rothman et al., 1991). Hepatocytes synthesize glucose through GNG, using different non-carbohydrates substrates (lactate, pyruvate, glycerol, and AA), to promote HGP (Hellerstein et al., 1997, Chung et al., 2015).

Lactate is oxidized by LDH to generate pyruvate. Pyruvate is transported into the mitochondria and converted to OAA by pyruvate carboxylase. Eventually, OAA is converted to glucose; when this happen, OAA is reduced to malate by mitochondrial MDH, exported into the cytoplasm, and oxidized by cytoplasmic MDH to regenerate OAA. This cytoplasmic OAA is converted to phosphoenolpyruvate by cytoplasmic phosphoenolpyruvate carboxylase (PEPCK). Phosphoenolpyruvate, after multiple biochemical reactions, is converted into F-1,6-bisP which is then dephosphorylated by fructose 1,6 bisphosphatase (FBPase) to generate F6P. Next, F6P is converted to G6P, transported into the ER, and dephosphorylated by glucose-6-phosphatase (G6Pase) to generate glucose.

Regarding to glycerol contribution to GNG, glycerol that comes from increased WAT lipolysis under fasting, enters into hepatocytes via aquaporin-9 (Jelen et al., 2012). Once in the hepatocytes, it is phosphorylated by glycerol kinase to generate glycerate-3 phosphate, which is converted to DHAP, a gluconeogenic precursor, by the mitochondrial glycerol 3-phosphate dehydrogenase (GPDH) (Han et al., 2016). Lastly, AA are converted to α-ketoacids through deamination reactions catalyzed by glutaminase, glutamate dehydrogenase, and/or aminotransferase. The α-ketoacids are further converted to intermediates of the TCA cycle, which also serve as precursors for GNG or directly into pyruvate, following then the pathway described above.

There are different levels of GNG regulation. Mitochondrial acetyl-CoA, a central metabolic substrate regulator (Pietrocola et al., 2015), it is a key allosteric activator of pyruvate carboxylase, leading to increasing OAA production and then triggering GNG. The chronic activation of GNG is ultimately achieved via transcriptional mechanisms. Major transcriptional factors that are shown to induce gluconeogenic genes include c-AMP response element binding (CREB), forkhead box O (FoxO)-1 (Oh et al., 2013) or peroxisome proliferator-activated receptor gamma coactivator 1 alpha (PGC-1α). Moreover, glucagon and epinephrine are also involved in the GNG induction, contrary to insulin that promotes its inhibition (Han et al., 2016). Lastly, the process is regulated by the own gluconeogenic enzymes such as PEPCK or G6Pase, and also the circadian clock, the endoplasmic reticulum, growth hormones, cytokines and gastrointestinal (GI) hormones such as glucagon-like peptide 1 (GLP-1) are involved (Rui, 2014).

a.Fed

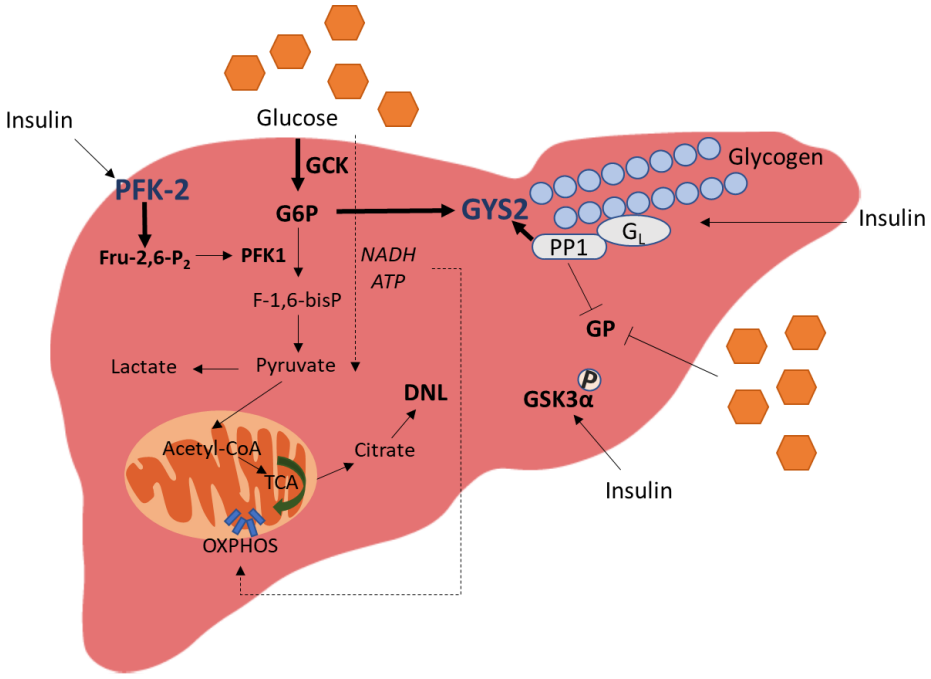

b. Fasting

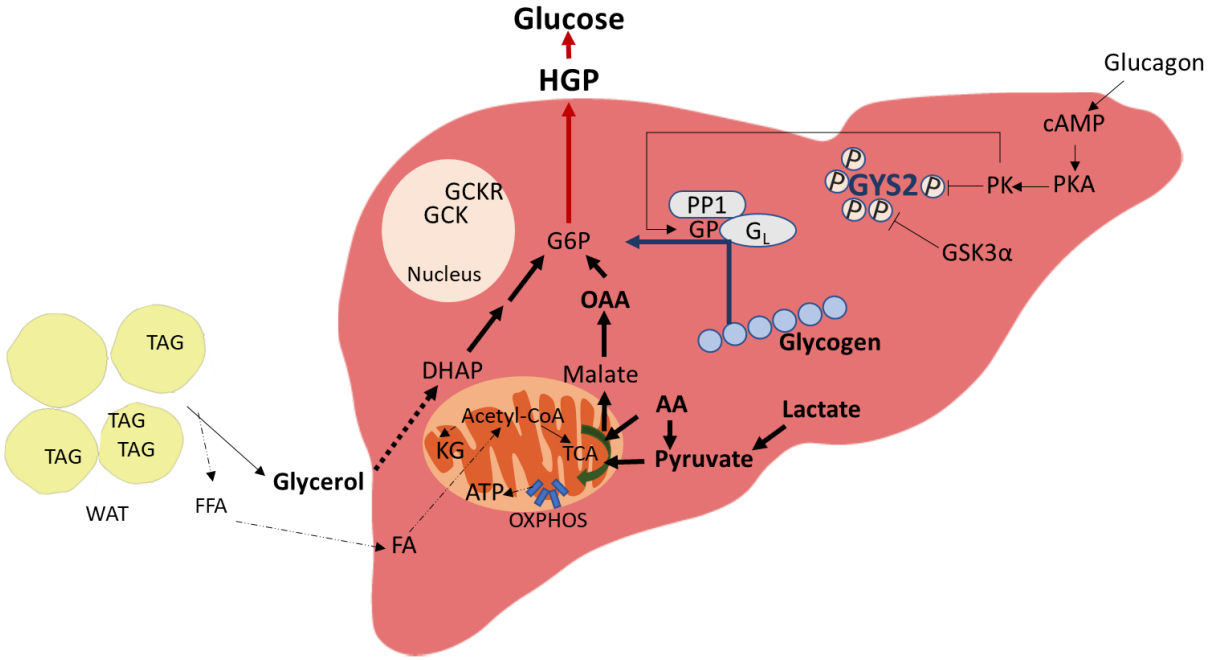

Scheme 2: Hepatic metabolism in fed and fasting states

a. Feeding promotes hepatic glucose uptake and glycolysis (glucose to pyruvate), repletes glycogen stores and induces fatty acid synthesis (DNL), while inhibits fatty acid β-oxidation. Glucose is transformed into glucose-6-phosphate (G6P) by glucokinase (GCK), which allosterically activates glycogen synthase 2 (GYS2), promoting hepatic glycogen accumulation. Glucose also allosterically inhibits glycogen phosphorylase (GP). Moreover, insulin decreases intracellular levels of cAMP and leads to the inhibition of the PKA-dependent processes: 1) activates PP1 with its glycogen-targeting subunit (G_L), dephosphorylating and inactivating GP and 2) it also dephosphorylates and activates GYS2. Additionally, insulin promotes GSK3α phosphorylation and inhibition, also contributing to GYS2 activation.
Moreover, insulin activates PFK-2, increasing fructose 2,6-bisphosphate (Fru-2,6-P_2) levels, the most potent positive allosteric effector of PFK, enhancing glycolysis.
b. Fasting increases hepatic glucose production (HGP) from GNG and glycogenolysis. GNG is led by different gluconeogenic precursors (glycerol from white adipose tissue (WAT) lipolysis, amino acids (AA) and oxaloacetate (OAA)). Glucagon increases intracellular concentration of cAMP and subsequent PKA activation, which induces the nuclear sequestration of GCK, phosphorylates and activates phosphorylase kinase (PK), which finally phosphorylates and inactivates GYS2 and activates GP by phosphorylating at Ser15. Active GP also binds to and inhibits the GL subunit of PP1, which prevents the PP1-dependent binding, dephosphorylation and inactivation of GYS2. The coordinated activation of GP and inhibition of GYS2 result in net glycogenolysis. Additionally, GSK3α phosphorylates and inhibits GYS2, contributing to glycogenesis inhibition. Lastly, during fasting, mitochondrial lipid β-oxidation and ketogenesis (KG) are also activated to generate ATP.

5. The MAP Kinase family

The Mitogen-activated protein kinases (MAPK), which transduce a variety of extracellular signals that regulate cellular responses (Sabio and Davis, 2014), are Ser/Thr kinases that belong to the CMGC group (named after the initials of some members). The CMGC group is composed by cyclin dependent kinases (CDK), MAPK, glycogen synthase kinase (GSK) and CDK-like kinases (CDLK) and it is an essential and large group of kinases found in all eukaryotes (Braconi Quintaje and Orchard, 2008).

There are three groups of MAP kinases: the extracellular signal-regulated kinases (ERK)-1/2, the (Barger et al., 2001) (α, β, γ and δ) MAP kinases (*MAPK14, 11, 12 and 13* genes respectively), and the c-Jun N-terminal kinases (JNK)-1/2/3 (*MAPK8, 9 and 10* genes respectively). While ERKs are mainly activated by mitogens and differentiation signals, JNK and p38 MAPK are activated by stress stimuli and are collectively named stress-activated kinases (SAPK) (Sabio and Davis, 2014). The MAPK are activated upon dual phosphorylation of tyrosine and threonine residues in a conserved Thr-X-Tyr loop sequence, where X is glutamate in the case of ERK, proline for JNKs and glycine for p38s. Phosphorylation of MAPK is catalyzed by the mitogen-activated protein kinase kinase (MAPKK, MKK, MAP2K or MEK), which are in turn activated upon phosphorylation of Serine/Threonine residues (Cuenda and Rousseau, 2007). Although there are exceptions, it is described that the activation of ERK1/2 is mediated by MEK1/2, p38s by MKK3/6, JNKs by MKK4/7 and ERK5 by MEK5. However, most of these studies were performed in immortalized fibroblasts and how specific MAPK isoforms are activated in response

to different stimuli in other cells types is largely unknown (Manieri and Sabio, 2015). Moreover, each MAPKK can be activated by more than one mitogen-activated protein kinase kinase kinase (MAPKKK, MAP3K or MEKK), in a stimulus-dependent manner. The MAPKKK is typically activated by interactions with a small GTPase and/or phosphorylation by protein kinases downstream from cell surface receptors (Cuevas et al., 2007). Once activated, MAPK mediate a wide range of functions through phosphorylation of several substrates, controlling vital signal transduction pathways that regulate processes such as cell proliferation, cell differentiation, and cell death. MAPK phosphatases (MKP) reverse the phosphorylation and return the MAPK to their inactive state. MKP-1 was the first discovered (Franklin and Kraft, 1997). Others involved phosphatases are PP2C (Ser/Thr phosphatase), PTP (Tyr phosphatase) (Takekawa et al., 2000, Takekawa et al., 1998), MKP-7 (Keyse, 2000, Tanoue and Nishida, 2003) and MKP-3 (Lawan and Bennett, 2017). MKPs have been demonstrated to play a variety of roles in metabolic homeostasis. Particularly MKP-1 have a critical role in the regulation of liver metabolism (Wu et al., 2006, Roth et al., 2009, Flach et al., 2011, Lawan et al., 2015).

Moreover, specific scaffold proteins that contribute to MAPK signaling have been identified. These proteins provide spatial temporal regulation of cascade activation, and/or localizing the components to specific cellular sites or substrates (Good et al., 2011). Some of these scaffold proteins are KSR and MP1 for the ERK module; JIP1, JIP2, JIP3, JIP4, and POSH for the JNK module; and JIP2, JIP4, and OSM for the p38 module (Dhanasekaran et al., 2007).

5.1. p38 MAPK

The p38 MAPKs were cloned for the first time in 1994 (Han et al., 1995). Particularly the p38α was the first isoform identified, as the mammalian MAPK orthologue of HOG1 from *Saccharomyces Cerevisae*. In parallel other two groups found this protein as the kinase activated by stress (called Reactivating Kinase, RK) and by IL-1 (called p-40) (Cuenda and Rousseau, 2007). Later, 3 additional isoforms were defined: p38β in 1994 (Cuenda and Rousseau, 2007), p38γ in 1996 (Li et al., 1996) and p38δ in 1997 (Jiang et al., 1997).

Each p38 protein is encoded by a different gene, located tandemly in two chromosomes. In the chromosome 15 in mice and 22 in humans are located p38β (*MAPK11)* and p38γ (*MAPK12*). By contrary p38δ (*MAPK13*) and p38α (*MAPK14*) are in the chromosome 17 in mice and 6 in humans.

The p38 MAPK have different tissue expression patterns (Sabio and Davis, 2014). The p38α is widely expressed, although it is less abundant in brain, where p38β MAPK is the major isoform (Beardmore et al., 2005). The p38δ MAPK isoform is highly expressed in a limited number of tissues, including neutrophils, small intestinal,

pancreas, testis and kidney (Cuadrado and Nebreda, 2010, Ittner et al., 2012, Sumara et al., 2009), while p38γ is expressed in all tissues, with high levels found in muscle (Lawan and Bennett, 2017).

The p38 MAPK can be classified depending on their substrate selectivity, their susceptibility to inhibition by certain compounds, or their sequence homology. Regarding to the substrate specify, they have some overlapping substrates and functional redundancy. For example, common substrates of p38 MAPK are MBP, PHAS-1, and transcription factors such as ATF2, SAP1, Elk-1, and p53 (O'Callaghan et al., 2014). But the functions of p38γ and δ have not been studied extensively *in vivo*, and very little is known about their substrates and functions. However, for example MAPKAPKS (MK2) *in vitro* are better phosphorylated by p38α and β than p38γ and δ (Sabio et al., 2004). Which is clear is that the significance of the stimulus type in determining p38 MAPK isoform activation is going to be crucial. Regarding the classification depending on their susceptibility to inhibition, *in vitro* and *in vivo* assays demonstrated that only p38α and β are inhibited by pyridinyl imidazoles (SB202190 and SB203580) (Wilson et al., 1997, Young et al., 1997, Eyers et al., 1998, Gum et al., 1998). However, p38γ and δ can be inhibited at higher concentrations by BIRB796 (pan-p38 MAPK inhibitor) (Pargellis et al., 2002, Kuma et al., 2005). p38γ can also be inhibited by pirfenidone (5-methyl-1-phenyl-2-(1H)-pyridone), protecting against idiopathic pulmonary disease (Oku et al., 2008, Huang et al., 2015, Lancaster et al., 2016). Moreover, recently our group has seen p38γ inhibition by pirfenidone, but also by RO3066 (a specific cyclin dependent kinase (CDK) inhibitor) protects against chemically-induced liver tumour formation (Tomas-Loba et al., 2019). The differential sensitivity to these drugs can be attributed to amino acid sequence variability at the ATP binding pocket where these compounds bind competitively, facilitated by interactions with nearby AA (O'Callaghan et al., 2014). Regarding to the last classification way, whereas p38α and β are 75% identical, p38γ and δ share 70% of homology. Moreover, p38γ and δ are 62% and 61% respectively identical to p38α.

It is known that MAPK play a central role in processes that regulate metabolism (Manieri and Sabio, 2015, Gehart et al., 2010); however, only p38α/β and JNK1/2 have been related with hepatic metabolism. Moreover, while the JNK pathway has been extensively studied, the role of p38 MAPK has received less attention (Lawan and Bennett, 2017, Sabio and Davis, 2010, Manieri and Sabio, 2015) and the specific role of the different p38 isoforms, particularly γ and δ in liver metabolism has not been explored. Therefore, the use of conditional knockout and transgenic mouse models is required to study the different function of each p38 isoform in liver homeostasis. Despite this, some studies have point out a role for p38α and β in GNG and glucose homeostasis. It seems p38α/β: 1) promote liver GNG through CREB phosphorylation and *PGC1α* expression (Cao et al., 2005); 2) control glucose homeostasis through CCAAT-enhancer-binding protein alpha (C/EBPα) and increase *PEPCK* gene expression (Qiao et al., 2006) and 3) improve glycaemia during obesity through X-box binding protein 1 (Xbp1s)

phosphorylation, translocation and ER stress reduction (Lee et al., 2011). In the same way, the hepatic specific deletion of p38α reduced fasting glucose and impaired GNG, showing p38α can control GNG in an AMPK-specific manner (Jing et al., 2015). Additionally, glucocorticoid receptor is also a target of different MAPK. In this context, phosphorylation by p38 seems to enhance its transcriptional activity (Miller et al., 2005); whereas phosphorylation by JNK and ERK1/2 inhibits its function (Itoh et al., 2002). Moreover, PPARα is also directly phosphorylated by p38, which enhances its activity (Barger et al., 2001) and p38 is also required for glucagon- and fasting- mediated suppression of hepatic lipogenesis, possibly through the inhibition of SREBP1c transcription (Xiong et al., 2007). Finally, it seems MKP-1, which is overexpressed in HFD fed mice, promoting hepatic steatosis (Lawan et al., 2015), it could be related with the p38α/β downregulation in HFD (Lee et al., 2011); negatively regulating hepatic triglyceride metabolism (Flach et al., 2011, Wu et al., 2006).

5.1.1 p38δ MAPK

p38δ MAPK was identified in 1997 (Jiang et al., 1997). p38δ MAPK activation is largely transient, with downregulation occurring within minutes of stimulation (Coulthard et al., 2009), due to the regulatory action of protein phosphatases (Zhou et al., 2008, Tanoue et al., 2001, Kraft et al., 2007). The role of p38δ MAPK in the different physiological processes is still poorly known; however, it has been described this kinase is involved in:

- Inflammation; particularly, combined p38γ and δ have recently been shown to play important roles in regulating cytokine production by macrophages and dendritic cells (Risco et al., 2012, Gantke et al., 2011, Gonzalez-Teran et al., 2013), T cell activation and neutrophil migration (Ittner et al., 2012, Gonzalez-Teran et al., 2016b) (Sumara et al., 2009) and T cell development (Risco et al., 2018). Therefore, being related in modulating tumorigenesis associated with inflammation (Zur et al., 2015), antifungal immunity (Alsina-Beauchamp et al., 2018), arthritis (Criado et al., 2014) (Gaestel et al., 2009, Arthur and Ley, 2013), acute lung injury (Ittner et al., 2012), chronic obstructive pulmonary disease (Alevy et al., 2012) and atherosclerotic inflammation (Rajamaki et al., 2016). Moreover, p38δ has also been involved in the regulation of IL-6 biosynthesis, upon ceramide signaling, which may have important role in sphingolipid metabolism, signal transduction, Gaucher disease, inflammation, and cancer (Kitatani et al., 2009).

-Keratinocyte fate, particularly it seems there is a specific balance between the prosurvival ERK1/2 and the proapoptotic p38δ MAPK signals, which is essential for determined keratinocyte fate (Efimova et al., 2003). Specifically, p38δ MAPK contributes to keratinocytes apoptosis in a PKDδ dependent manner in response to okadaic acid (OA) and hydrogen peroxide (Efimova et al., 2004, Kraft et al., 2007). However, p38δ MAPK also increases the expression of involucrin, a marker of keratinocyte terminal differentiation, which is a critical

process for the correct epidermal homeostasis (Balasubramanian et al., 2002, Dashti et al., 2001); and p38δ MAPK can also regulate the expression of ZO-1, an epidermal tight junction membrane protein, which is also associated with keratinocyte differentiation (Siljamaki et al., 2014). To understand the role of p38δ MAPK in keratinocytes regulation is important because *MAPK13* gene expression has been found upregulated in psoriasis (Haider et al., 2006).

-Cancer, where p38δ MAPK can function as pro- or anti-oncogenic factor depending on the cell type. p38δ MAPK expression and activation are significantly increased in a variety of carcinoma cell lines such as human primary cutaneous squamous carcinoma cells (Haider et al., 2006, Schindler et al., 2009), head and neck squamous carcinoma cells and tumors (Junttila et al., 2007), cholangiocarcinoma, liver cancer (Tan et al., 2010), colon cancer (Del Reino et al., 2014) and breast cancer and lung metastasis (Wada et al., 2017). Moreover, it has been described that p38δ MAPK controls mTOR activity through a double mechanism; phosphorylating p62 which activates mTORC1 and consequently promotes autophagy and tumor growth (Linares et al., 2015).
By the other hand, p38δ MAPK works as tumor suppressor in mouse embryonic fibroblast (Cerezo-Guisado et al., 2011) and in esophageal squamous cell carcinoma (OESCC), where reintroduction of p38δ MAPK significantly impaired cell proliferation, migration, and invasion (O'Callaghan et al., 2013). Interestingly, hypermethylation of the *MAPK13* gene promoter region that downregulates its expression, has recently been characterized in both malignant pleural mesothelioma (Goto et al., 2009) and primary cutaneous melanoma (Gao et al., 2013).

-Other functions: 1) Hematopoiesis, particularly p38δ is involved in the erythrocyte membrane remodeling and enucleation (Hale et al., 1999). 2) Combined p38γ and p38δ activates mTOR pathway through DEPTOR phosphorylation and subsequent degradation, controlling heart growth (Gonzalez-Teran et al., 2016a). 3) p38δ MAPK can decrease the activity of the transcription factor TonEBP/ OREBP upon high NaCl, which is activated in the renal inner medulla producing cell cycle delay, oxidative stress, DNA damage and apoptosis (Zhou et al., 2008). 4) p38δ MAPK participates in TGFβ-1 signaling pathway, a potent inducer of ECM synthesis that leads to renal fibrosis (Wang et al., 2002). 5) p38δ-mediated SQSTM1 phosphorylation that is a critical signal for the aggresome formation, which serves to organize misfolded proteins into a single location, in cells under proteasomal stress (Zhang et al., 2018). 6) p38δ controls microtubule assembly through Tau phosphorylation (Goedert et al., 1997, Buee-Scherrer and Goedert, 2002); but also Tau dissociation from the cytoskeleton upon hyperphosphorylation, which contribute to the development of neurofibrillary tangles, structures typically presented in Alzheimer's disease (Goedert, 2001, Bramblett et al., 1993, Lee et al., 2001). 7) Lastly, p38δ is involved in cytoskeleton regulation through stathmin phosphorylation (Lee et al., 2001), enhancing cell survival under stress conditions.

- Role of p38δ MAPK in metabolism: 1) p38δ decreases pancreatic insulin secretion, through

phosphorylation and inhibition of the protein kinase D1 (PKD1); moreover, mice lacking p38δ have a fivefold lower rate of pancreatic β cell death in response to oxidative stress and are protected against HFD induced insulin resistance (Sumara et al., 2009). 2) p38δ MAPK expression is elevated in livers of obese patients with NAFLD and in livers of mice fed with a methionine choline deficient (MCD) diet (Gonzalez-Teran et al., 2016b) and p38δ expression correlates with liver fibrosis in human (data do not published). 3) Mice lacking p38γ/δ in myeloid cells, which show defective migration, are resistant to diet-induced fatty liver and glucose intolerance (Gonzalez-Teran et al., 2016b). 4) p38δ MAPK is involved in brown adipose tissue thermogenesis because it is activated by cold exposure and specific p38δ lack in adipose tissue promoted overweight together with reduced EE (Matesanz et al., 2018).

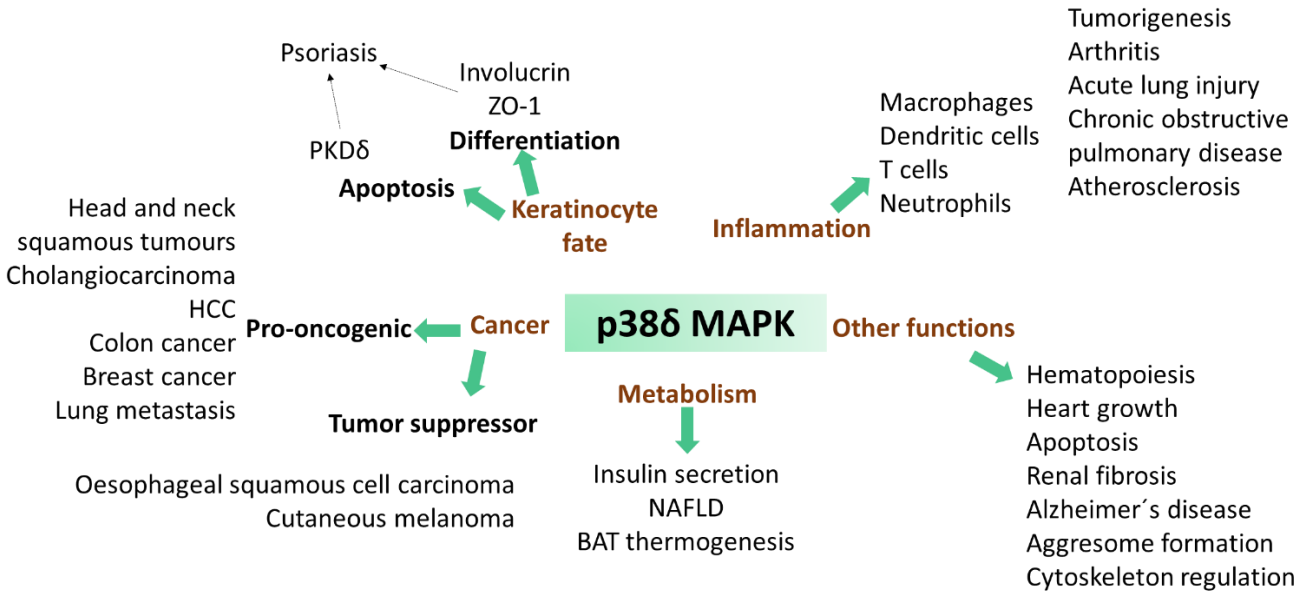

Scheme 3: p38δ MAPK functions

p38δ MAPK controls inflammation; keratinocyte fate, which might have an impact in psoriasis, since its expression is increased in this disease; besides, p38δ MAPK is involved in cancer, acting as pro- or anti-oncogenic factor. Additionally, p38δ MAPK has been related with other functions such as hematopoiesis or Alzheimer´s disease. However, its role in metabolism has not been almost explored. Regarding this, it is only known that p38δ MAPK is involved in pancreatic insulin secretion and β cell death, in brown adipose tissue (BAT) thermogenesis and in NAFLD, since its expression is increased in the liver of obese patients with NAFLD and the lack of p38γ and δ in myeloid cells protected against diet-induced fatty liver.

Therefore, p38δ MAPK is involved in several functions, mainly in inflammation; although, some of these roles have not been precisely defined so far. Particularly its function in metabolism and specifically in liver metabolism has not been almost explored. Thus, this thesis project has been focused in: 1) To progress in the understanding of the p38 MAPK regulation and functions *in vivo*; and particularly in the role of the p38δ MAPK isoform in the

hepatic metabolism. 2) To better understand hepatic metabolism, a complex network, but crucial for whole body homeostasis. 3) To find novel target to treat metabolic diseases; particularly, T2D and NAFLD, two of the most extended diseases nowadays, without effective treatments and with high economic and mortality impact.

Objectives

1. To explore the role of the hepatic p38δ MAPK in liver metabolism

1.1 To evaluate the effect of the hepatic specific p38δ MAPK deletion in whole body homeostasis.

1.2 To identify mechanisms by which p38δ MAPK is involved in the blood glucose levels regulation.

1.3 To unveil the molecular mechanism through which p38δ MAPK controls glycogen metabolism.

1.4 To determine the effect of the hepatic specific p38δ MAPK deletion in hepatic lipid metabolism.

2. To explore the role of p38δ MAPK in obesity-related T2D and NAFLD

2.1 To study the effect of the hepatic specific p38δ MAPK deletion in HFD-fed mice, in the protection against hyperglycemia and insulin resistance.

2.2 To determine whether the hepatic specific p38δ MAPK deletion in HFD-fed mice protects against NAFLD.

2.3 To unveil the molecular mechanism through which the lack of p38δ MAPK protects against obesity-related T2D and NAFLD.

2.4 To explore the role of p38δ MAPK in the glycolysis regulation.

2.5 To explore whether the hepatic specific deletion of p38δ MAPK improves hyperglycemia and NAFLD in obese mice.

Objetivos

1. Estudiar el papel de la estrés quinasa hepática p38δ MAPK en el metabolismo del hígado

1.1 Evaluar el efecto de la deleción específica de p38δ MAPK en hepatocitos sobre la homeostasis global del organismo.

1.2 Identificar los mecanismos por los que p38δ MAPK regula los niveles de glucosa en sangre.

1.3 Identificar el mecanismo molecular por el que p38δ MAPK controla el metabolismo hepático del glucógeno.

1.4 Determinar el efecto de la deleción específica de p38δ MAPK en hepatocitos sobre el metabolismo hepático lipídico.

2. Explorar el papel de la estrés quinasa hepática p38δ MAPK en la diabetes tipo 2 y en la enfermedad del hígado graso no alcohólico asociadas a la obesidad

2.1 Estudiar el efecto de la deleción específica de p38δ MAPK en hepatocitos de ratones alimentados con dieta alta en grasa y colesterol sobre la protección frente a hiperglucemia y resistencia a insulina.

2.2 Determinar si la deleción específica de p38δ MAPK en hepatocitos de ratones alimentados con dieta alta en grasa y colesterol protege frente al desarrollo de hígado graso no alcohólico.

2.3 Identificar los mecanismos moleculares por los que la falta de p38δ MAPK en hepatocitos protege frente a diabetes tipo 2 e EHGNA asociados a la obesidad.

2.4 Explorar el papel de p38δ MAPK en la regulación de la glucólisis.

2.5 Explorar si la deleción específica de p38δ MAPK en hepatocitos de ratones obesos protege frente a hiperglucemia e hígado graso no alcohólico.

Materials and methods

Animals

8- and/or 22-week-old male mice were housed in a pathogen-free animal facility under a 12 h light/dark cycle at constant temperature and humidity, and water *ad libitum*. For all studies, mice p38δLoxP (B6.129-Mapk13tm1/J) (Gonzalez-Teran et al., 2016b) or p38δLoxP/Fgf21LoxP (B6.129-Mapk13tm1/Fgf21tm1.2Djm/J) were crossed with AlbCRE (B6.Cg-Tg(Alb-cre)21Mgn/J) (Postic and Magnuson, 2000). All these animals were maintained on a C57BL/6J background (Jackson Laboratory) (back-crossed 10 generations). The mice employed in this study were Alb^{cre} (CRE^{+}), $Alb^{p38\delta KO}$ (CRE^{+} $p38\delta^{LoxP/LoxP}$) and $Alb^{p38\delta/FGF21KO}$ (CRE^{+} $p38\delta^{LoxP/LoxP}$ /$FGF21^{LoxP/LoxP}$).

Mice were fed with a standard control chow diet (CD) (D183/17160, Safe) or a high fat diet: 60% kcal fat with 1,5% of cholesterol (HFD) (Research Diets Inc.) for 8-12 weeks ad libidum.

Mice were sacrificed after overnight fasting (16 h), upon 2 h feeding or 15 min intraperitoneal insulin injection (0.75 IU/kg); and also, after 4 h morning food deprivation. Tissues were weighted and snap-frozen in liquid nitrogen or process for histological analyses.

All animal procedures conformed to EU Directive 86/609/EEC and Recommendation 2007/526/EC regarding the protection of animals used for experimental and other scientific purposes, enacted under Spanish law 1201/2005. The procedures have been reviewed by the Institutional Animal Care and Use Committee (IACUC) of Centro Nacional de Investigaciones Cardiovasculares, and approved by Consejeria de Medio Ambiente, Administración Local y Ordenación del Territorio of Comunidad de Madrid.

Genotype was confirmed by PCR analysis of genomic DNA from tail. For liver and pancreas, 0.5 cm tissue were cut and overnight incubated at 55 °C with 20 mg/ml proteinase K (Sigma) and T:N:E:S buffer (50mM Tris pH=7.4, 100mM EDTA pH=8.0, 400mM NaCl and 0,5% SDS). Then we proceeded as follow: 150 µl NaCl saturated 6M, shake vigorously and stand for 5 min, 5 min at 14,000 rpm, 500 µl 100% ethanol, 5 min at 14,000 rpm, remove ethanol and add 100 µl 100% ethanol, 5 min at 14,000 rpm, remove ethanol, evaporate and add sterile water. Then, 0.5 µl was used for PCR to check CRE-excised (555 bp) and wild type *MAPK13* (799 bp). Primers used:

BI5-12L: 5´-GCT CAG CTT CTT GAT GGC CAC-3´

Delta-2: 5´-ACG TAC CTG GGC GAG GCG GCA-3´

Magnetic resonance imaging

Whole-body composition for HFD-fed mice was analyzed by magnetic resonance imaging (Whole body composition analyzer; EchoMRI, Houston, TX, USA) in collaboration with Dr. Nogueiras' Lab at Santiago de Compostela University. Whole-body composition for CD-fed mice Bruker Mini-Spec Analyzer (Bruker, TX) was used in collaboration with Yale Mouse Metabolic Phenotyping Center (MMPC) at Yale University.

Indirect calorimetry system

Mice were housed under controlled temperature and lighting with free access to food and water. Food intake, EE, respiratory quotient (RQ) and physical activity were monitored for 3 days in metabolic cages (TSE LabMaster, TSE Systems, Bad Homburg, Germany) for HFD studies and Oxymax system from Columbus Instruments (Columbus, OH) for CD studies as previously described (Nogueiras et al., 2009, Czyzyk et al., 2012) respectively. Mice were acclimated for 48 h to the test chambers and then were monitored for an additional 72 h. Data collected from the last 72 h was used to calculate all parameters for which results are reported. Studies were done in collaboration with Dr. Nogueiras' Laboratory at Santiago de Compostela University and with Yale Mouse Metabolic Phenotyping Center (MMPC) at Yale University, respectively.

Glucose Tolerance Test

Awake mice were fasted overnight (16 h) and administered with an intraperitoneal injection of glucose (D-(+)-glucose monohydrate) (1 g/kg body weight). Glycemia was measured in tail vein blood samples at the indicated time points. Glycemia was determined using glucometers.

For the oral tolerance test, HFD-fed mice were 4 hours morning food deprived and administered glucose (3g/ kg) by gavage. Blood samples were taken for posterior insulin levels measurement. Insulin was quantified in serum by a multiplexed ELISA with a Luminex 200 analyzer (Bio-Rad) following manufacture instructions.

Insulin Tolerance Test

Insulin (Humulin Regular, Lilly) was injected intraperitoneally at a dose of 0.75 IU/kg body weight to fed mice, after a short food deprivation (1h). Glycemia was measured in tail vein blood samples at the indicated time points. Glycemia was determined using a glucometers.

Insulin Release

Chow-fed mice were injected with 2 g/kg of glucose and blood collected by submaxillary puncture at 0, 10, and 30 min after injection. Insulin was quantified in serum by a multiplexed ELISA with a Luminex 200 analyzer (Bio-Rad) following manufacture instructions.

Hyperinsulinemic-euglycemic clamp

After surgical implantation of an indwelling catheter in the right jugular vein, the mice were allowed to recover for 1 week prior to clamp experiments. Basal infusion and hyperinsulinemic-euglycemic clamp studies were used to assess whole-body and hepatic insulin sensitivity in HFD-fed 4h fasted mice, starting fasting in the morning (8 am). To *assess* insulin's acute ability to suppress GNG, mice were infused with basal bolus injection (5 µl 3-(^{3}H)-glucose (1µCi/min)) (Perkin Elmer) via the jugular vein, continued by a continues basal solution infusion (1 µl/min of 30 µl 3-(^{3}H)-glucose (1mCi/ml)) for 60 min. Blood samples were taken at 30 and 60, 65 and 70 min to assess basal glucose turnover. At 60 min, a 120-min insulin (Novorapid) infusion was initiated, previously by

an insulin bolus injection (2.5 µl of insulin 1U) via the jugular vein, continued by a continuous clamp solution infusion (1 µl/min of (body weight*2) µl of insulin 1U/ml + 30 µl 3-(^{3}H)-glucose (1µCi/min))(clamp at 0.2U/kg/h). Blood glucose was measured every 10 min to see drop in blood glucose and then, plasma glucose concentrations were measured every 10-15 min with a variable infusion of 20% glucose (Lavoisier) to maintain euglycemia, adjusting glucose infusion rate. When mice were clamped (approximately 40-60 min later), 3 blood samples from the vein tail were taken every 10 min.

Then, a 2-µCi bolus injection of 2-deoxy-*d*-(1-^{14}C)-glucose (Perkin Elmer) was intraperitoneally injected at 90 min to determine tissue-specific glucose uptake, which was calculated from the area under the curve of 2-deoxy-*d*-[1-^{14}C]-glucose detected in plasma and the tissue content of 2-deoxy-*d*-(1-^{14}C)-glucose, as previously described (Youn and Buchanan, 1993, Jurczak et al., 2012).

Mice were euthanized with cervical dislocation. Tissues were snap-frozen in liquid nitrogen within 10 and 30 seconds of euthanasia, respectively, and stored at −80°C for further analysis.

Glucose turnover was calculated as the ratio of the 3-(^{3}H)-glucose infusion rate (GIR) to the specific activity of plasma glucose at the end of the basal infusion and during the last 30 min of the hyperinsulinemic-euglycemic clamp study. HGP represents the difference between the GIR and the rate of glucose appearance.

It was done in collaboration with Dr. Luquet's Laboratory, at Paris Diderot University.

Positional isotopomer nuclear magnetic resonance (NMR) tracer analyses (PINTA) *(Perry et al., 2017)*

CD-fed overnight fasting mice were infused with (3-^{13}C)-lactate (Sigma, St. Louis, MO; 120 µmol/(kg-min) prime for 5 min, 40 µmol/(kg-min) continuous infusion) and (3-^{3}H)-glucose (PerkinElmer, Waltham, MA) 0.1mg/(kg-min) prime for 5 min and 0.3mg/(kg-min) for 120 min, after which blood was obtained from the vein tail, immediately centrifugated and plasma obtained. Then, mice were sacrificed and their livers snap-frozen *in situ* using metal tongs pre-chilled in liquid nitrogen. Livers were storage at -80°C until their processing.

Then, ∼600 mg livers were lysed in 2 ml 7% perchloric acid, sit on ice 5 min and centrifuged at 4,000 rpm for 20 min 4°C. Supernatants were adjusted at pH=6.8-7.2 and centrifuged at 4,000rpm for 20 min 4°C. Again, supernatants were frozen in liquid nitrogen and put in the lyophilizer overnight. Then, residual was dissolved in 500 µl milliQ water, vortex 5 seconds and spin at 4,000 rpm for 10 min 4°C. 250 µl ethanol was added to supernatants, vortex 5 seconds and spin at 4,000 rpm for 10 min 4°C. Supernatants were transferred and ethanol was removed with gentle nitrogen flow and speedvac. Samples were kept at 4°C until NMR measure, then resuspend in 450 µl of heavy water (D_2O) phosphate buffer solution, vortex, and centrifuged to 4,000 rpm 10 min to 4°C.

The flux calculations were done using (^{13}C)-glucose positional enrichment in glucose and liver, determined by NMR and gas chromatography/mass spectrometry (GC/MS) as described below. Pyruvate carboxylase flux (V_{PC})

is the rate of pyruvate carboxylase flux as determined from the anaplerotic flow into OAA. Citrate synthase flux (V_{CS}) is defined as the flux of the CS reaction in the citric acid cycle. The calculated anaplerotic flux can also include malic enzyme flux but under the conditions studied malic enzyme flux is negligible compared to anaplerotic flux (Petersen et al., 2016a, Perry et al., 2016). To measure the contribution of glycerol and glycogen to GNG we subtracted the rates of V_{PC} from the total EGP, assuming that the three sources of glucose production are glycogenolysis and GNG from V_{PC} and glycerol. We used GC/MS to measure $m+1$ and $m+2$ (^{13}C) glucose enrichment. The total $m+1$ and $m+2$ (^{13}C)-glucose enrichment was measured using a pentaacetate derivative: plasma and liver samples were deproteinized using five volumes of methanol, dried and derivatized with 75 µl of 1:1 acetic anhydride:pyridine. After heating to 65 °C for 20 min, the reaction was finished by adding 25 µl methanol, and $m+1$ and $m+2$ (as well as $m+3$…$m+6$) were determined by GC/MS (CI mode, *m/z* 331 [*m*], 332 [$m+1$], 333 [$m+2$],…337 [$m+6$]). The $m+1$ and m + 2 (^{13}C) enrichments of the glucose C4C5C6 fragment were determined by generating the aldonitrile pentapropionate derivative: plasma and NMR liver extract samples were dried under N_2 gas, and 50 µl hydroxylamine hydrochloride (20 mg/ml in pyridine) were added. The samples were heated at 90 °C for 60 min, then 100 µl propionic anhydride was added, after which the samples were heated at 60 °C for 30 min. Finally the samples were evaporated under N_2 gas, resuspended in ethyl acetate, and the $m+1$ and $m+2$ enrichment of the glucose C4C5C6 fragment was measured by GC/MS (Antoniewicz et al., 2011). It was done in collaboration with Dr. Shulman's Laboratory, at Yale University.

Histology

Tissue samples were fixed in 10% formalin, dehydrated and embedded in paraffin. Sections (5 µm) were cut and stained with hematoxylin and eosin (American Master Tech Scientific) for histopathological examination. Liver glycogen was stained with Periodic Acid Schiff (PAS) (Sigma). Four images (x20) were taken from each liver.

Lipid accumulation was assessed with Oil-Red staining (American Master Tech Scientific). Sections (8 µm) were prepared from tissue frozen in OCT compound (Tissue-Tek).

Luminex

Insulin concentration was measured by multiplexed ELISA with a Luminex 200 analyzer (Millipore) following manufacture instructions.

ELISA Fgf21

Serum FGF21 was determined using the Mouse/Rat FGF-21 ELISA kit (MF2100, R&D Systems). 10 µl plasma was used for each sample.

RNA-Sequencing

Total RNA was isolated from liver using the RNeasy Mini kit (Quiagen) with on-column DNase I-digestion. Samples were pooled two by two to obtain 1 µg of total RNA (500 ng from each pooled-sample) and RNA quality was verified using agarose gel and NanoDrop spectrophotometer (checking OD 260/280 was 1.9-2.0).

Total RNA was processed with TruSeq RNA sequencing with Illumina Genome Analyzer IIx Sequencing System. Total RNA processing with TruSeq RNA Sample Preparation and sequencing were performed by Genomic Unit at CNIC. Data obtained from RNA sequencing were analyzed using Ingenuity® Pathway Analysis (IPA).

Measurement of hepatic triglycerides

Hepatic triglyceride content was measured in livers from mice starved overnight. Total lipids were extracted from liver samples (25 mg) in isopropanol (50mg/ml). Lysates were centrifuged at 10,000rpm for 15 min at 4ºC. 10 µl supernatant was used to measure triglycerides with a commercial kit (Sigma).

Hepatic de novo lipogenesis measure

DNL was performed as previously described (Nassir et al., 2013) with slight modifications (Aspichueta et al., 2005). In brief, freshly isolated tissue slices (40 mg) were incubated in high glucose DMEM with insulin (150nM) and [H^3] Acetic acid 20 µCi/ml for 4 hours. Tissue slices were washed five times in cold PBS, homogenated in PBS and lipids were extracted as previously described (Folch et al., 1957). Then, lipids were separated by TLC (Ruiz and Ochoa, 1997) the band corresponding to each lipid was scraped and the radioactivity was measured in a scintillation counter. It was done in collaboration with Dra. Aspichueta's Laboratory, at Pais Vasco University.

Hepatic fatty acid β-oxidation measure

The rate of fatty acid oxidation was determined by measuring the amount of $^{14}CO_2$ (complete oxidation) and the amount of ^{14}C labelled acid-soluble metabolites (ASM) (incomplete oxidation) released. β-oxidation was assessed as described before (Gao et al., 2015, Hirschey et al., 2010). Fresh liver pieces were homogenated in a Potter homogenizer (5 strokes) in cold buffer (25 mM Tris-HCl, 500 nM sucrose, 1 mM EDTA-Na_2 pH 7,4) and sonicated for 10 s. Then, the homogenates were centrifuged at 500 xg for 10 min at 4 °C. Approximately 500 µg of protein from the homogenates supernatant was used for the assay in a volume of 200 µl. The reaction started by adding

400 µl of assay mixture containing 0.5 µCi/ml [1-^{14}C] palmitic acid to the samples and was incubated for 1 h at 37 °C in eppendorf tubes with a Whatman paper circle in the cap. The reaction was stopped by adding 300 µl of 3 M perchloric acid and 1 M NaOH was added to impregnate the whatman cap.

After 2 h the Whatman caps were retired and the radioactivity associated was measured in a scillation counter. The eppendorf tubes were centrifugated at 21,000 g 10 min at 4 °C. 400 µl from the supernatant were collected and the radioactivity was counted in a scintillation counter. The supernatant contained the acid soluble

metabolites (ASM) and the Whatman caps captured the released CO_2. It was done in collaboration with Dra. Aspichueta's Laboratory, at Pais Vasco University.

Hepatic long-chain acyl CoA content

LCCoA and very LCCoA were extracted from frozen tissue samples (~100 mg) and purified using a solid phase extraction method described previously by Deutsch et al. (Deutsch et al., 1994) with minor modifications for desalting. A known amount of heptadecanoyl-CoA was added as an internal standard. OPC columns (Applied Biosystems) were used for solid phase extraction. Samples were dissolved in 100 µl of methanol/H2O for LC-MS/MS analysis (Applied Biosystems 6500 QTRAP). The quantitative analysis of the LCCoA and very LCCoA metabolites: $C_{12:3}$, $C_{12:2}$ $C_{12:1}$, C_{12}, $C_{14:3}$, $C_{14:2}$, $C_{14:1}$, C_{14}, $C_{16:3}$, $C_{16:2}$, $C_{16:1}$, C_{16}, $C_{18:3}$, $C_{18:2}$, $C_{18:1}$, $C_{20:5}$, $C_{20:4}$, $C_{22:6}$ were selectively monitored with the next ion pairs 470.9/862.26, 471.9/864.28, 472.9/866.29, 473.9/868.5, 484.9/890.29, 485.9/892.31, 486.9/894.32, 487.9/896.30,498.9/918.32, 499.9/920.34, 500.9/922.36, 501.9/924.37, 513/946.36, 514.1/948.37, 515.7/950.39, 516/952.40, 525.1/970.36, 526.1/972.37 and 538.1/996.37 , respectively. It was done in collaboration with Dr. Shulman's Laboratory, at Yale University.

Measurement of hepatic acetyl-CoA concentrations

To measure hepatic acetyl-CoA concentrations, ~100 mg liver tissue was homogenized in 1 mL ice cold 10% trichloroacetic acid. An internal standard (5 nmol) (1,2-$^{13}C_2$)-acetyl-CoA was added before homogenization. The samples were mixed on a rotating shaker for 30 min at 4°C and centrifuged at 4,000 g for 5 min at 4°C. The supernatant was then loaded on a C18 cartridge, which had been preconditioned by 3 mL HPLC-grade methanol, then 4 mL 1 mM HCl were added. After the supernatant flowed through the cartridge, it was washed with 3 mL 1 mM HCl and 1 mL distilled water. The flow-through was then discarded. Finally, acetyl-CoA was eluted from the cartridge with 2 mL ethanol-water (65-35%, v/v) containing 0.1 M ammonium acetate followed by 2 mL 50% HPLC-grade methanol-water. The samples were dried in a Speed Vac for the minimum time necessary (~6 h), resuspended in 100 µL distilled water, and transferred to LC-MS/MS vials.

LC-MS/MS method development and analysis were performed on an Applied Biosystems 6500 QTRAP, equipped with a Shimadzu ultrafast liquid chromatography system using an electrospray ionization source with positive-ion detection. The quantitative analysis of the CoA metabolites was simultaneously monitored in MRM mode. Acetyl-CoA and (1,2-$^{13}C_2$)-acetyl-CoA were selectively monitored with the ion pairs of 810.0/303.1 and 812.0/305.1, respectively. The optimized MS parameters were: curtain gas 35; collision gas med, ionization potential 4500 V, probe temperature 5000C; ion source gas 1 50; ion source gas 2 65; declustering potential 120 V; entrance potential 10 V. The collision energy (40-160 V) and collision cell exit potential (8-20 V) were found to be ion-pair-dependent, and they were optimized for each individual metabolite. It was done in collaboration with Dr. Shulman's Laboratory, at Yale University.

Plasma biochemical analysis

Plasma glucose concentrations were measured using the YSI 2700 Select Biochemistry Analyzer, upon immediate blood centrifugation, 30 s at 10,000 rpm.

Plasma β-hydroxybutyrate (3HB) concentrations was measured by COBAS (Roche Diagnostics) from 8 µl plasma.

Plasma amino acid concentrations (alanine, serine, leucine, isoleucine, phenylalanine, glutamate+glutamine) were measured by GC-MS after spiking 8 µl plasma with an internal standard containing 1 mM of each analyte of interest with an (m+1) ^{2}H or ^{13}C isotopic label, the dried under nitrogen gas and derivatized with 75 µl N-Butanol 4 N HCl (Sigma). Next, samples were heated for 60 min at 60°C and dried under nitrogen gas. They were reacted with 100 µl of 1:7 trifluoracetic acid (Thermo Fisher Scientific, Waltham, MA): methylene chloride (Sigma) and run immediately in the GC/MS. AA concentrations were calculated by comparing the ration of (m+1) ^{13}C to natural abundance peak areas in the plasma samples to a standard curve.

Plasma glycerol concentrations were measured by GC-MS. 10 µl plasma samples were spiked with an equal volume of (2-^{13}C)-glycerol (89 µM). Then equal plasma volumes of zinc sulfate and barium hydroxide were added, centrifugate at room temperature 10 min and Speed Vac overnight. Then, 75 µl 1:1 acetic anhydride:pyridine was added and heat at 65°C for 20 min. After cooling, and before running in the GC/MS, 25 µl ethanol were added. Glycerol was measured comparing the ratio of (m0) to (m+1) glycerol in the samples to a standard curve. It was done in collaboration with Dr. Shulman's Laboratory, at Yale University.

Glycogen content

Briefly, ~10 mg of tissue was homogenized in 100 µl of water on ice. Boiled homogenates (95 ^{o}C) for 5 minutes were centrifuged at 13,000 g for 5 minutes at 4 ^{o}C. Glycogen content was estimated from glucose released measured, as glucose units analysed colorimetrically with an appropriate standard curve and with the Glycogen Assay Kit (Sigma). For measurement 30 µl hydrolisis buffer was added to 20 µl lysate.

Glycogen synthase activity

~100mg of tissue was pulverized in liquid nitrogen and then homogenized in 1ml of ice-cold homogenization buffer (50 mM Tris-HCl pH=7.5, 2 mM EGTA, 10 mM EDTA, 1% Triton X-100, 50 mM NaF, 5 mM pyrophosphate and added fresh 0.27M sucrose, 1 mM sodium orthovanadate, 10 µg/ml leupeptin, 10 µg/ml aprotinin, 1 mM PMSF and 0.1% β-mercaptoethanol). GYS2 activity in liver lysates was measured by a modification of the method of Thomas et al. (Thomas et al., 1968) with or without saturating G6P (10 mM) (Sigma G7879). GYS2 activity assay buffer: 8.9 mM UDP-^{14}C –glucose (0.07 µCi) (Perkin Elmer)(for +G6P mix or double for –G6P mix), 6.7 mg/ml glycogen (G-8876, Sigma), 6.7 mM potassium phosphate, 33.3 mM NaF, 0.67 mM EDTA and 0.1 M KCl, pH=6.8. 20 µl samples and 40 µl assay buffer per sample were used. The reaction was allowed for 30 min at 30 ^{o}C in agitation. 50 µl of the reaction mix was put on small piece (2.5 cm x 2.5 cm) of paper 31 ET CHR (Whatman

3031-915) and quickly put into cold (-20ºC) 66% ethanol. Pieces of paper were washed for ten minutes, for 3 times at room temperature. Then pieces of paper were quickly washed with acetone and allowed to dry. Then, they were counted in liquid scintillation counter. The cpm from generated glycogen must be ~10% cpm of reaction mix.

Previous treatment of UDP-^{14}C –glucose and glycogen are required. UDP-^{14}C –glucose was put in a speed back at 45ºC to evaporate ethanol:water (7:3) and solubilized in 2% ethanol at kept at -20ºC. Glycogen also was previously treated to remove inorganic phosphate by chromatography with AG 501-X8 (D) (Biorad 142-6425). 10 g of glycogen was added gradually into 90 ml distillated water at 37ºC and shake until total solution; then, add water to 100 ml. Pass water to get a good flow through the column and then to pass the glycogen solution; discard the first 6 ml and recover the rest. Mix 1 volume of glycogen solution with 2 volume of cold absolute ethanol, adding gradually ethanol into glycogen solution in a glass baker and leave stirring overnight at 4ºC. Centrifuge at 39,086 g 30 min at 4ºC, to collect sediments and add 95 ml 66% ethanol, break pellet with a spatula and leave 2 h stirring at RT, then leave stirring overnight at 4ºC. Centrifuge at 39,086 g, 30 min at 4ºC, collect sediments and leave overnight in order to dry at 37ºC. Finally powder glycogen and keep in the fridge.

Determination of the glycolytic flux

The glycolytic flux was assessed by assessing the rate of conversion of D-[3-^{3}H]glucose into $^{3}H_2O$, as previously described (Herrero-Mendez et al., 2009). In essence, liver slices (80-100 mg) were pre-incubated for 30 min in 2 ml of a Krebs–Henseleit buffer (11 mM Na_2HPO_4, 122 mM NaCl, 3.1 mM KCl, 0.4 mM KH_2PO4, 1.2 mM $MgSO_4$, 1.3 mM $CaCl_2$; pH 7.4) supplemented with 20 mM D-glucose at 37 ºC, followed by incubation in the presence of 10 µCi/ml of D-[3-^{3}H]glucose in fresh Krebs-Henseleit buffer (2 ml) in glass 25-ml Erlenmeyer flasks equipped with a central well containing a tube with 0.5 ml of water. The flask atmosphere was gassed with a $O2/CO2$ (95/5) mixture for 20 s and stopped with a rubber cap, and the flasks were incubated in a thermostatized orbital shaker (Forma Benchtop Orbital Shaker, Model 420, Thermo Fischer) for 4 hours at 37°C (linearity was tested during this time). The incubations were finished by injecting 0.2 ml of 20 % (v/v) $HClO_4$ through the rubber cap, and flasks were further incubated for 72 h to allow the equilibration of $^{3}H_2O$ between the incubation medium and the water of the central well. The rate of glycolysis was expressed as nmol of D-[3-^{3}H] glucose incorporated into $^{3}H_2O$ per h and per mg tissue.

Lactate concentrations were measured in the buffer after the 4 h incubation period spectrophotometrically by determining the increments in absorbance at 340 nm in a mixture containing 1 mM NAD^+ and 22.5 U/ml lactate dehydrogenase in 0.25 M glycine/0.5 M hydrazine/1 mM EDTA buffer at pH 9.5.

It was done in collaboration with Dr. Bolaños´s Laboratory, at Salamanca University.

PFK2 activity measure

For PFK2 activity measure, frozen liver was pulverized in liquid N_2, weight and homogenized with a 26-gauge needle 10-12 times in isolation buffer (50 mM NaF, 50 mM KCl, 30 mM 2-Mercaptoethanol, 2 mM EDTA-diK^+, 0.1 PMSF, 100 mM HEPES; pH 7.5). Tissue was centrifugated (25,000 x *g*, 30 min) and the resulting supernatant used for the determination of PFK2 activity in reaction buffer (100 mM HEPES, 200 mM KCl, 10 mM KH_2PO_4, 14 mM $MgCl_2$, 30 mM 2-Mercaptoethanol, 10 mM Fructose-6-P, 30 mM Glucose-6-P, 260 mM ATP; pH 7.1) for 20 min. The incubations were finished with NaOH 0.25 M. Fructose-2-6-bisphosphate (Fru-2,6-B_2) synthesized during the reaction was used to spectrophotometrically measure PFK1 activity by determining the increments in absorbance at 340 nm for 20 min (2 min intervals) at 30 ºC in a mixture containing 0.1 M Tris-HCl, 14 mM $MgCl_2$, 0.1 M Fructose-6-P, 3 mg NADH, 1uL Aldolase, 1 uL Triose phosphate isomerase (TIM)-glycerol phosphate deshidrogenase (GDH), 1.5 uL PFK-1(PPi-depend), 10 mM PPi; pH 8) using the coupled enzymatic reaction as described by Van Schaftingen (Van Schaftingen and Hers, 1986) . Slopes obtained were used to relativize PFK2 activity. It was done in collaboration with Dr. Bolaños´s Laboratory, at Salamanca University.

Inmunoblot analysis

Tissue extracts were prepared in Triton lysis buffer (20mM Tris (pH 7.4), 1% Triton X-100, 10% glycerol, 137mM NaCl, 2mM EDTA, 25mM β-glycerophosphate, 1mM sodium orthovanadate, 1mM phenylmethylsulfonyl fluoride and 10µg/mL of aprotinin and leupeptin). Extracts (20-50µg protein) and immunoprecipitates (prepared from 500µg-2mg protein) were examined by immunoblot. For the immunoprecipitation assay, liver extracts were incubated with 4 µg of p38δ antibody (homemade) or anti-GFP (Santa Cruz sc-5385) coupled to protein-G-Sepharose. After overnight incubation at 4^{o}C, the captured proteins were centrifuged at 10,000 g, the supernatants discarded and the beads washed four times in lysis buffer. Beads were boiled for 5 minutes at 95 ^{o}C in 10µl sample buffer. Lysates were separated by SDS-PAGE and incubated in a 1/1000 dilution with antibodies against phospho-AKT (Thr308) antibody (Cell Signalling Technology cat# 9275S), phospho-AKT (Ser473) antibody (Cell Signalling Technology cat# 9271s), AKT antibody (Cell Signalling Technology cat# 9272s), phospho-Ser/Pro antibody (Cell Signalling Technology cat# 2325S), phospho-Thr/Pro antibody (Cell Signalling Technology cat# 9391S), p-PFKFB3 (ser467) antibody (Bioss cat# bs-3331R), PFKFB3 antibody (Cell Signalling Technology cat# 13123S), phospho-GYS (Ser461) antibody (Cell Signalling Technology cat# 3891), GYS (15B1) antibody (Cell Signalling Technology cat# 3886), phospho-GSK3α (Ser21) antibody (36E9)(Cell Signalling Technology cat# 9316), GSK3α (D80E6) antibody (Cell Signalling Technology cat# 4337), p38δ MAPK (Cell Signalling Technology cat# 2308s), GAPDH FL-335 (Santa Cruz cat# sc-25778) , α-tubulin (DM1A) (Sigma cat# T6199) or vinculin (hVIN-1) antibody (Sigma cat# V9131.). After washes, membranes were incubated with and appropriate horseradish peroxidase-conjugated secondary antibody (1:5000) (GE Healthcare), and signal was

detected using an enhanced chemiluminiescent substrate for the detection of horseradish peroxidase (Clarity Western ECL substrate).

Adeno-associated virus vector

AAV plasmids were cloned and propagated in the Stbl3 *E. coli* strain (Life Technologies). pCMV Flag p38δ F324S was cloned into a liver-specific HRC-hAAT promoter plasmid to generate pAAV-HRC-hAAT-p38δact ($AAV^{p38\delta^*}$). As control pAAV-U6-scramble shRNA-CMV-GFP (AAV^{U6}) was used. These AAV plasmids were packaged into AAV-2/8 capsids to specifically target the liver, produced by the Viral Vector Unit (CNIC) or in Harvard University (Gonzalez-Teran et al., 2016a). Adeno-associated viruses (serotypes AAV2/8) were produced in HEK-293T cells and collected from the supernatant. AAV2/8-CAG-Cre-WPRE (AAV^{CRE}) was obtained from Harvard University.

Administration of adeno-associated virus vectors

For systemic administration, AAV^{CRE} virus were diluted in PBS to get $0.5x10^{11}$ PV/ml for adult mice and injected via the tail vein. For pup injection (p1-2), $AAV^{p38\delta^*}$virus or control AAV^{U6} were injected in the carotid artery upon dilution in PBS to get $2x10^{11}$ PV/ml.

In vitro kinase assay

One microgram of human GST-PFKFB3 protein was incubated in kinase buffer containing 50mM Tris/HCl pH=7.5, 0.1 mM EGTA, 0.1 mM sodium orthovanadate and 0.1% β-mercaptoethanol with 1 µg of active recombinant p38δ (provided by MRC Protein Phosphorylation and Ubiquitylation Unit, Dundee, UK) in 25µl of total volume for 30 min at 37ºC in the presence of 200 µM cold ATP. The reaction was stopped by adding SDS-containing sample buffer, and proteins were resolved by SDS–PAGE and visualized by staining with colloidal Coomassie Blue.

In vivo kinase assay

Cells were plated at 70% confluence in DMEM/10%FBS 6-8 h before transfection. Cells were transfected using the calcium phosphate method (Sabio et al., 2004) with the next cDNA expression plasmids: pDEST-TAP-GYS2 kindly provided by Joan J. Guinovart (IRB, Spain), pCMV-HA-Flag $p38\delta^{F324S}$, kindly provided by David Engelberg (The Hebrew University of Jerusalem, Israel) and pEGFP-C1-PFKFB3 (K6), kindly provided by Juan Pedro Bolaños (Universidad de Salamanca, Spain). The culture medium was replaced 14 h after transfection with fresh complete medium, and cells were harvested 48 h later.

Cellular extracts were prepared in Triton lysis buffer [20mM Tris (pH 7.4), 1% Triton X-100, 10% glycerol, 137mM NaCl, 2mM EDTA, 25mM β-glycerophosphate, 1mM sodium orthovanadate, 1mM phenylmethylsulfonyl fluoride and 10µg/mL of aprotinin and leupeptin]. PFKFB3 and GYS2 proteins were immunoprecipated (from 500µg-2mg protein) using anti-GFP (Santa Cruz sc-5385) or anti-FLAG (Sigma F1804) antibodies respectively (1-2 µg),

coupled to 20µl Dynabeads (Invitrogen). After incubation for 4 hours at 4°C, the captured proteins were washed 8 times with lysis buffer.

LC-MS/MS

For *in vitro* kinase assay, the band containing GST-PFKFB3 was excised. For *in vivo* kinase assay, PFKFB3 or GYS2 immunoprecipitation proteins were treated with 50mM DTT in BA at 56 °C for 30 min, to reduce disulfide bonds; follow by 50 mM iodoacetamide in BA for 20 min in darkness, to derivatize cysteine residues. The protein was in-gel digested with trypsin (Promega)(ratio 12:1, weight/weight) overnight at 37 °C in BA and 5 % acetonitrile, and the resulting peptides were extracted from the gel with BA and 0.5 % trifluoracetic acid. Then, trifluoroacetic acid to 1 % was added to desolate the peptides in C18 Oasis-HLB columns, follow by spin vacuum dry.

Liver tissues samples were lysed in lysis buffer (50 mM Tris-HCl pH 8,5; 2% SDS and 50 mM DTT) and mechanical shock (MagnaLyser, 3 cycles of 60 s/65000 rpm). Then, samples were boiled for 10 min, incubated for 20 min in agitation and centrifuged. Protein concentration was quantified with infrared spectrometer (Direct Detect, Millipore). Samples were digested with the sample preparation protocol (FASP) (Wisniewski et al., 2009). For the quantitative analyses, peptides were dissolved in 150 mM triethylamonic bicarbonate tampon (TEAB). Peptides concentration was measured by Direct Detect (Millipore) and the same amount was labeled for 1 h at room temperature with their respective isobaric reactive (Tandem mass tag (TMT), Thermo Fisher). Lastly, trifluoroacetic acid was added, samples were mixed, vacuum concentrated, desalted with C18 Oasis-HLB cartridges and dried.

Peptides were measured by nanoscale-microcapillary reversed phase liquid chromatography tandem mass spectrometry (LC-MS/MS), using C-18 columns (75 µm I,D, x 25 cm, 2 µm particle size, Acclaim PepMap RSLC, 100 C18; Thermo Fisher Scientific) in a continuous acetonitrile gradient for 40 min (phosphorylation sites identification assay) or 6 h (proteome study). Peptides were eluted in an emisor nanospray (200 nL/min) and the peptides fragmentation in an Orbitrap Fusion mass spectrometer (Thermo Fisher). For the proteome study, the labeled samples were also fractionated by reverse phase chromatography at high pH (Thermo Fisher). The resolution for the spectrum acquisition of the parental ion mass was 70.000 MHW, follow by HCD fragmentation spectrums of more intensive ions. The dynamic exclusion was 40 s.

For the identification and quantification of proteins, acquired spectrums were analyzed with Proteome Discoverer program (2.1 version, Thermo Fisher Scientific), using the search algorithm SEQUEST-HT (Thermo Fisher Scientific), using Uniprot database with the next parameters: trypsin digestion with maximum of 2 failed cuts, tolerance of 2 Da and 0.03 Da in the ion precursor mass and fragmented ions respectively, carbamidomethyl cysteine, N-terminal extreme modification and Lys by TMT as fix modifications. Lastly,

methionine modifications were analyzed as dynamic oxidation. For the protein modification, the Ser and Thr phosphorylation was added as variable modification.

Identified peptides were validated using the probability ratio method (Martinez-Bartolome et al., 2008) and the false discovery rate (FDR) was calculated as previously described (Navarro and Vazquez, 2009, Bonzon-Kulichenko et al., 2015). Identified peptides were filtered with FDR≤1%. The proteins were quantified in base of reporter ions intensity from all identified peptides. For the fragmentation spectrum assignment or modified residues, Scaffold program was used (Proteome Software, Oregon) with the findings from the Proteome Discoverer. Quantitative data was analyzed by QuiXoT (Navarro et al., 2014). To detect functional alteration Systems Biology Triangle (SBT) was used (Garcia-Marques et al., 2016). It was done in collaboration with Proteomics Unit at CNIC.

RNA isolation and quantitative real-time-PCR analysis

Total RNA was isolated from liver with the RNeasy Mini Kit (Qiagen) with on-column DNase I digestion. RNA was quantified using a NanoDrop spectrophotometer. Complementary DNA synthesis was carried out using the High-Capacity complementary DNA Reverse Transcription Kit (Applied Biosystems). Expression of the housekeeping gene *β-actin* was used for normalization. RT-qPCR was performed using Fast SYBR Green (Applied Biosystem) on a 7900HT Fast Real-time PCR system (Applied Biosystem). Primer sequences were as follows (F. forward; R. reverse).

β-actin F: 5´ GGCTGTATTCCCCTCCATCG 3´

β-actin R: 5´ CCAGTTGGTAACAATGCCATGT 3´

MAPK13 F: 5´ ATGAGCCTCACTCGGAAAAGG 3´

MAPK13 R: 5´ GCATGTGCTTCAAGAGCAGAA 3´

ATP measurement in isolated mitochondria

Mitochondria were extracted from the liver (Frezza et al., 2007). After isolation, mitochondrial protein concentration was determined by Bradford assay (BioRad) and 10-50 µg protein were incubated in 160 µl experimental buffer A (150 mM KCl, 25mM Tris-HCl, 2 mM EDTA, 0.1 % BSA FA, 10 mM K-phsophatate, o.1 mM MgCl2, pH=7.4), 1mM substrate and 20 µl fresh experimental buffer B (0.5 M Tris-acetate, pH-7.75; 0.8 mM luciferine, 20 mg/ml luciferase). ATP synthesis was measured using a kinetic luminescence assay, as described in (Vives-Bauza et al., 2007) with the next ATP standard curve (10, 5, 2.5, 1.25, 0.6, 0.3, 0.15 and 0.075 mM).

Statistical Analysis

Differences between experimental groups were examined for statistical significance by unpaired two-tailed Student's *t*-test, one or two-way ANOVA coupled to Bonferroni's post-test or by multiple-comparison using the Holm-Sidak method. Significance defined as a p-value<0.05. GraphPad Prism 7.0 (San Diego, CA) was used for all

statistical analysis. In most cases, minimum n=5 mice per group were used; although specific number is indicated in the figure legends. Data are presented as the mean ± SEM. Image J was used to quantify western blot analysis.

Results

1. Hepatic specific overexpression of active p38δ MAPK increases blood glucose levels and promotes insulin resistance

Liver is a central regulator of whole body metabolism (Postic et al., 2004) whose homeostasis and function exert and important role in obesity, insulin resistance and T2D (Rui, 2014). Metabolic deregulation and hepatic steatosis have been linked to stress kinases. While the role of JNK in the development of T2D and hepatic steatosis has been widely studied (Sabio et al., 2008, Sabio et al., 2010, Han et al., 2013, Hirosumi et al., 2002, Sabio et al., 2009), less is known about the role of the MAPK. Our group has shown that p38δ MAPK expressed in neutrophils can modulate liver metabolism (Gonzalez-Teran et al., 2016b). However, the function of hepatic p38δ MAPK in the development of insulin resistance and NAFLD is unknown. Interestingly, the expression of p38δ MAPK increases in obese humans with NAFLD and in mice with NASH-induced by MCD diet (Gonzalez-Teran et al., 2016b), suggesting that hepatic p38δ MAPK may have a role in fatty liver disease pathophysiology.

To evaluate whether hepatic p38δ MAPK overexpression in hepatocytes directly promotes metabolic alterations, we overexpressed active p38δ MAPK in the livers of wild type mice (CXBL6/7J), injecting at p1, with adeno-associated virus (AAV) serotype 2/8 that are highly greater transduces in liver (Nam et al., 2007). Moreover p38δ expression is leading by the apolipoprotein E locus control region (HCR), human alpha1-antitrypsin (hAAT) promoter which enhances *in vivo* hepatic gene expression (Miao et al., 2000).

Confirming the central role of hepatic p38δ MAPK in whole-body homeostasis, hepatocytes specific overexpression of the active form of p38δ (Figure 1A) increased blood glucose levels and promoted insulin resistance (Figure 1B) in 8 weeks old CD-fed mice.

A

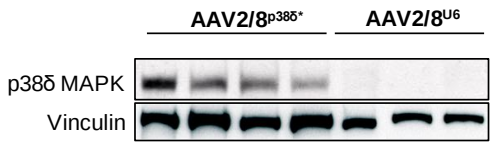

B

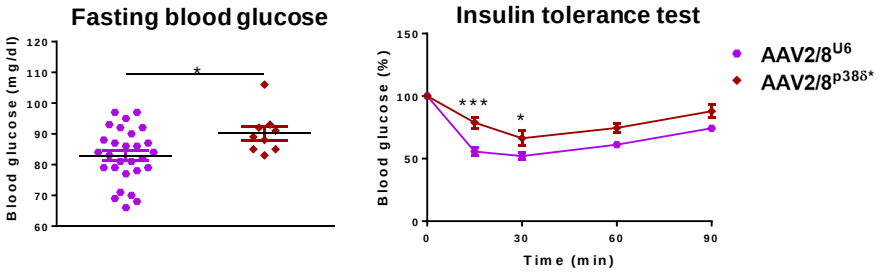

Figure 1: Hepatic specific overexpression of active p38δ promote insulin resistance and increased blood glucose levels in CD-fed mice

CXBL6/7J mice were injected at p1 with adeno-associated virus serotype 2/8 expressing the human active p38δ protein (AAV2/8$^{p38\delta*}$) or the corresponding control virus (AAV2/8^{U6}). Mice were fed with CD for 8 weeks. A) Immunoblot analysis of p38δ expression were done in livers from control and AAV2/8$^{p38\delta*}$ mice. Vinculin protein expression was monitored as loading control, (n=4). B) Left: Blood glucose levels in control Alb^{cre} and Alb$^{p38\delta KO}$ mice after overnight fasting (16 hours). Right: Insulin tolerance test. Blood glucose concentration was measured in mice upon intraperitoneal insulin injection (0.75 IU/kg) upon 1 h of food deprivation. (mean ± SEM, n=13-15). *$p < 0.05$, ***$p < 0.001$ (two-way ANOVA coupled to Bonferroni's post-tests or unpaired *t* test).

2. Generation of the hepatic specific p38δ MAPK knockout mice (Alb$^{p38\delta KO}$)

To evaluate the role of hepatic p38δ MAPK in metabolism, we generated genetically engineered mice that lack p38δ specifically in hepatocytes. The experimental mouse model was generated by crossing mice in which *MAPK13* gene was flanked by *LoxP* sequence (*MAPK13$^{f/f}$),* with mice expressing CRE recombinase under the control of the hepatic specific albumin (Alb) promoter (Alb^{cre}) (Powell et al., 1984, Gorski et al., 1986, Izban and Papaconstantinou, 1989, Postic et al., 1999). We obtained the hepatic specific p38δ knockout mice (Alb$^{p38\delta KO}$) and we used the mice expressing CRE protein (Alb^{cre}) as control. Unspecific recombination in other tissues has not been previously observed (Postic et al., 1999, Michael et al., 2000, Hayhurst et al., 2001, Thierbach et al., 2005); however, we first analyzed the specific deletion of p38δ MAPK in the liver, using pancreas as negative control, where this kinase is highly expressed (Sumara et al., 2009). PCR analysis to check *MAPK13* deletion was performed. We observed p38δ deletion in the livers from Alb$^{p38\delta KO}$ mice, but not in pancreas from Alb$^{p38\delta KO}$ (Figure 2B). Moreover, western blot analysis upon p38δ MAPK inmunoprecipitation showed that levels of p38δ was reduced in liver lysates from Alb$^{p38\delta KO}$ compared with the control Alb^{cre} mice (Figure 2C); while in pancreas, p38δ MAPK expression was similar in both genotypes (Figure 2D). These data indicate a specific deletion of p38δ in hepatocytes.

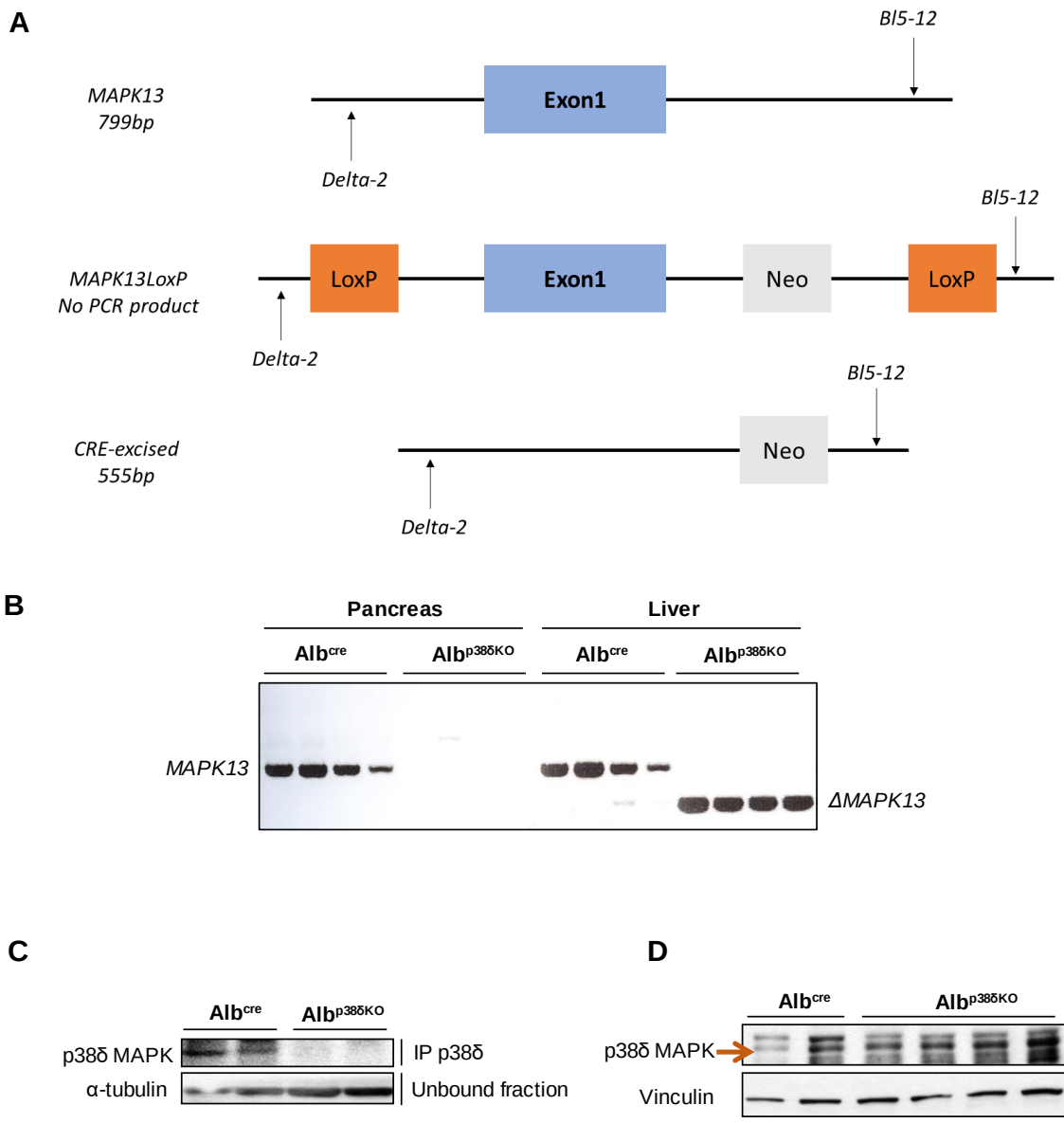

Figure 2: Evaluation of the Alb$^{p38\delta KO}$ mice

The specific deletion of p38δ was assessed in livers and pancreas from hepatic specific p38δ deficient mice (Alb$^{p38\delta KO}$) and control mice (Alb^{cre}). A) Scheme of *MAPK13, MAPK13*LoxP and *MAPK13* upon CRE recombination, showing binding sites of primers used to check p38δ MAPK hepatic specific deletion. B) *Cre*-mediated deletion of the intron 1 in the *MAPK13* gene in liver. Genomic DNA isolated from pancreas and liver was examined by PCR analysis using primers that detect CRE-excised or wild type gene. C) p38δ MAPK was immunoprecipitated (IP) from liver extracts and immunoblot analysis was performed. α-tubulin protein expression was used as a loading control. D) Immunoblot analysis of p38δ in pancreas lysates. Vinculin protein expression was used as a loading control.

3. Alb$^{p38\delta KO}$ mice are protected against obesity-induced insulin resistance and hyperglycemia

To evaluate whether specific depletion of p38δ MAPK in hepatocytes protects against obesity and obesity-related diseases, 8 weeks old Alb^{cre} and Alb$^{p38\delta KO}$ mice were fed with a HFD (60% kcal fat with 1,5% of cholesterol), for 8-10 weeks. Both Alb^{cre} and Alb$^{p38\delta KO}$ mice became obese and no differences were found between genotypes in body weight, fat mass or lean mass upon HFD (Figure 3A). Moreover, no differences in glucose tolerance by intraperitoneal glucose tolerance test (GTT) or in plasma insulin levels during the oral GTT were found (Figure 3B). Nevertheless, Alb$^{p38\delta KO}$ mice had reduced blood glucose levels after overnight fasting and higher insulin sensitivity during insulin tolerance test (ITT), to judge by greater decrease in blood glucose levels upon insulin injection in Alb$^{p38\delta KO}$ mice compared to control mice (Alb^{cre}) (Figure 3C).

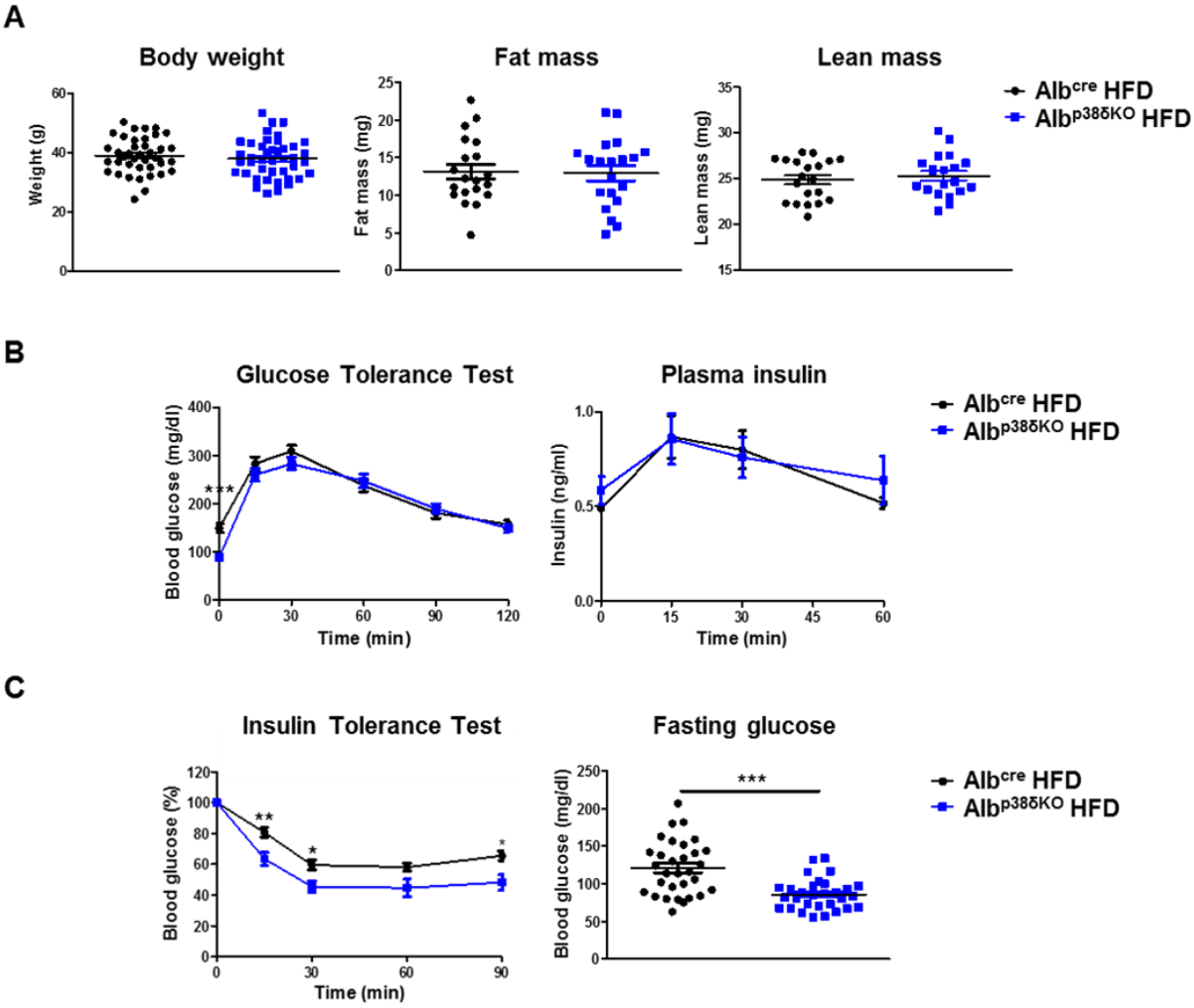

Figure 3: Alb$^{p38\delta KO}$ mice have decreased fasting blood glucose and are protected against HFD-induce insulin resistance

A) Body weight, fat and lean mass of hepatic specific p38δ deficient mice (Alb$^{p38\delta KO}$) and control mice (Alb^{cre}) fed with HFD (8 weeks), (mean ± SEM, n=19-39). B) Intraperitoneal glucose tolerance test and plasma insulin release. Blood glucose concentration was measured in mice given intraperitoneal injections of glucose (1 g/kg) upon overnight fasting (mean ± SEM, n=13-15). Plasma insulin levels were measured from vein tail blood samples during oral glucose tolerance test (3g/kg) upon 4 hours of food deprivation (mean ± SEM, n=8-10). C) Insulin tolerance test and fasting blood glucose levels. Blood glucose concentration was measured in mice upon intraperitoneal insulin injection (0.75 IU/kg) after 1 h of food deprivation (mean ± SEM, n=13-15). Fasting blood glucose was measured after overnight fasting (16 hours) (mean ± SEM, n=31-33). *$p < 0.05$, **$p < 0.01$, ***$p < 0.001$ (two-way ANOVA coupled to Bonferroni's post-tests or unpaired *t* test).

4. Hepatic insulin sensitivity in HFD-fed Alb$^{p38\delta KO}$ mice protects against whole body insulin resistance

HFD-fed Alb$^{p38\delta KO}$ mice were protected against insulin resistance. Then, we next performed the hyperinsulinemic-euglycemic clamps (Ayala et al., 2006, Ayala et al., 2010) to check insulin sensitivity *in vivo* conscious mice. During hyperinsulinemic-euglycemic clamps, constant insulin infusion promote hyperinsulinemia, together with maintained euglycemia by variable GIR. GIR is the reflection of insulin sensitivity. Moreover, using constant infusion of (3-^{3}H)-glucose, we can measure the hepatic endogenous glucose production (EGP) and the glucose disappearance (Rd or peripheral glucose uptake), allowing to differentiate between hepatic and peripheral insulin sensitivity.

Hyperinsulinemic-euglycemic clamps after 4 hours of food deprivation showed that Alb$^{p38\delta KO}$ mice presented bigger suppression of HGP upon insulin, indicating increased hepatic insulin sensitivity (Figure 4A). However, no changes were found in peripheral glucose uptake upon insulin (Figure 4A), suggesting specific hepatic insulin sensitivity in mice lacking p38δ in hepatocytes. Moreover, larger GIR (Figure 4A) confirmed increased insulin sensitivity in Alb$^{p38\delta KO}$ mice, in concordance with the higher insulin sensitivity found in the ITT (Figure 3C). Nevertheless, no significant differences were found in the basal HGP after 4 hours of food deprivation, but neither blood glucose levels were different at this time point (Figure 4B).

Lastly, we injected intraperitoneal 2-deoxy-*d*-[1-^{14}C]-glucose (2DG), to check directly peripheral tissue glucose uptake. 2DG cannot undergo further glycolysis in most cells, due to hexokinase phosphorylates 2DG, trapping the product 2-deoxyglucose-6-phosphate into the cells. Therefore, we can quantify the levels of (^{14}C)-2-deoxyglucose-6-phosphate as measured of glucose uptake. No differences in glucose uptake were found between genotypes, again confirming specific hepatic insulin sensitivity in mice lacking p38δ in hepatocytes (Figure 4C).

Therefore, hepatic p38δ deletion promotes specific liver insulin sensitivity and consequently decreases whole body insulin resistance.

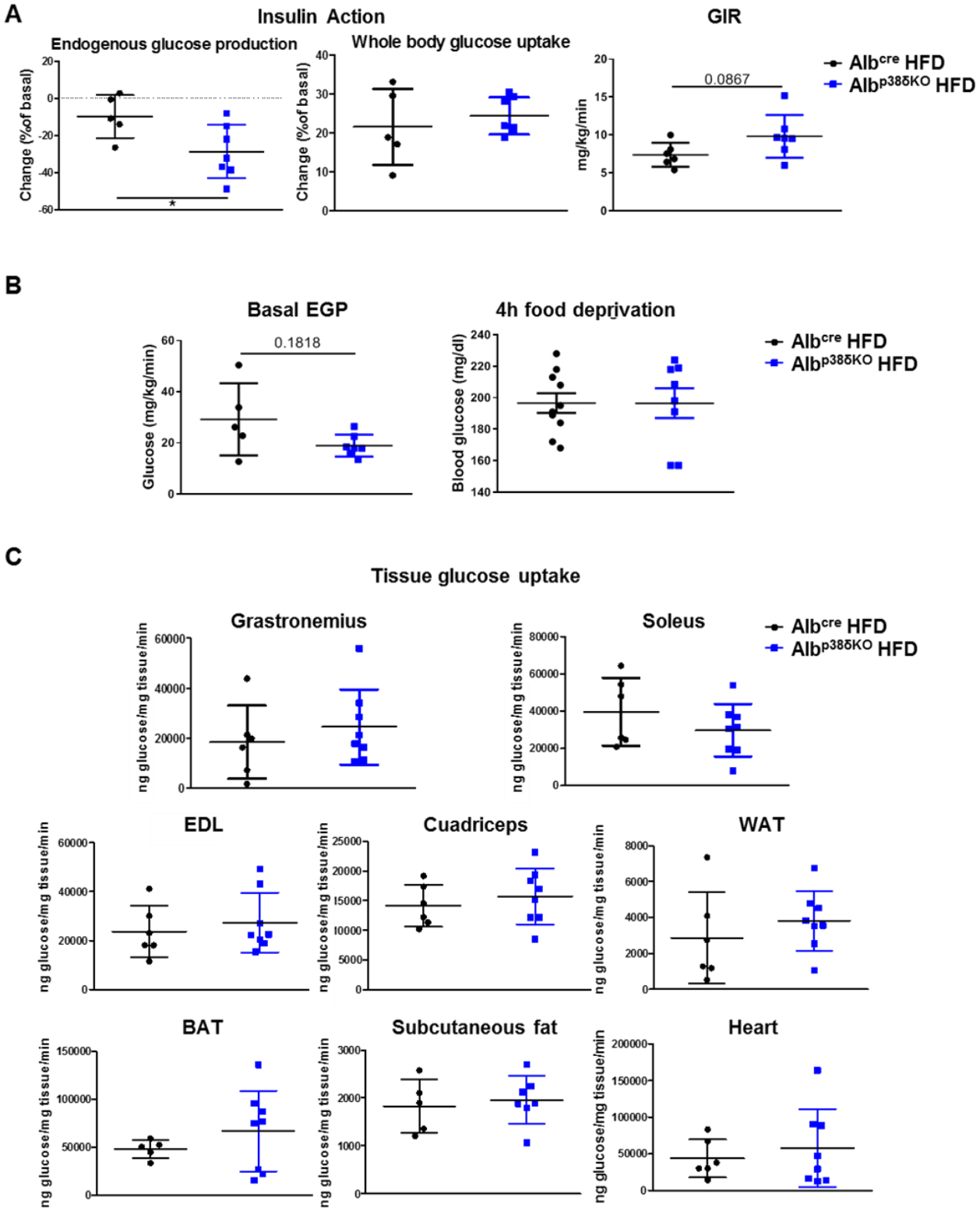
A
Insulin Action
Endogenous glucose production
Change (%of basal)
Whole body glucose uptake
Change (%of basal)
GIR
mg/kg/min
0.0867
Alb^cre HFD
Alb^p38δKO HFD
B
Basal EGP
Glucose (mg/kg/min)
0.1818
4h food deprivation
Blood glucose (mg/dl)
Alb^cre HFD
Alb^p38δKO HFD
C
Tissue glucose uptake
Grastronemius
Soleus
ng glucose/mg tissue/min
Alb^cre HFD
Alb^p38δKO HFD
EDL
Cuadriceps
WAT
BAT
Subcutaneous fat
Heart

Figure 4: Alb$^{p38\delta KO}$ mice are protected against whole body insulin resistance due to increase hepatic insulin sensitivity

A) Insulin sensitivity was measured using hyperinsulinemic-euglycemic clamps with conscious HFD- fed Alb$^{p38\delta KO}$ and Alb^{cre} mice. The hepatic insulin action was expressed as insulin-mediated percent suppression of basal HGP and as insulin-mediated glucose uptake of basal Rd. GIR is the steady-state glucose infusion rate (mean ± SEM, n=5-7). B) Basal HGP(EGP) and blood glucose levels after 4 hours of food deprivation. C) (^{14}C)-2-deoxyglucose-6-phosphate levels in muscle (gastrocnemius, soleus, quadriceps and extensor digitorum longus (EDL)), white adipose tissue (WAT), brown adipose tissue (BAT), subcutaneous fat and heart. *$p < 0.05$ (unpaired *t* test).

5. Exploring insulin signaling in the liver

To further explore the hepatic specific insulin sensitivity in HFD-fed Alb$^{p38\delta KO}$ mice we explored AKT/GSK3α/GYS2 pathway, the canonical pathway for insulin signaling and whose lost in hepatocytes drives to severe insulin resistance and hepatic dysfunction (Michael et al., 2000). Upon insulin or feeding, AKT becomes active and phosphorylates GSK3α at Ser21, which inhibits its activity. GSK3α is the main liver isoform. Then, GSK3 cannot phosphorylate GYS2 among others, at Ser641, allowing GYS2 activation and glycogen production. No differences were found in AKT phosphorylation (at Thr308 and Ser473) upon insulin stimulation (Figure 5A). In agreement, we did not find differences in GSK3α phosphorylation (at Ser21) after feeding (Figure 5B), neither in GYS2 Ser641 phosphorylation in Alb$^{p38\delta KO}$ mice (Figure 5B). Therefore, these data indicate that increased Alb$^{p38\delta KO}$ mice hepatic insulin sensitivity might be due to downstream mechanisms, different to insulin signaling through AKT/GSK3α/GYS2 pathway**.** Since GNG and glycogenolysis are usually decreased upon insulin, through AKT activation; no differences in AKT phosphorylation suggests that the high HGP inhibition upon insulin observed in Alb$^{p38\delta KO}$ mice compared to control mice during the clamp (Figure 4A), might not be mediated by changes in GNG, neither glycogenolysis; which are the two main pathways that contribute to HGP.

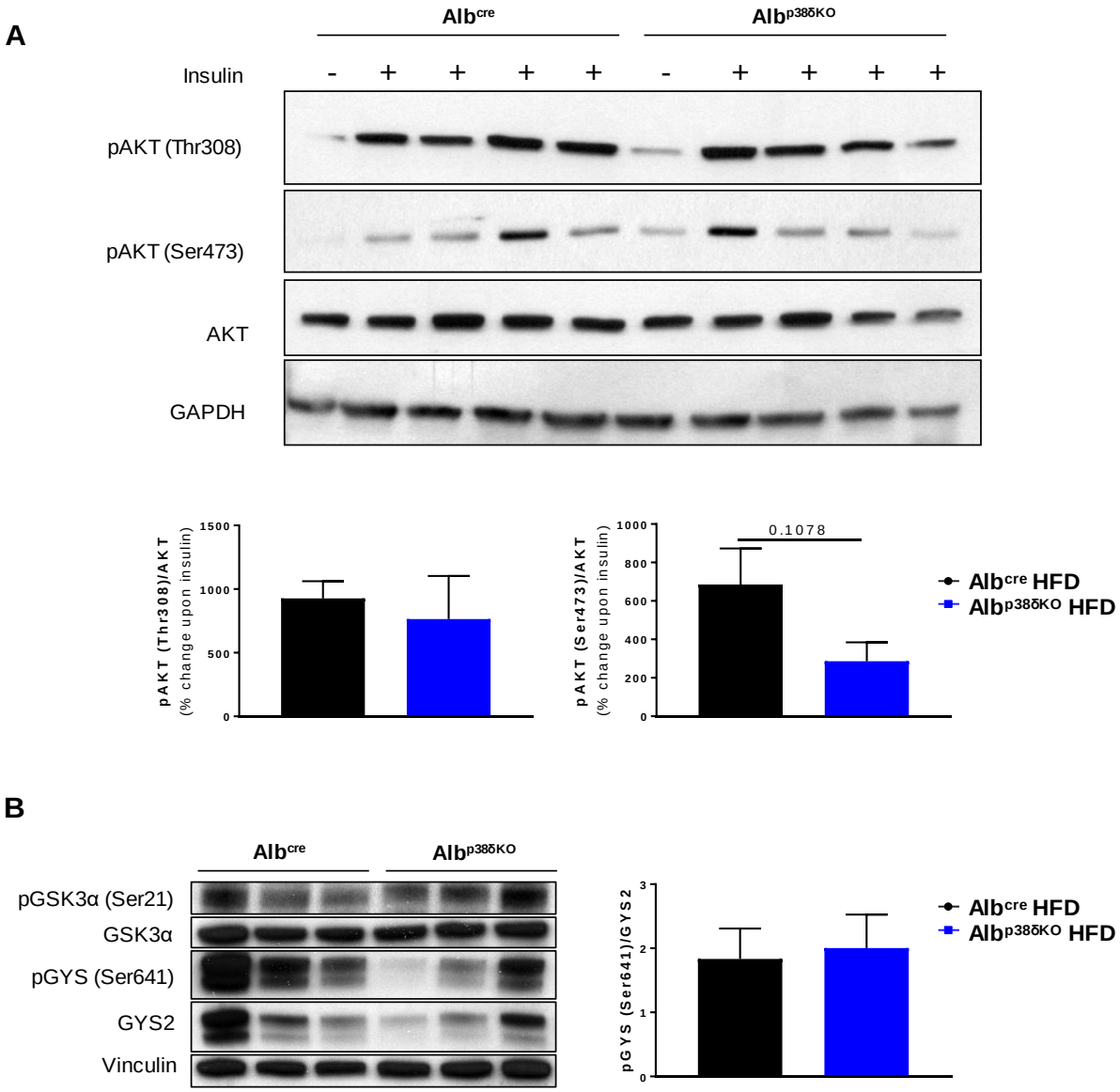

Figure 5: Alb$^{p38\delta KO}$ mice are protected against hepatic insulin resistance by mechanisms downstream AKT

A) To check insulin signaling, immunoblot analysis of AKT phosphorylation (Ser473 and Thr308) and AKT were done in livers from 8 weeks HFD-fed control and Alb$^{p38\delta KO}$ mice in basal upon overnight fasting (16 hours) and after 15 minutes of intraperitoneal insulin injection (0.75 IU/kg). GAPDH protein expression was monitored as loading control. B) Immunoblot analysis of pGSK3α Ser21, GSK3α, pGYS Ser641 and GYS2 was done in livers extracts from 8 weeks HFD-fed control and Alb$^{p38\delta KO}$ mice sacrificed upon 2 h feeding. Vinculin was used as loading control. Image J was used to quantify GYS phosphorylation at Ser641 and AKT phosphorylation at Thr308 and Ser473 residues (mean ± SEM, n=3-12) (Welch´s unpaired *t* test).

6. Alb$^{p38\delta KO}$ mice are protected against hyperglycemia because they have reduced glycogenesis and consequently liver glycogen storage

Alb$^{p38\delta KO}$ mice were protected against hyperglycemia (Figure 3C) and hepatic insulin resistance, as higher HGP inhibition upon insulin during the clamp was observed in these mice (Figure 4A). Pyruvate tolerance test injecting intraperitoneally the gluconeogenic substrate sodium pyruvate confirmed no differences in GNG from pyruvate (Figure 6A). Moreover, no changes in basal HGP in mice after 4 h of food deprivation (Figure 4B), when glycogenolysis plays the main role in the HGP also suggested no differences in glycogenolysis. Therefore, since GNG, glycogenolysis, neither peripheral glucose uptake (Figure 4C) were altered, to explain low fasting blood glucose levels, we measured hepatic glycogen content because it is the main glucose storage in the body. Alb$^{p38\delta KO}$ mice showed decreased liver glycogen levels (Figure 6B). Liver glycogen is usually accumulated in response to fed (insulin and mainly glucose input). The liver glycogen synthase is a key enzyme in the glycogen synthesis and it is control by a complex interplay between the allosteric activator G6P, the reversible phosphorylation through AKT/GSK3 and the glycogen-associated form of protein phosphatase 1 (Roach, 2002, Ros et al., 2009, von Wilamowitz-Moellendorff et al., 2013). We did not find differences in GYS2 Ser641 upon feeding, which is one of the inhibitory sites that are phosphorylated by GSK3; however, to understand the molecular mechanism responsible of the reduction in the liver glycogen storage, we directly measured GYS2 activity in livers from Alb$^{p38\delta KO}$ and control mice. The activation of GYS2 after feeding was decreased in Alb$^{p38\delta KO}$ mice (Figure 6C) in agreement with the reduction in the hepatic glycogen content that these mice showed. However, no significant changes were found in GYS2 activity in Alb$^{p38\delta KO}$ mice in fast or in fed conditions compared to control mice (Figure 6D). We found that whereas upon feeding GYS2 was properly activated in control mice (Alb^{cre}), this activation was impaired in the knockout mice (Figure 6D).

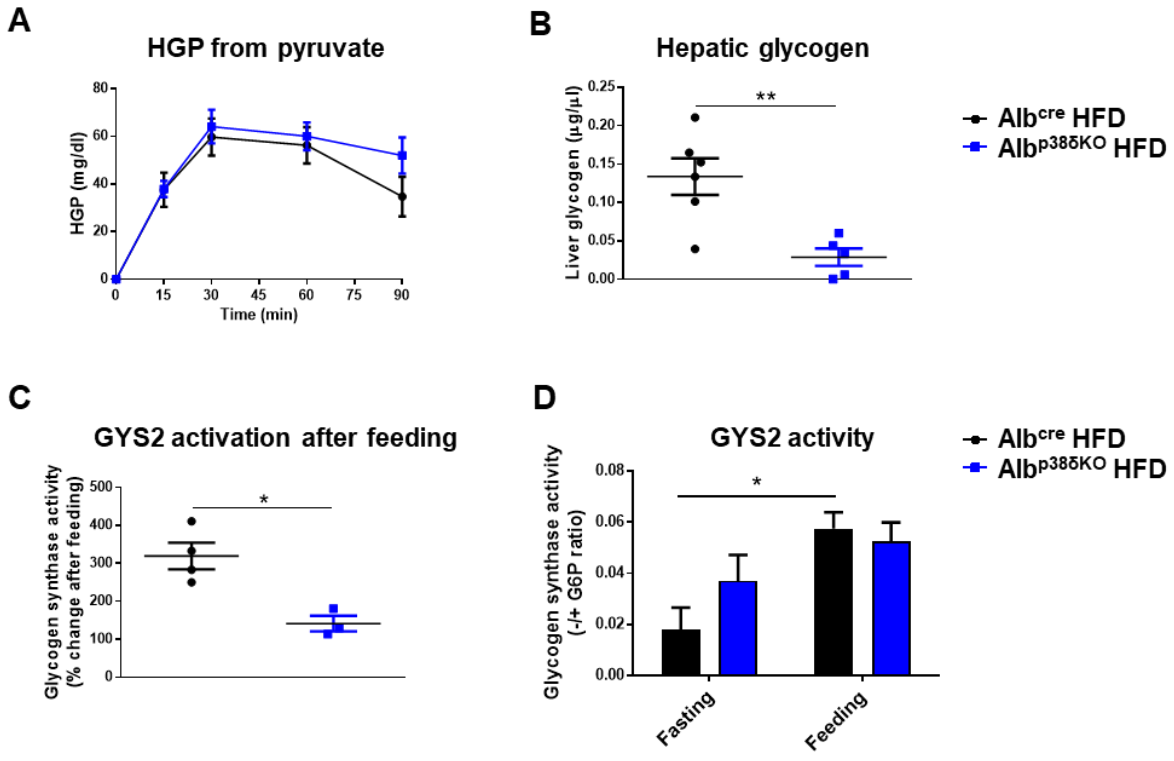

Figure 6: Reduced liver glycogen storage protects Alb$^{p38\delta KO}$ mice against hyperglycemia

A) HGP from GNG upon intraperitoneal injection of sodium pyruvate (2mg/kg) in 8 weeks HFD-fed control and liver p38δ deficient mice. Blood glucose levels from each genotype are relativized to basal blood glucose levels (time 0) (mean ± SEM, n=9-15). B) Glycogen content measured in liver under fed conditions in 8 weeks HFD-fed control and liver p38δ deficient mice (mean ± SEM, n=5-6). C and D) Glycogen synthase (GYS) 2 activity in liver extracts (µg) from 8 weeks old HFD-fed control and liver p38δ deficient mice. Activity measures by UDP-^{14}C-glucose (nmol/L) incorporation to glycogen with or without saturating G6P levels for 20 minutes. GYS2 activity was calculated as ratio ^{14}C-glycogen in −G6P/+G6P conditions. Values were calculated from duplicate activity measurements. Data is shown as percentage of change after feeding (respect to fast conditions) (C) GYS2 activity in fasting and feeding (D) (mean ± SEM, n=3-4). *$p < 0.05$, **$p < 0.01$ (two-way ANOVA coupled to Bonferroni's post-tests or unpaired *t* test).

7. p38δ MAPK phosphorylates and controls GYS2 activity

Then, we evaluated whether p38δ could directly phosphorylate and activate GYS2. To explore this possibility, we performed an *in vivo* kinase assay (transfecting recombinant human GYS2 in HEK 293T cells, followed by GYS2 immunoprecipitation and mass spectrometry analyses. We found that p38δ MAPK phosphorylates GYS2 in three residues, Thr278, Ser627 and Ser683 (Figure 7A). Interestingly, Ser627 and Ser683 residues, are close to the central domain (Ser641, 645, 649 and 653) that inactivates GYS (Mora et al., 2005, Jensen et al., 2012, Coghlan et al., 2000, Cline et al., 2002). Moreover, p38δ phosphorylation sites are also close to G6P activation domain (13-amino-acid segment) (Hanashiro and Roach, 2002, von Wilamowitz-Moellendorff et al., 2013). The proximity

of p38δ-mediated GYS2 phosphorylation sites to the main described regulatory sites that control the activity of the enzyme, suggests that p38δ could be modulating GYS2 inhibition or activation mediated by these stimuli.

A

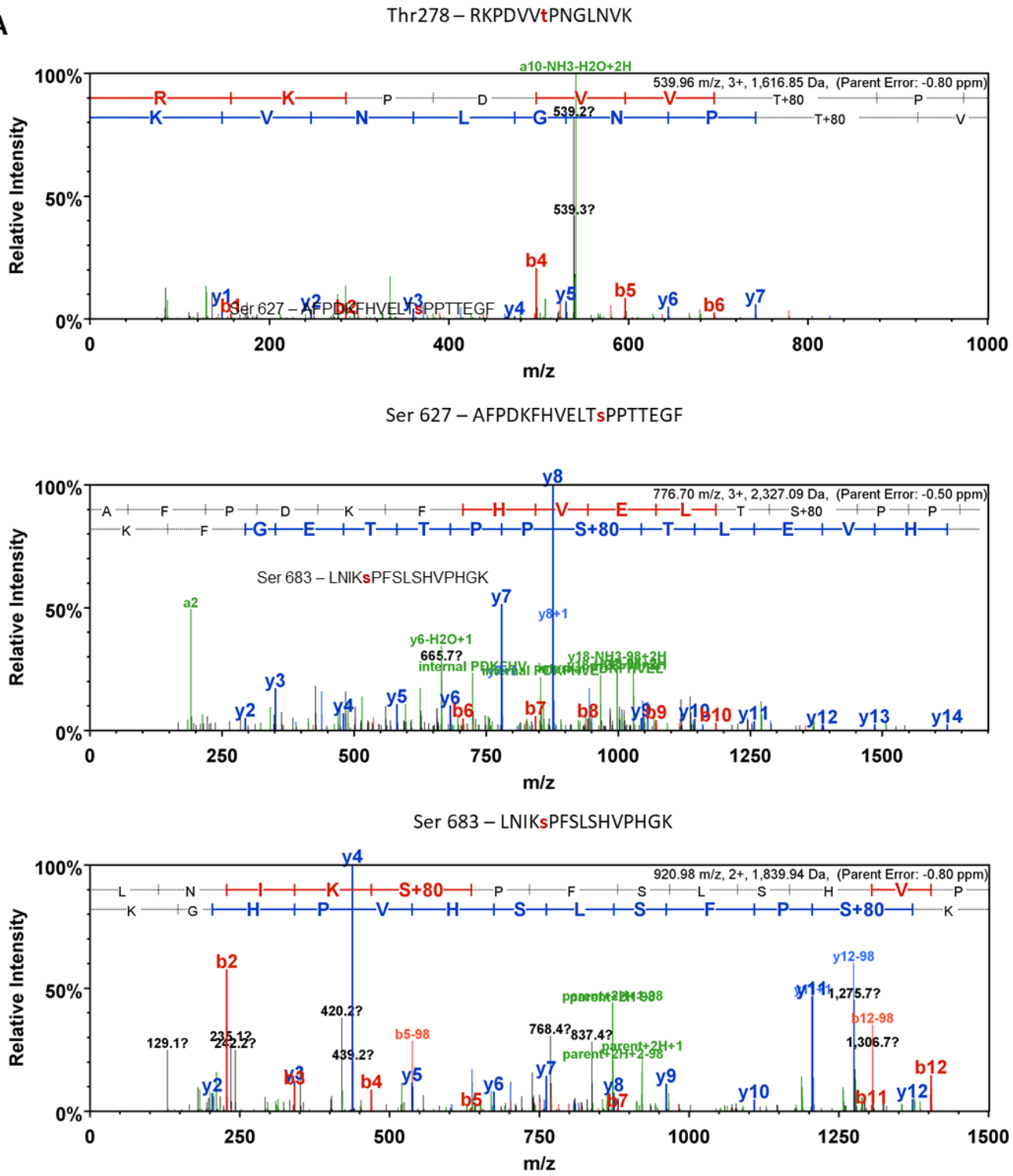

Figure 7: MS analysis of *in vivo* phosphorylation of GYS2 by active p38δ MAPK

Human pDEST-TAP-GYS2 plasmid was expressed in HEK-293T cells alone or together with pCMV-HA-Flag p38δ^{F324S}, which expresses the constitutively active p38δ. HEK-293T were starved overnight (16 hours). GYS2 phosphorylation was analyzed from Flag immunoprecipitation (2 µg) by LC-MS/MS. After in-gel trypsin digestion, peptides were monitored using the Orbitrap mass spectrometer as described in the Methods section. The panels show deduced MS/MS spectra by Scaffold (Proteome Software, Oregon) in GYS2 protein, validating the phosphorylation in the indicated sites in the protein (in lower case letters). Note that LC-MS/MS spectra confirm peptide phosphorylation at Ser and Thr residues in the consensus sequences SP and TP, respectively. No phosphorylation was detected in the control samples (data not shown).

8. CD-fed Alb$^{p38\delta KO}$ mice also have reduced liver glycogen storage that promotes low blood glucose levels

Our data showed that p38δ MAPK plays a main role controlling glucose metabolism in mice fed with HFD. Therefore, we decided to explore also the role of p38δ in normal conditions, using mice fed with a normal/CD. CD-fed Alb$^{p38\delta KO}$ mice did not show differences in fat mass, however they exhibited less lean mass and body weight (Figure 8A). They also presented reduced fasting blood glucose levels, even with less plasma insulin levels; however, CD-fed Alb$^{p38\delta KO}$ mice showed increased postprandial blood glucose levels (Figure 8B). Interestingly in concordance with our results in HFD, CD-fed Alb$^{p38\delta KO}$ mice had reduced hepatic glycogen content (Figure 8C) and glycogenesis rate (Figure 8D) without differences in GNG upon sodium pyruvate injection (Figure 8E). This suggested that the reduced liver glycogen content in Alb$^{p38\delta KO}$ mice might be responsible of the reduced blood glucose levels. Moreover, in agree with a direct regulation of GYS2 by p38δ MAPK phosphorylation, no differences in Ser641 phosphorylation were found between genotypes upon feeding (Figure 8H). However, contrary to previous studies (Irimia et al., 2017), the lack of glycogen did not produce insulin resistance (Figure 8F), neither NAFLD in CD-fed Alb$^{p38\delta KO}$ mice (Figure 8G). Therefore, our data point out that p38δ is essential to correct glycogen storage and subsequent blood glucose levels regulation in normal and in high fat conditions.

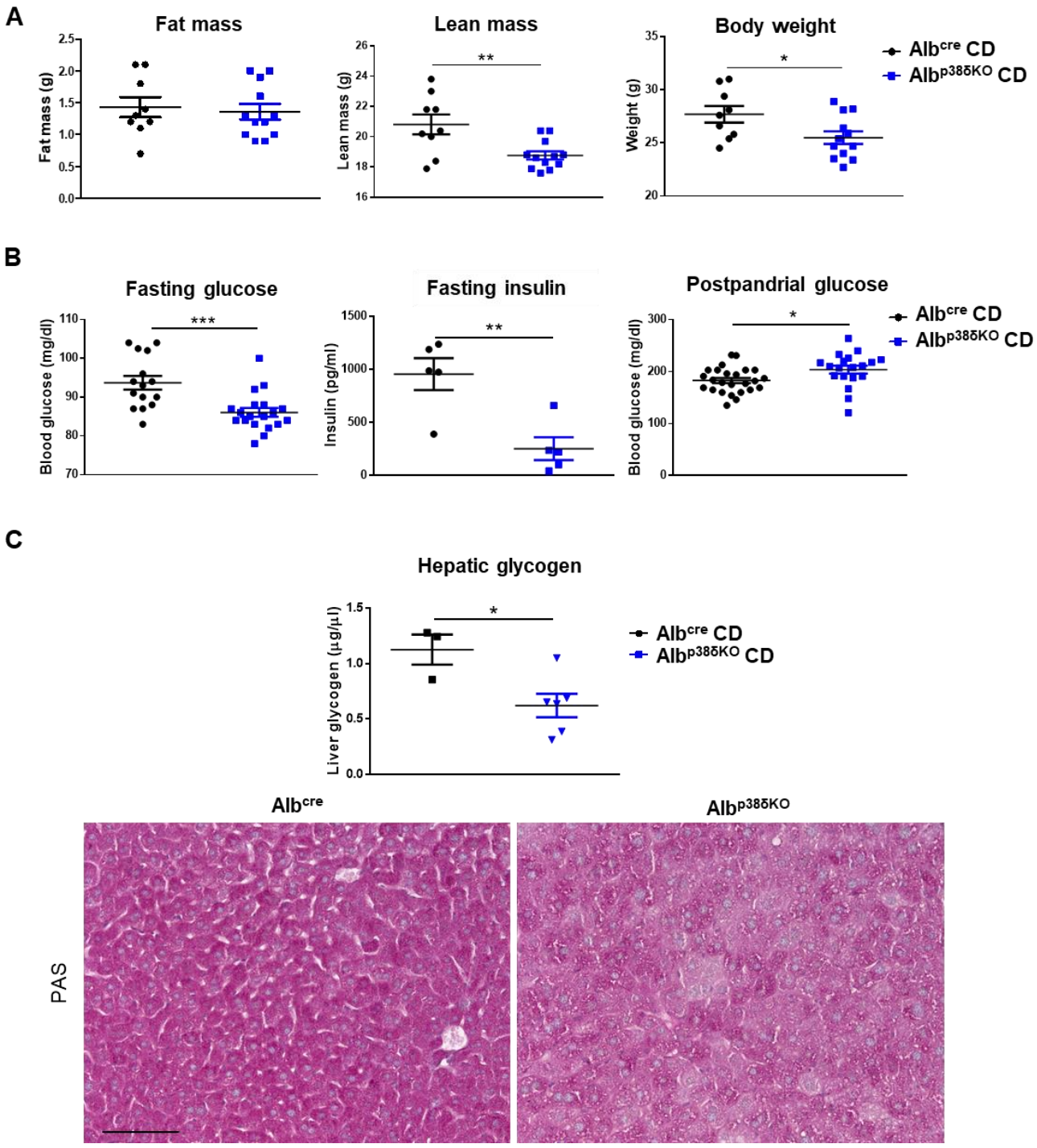
A
Fat mass
Fat mass (g)
Lean mass
Lean mass (g)
Body weight
Weight (g)
Alb^cre CD
Alb^p38δKO CD
B
Fasting glucose
Blood glucose (mg/dl)
Fasting insulin
Insulin (pg/ml)
Postpandrial glucose
Blood glucose (mg/dl)
C
Hepatic glycogen
Liver glycogen (µg/µl)
Alb^cre
Alb^p38δKO
PAS

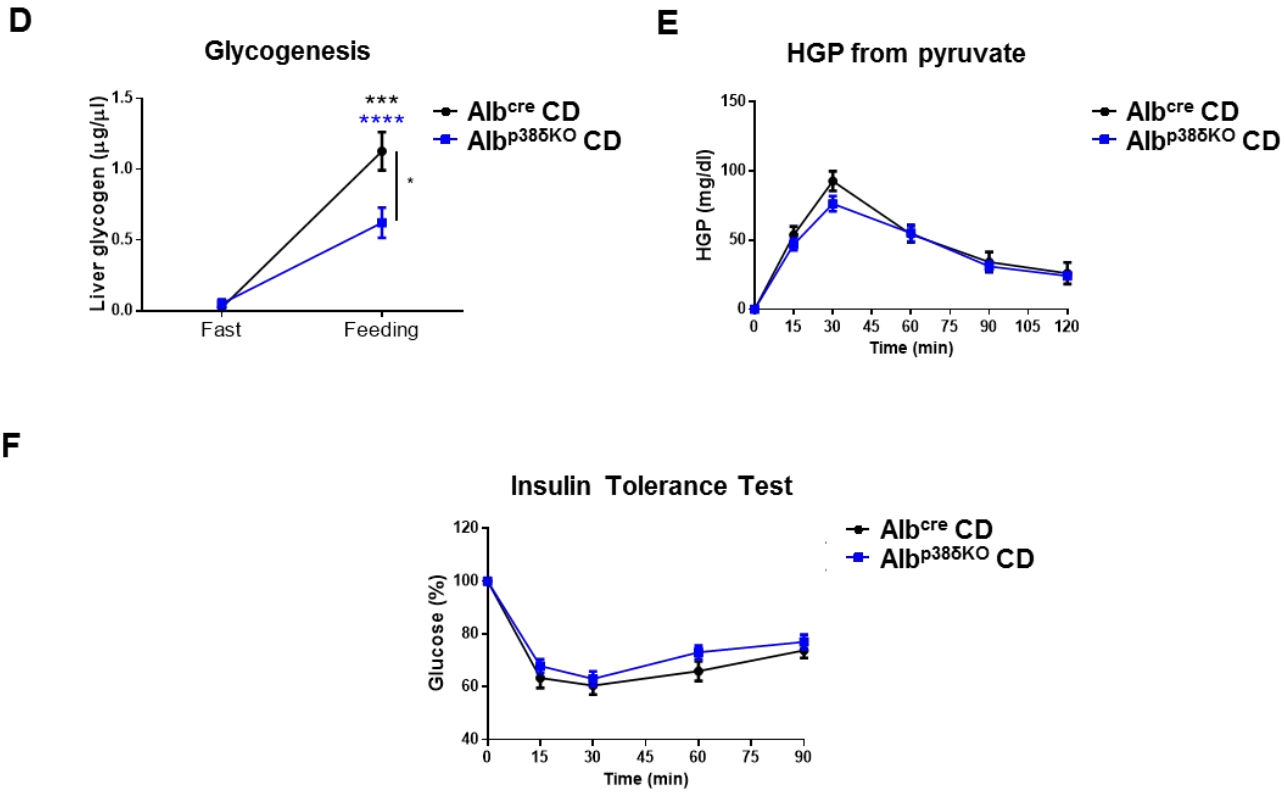
D
Glycogenesis
Liver glycogen (µg/µl)
1.5
1.0
0.5
0.0
***
****
*
Fast
Feeding
Alb^cre CD
Alb^p38δKO CD
E
HGP from pyruvate
HGP (mg/dl)
150
100
50
0
0 15 30 45 60 75 90 105 120
Time (min)
Alb^cre CD
Alb^p38δKO CD
F
Insulin Tolerance Test
Glucose (%)
120
100
80
60
40
0 15 30 45 60 75 90
Time (min)
Alb^cre CD
Alb^p38δKO CD
G
Alb^cre
Alb^p38δKO
H&E

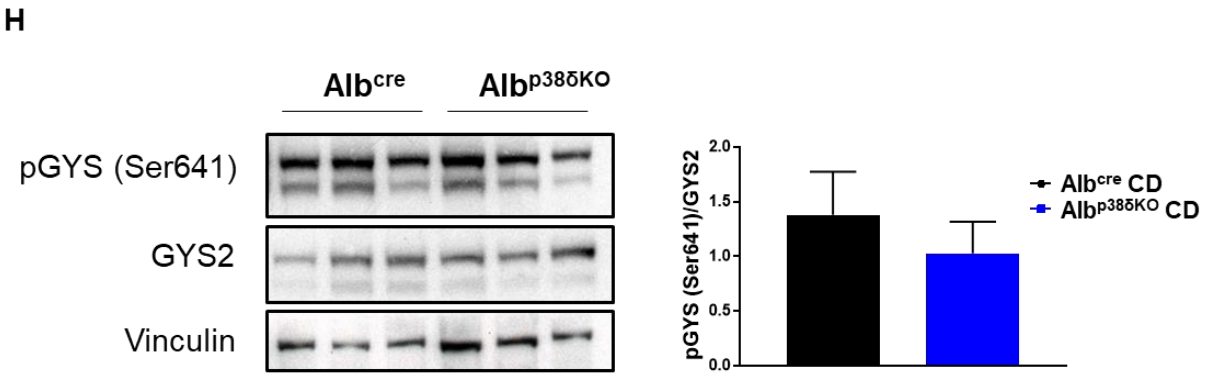

Figure 8: Alb$^{p38\delta KO}$ also show reduced liver glycogen storage and blood glucose levels in chow diet (CD).
A) Fat mass, lean mass and body weight of hepatic specific p38δ deficient mice (Alb$^{p38\delta KO}$) and control mice (Alb^{cre}) fed with CD (8 weeks), (mean ± SEM, n=9-12). B) Plasma glucose and insulin levels upon overnight fasting (16 hours) in CD-fed control and Alb$^{p38\delta KO}$ mice (left and central graphs). Plasma insulin levels were measured from cheek blood samples by Luminex analyses. Right: Postprandial glucose (mean ± SEM, n=15-19). C) Up: Glycogen content measured in the liver under fed conditions in CD-fed control and hepatic p38δ deficient mice (mean ± SEM, n=3-6). Down: Representative liver sections stained with Periodic acid–Schiff (PAS) staining. Scale bar=50µm D) Glycogenesis rate was measured as difference between liver glycogen levels in CD-fed control and knockout mice after overnight fasting and 2 hours feeding (mean ± SEM, n=3-6). E) HGP from GNG upon intraperitoneal injection of sodium pyruvate (2mg/kg) in 16-18 weeks old CD-fed control and hepatic p38δ deficient mice. Blood glucose levels from each genotype are relativized to basal blood glucose levels (time 0). F) Insulin tolerance test CD-fed mice. Blood glucose concentration was measured in mice upon intraperitoneal insulin injection (0.75 IU/kg) after 1 h of food deprivation (mean ± SEM, n=15-20). G) Representative liver sections from control (Alb^{cre}) and Alb$^{p38\delta KO}$ mice fed a CD stained with hematoxylin and eosin. Scale bar=50µm (mean ± SEM, n=5). H) Inmunoblot analysis of pGYS2 and GYS2 expression in the livers of mice upon 2h feeding. Image J was used to quantify GYS phosphorylation at Ser641. (mean ± SEM, n=3) *$p < 0.05$, **$p < 0.01$, ***$p < 0.001$, ****$p < 0.0001$ (two-way ANOVA coupled to Bonferroni's post-tests or unpaired *t* test).

9. Measure of hepatic flux rates that contribute to EGP by positional isotopomer NMR analysis

To further study HGP and to confirm whether reduced glycogen storage promotes blood glucose levels reduction in mice lacking p38δ in hepatocytes, we performed the positional isotopomer NMR tracer analysis (PINTA) in CD-fed mice. This new methodology allows to directly measure hepatic flux that contributes to the HGP *in vivo*, by simply assessing the positional isotopomer enrichments of the C_4 and C_5 carbons of plasma glucose using combined ^{13}C NMR/gas chromatography-mass spectrometry analysis of plasma following infusion of (3-^{13}C)-lactate and glucose tracer to assess rates of HGP (Perry et al., 2017).

Since we did not see differences in basal HGP after 4h food deprivation in HFD-fed mice, we decided to expose CD-fed mice to longer fasting time (16h). However, no differences in global endogenous glucose production was found (Figure 9A). When we directly measured pyruvate carboxylase flux (V_{PC}), which generates the main gluconeogenic substrate OAA; we found a slight, not significant increase in its activity in Alb$^{p38\delta KO}$ mice (Figure 9B). This also supports that there are no differences in GNG between genotypes. In agreement with no changes

in V_{PC}, no differences in liver acetyl-CoA levels, which is the main pyruvate carboxylase allosteric activator (Jitrapakdee et al., 2008), were found between genotypes (Figure 9E). However, plasma AA levels, which are also gluconeogenic substrates, were increased in $Alb^{p38\delta KO}$ mice (Figure 9F), explaining the slight increase in the $V_{PC.}$ However, when we measured the HGP from glycerol and glycogen, $Alb^{p38\delta KO}$ mice showed a reduction compared to control mice (Figure 9C). Glycerol that contributes to GNG comes mainly from white fat lipolysis. As $Alb^{p38\delta KO}$ mice did not show differences in plasma glycerol levels (Figure 9D), low liver glycogen content may be the main responsible for the decrease EGP observed in $Alb^{p38\delta KO}$ mice. PINTA also measures CS flux (V_{CS}) *in vivo*, a key enzyme in the Krebs cycle, an important pathway for hepatic mitochondrial fatty acid β-oxidation; but which is also required for the endergonic steps of GNG, among other things to generate OAA, the main gluconeogenic substrate. V_{CS} was decreased in $Alb^{p38\delta KO}$ (Figure 9G), suggesting impaired mitochondrial Krebs cycle. Moreover, the V_{CS} decrease could contribute to reduce OAA levels, and in consequence the partial GNG activation, which will not be enough to increase blood glucose levels upon total glycogen liver depletion in $Alb^{p38\delta KO}$mice.

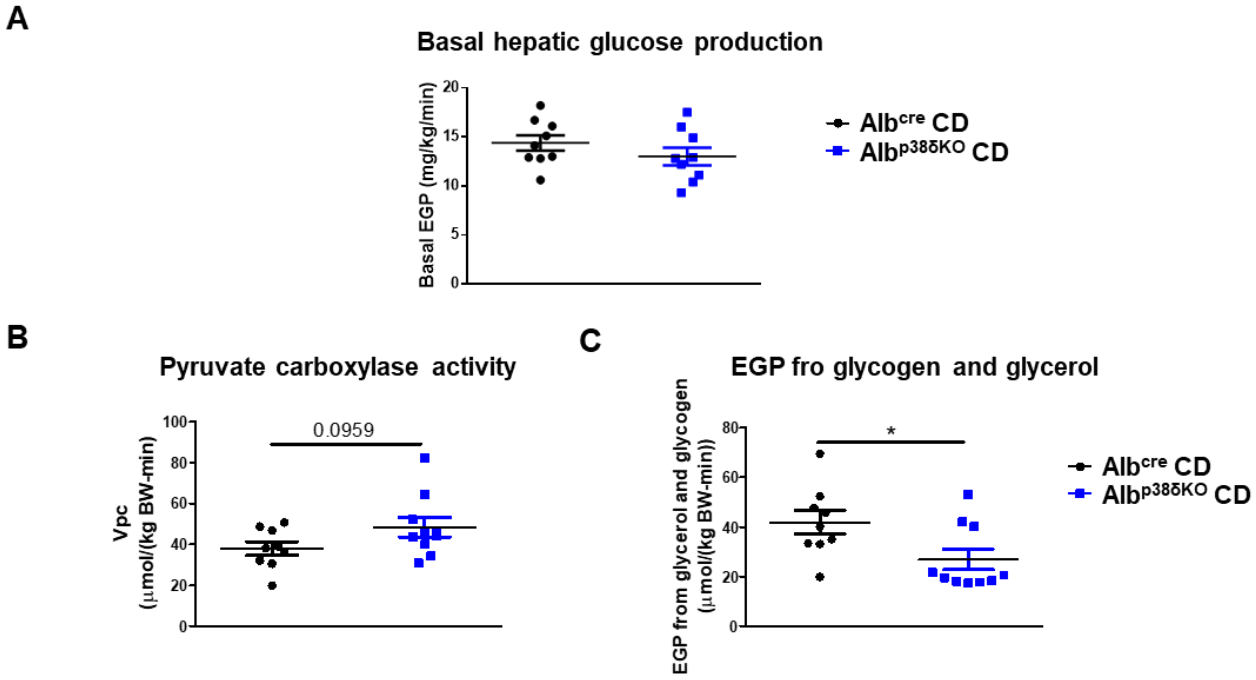

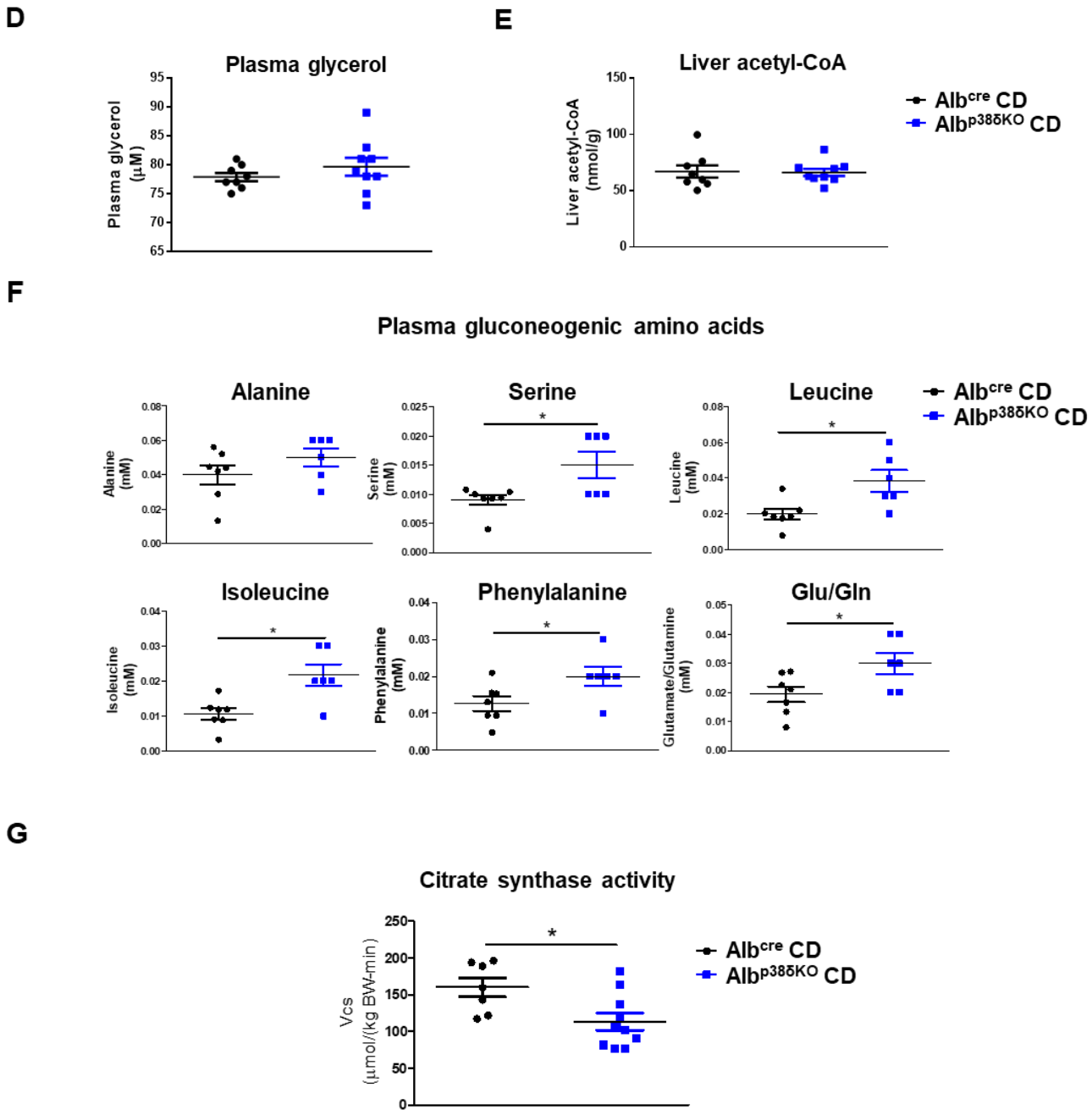

Figure 9: Reduced hepatic glycogen content and CS activity decrease EGP in Alb$^{p38\delta KO}$

Positional isotopomer NMR tracer analysis (PINTA), using combined NMR/gas chromatography-mass spectrometry analysis of plasma following infusion of (3-^{13}C)-lactate (120 µmol/(kg-min) prime for 5 min, 40 µmol/(kg-min) continuous infusion for 120 min) and glucose tracer ((3-^{3}H)-glucose, 0.1mg/(kg-min) prime for 5 min, 0.3mg/(kg-min) for 120 min), in 16-18 weeks old CD-fed mice after overnight (16 hours) fasting. A) Basal hepatic glucose production. B) Liver pyruvate carboxylase flux, determined from the anaplerotic flow into OAA. C) HGP from glycogen and glycerol, measured subtracting the rates of V_{PC} from the total EGP. D) Plasma glycerol measured by gas chromatography –mass spectrometry (GC-MS). E) Liver acetyl-CoA content was measured by liquid chromatography-mass spectrometry (LC-MS/MS). F) Plasma amino acids (AA) levels

measured by GC-MS. G) Liver CS flux, defined as the flux of the CS reaction in the Krebs cycle. (mean ± SEM, n=7-10) **p* < 0.05 (unpaired *t* test).

10. Increased KG in Alb$^{p38\delta KO}$ chow fed mice

Alb$^{p38\delta KO}$ mice fed with CD also showed reduced blood glucose levels. When glucose is insufficient, cells usually shift to oxidize lipids; however decreased V_{CS} in CD-fed knockout mice (Figure 9G), suggested reduced Krebs cycle and lipid β-oxidation. However, we did not find changes in ^{14}C-palmitate incomplete and complete oxidation in livers extracts from CD-fed mice (Figure 10A). In the same way, no differences were found in *de novo* lipogenesis; only diacylglycerides production was reduced (Figure 10B). But interestingly, Alb$^{p38\delta KO}$ mice accumulated more C_{18} long-chain acyl-CoA in the liver (Figure 10C).

As Alb$^{p38\delta KO}$ mice had low blood glucose levels, and lipid β oxidation did not change; we explored KG pathway, because mainly ketone bodies (acetoacetate (AcAc) and 3HB, are usually produced when there is not available glucose in blood and there are not enough glycogen stores to supply energy demand of extrahepatic tissues (Grabacka et al., 2016, Puchalska and Crawford, 2017). We found increased 3HB plasma levels in Alb$^{p38\delta KO}$ mice (Figure 10D); suggesting, Alb$^{p38\delta KO}$ mice use KG as main pathway to get energy, due to low glucose availability. However, surprisingly fasting Fgf21 plasma levels were found reduced (Figure 10E).

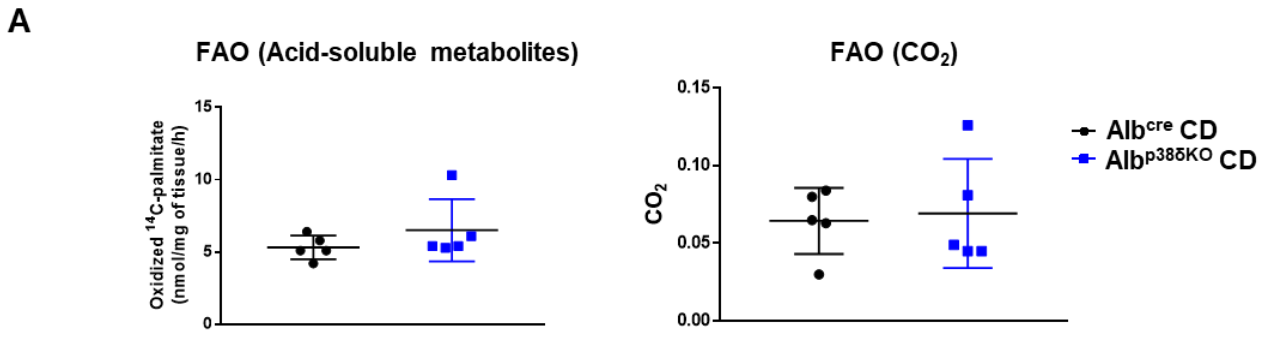

B

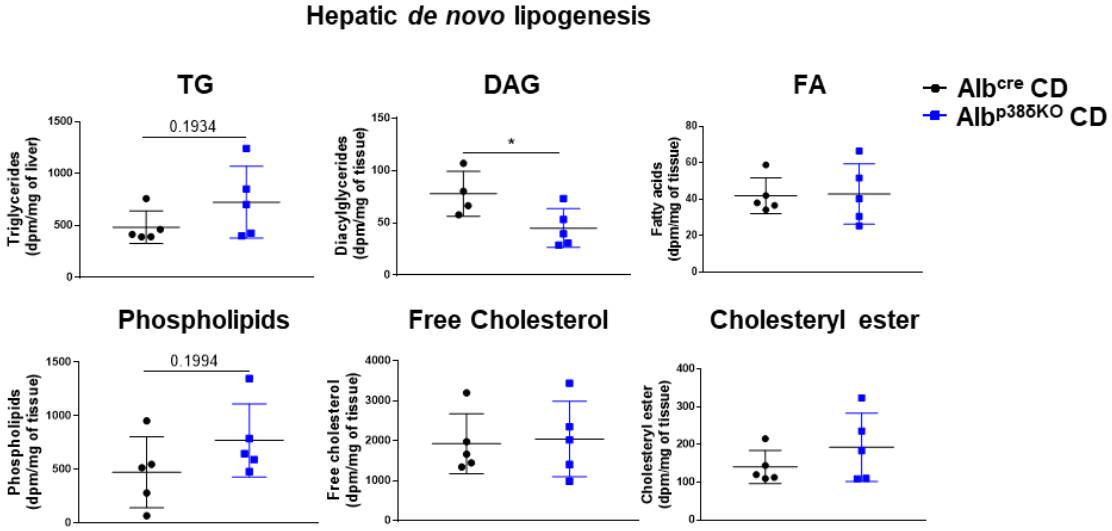
Hepatic *de novo* lipogenesis
TG
DAG
FA
Triglycerides (dpm/mg of liver)
Diacylglycerides (dpm/mg of tissue)
Fatty acids (dpm/mg of tissue)
0.1934
*
Albcre CD
Albp38δKO CD
Phospholipids
Free Cholesterol
Cholesteryl ester
Phospholipids (dpm/mg of tissue)
Free cholesterol (dpm/mg of tissue)
Cholesteryl ester (dpm/mg of tissue)
0.1994

C

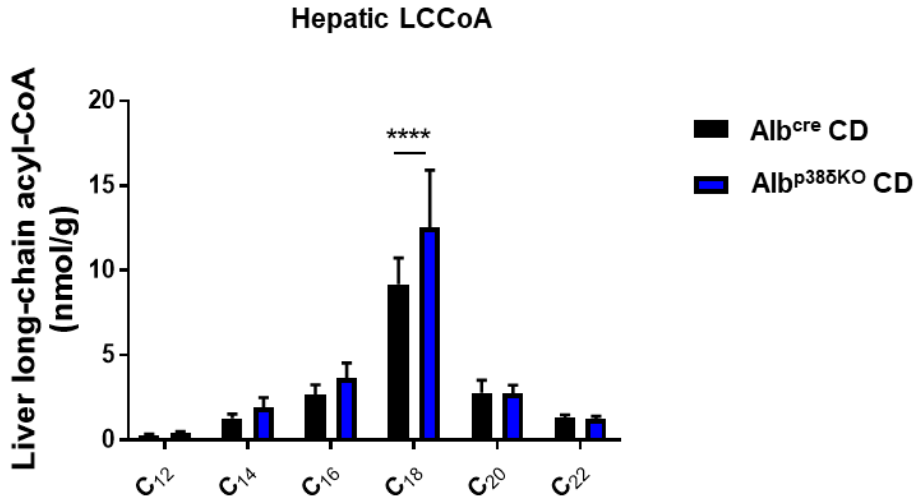
Hepatic LCCoA
Liver long-chain acyl-CoA (nmol/g)
****
Albcre CD
Albp38δKO CD
C12
C14
C16
C18
C20
C22

D

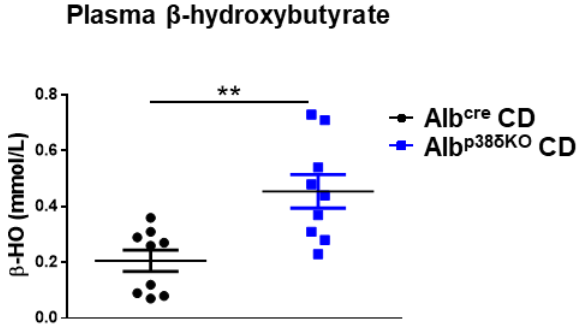
Plasma β-hydroxybutyrate
β-HO (mmol/L)
**
Albcre CD
Albp38δKO CD

E

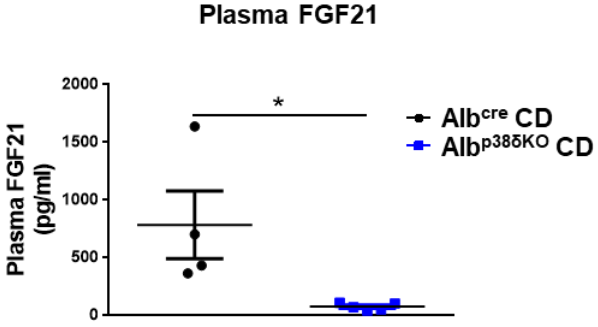
Plasma FGF21
Plasma FGF21 (pg/ml)
*
Albcre CD
Albp38δKO CD

Figure 10: CD-fed Alb$^{p38\delta KO}$ mice use KG as energy source during fasting

A) Complete and incomplete ^{14}C-palmitate β-oxidation rate in liver extracts from CD-fed control and hepatic specific p38δ knockout mice. Complete oxidation was measured as $^{14}CO_2$ levels and incomplete oxidation was measured as levels of acid-soluble metabolites containing the ^{14}C radiolabeled (mean ± SEM, n=5). B) *De novo* triglycerides (TG), diacylglycerols (DAG), fatty acids (FA), phospholipids, free cholesterol and cholesteryl-ester synthesis upon ^{3}H-acetate incorporation in liver extracts from control and hepatic specific p38δ knockout mice (mean ± SEM, n=5. C) Liver fasting long-chain acyl CoA profile measured by LC-MS/MS (mean ± SEM, n=9). D) Plasma β-hydroxybutyrate levels were measured by COBAS (mean ± SEM, n=9). E) FGF21 plasma levels of CD-fed mice fasted overnight was measured by ELISA (mean ± SEM, n=4-5). *$p < 0.05$, **$p < 0.01$, ****$p < 0.0001$ (unpaired *t* test or multiple-comparison using the Holm-Sidak method).

11. Hepatic specific p38δ deletion protects against obesity-induced NAFLD

Insulin resistance is associated with the development of NAFLD (Williamson et al., 2011), but also NAFLD induces insulin resistance (Gruben et al., 2014). Therefore, as Alb$^{p38\delta KO}$ mice were protected against hepatic and whole-body insulin resistance, we decided to explore hepatic steatosis. Reduced liver weight in HFD-fed Alb$^{p38\delta KO}$ mice correlated with reduced lipid droplets and triglycerides levels in the liver of these mice compared with control mice (Alb^{cre}) (Figure 11A). Suggesting that HFD-fed Alb$^{p38\delta KO}$ mice were protected against NAFLD and in consequence this might explain their protection against insulin resistance. Actually, liver RNA-seq analysis indicated that NF-κB pathway, a main driver of insulin resistance, is downregulated in livers from Alb$^{p38\delta KO}$ mice (activation z-score in control mice= 2.614, p-value=) (data do not show in upstream regulator graph from RNA-seq analysis).

To evaluate whether changes in liver lipid metabolism might be involved in the protection against NAFLD we evaluated DNL and the lipid β-oxidation. Alb$^{p38\delta KO}$ mice presented reduced DNL of triglycerides, DAG, free cholesterols and cholesteryls ester measured upon ^{3}H-acetate incorporation in liver extracts (Figure 11B). This reduction could be due to the lack of intermediates substrates needed to build lipids, as a consequence of glycolysis reduction observed (Figure 11C). We next evaluated lipid β-oxidation pathway, upon ^{14}C-palmitate incorporation in liver extracts. Alb$^{p38\delta KO}$ mice showed higher incomplete oxidation than control mice (Figure 11C), to judge by increased ASM containing the ^{14}C radiolabeled found in the liver of Alb$^{p38\delta KO}$ mice after ^{14}C-palmitate incorporation. ASM include: palmitoyl-carnitine, acetyl-carnitine, acetyl-CoA, ketone bodies, gluconeogenic intermediates, cataplerotic Krebs cycle intermediates and fatty acyl-CoAs shorter than 6 carbons (Huynh et al., 2014). However, no differences were found in the lipid complete β-oxidation, which involves completed Krebs cycle and OXPHOS function, with the subsequent CO_2 production (Figure 11C). The increase only in the incomplete lipid β-oxidation might indicate a deficient mitochondrial function.

To further explore the mitochondria functionality, we directly measured ATP production in isolated mitochondria from livers of $Alb^{p38\delta KO}$ and control mice. We found a reduction in the ATP production in isolated mitochondria from knockout mice, when palmitoyl-CoA was used as substrate for respiration (Figure 11D). However, no differences were found with other substrates: succinate, neither with glutamate/malate (Figure 11D). These results confirmed a defect in the mitochondria during lipid β-oxidation in mice lacking p38δ in hepatocytes, probably at the Krebs cycle levels, accordingly with the reduced complete ^{14}C-palmitate β-oxidation previously described (Figure 11C).

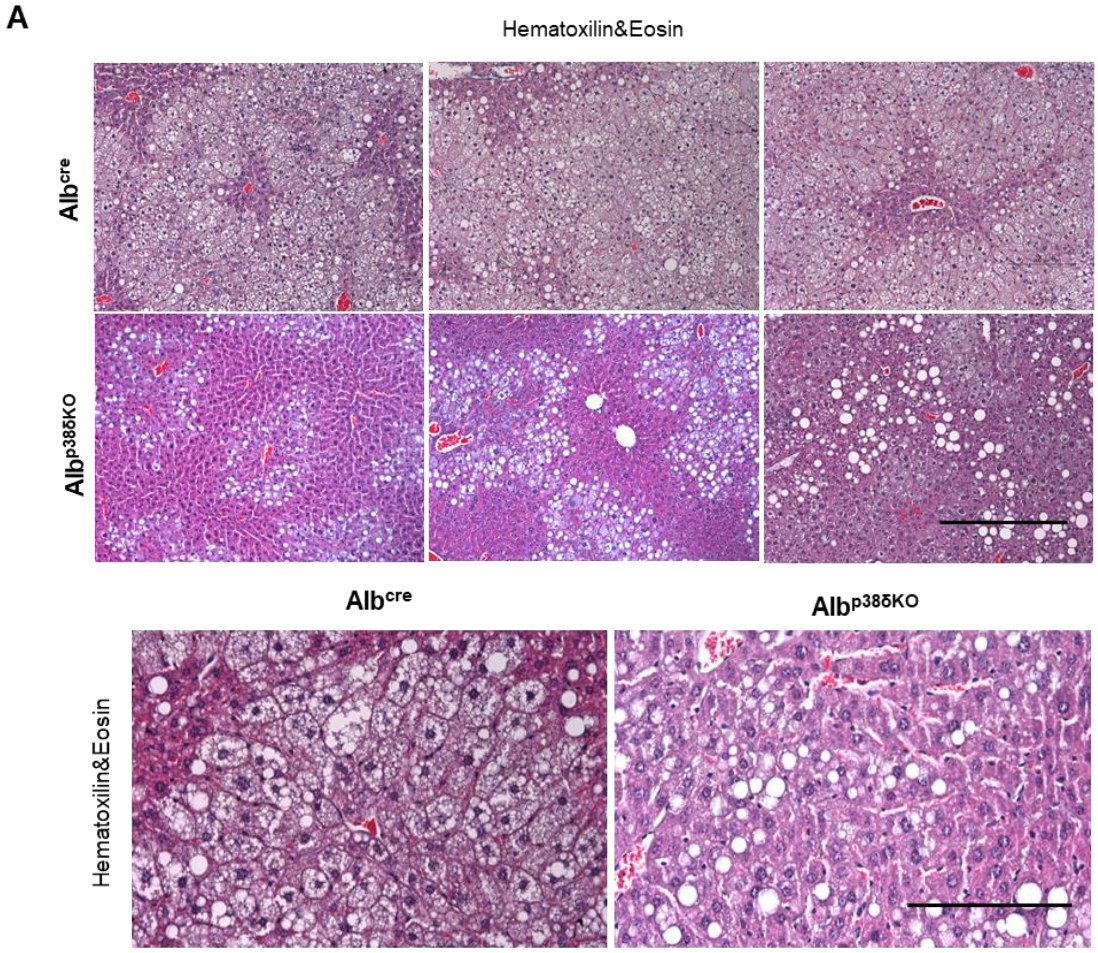

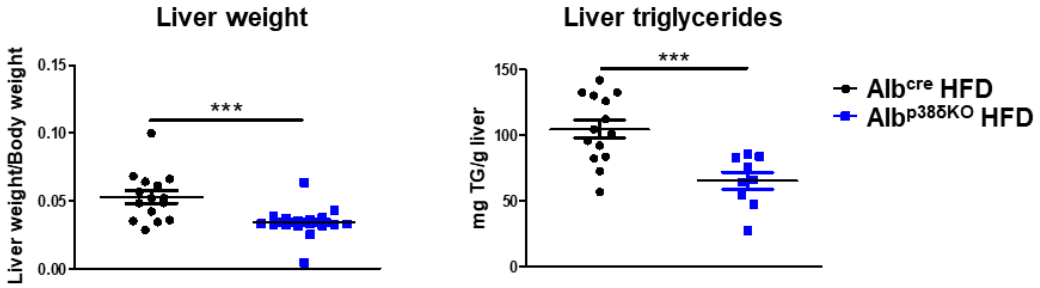
Liver weight
Liver weight/Body weight
0.15
0.10
0.05
0.00
***
Liver triglycerides
mg TG/g liver
150
100
50
0
***
Alb^cre HFD
Alb^p38δKO HFD

B

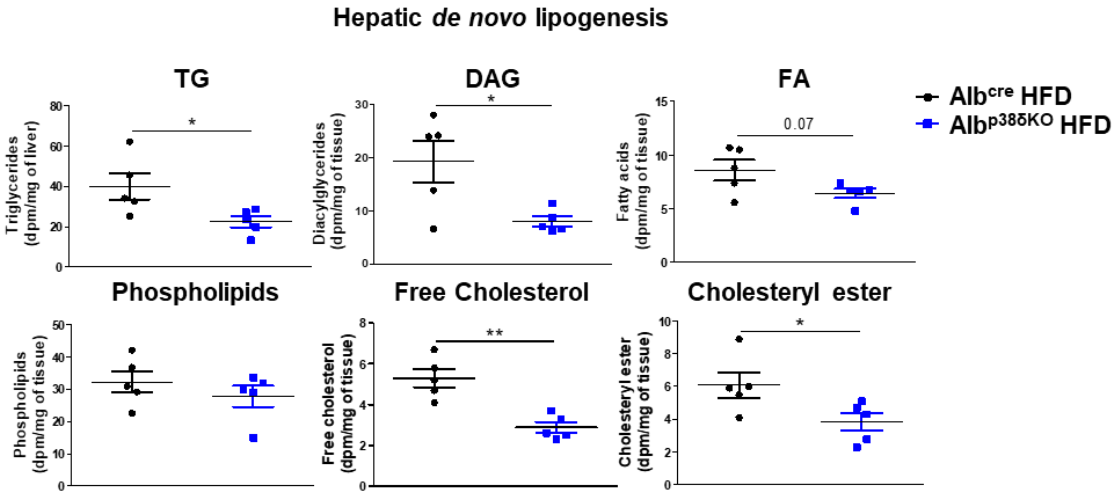
Hepatic *de novo* lipogenesis
TG
Triglycerides (dpm/mg of liver)
*
DAG
Diacylglycerides (dpm/mg of tissue)
*
FA
Fatty acids (dpm/mg of tissue)
0.07
Alb^cre HFD
Alb^p38δKO HFD
Phospholipids
Phospholipids (dpm/mg of tissue)
Free Cholesterol
Free cholesterol (dpm/mg of tissue)
**
Cholesteryl ester
Cholesteryl ester (dpm/mg of tissue)
*

C

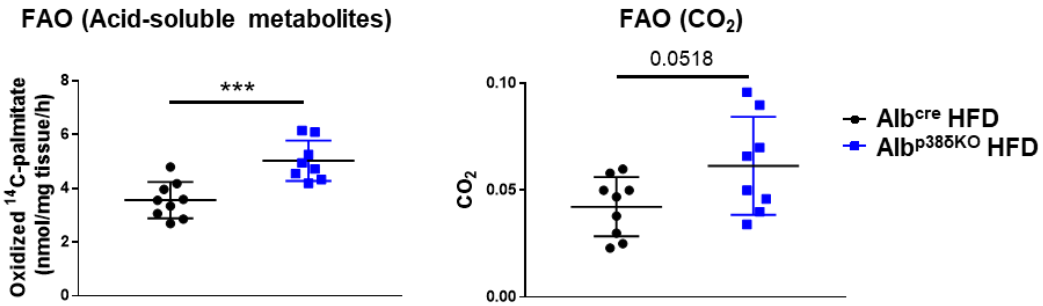
Hepatic lipid β-oxidation
FAO (Acid-soluble metabolites)
Oxidized ¹⁴C-palmitate (nmol/mg tissue/h)
***
FAO (CO₂)
CO₂
0.0518
Alb^cre HFD
Alb^p38δKO HFD

D

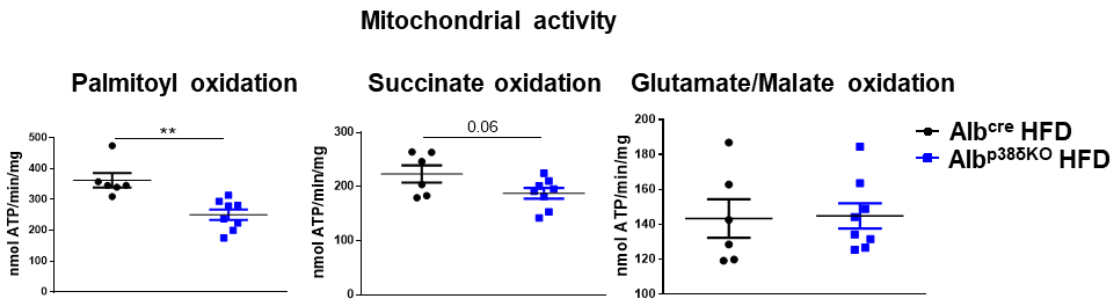
Mitochondrial activity
Palmitoyl oxidation
nmol ATP/min/mg
**
Succinate oxidation
nmol ATP/min/mg
0.06
Glutamate/Malate oxidation
nmol ATP/min/mg
Alb^cre HFD
Alb^p38δKO HFD

Figure 11: Alb$^{p38\delta KO}$ mice are protected against NAFLD as a consequence of decreased DNL and augmented incomplete lipid β-oxidation

A) Representative liver sections from control (Alb^{cre}) and Alb$^{p38\delta KO}$ mice fed a HFD for 8 weeks stained with hematoxylin and eosin. Scale bar=200µm. Down: Liver weight to body weight ratios (left) and liver triglycerides for control and Alb$^{p38\delta KO}$ mice fed a HFD for 8 weeks (right) (mean ± SEM, n=9-19). B) *De novo* triglycerides (TG), diacylglycerols (DAG), fatty acids (FA), phospholipids, free cholesterol and cholesteryl-ester synthesis upon ^{3}H-acetate incorporation in liver extracts from control and hepatic specific p38δ knockout mice (mean ± SEM, n=5. C) Complete and incomplete ^{14}C-palmitate β-oxidation rate in liver extracts from HFD-fed control and hepatic specific p38δ knockout mice. Complete oxidation was measured as $^{14}CO_2$ levels and incomplete oxidation was measured as levels of acid-soluble metabolites containing the ^{14}C radiolabeled (mean ± SEM, n=8-9). D) Palmitoyl, succinate and glutamate+malate-driven ATP synthesis in isolated mitochondria from HFD-fed control and knockout livers (mean ± SEM, n=6-8 mitochondrial homogenized from 3-4 mice) *$p < 0.05$, **$p < 0.01$, ***$p < 0.001$ (unpaired *t* test).

12. Exploring mechanisms that protect mice lacking p38δ in hepatocytes against NAFLD

To explore the underlaying mechanisms involved in the increase of the incomplete lipid β-oxidation and the decrease of *de novo* lipogenesis, we performed RNA-sequencing analyses in livers from control and HFD-fed mice lacking p38δ in hepatocytes upon overnight fasting. Negative z-score indicates upregulation in Alb$^{p38\delta KO}$ livers. We found PPARα pathway was upregulated in livers from Alb$^{p38\delta KO}$ mice (z-score= -2.209, p-value= 4.00E^{-14}) (Figure 12A). PPARα is the main hepatic pathway that drives fatty acid oxidation by peroxisomes, mitochondria and also ER (Evans et al., 2004, Pyper et al., 2010). Therefore, PPARα pathway upregulation in fasted Alb$^{p38\delta KO}$ livers is in agreement with high lipid β-oxidation and protection against hepatic steatosis found in these mice. Furthermore, PPARδ pathway, which also promotes lipid oxidation and decreases lipogenesis (Nagasawa et al., 2006, Wu et al., 2011, Bojic et al., 2014), was upregulated in the livers from fasted Alb$^{p38\delta KO}$ mice (z-score -1.227, p-value= 1.10E^{-14}) (Figure 12A); supporting again the high lipid oxidation and low lipogenesis found in these mice.

To further explore whether PPARα might mediate the increase lipid oxidation in Alb$^{p38\delta KO}$ mice, we checked blood levels of FGF21, a main mediator of PPARα effects that protects against hepatic steatosis (Lundasen et al., 2007, Inagaki et al., 2007, Badman et al., 2007, Xu et al., 2009a). FGF21 plasma levels were only slightly higher in fasted obese Alb$^{p38\delta KO}$ mice compared to control mice (Figure 12B). However, interestingly FGF21 plasma levels were definitively reduced in Alb$^{p38\delta KO}$ after feeding (Figure 12B).

To further explore whether FGF21 was triggering the high lipid oxidation in mice lacking p38δ in hepatocytes, we generated the double hepatic specific FGF21/p38δ knockout mice (Alb$^{p38\delta/FGF21KO}$). Surprisingly, Alb$^{p38\delta/FGF21KO}$ mice still presented high lipid incomplete oxidation compared to control mice, and interestingly they had higher complete oxidation than Alb$^{p38\delta KO}$ mice (Figure 12C).

A

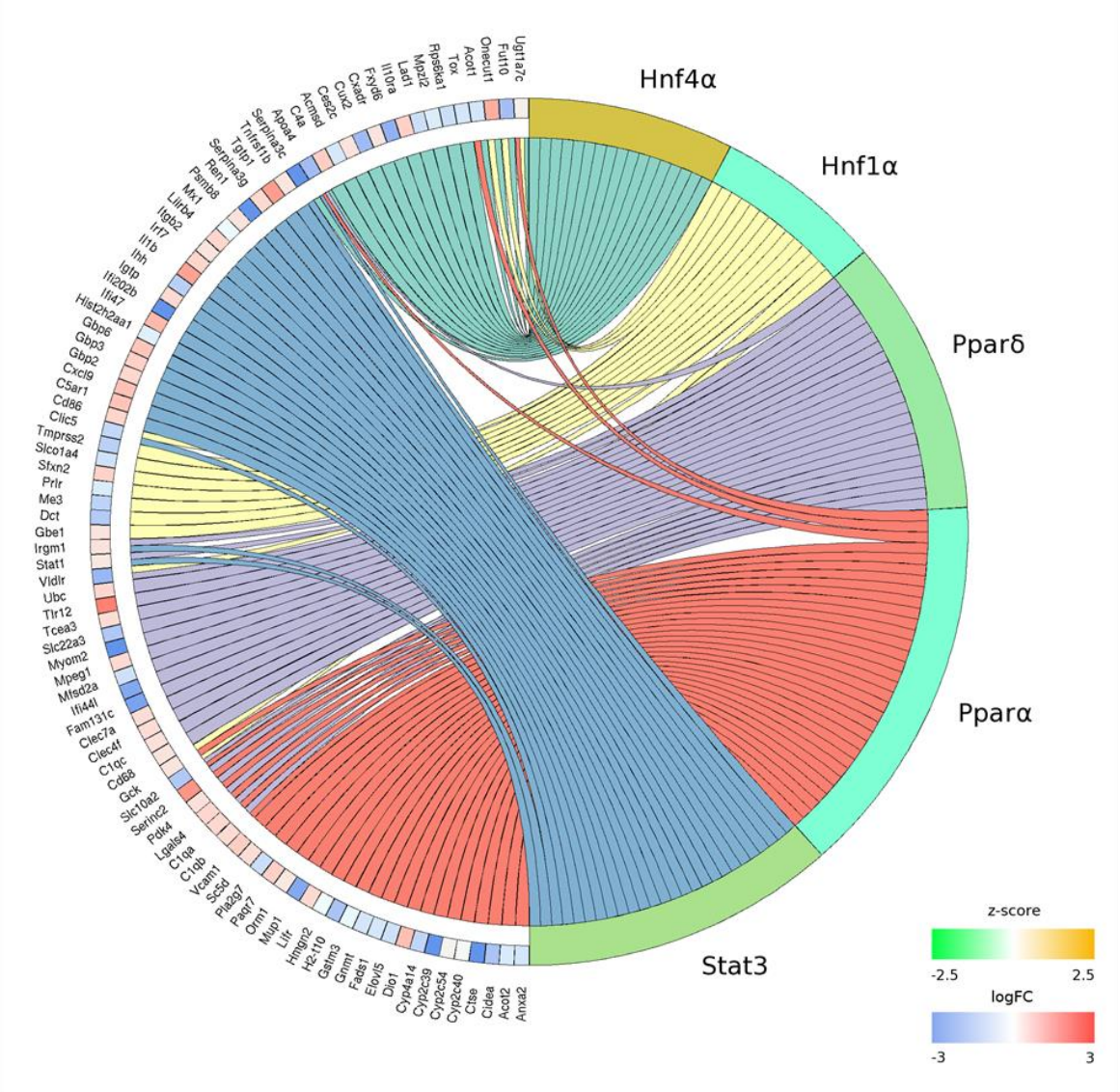
Hnf4α
Hnf1α
Pparδ
Pparα
Stat3
z-score
-2.5
2.5
logFC
-3
3

B

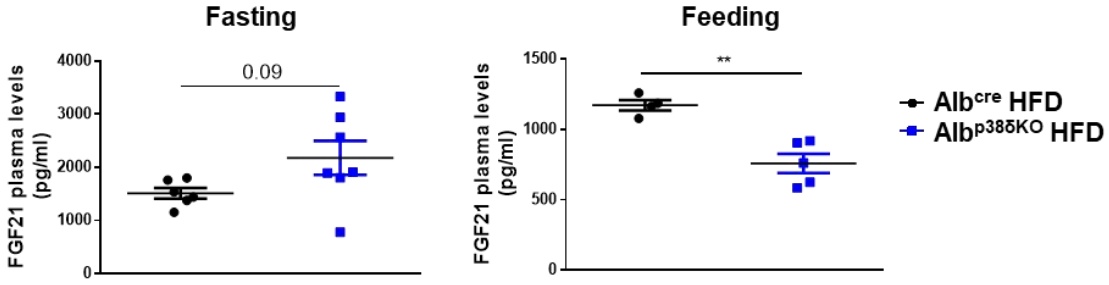
Fasting
Feeding
FGF21 plasma levels (pg/ml)
0.09
**
Alb^cre HFD
Alb^p38δKO HFD

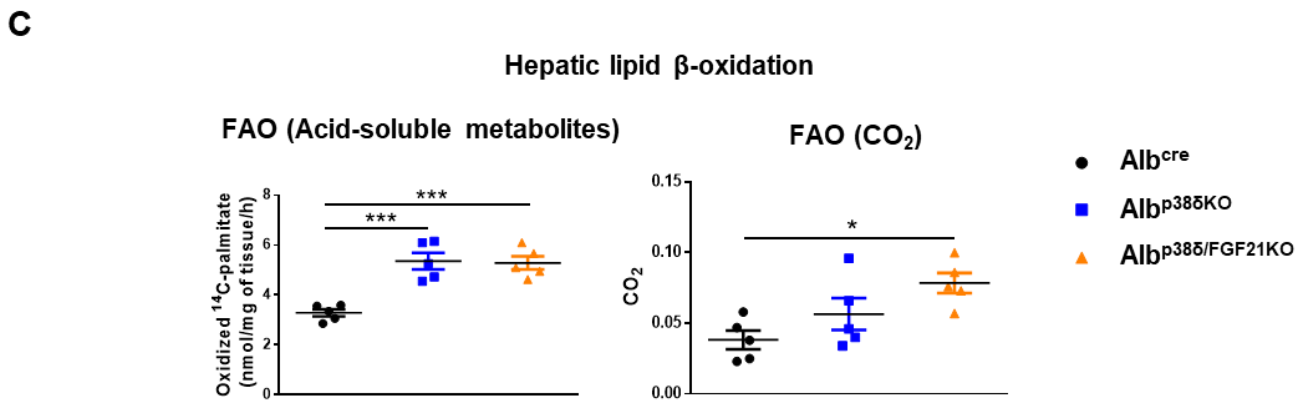

Figure 12: PPARα upregulation could protect Alb$^{p38\delta KO}$ mice against NAFLD

A) Gene expression of liver tissue from 8 weeks HFD-fed control and liver p38δ deficient mice upon overnight fasting was assessed by RNA-sequencing and results analyzed by Ingenuity® Pathway Analysis. Graphical representation of upstream regulators increases in livers of Alb$^{p38\delta KO}$ mice. Negative z-score (green color) implies activation in the Alb$^{p38\delta KO}$ mice. Negative LogFC values (blue color) means higher gene expression in Alb$^{p38\delta KO}$ mice. B) FGF21 in the blood of 8 weeks HFD-fed mice fasted overnight or after 2 hours refed was measured by ELISA (mean ± SEM, n=4-7). C) Complete and incomplete ^{14}C-palmitate β-oxidation rate in liver extracts from HFD-fed hepatic specific p38δ knockout, hepatic specific FGF21/p38δ knockout and control mice. Complete oxidation was measured as captured $^{14}CO_2$ levels and incomplete oxidation was measured as levels of acid-soluble metabolites containing the ^{14}C radiolabeled (mean ± SEM, n=5). *$p < 0.05$, **$p < 0.01$, ***$p < 0.001$ (unpaired *t* test).

13. p38δ MAPK controls glycolysis through direct PFKFB3 phosphorylation

To further explore the molecular mechanism behind the protection against NAFLD, we explored glycolysis, since it is the main pathway that generates intermediates for DNL. Hepatic glycolytic flux and lactate levels were decreased in HFD-fed Alb$^{p38\delta KO}$ mice (Figure 13A). Then, we focused our attention in PFKFB or PFK2 enzymes because these enzymes catalyze the synthesis and the degradation of Fru-2,6-P_2, which is the most potent allosteric activator of PFK1, a key glycolytic enzyme. Accordingly, to less glycolysis rate, less PFK2 activity was found in the livers from HFD-fed Alb$^{p38\delta KO}$ mice (Figure 13B), suggesting also decreased PFKFB activity. Moreover, since it has been previously described that p38/MK2 phosphorylates the isozyme 3 of PFKFB, at Ser461, increasing its activity (Novellasdemunt et al., 2013) and in the PFKFB3 sequence there are canonical phosphorylation motifs for MAPK; we wondered whether p38δ MAPK could phosphorylate and control directly PFKFB3 activity, triggering glycolysis.

Then, we explored PFKFB3 phosphorylation by p38δ MAPK through *in vitro* (by kinase assay and mass spectrometry (MS)) and *in vivo* (transfecting recombinant rat *PFKFB3* in HEK 293T cells, followed by PFKFB3 immunoprecipitation and MS analyses). We found that p38δ MAPK phosphorylates human PFKFB3 in two residues, Ser467, also previously described in a phosphoproteomic study (Robles et al., 2017); and Thr463 (Figure 13C) (For rat PFKFB3, these residues correspond with Thr492 and Ser496).

To evaluate the physiological role of p38δ MAPK phosphorylating PFKFB3, we checked Ser467 and Thr463 phosphorylation sites in fasted and fed animals. As only the phospho-Ser467 antibody is available, we also used a Phospho-MAPK Substrates (PXS*P or S*PXR/K) and Phospho-MAPK Substrates Motif [PXpTP] antibodies, they detect phospho-serine and phospho-threonine in the specific motif of phosphorylation of MAPK (S/T)PXR/K (Cuenda and Rousseau, 2007). We observed that upon feeding, PFKFB3 phosphorylation (Ser/Pro, Thr/Pro and Ser467 sites) increased in livers lysates from control mice, but not in $Alb^{p38\delta KO}$ mice (Figure 13D). Firstly, these results indicated that p38δ MAPK is able to phosphorylate PFKFB3 in Thr463 and Ser467 residues *in vivo*. Secondly, we confirmed that the PFKFB3 phosphorylation by p38δ MAPK might promote glycolysis after feeding, because mice without p38δ in hepatocytes showed reduced PFKFB3 phosphorylation and less glycolysis rate.

A

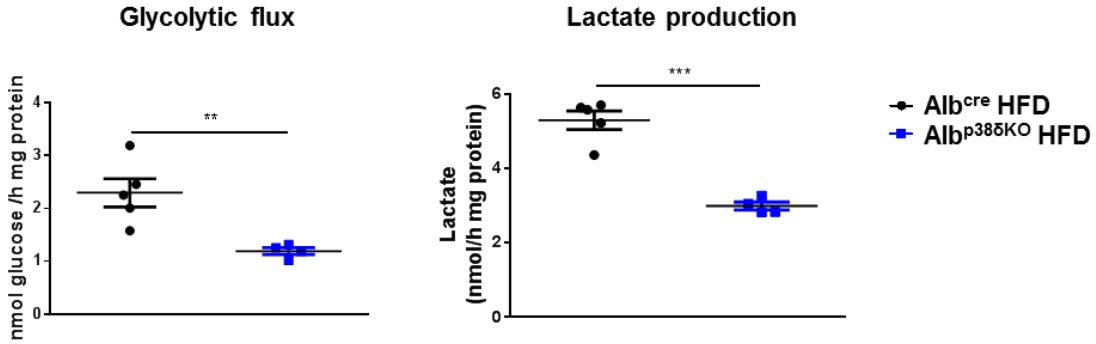
Glycolytic flux
nmol glucose /h mg protein
**
Lactate production
Lactate (nmol/h mg protein)
***
Alb^cre HFD
Alb^p38δKO HFD

B

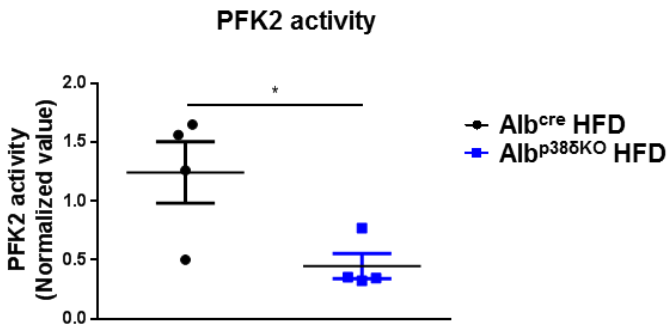
PFK2 activity
PFK2 activity (Normalized value)
*
Alb^cre HFD
Alb^p38δKO HFD

C

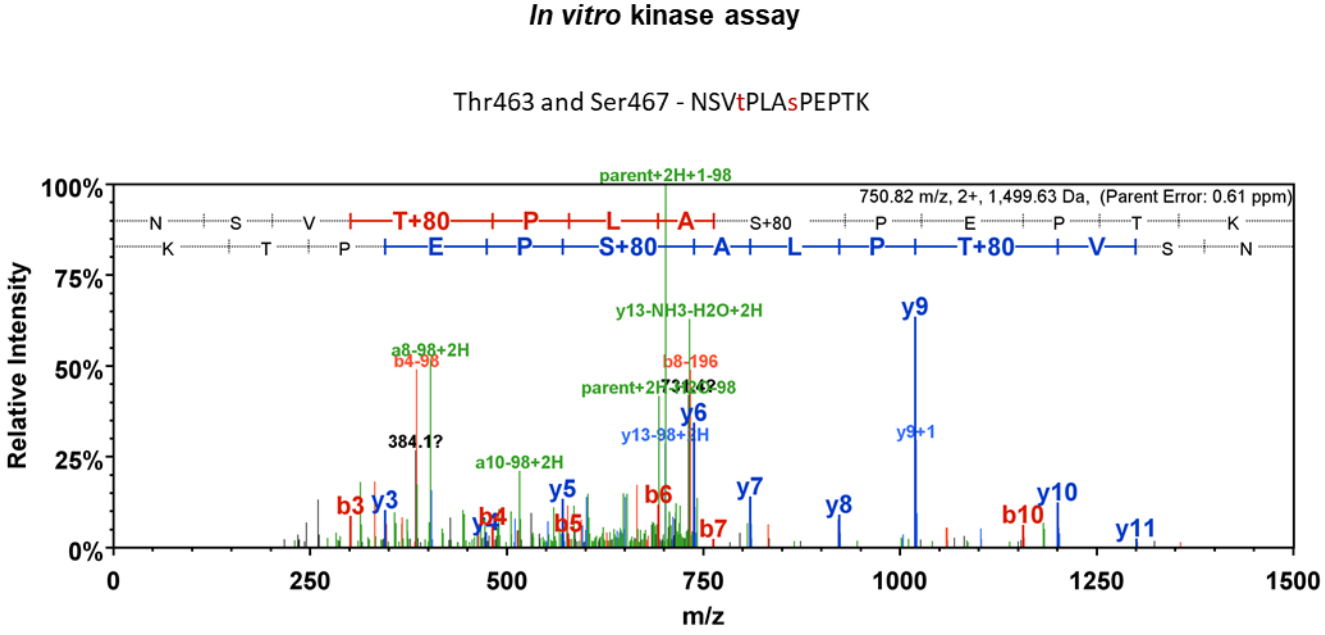
In vitro kinase assay
Thr463 and Ser467 - NSVtPLAsPEPTK
750.82 m/z, 2+, 1,499.63 Da, (Parent Error: 0.61 ppm)
Relative Intensity
m/z

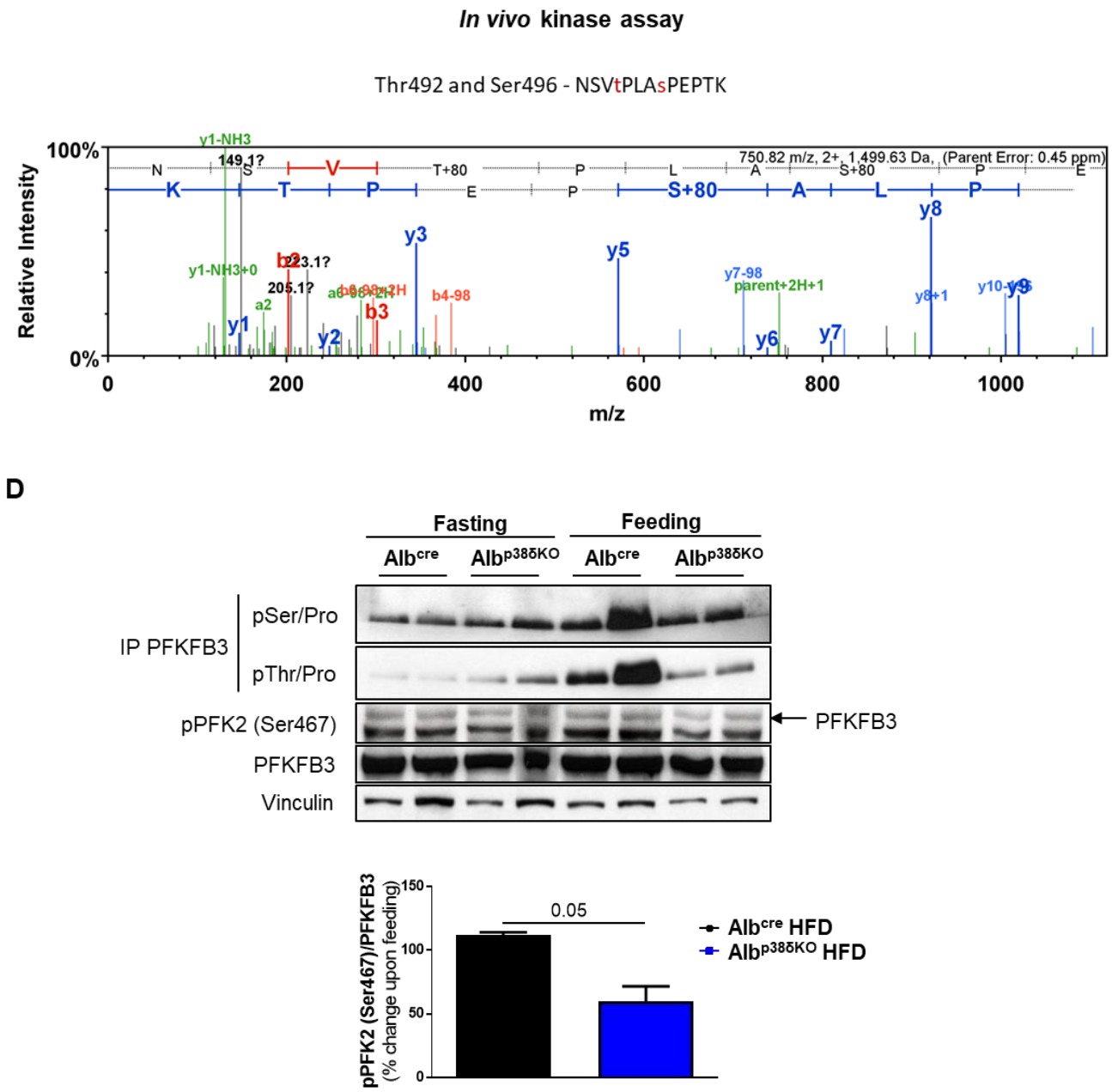

Figure 13: p38δ MAPK phosphorylates PFKFB3 *in vivo* and *in vitro*, promoting glycolysis

A) Glycolytic flux was assessed in liver extracts, measuring the conversion of D-(3-^{3}H)-glucose into ^3H_2O and also lactate levels produced during the reaction (mean ± SEM, n=4-5). B) PFK2 activity was assessed in fresh liver cuts from 8 weeks HFD-fed control and Alb$^{p38\delta KO}$ mice as relative values respect to the control and using slopes obtained from the PFK1 activity. Fructose-2-6-bisphosphate (Fru-2,6-B_2) synthesized during the reaction was used to spectrophotometrically measure PFK1 activity by determining the increments in absorbance at 340 nm for 20 min at 30 ºC (mean ± SEM, n=4-5, and technical duplicates). C) Identification of PFKFB3 phosphorylation sites by p38δ through LC-MS/MS. (Up) In an *in vitro* kinase assay, recombinant human PFKFB3 protein (1 µg) was incubated alone or in the presence of constitutively active p38δ kinase (1 µg) and 0.2 mM of cold ATP for 30 min at 37ºC. (Down) In an *In vivo* kinase assay rat pEGFP-C1-PFKFB3 (K6)

plasmid was expressed in HEK-293T cells alone or together with pCMV-HA-Flag p38δ^{F324S} which expresses the constitutively active p38δ MAPK. HEK-293T were starved overnight (16 hours). PFKFB3 phosphorylation was analyzed from GFP immunoprecipitation (2 µg) by LC-MS/MS. After in-gel trypsin digestion, peptides were monitored using the Orbitrap mass spectrometer as described in the Methods section. The panels show deduced MS/MS spectra by Scaffold (Proteome Software, Oregon) in PFKFB3 protein, validating the phosphorylation in the indicated sites in the protein (in lower case letters). Note that LC-MS/MS spectra confirm peptide phosphorylation at Ser and Thr residues in the consensus sequences SP and TP, respectively. No phosphorylation was detected in the control samples (data not shown). D) Immunoblot analysis of pPFKFB3 (Ser/Pro and Thr/Pro) upon PFKFB3 inmunoprecipitation (2 µg), pPFK2 Ser467 and PFKFB3 were done in livers extracts from 8 weeks HFD-fed control and Alb$^{p38\delta KO}$ mice upon overnight fasting (16 hours) or 2 hours refed. Vinculin protein expression was monitored as loading control. Image J was used to quantify PFK2 phosphorylation at Ser467. Data is shown as % change upon feeding. **p* < 0.05, (unpaired *t* test).

14. Global energy balance in Alb$^{p38\delta KO}$ mice

Since Alb$^{p38\delta KO}$ mice seemed to have increased lipid metabolism instead of glucose metabolism, we next examined global energy metabolism using metabolic cages. No differences in energy ex penditure, food intake, RQ and locomotor activity were found between HFD-fed and control mice; however, CD-fed Alb$^{p38\delta KO}$ showed reduced RQ, without differences in any of the other measured parameters (Figure 14).

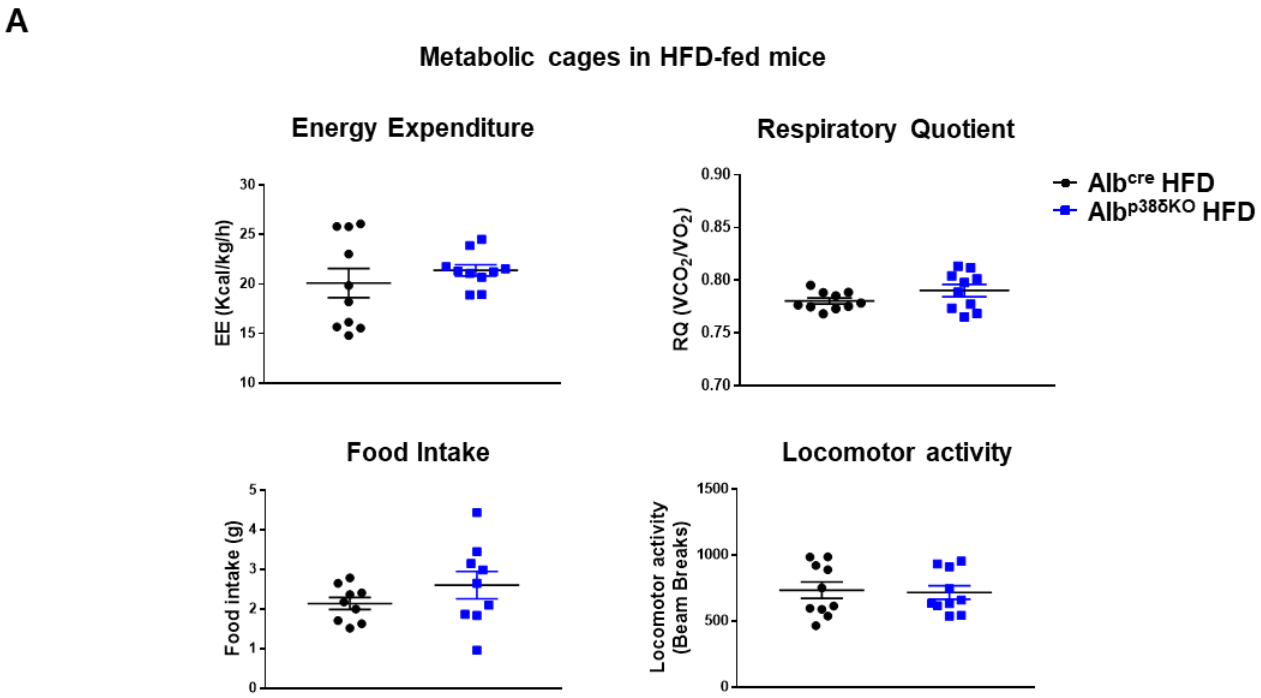

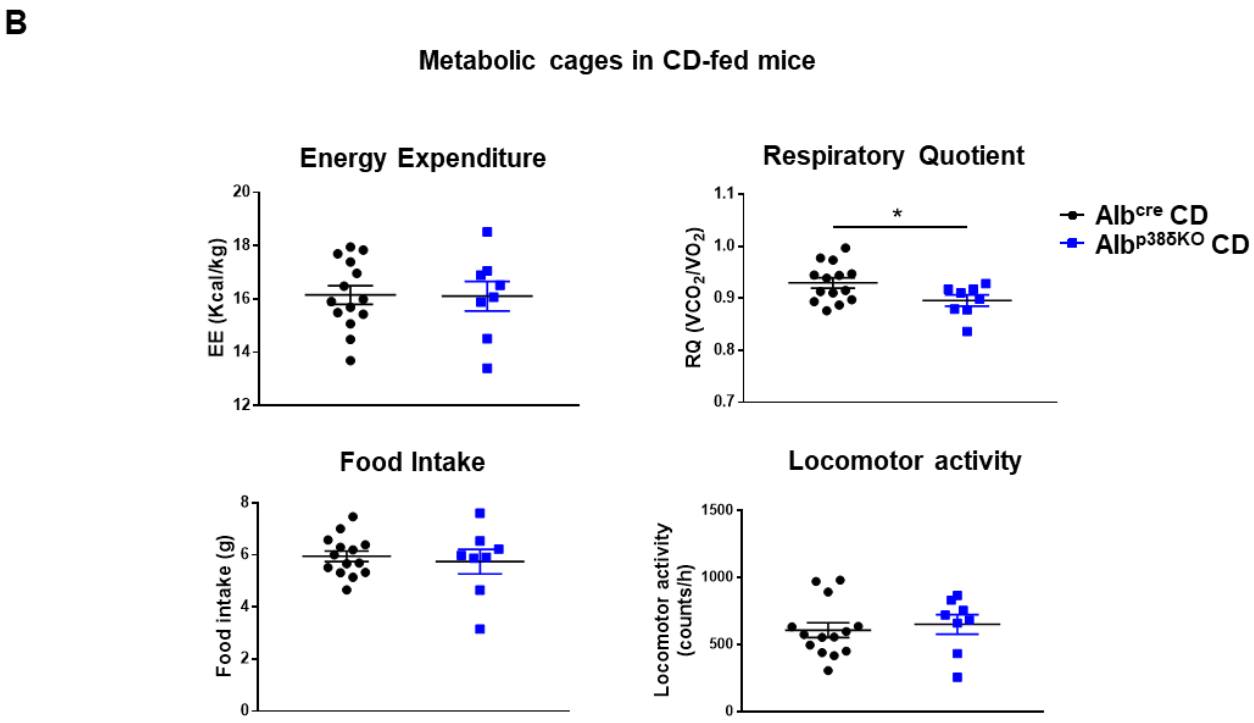

Figure 14: No changes in global energy balance in HFD-fed control and Alb$^{p38\delta KO}$ mice; however, CD-fed mice showed reduced respiratory quotient

Energy expenditure, locomotor activity, respiratory quotient (RQ) and food intake was determined using metabolic cages for 72 hours in 16-18 weeks old control and Alb$^{p38\delta KO}$ mice fed with A) HFD (mean ± SEM, n=10) or B) HFD for 8 weeks (mean ± SEM, n=8-14). *$p < 0.05$ (unpaired *t* test).

15. p38δ MAPK could be a target to treat obesity-related insulin resistance and hepatic steatosis

As obese mice lacking p38δ in hepatocytes mice were protected against T2D (insulin resistance, hyperglycemia) and hepatic steatosis and because of high levels of p38δ expression have been found in humans with NAFLD (Gonzalez-Teran et al., 2016b), we checked the therapeutic potential of targeting p38δ in liver. For this we downregulated p38δ specifically in livers of mice fed with HFD for 6 weeks. We used mice in which the p38δ gene (*MAPK13*) was flanked by LoxP sites (*MAPK13$^{f/f}$*) and CXBL6/7J mice as control. To delate p38δ, we injected intraperitoneally AAV serotype 2/8, which expressed specifically in the liver CRE recombinase protein in both mice genotypes. After CRE expression, LoxP sites are recombined and *MAPK13* gene is deleted. 2 weeks after the injection we found that the hepatic *MAPK13* gene expression downregulation (Figure 15A), was associated with protection against HFD-induced hyperglycemia, insulin resistance (Figure 15B) and NAFLD (Figure 15C). Therefore, this data suggests that the inhibition of hepatic p38δ could be an effective treatment to treat T2D and it also supports that p38δ is a central glucose metabolism regulator.

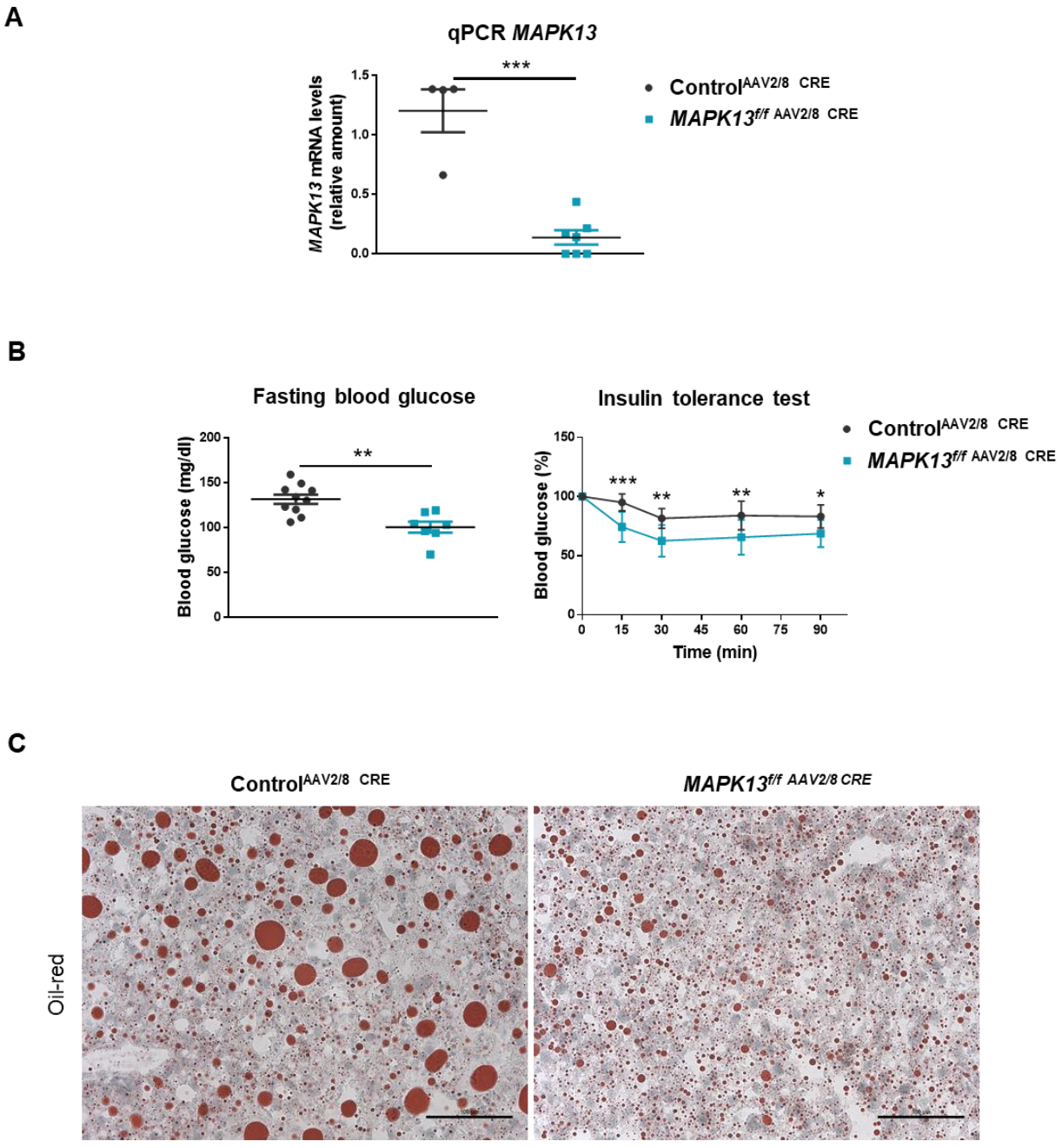

Figure 15: The hepatic p38δ could be a target to treat T2D

6 weeks HFD-fed *MAPK13*$^{f/f}$ and CXBL6/7J control mice were intravenously injected with AAV serotype 2/8 expressing Cre recombinase protein, to specifically delete p38δ in hepatocytes (*MAPK13*$^{f/f\ AAV2/8\ Cre}$). Control are shown as Control$^{AAV2/8\ Cre}$. 2 weeks after the injection A) Blood glucose levels were measured after overnight fasting (16 hours). B) Insulin tolerance test was performed. Blood glucose concentration was measured in mice upon intraperitoneal insulin injection (0.75 IU/kg) upon 1 h of food deprivation (mean ± SEM, n=7-10). C) Representative liver sections stained with Oil-red to measure lipids. Scale bar=100µm (mean ± SEM, n=3-5) *$p < 0.05$, **$p < 0.01$, ***$p < 0.001$ (two-way ANOVA coupled to Bonferroni's post-tests and unpaired *t* test).

Discussion

Metabolism is a main driving force of life, because it allows to each cell to get and to produce energy. The importance of the correct metabolism regulation and the impact of its deregulation are nowadays having a huge incidence in human health (obesity and its related diseases). Obesity is a global health problem, which has reached pandemic proportions, affecting more than 600 million people worldwide (Verma and Hussain, 2017). The main concern of obesity is the greater risk to develop serious disorders, such as T2D; which is also a global health care problem that will reach pandemic levels, because forecast points out that in 2040 this disease will affect 642 million people worldwide (IDF, 2017). T2D is characterized by insulin resistance and high blood glucose levels. Glucose related diseases are pathological conditions with different etiologies, in which the blood glucose cannot be maintained within the normal range, such as happens not only in hyperglycemia, but also in hypoglycemia; both with important health consequences (Sharabi et al., 2015).

The liver is one of the main tissues that contributes to maintain normoglycemia (blood glucose levels around 90 mg/dl), through HGP and glycogen storage. But also, the liver has a central role in the control of whole-body metabolism, being also involved in lipid and protein metabolism and removing harmful toxins. Therefore, the liver has a main role in the pathophysiology of metabolic diseases, being deeply affected in obesity, which promotes NAFLD; but the liver is also a main driver of insulin resistance. NAFLD is also highly prevalent in T2D (Bhatt and Smith, 2015) and the higher risk of this hepatic disease is that in some cases, NAFLD may progress to NASH (when there is inflammation and cell injury), cirrhosis (hepatic fibrosis), and even liver failure or HCC. Although, NAFLD is the most extended chronic liver disease, there are also many others types of genetic/metabolic liver diseases such as: glycogen or lipid storage deficiencies, urea cycle disorders or peroxisomal disorders, with highly complex pathophysiology and which have not been much explored. Therefore, to better understand liver function will allow to find new targets to treat liver related diseases which have huge impact in whole-body homeostasis; between them NAFLD and also to treat other extended diseases such as T2D.

Actually, find new treatments is crucial, because currently there are not effective treatments for T2D (Marin-Penalver et al., 2016), neither NAFLD (Patel and Siddiqui, 2019). Nowadays, the first line to treat T2D is based on lifestyle modifications and metformin administration, with the use of a second and third-line of pharmacological agents: sulfonylureas, meglitinides, insulin, thiazodilinione (TZD) or alpha-glucosidase inhibitors; and recently also glucagon-like peptide 1 analog, dipeptidil peptidasa-4 inhibitor (iDPP4) and sodium/glucose cotransporter 2 inhibitor (iSGLT2), depending on patients' metabolic or genetic profile (Marin-Penalver et al., 2016). For NAFLD and NASH treatment, current therapies involved drugs focus on reducing weight; antidiabetic drugs, such as metformin or TZD; farnesoid X receptor agonist; anti-inflammatory agents, such as vitamin E; immune modulators and statins (Patel and Siddiqui, 2019). Some of these drugs targets key metabolic proteins, such as

AMPK or G3PDH (metformin) or PPARγ and α (TZD). However, the side effects of the treatments, without final control, neither disease resolution; makes the necessity to research into new targets and therapies. Moreover, this indicates that there are other key metabolic regulators still unexplored.

We have previously described in the introduction main pathways involved in the development of obesity-related T2D and NAFLD. To summarize, high FFA levels promote insulin resistance which increases the hepatic glucose production, directly promoting hyperglycemia; which the subsequent pancreatic β cell secretory failure and apoptosis. By other hand, alterations in lipid metabolism (uptake, oxidation and synthesis) are main factors for NAFLD development. But also, NAFLD is a main driver of insulin resistance. MAPK participate in a multitude of processes that control hepatic metabolism. There is strong evidence regarding to the role of JNK in liver pathophysiology and insulin resistance (Sabio and Davis, 2010, Pal et al., 2016). By contrast, the role of ERK is still controversial (Lawan and Bennett, 2017) and the role of p38 MAPK in liver metabolism has not been almost studied (Manieri and Sabio, 2015). However, since JNK and p38 MAPK are stress kinases, which are activated by stress stimuli, such as inflammation (Sabio and Davis, 2014) or FFA (Jaeschke and Davis, 2007, Kant et al., 2013), which are main components of obesity; stress kinases may play a main role in the hepatic metabolic dysfunction. Regarding to p38 MAPK, what is basically known, using pharmacological inhibitors and siRNA, is that p38α and β control GNG (Cao et al., 2005). Moreover, it is known that p38 MAPK can phosphorylate and control main transcription factors and coactivators involved in GNG and lipid metabolism, such as PGC1α (Puigserver et al., 2001) or PPARα (Juge-Aubry et al., 1999, Barger et al., 2001), respectively. However, it is not clear whether they are involved in insulin resistance (Lee et al., 2011, Pereira et al., 2016, Lawan et al., 2015). Interestingly, preliminary results from our lab suggest that lack of p38α in hepatocytes does not affect glucose homeostasis or lipid metabolism. One of the less unexplored kinases is the p38δ MAPK, which might have a main role in liver metabolism, since it expression is increased in the livers of patients with NAFLD (Gonzalez-Teran et al., 2016b). However, there is nothing described about its role in liver metabolism and its impact on whole body homeostasis. Moreover, due to the complexity of the MAPK network, which must be precisely regulated, and due to MAPK are key factors managing cell function and metabolism; further investigation is needed to clarify MAPK tissue-specific function, to understand communication between different family members and to find new and specific upstream and downstream targets for each member. Therefore, the main purpose of this Thesis was to further dissect the role of p38δ MAPK in liver function, particularly in glucose and lipid metabolism and its impact in whole-body homeostasis; and also to evaluate its role in obesity-induced T2D and NAFLD. Moreover, this Thesis gives new insights into MAPK network. Importantly, we have found that the hepatic p38δ MAPK is a central metabolic regulator, being a central point in the glucose metabolism, controlling glycogenesis and glycolysis; but also the hepatic p38δ MAPK might have a central role in the lipid metabolism, modulating the

lipid oxidation; having a central role controlling PPARα upregulation and FGF21 expression. Moreover, in this Thesis we open many different lines to further explore, which might help to better comprehend hepatic metabolism and definitively human physiology.

1. The hepatic p38δ MAPK is a novel and essential glucose metabolism regulator

Maintaining blood glucose concentration within a relatively narrow range through periods of fasting or excess nutrient availability is essential for the survival of the organism. The decrease in plasma glucose levels (hypoglycemia) can lead to impaired brain function and death. Conversely, increased plasma glucose levels (hyperglycemia), a major clinical symptom of diabetes, dramatically increase the risk of various macrovascular and microvascular complications. Normoglycemia is a tightly balance between glucose uptake and endogenous glucose production. The liver maintains normal whole-body glucose levels during fasting by regulating *de novo* glucose production (GNG) from non-carbohydrate precursors such as lactate, AA and glycerol (Hellerstein et al., 1997, Chung et al., 2015) and by regulating glycogen breakdown (glycogenolysis).

We have found that the hepatic p38δ MAPK has a main role in liver mediated blood glucose levels regulation, since the overexpression of the active p38δ MAPK in hepatocytes of wild-type mice, increased blood glucose levels (Figure 1B). This result was also reinforced because mice lacking p38δ in hepatocytes ($Alb^{p38\delta KO}$) showed reduced blood glucose levels upon high fat or normal diet compared to control mice (Figure 3C and 8B). Moreover, we demonstrated that p38δ MAPK controls glycogen metabolism, because $Alb^{p38\delta KO}$ mice have reduced glycogen liver storage independently of the type of diet (Figure 6B and 8C). Lastly, p38δ MAPK also controls glycolysis, because HFD-fed $Alb^{p38\delta KO}$ mice showed reduced glycolytic flux (Figure 13A). Therefore, all these data definitively point out that p38δ MAPK might be a master regulator of glucose metabolism, controlling directly glycogen metabolism and blood glucose levels; and probably also glycolysis.

Previous works have identified that other MAPK participate in blood glucose regulation. We have previously mentioned that p38α and β might promote GNG (Cao et al., 2005) (Jing et al., 2015); but also, hepatic JNK1/2 deletion decreases fast glucose levels (Vernia et al., 2014) and ERK-2 liver specific deletion enhances fast blood glucose levels (Kujiraoka et al., 2013). Moreover, the MAPK phosphatases, MKP-1 and MKP-3, are also involved in glucose metabolism. MKP-1 decreases GNG (Lawan et al., 2015) and MKP-3 increases blood glucose levels through direct interaction and dephosphorylation of FOXO-1 (Wu et al., 2010, Jiao et al., 2012, Feng et al., 2014). However, here we show that p38δ MAPK is not involved in GNG regulation, but it directly promotes glycogenesis and glycolysis. Moreover, this is the first time that it is shown that one of the MAPK is a main regulator of blood

glucose levels, through direct *in vivo* measure of hepatic flux (PINTA) (Figure 9C). In addition, although it has been proposed that JNK is involved in muscle glycogen formation, increasing glycogenesis (Vijayvargia et al., 2010, Moxham et al., 1996) and that p38β can phosphorylate muscle GYS (Kuma et al., 2004); there is not any study about the role of any MAPK in hepatic glycogen metabolism, therefore being this the first *in vivo* work demonstrating that a MAPK directly controls hepatic glycogen storage through GYS2 and glycogenesis regulation.

Moreover, it has been shown that p38 controls PFKB3 activity through MK2 phosphorylation at Ser641 (Novellasdemunt et al., 2013, Bolanos, 2013) and Bad phosphorylation by JNK1 is required for PFK-1 and glycolysis activation (Deng et al., 2008); however, here we show for first time one of the MAPK directly phosphorylates PFKFB3, probably promoting glycolysis.

1.1 p38δ MAPK directly controls liver glycogen metabolism

The liver is the main organ that regulates glycogen metabolism and GYS2 is the main enzyme involved in this process. Mice with a disruption in *GYS1* gene (muscle isoenzyme), improve their glucose tolerance (Pederson et al., 2005a, Pederson et al., 2005b); pointing out the main role of GYS2 compared to GYS1 in keeping normoglycemia. Liver and also muscle glycogen reduction has been found in individuals with T2D (Magnusson et al., 1992, Shulman et al., 1990). In the same way, GYS2 hyperphosphorylation and decreased activity have been related with postprandial hyperglycemia in obese patients with T2D (Hojlund et al., 2009). However, we have seen that HFD-fed $Alb^{p38\delta KO}$ mice that have reduced liver glycogen content (Figure 6B) showed reduced hyperglycemia (Figure 3C). This discrepancy might be explained because whereas in T2D, due to insulin resistance, GNG is upregulated contributing to hyperglycemia (Magnusson et al., 1992); in obese $Alb^{p38\delta KO}$, GNG was properly suppressed in response to insulin during hyperinsulinemic-euglycemic clamp (Figure 4A). Moreover, and mainly, the livers of HFD-fed $Alb^{p38\delta KO}$ mice might present energy and substrates deficiency, required for gluconeogenic anabolism; considering that glycolysis was reduced (Figure 13A) and the Krebs cycle might be impaired because only incomplete lipid β-oxidation was increased in these mice (Figure 11C).

In previous works, mice lacking GYS2 in hepatocytes (LGSKO) developed insulin resistance and NAFLD (Irimia et al., 2017). Contrary to this, CD-fed $Alb^{p38\delta KO}$ mice, which had reduced liver glycogen content (Figure 8C), did not develop insulin resistance, neither NAFLD (Figure 8F and 8G). It is described that the compromised glucose disposal as glycogen may contribute to hepatic steatosis by converting the excess of carbohydrates into FA by the DNL pathway (Schwarz et al., 2003). This happens in LGSKO mice, which showed 40% increase

in DNL (Irimia et al., 2017). However, CD-fed Alb$^{p38\delta KO}$ mice did not show increased DNL, and the DAG synthesis was even decreased (Figure 10B). Therefore, these data suggest that although Alb$^{p38\delta KO}$ mice have reduced liver glycogen, since they do not increase DNL, they were protected against NAFLD and insulin resistance.

The lack of p38δ MAPK in hepatocytes mimics the pathophysiology of glycogen storage disease 0 (GSD0). Patients with this disorder have loss-of-function mutations in *GYS2* gene (Weinstein et al., 2006). GSD0 is characterized by glycogen synthesis impairment and consequently by fasting ketotic hypoglycemia (Irimia et al., 2010, Weinstein et al., 2006). CD diet-fed Alb$^{p38\delta KO}$ mice also showed fasting ketotic mild hypoglycemia, to judge by low blood glucose (Figure 8B) and high plasma 3HB levels after overnight fasting (Figure 10D). Therefore, this suggests that mutations in *MAPK13* or deficiencies in p38δ activity might results in the development of GSD0. In fact, Alb$^{p38\delta KO}$ mice show phenotype more similar to GSD0 than LGSKO mice, because LGSKO mice have normal blood glucose levels after fasting, due to increase GNG and they do not develop postprandial hyperglycemia (Irimia et al., 2017). However, Alb$^{p38\delta KO}$ mice not only showed fasting hypoglycemia, without changes in GNG (Figure 8E and 9B), but also, they presented increased blood glucose levels in fed conditions (Figure 8B), similarly to GSD0.

Additionally, here we show that p38δ MAPK can directly control GYS2 activity (Figure 6C and 6D) through the phosphorylation of three new residues: Thr278, Ser627 and Ser683 (Figure 7A). After feeding GYS2 is dephosphorylated on the inhibitory residue Ser641 and gets activated, promoting glycogen formation, to storage the excess of carbohydrates. Since Alb$^{p38\delta KO}$ mice showed less liver glycogen after feeding (Figure 6B), they might have decreased GYS2 activity, as our data showed (Figure 6C). However, GYS2 phosphorylation at Ser641, which inhibits GYS2 activity, was not change in these mice. Therefore, this suggests that p38δ MAPK might modulate GYS2 activation independently of Ser641 phosphorylation and that the lack of the GYS2 phosphorylation done by p38δ MAPK (at Thr278, Ser627 and Ser683 residues) might be responsible of the GYS2 function impairment in the livers of Alb$^{p38\delta KO}$ mice.

However, no differences were found in GYS2 activity in fed conditions between genotypes (Figure 6D), what points out that p38δ MAPK might be mediating only GYS2 activation after feeding in response to other regulatory stimuli. Whereas GYS2 activity increased in the livers of control mice after feeding, GYS2 activation in the livers of HFD-fed Alb$^{p38\delta KO}$ mice was not properly induced (Figure 6D). This is probably because GYS2 activity was slightly increased during fasting in the livers of these mice (Figure 6D); therefore, other possibility is that p38δ MAPK mediates GYS2 inhibition during fasting and this inhibition might be crucial for its correct regulation and for proper hepatic glycogen storage. In agree with this, no differences in

GYS2 phosphorylation at Ser641 were found in CD-fed Alb$^{p38\delta KO}$ mice upon feeding (Figure 8H), although these mice also presented less glycogen content (Figure 8C). Since the GYS2 sites that are phosphorylated by p38δ MAPK (Thr278, Ser627 and Ser683) are close to the GSK3 inhibitory phosphorylation sites (Ser641, 644, 648 and 652) (Mora et al., 2005, Jensen et al., 2012) (Coghlan et al., 2000, Cline et al., 2002), probably p38δ-mediated GYS2 phosphorylation are controlling the correct GSK3-mediated GYS2 phosphorylation and inhibition in fasting; with other words, probably GSK3 phosphorylation in GYS2 is dependent on its previous phosphorylation by p38δ. However, since the sites phosphorylated by p38δ MAPK are also close to the G6P activator domain (Arg579, 580, 582, 586, 588 and 591) (Hanashiro and Roach, 2002), p38δ MAPK could also modulate the proper G6P-mediated allosteric GYS2 activation upon feeding; actually, G6P-insensitive GYS2 mutant exhibits markedly lower glycogen accumulation in hepatocytes (von Wilamowitz-Moellendorff et al., 2013). Therefore, both hypotheses might be further explored and also fasting hepatic G6P levels might be measured, to discard that there are differences in hepatic G6P levels that promote basal GYS2 activation in fasting or not complete GYS2 stimulation after feeding. Moreover, it will be interesting to explore how p38δ-mediated GYS2 phosphorylation affects the Ser 7 of GYS2, because it has been shown it is the critical regulatory phosphorylation site of this enzyme (Ros et al., 2009). Therefore, future GYS2 activity studies, generating non-phosphorylatable and constitutive phosphorylated mutants for the GYS2 sites that are phosphorylated by p38δ, and using different conditions might completely confirm how p38δ controls GYS2 function. What is clear is that p38δ-mediated GYS2 phosphorylation seems to be a key regulator point for the correct GYS2 activation and hepatic glycogen accumulation. Moreover, here we show a novel substrate for p38δ MAPK.

1.2. Regulation of HGP in Alb$^{p38\delta KO}$ mice

HGP is a central mechanism to maintain blood glucose levels during overnight fasting. The contribution of glycogenolysis and GNG to overall glucose production is approximately equal. However, glycogenolysis plays the main role in the first fasting hours, whereas GNG increases when glycogen is being depleted (Hellerstein et al., 1997, Chung et al., 2015, Rothman et al., 1991, Southampton-University, 2017, Perry et al., 2018). Since HFD-fed Alb$^{p38\delta KO}$ mice showed reduced fasting blood glucose levels (Figure 3C), to asses HGP we performed hyperinsulinemic-euglycemic clamp, which is also the master technique to assay insulin sensitivity *in vivo*. Mice HFD-fed Alb$^{p38\delta KO}$ mice did not show significant differences in the basal HGP, neither in blood glucose levels after 4h fasting (Figure 4B). At this time, glycogenolysis is the main contributor to HGP; therefore, glycogenolysis might not be altered after this short fasting period in Alb$^{p38\delta KO}$ mice and these mice would still have enough hepatic glycogen storage to maintain blood glucose levels. Moreover, since no

changes were found in peripheral glucose uptake during clamp (Figure 4C), low blood glucose levels might be consequence of the hepatic regulation. Therefore, HFD-fed Alb$^{p38\delta KO}$ mice are protected against hyperglycemia due to reduced hepatic glycogen storage as a consequence of disrupt GYS2 regulation and glycogenesis.

To confirm this, we measured *in vivo* hepatic flux that contributes to EGP by PINTA in CD-fed mice, which also presented reduced fasting blood glucose levels (Figure 8B). Supporting our hypothesis, EGP from glycogen and glycerol was decreased in Alb$^{p38\delta KO}$ mice (Figure 9C). Since glycerol plasma levels did not change in Alb$^{p38\delta KO}$ mice (Figure 9D), glycogen liver storage reduction might be the main contributor to decrease EGP. However, since glycerol is converted into glycerophosphate and mitochondrial GPDH transforms glycerophosphate into DHAP that can be used for GNG; and the expression of mitochondrial GPDH was found reduced in proteomics analysis done in the livers of HFD-fed Alb$^{p38\delta KO}$ mice (data not shown); glycerol could also have a main role in the observed EGP reduction. Moreover, since mitochondrial GPDH has a main metabolic function, linking lipid and carbohydrate metabolism, mitochondrial and cytosolic processes and controlling cell bioenergetics (Mracek et al., 2013), mitochondrial GPDH activity might be further explore.

Interestingly, although for PINTA we increased fasting time to 16 h, no differences were found in basal EGP between genotypes, probably because at this point GNG might be also contributing to EGP. Actually, although we did not find significant differences in GNG in Alb$^{p38\delta KO}$ mice (Figure 8E), PC flux was slightly increase in these mice (Figure 9B), what might compensate net EGP after 16h fasting in CD-fed Alb$^{p38\delta KO}$ mice; however, it is not enough to keep normoglycemia as our data showed. Something similar happens in mice lacking GYS2 in hepatocytes (LGSKO), in which no differences were found in net HGP. However, whereas in Alb$^{p38\delta KO}$ mice, GNG, neither glycogenolysis were altered; in LGSKO mice, GNG was importantly increased, but glycogenolysis was decreased (Irimia et al., 2010). The mild V_{PC} increase in CD-fed Alb$^{p38\delta KO}$ mice might come from AA input. In fact, plasma AA levels were found increased in CD-fed Alb$^{p38\delta KO}$ mice (Figure 9F), what suggests that muscle proteolysis may be activated. Actually, the generation of gluconeogenic AA by tissue proteolysis is largely responsible for the net addition of carbons into the glucose pool via anaplerosis, during fasting periods under low blood glucose conditions. Despite AA input, GNG might not be increased in CD-fed Alb$^{p38\delta KO}$ mice to maintain normoglycemia; firstly, due to alanine that is the major gluconeogenic amino acid (via the glucose-alanine cycle) (Felig, 1973) was only slightly increased in plasma levels from these mice. Secondly, GNG requires a continuous supply of high energy cofactors (NADH and ATP) derived from Krebs cycle activity and respiration, but CD-fed Alb$^{p38\delta KO}$ mice might present impaired Krebs cycle as reduced CS activity indicated (Figure 9G).

Alb$^{p38\delta KO}$ mice were protected against hyperglycemia without changes in glucose synthesis or glycogen breakdown, pointing out that to decrease hepatic glycogen synthesis and GYS2 activity could be also a good strategy for T2D treatment, although typically it has been found that glycogen synthesis is impaired in T2D (Krssak et al., 2004). Previous approaches have also suggested to specifically target the liver, mainly GNG and glycogenolysis, or also to inhibit GSK3, to normalize blood glucose (Rines et al., 2016). Interestingly, downregulation of p38δ in the livers from mice fed with HFD for 6 weeks, drastically decreased blood glucose levels, protecting mice against hyperglycemia and insulin resistance (Figure 15B). Moreover, hepatic p38δ downregulation also protected against NAFLD. Therefore, the inhibition of p38δ MAPK in hepatocytes may be further explore as target to treat obesity related T2D and NAFLD. Lastly, it is also important to consider that in normal diet, the lack of p38δ in hepatocytes promotes hypoglycemia, which is also an important pathological condition as we have previously discussed.

1.3. p38δ MAPK directly controls glycolysis

The liver can switch from net hepatic glucose storage to glucose output, by regulating the activity of key glycolytic and gluconeogenic enzymes. However, although the lack of p38δ MAPK in hepatocytes reduced hepatic glucose output, glycolysis was also decreased (Figure 13A). PFK enzymes are one of the main kinases involved in glycolysis regulation and their levels and activities are increased in postprandial state (Rui, 2014). Between the 4 different PFK2 isozymes, PFKFB3 has been the main isozyme involved in glycolysis link to cell proliferation through p38α-MK2-mediated PFKFB3 phosphorylation at Ser461 and transcriptional activation (Novellasdemunt et al., 2013, Bolanos, 2013). Moreover, *Pfkfb3* has been found upregulated in a diabetic mouse model (Duran et al., 2009). We have found that p38δ MAPK phosphorylates PFKFB3 in two new phospho sites, Ser467 and Thr463 (Figure 13D). Since Alb$^{p38\delta KO}$ mice showed reduced glycolytic flux (Figure 13A) and these phosphorylations were decreased after feeding in the livers of these mice (Figure 13C); p38δ MAPK might phosphorylate PFKFB3 *in vivo* inducing glycolysis. Therefore, here we give for first time a physiological meaning to Ser467 and Thr463 PFKFB3 residues and we show a new key regulation point of hepatic glycolysis through p38δ-mediated PFKFB3 phosphorylation. However, since PFKFB3 is ubiquitous expressed (Atlas) and PFKB1 is the main liver isozyme (Atlas), further studies might determine the regulation of the different PFK-2 isozymes by p38δ MAPK and whether there is other isozyme involved in the glycolysis decrease observed in Alb$^{p38\delta KO}$ mice.

Typically and contrary to our data, glycolysis reduction has been related with hyperglycemia and insulin resistance (Torres et al., 2009, Michael et al., 2000), while glycolysis enhancement decreases blood glucose levels (Wu et al., 2001, Wu et al., 2002). Actually, metformin, a current treatment to T2D, increases

glycolysis targeting AMPK (Miller and Birnbaum, 2010, Silva et al., 2010). By contrast, our results indicate that although $Alb^{p38\delta KO}$ mice have reduced glycolysis, they are still protected against hyperglycemia. However, in the context of low blood glucose levels due to glycogen storage reduction, this could be an advantage to maintain survival, not decreasing more blood glucose levels and promoting all glucose takes by the liver is accumulated as glycogen. Moreover, it has been reported that PFKFB3 inhibition induces autophagy (Klarer et al., 2014, Yang et al., 2014), a mechanisms which could promote cell survival during low energy conditions (Yang et al., 2013). However, this might be further explore because there is still controversy regarding to the role of PFKFB3 and autophagy, and particularly regarding to the role of p38α-induces proteasome-dependent degradation of PFKFB3 and autophagy inhibition or activation in cancer cells (Desideri et al., 2014). What is clear is that the role of p38δ-mediated PFKFB3 phosphorylation could also have an important role in tumor progression, since PFKFB3 has been described as main drivers of the Warburg effect (switch to anaerobic glycolysis) in different types of cancer (Lu et al., 2017). Lastly, since one of the major functions of liver glycolysis is to provide carbons from glucose for DNL (Rui, 2014); in a context of HFD, to decrease glycolysis will reduce intermediates that could be used for lipid synthesis, intrahepatic accumulation and consequently NAFLD development and insulin resistance. Since p38δ MAPK expression is increased in the livers of obese people with NAFLD (Gonzalez-Teran et al., 2016b), it could be that p38δ is activated during high-energy states, contributing to increase glycolytic flux driving DNL and also glycogen accumulation; what will give high availability of energy and substrates to hepatocytes. Therefore, p38δ MAPK could be also involved in the progression from NAFLD/NASH to HCC and it might be further explored. Actually, recently our group have found that to target p38γ, the most similar kinase to p38δ, protects against HCC development (Tomas-Loba et al., 2019).

2. The role of hepatic p38δ MAPK in lipid metabolism

The liver also plays a key role in lipid metabolism, importing and manufacturing FFA, storing and exporting lipids. Homeostatic disruption of any of these processes can lead to the development of NAFLD. We will discuss later the role of p38δ MAPK in the protection against obesity-induced NAFLD and insulin resistance. However, we have also seen that p38δ MAPK might have a function controlling hepatic lipid metabolism, since CD-fed $Alb^{p38\delta KO}$ mice showed differences in DAG and C_{18}-CoA accumulation in the liver, which might be further explored. Particularly, $Alb^{p38\delta KO}$ mice presented higher C_{18}-CoA levels in the liver than control mice. We also observed slight increase in C_{12}-CoA, C_{14}-CoA and C_{16}-CoA in livers of $Alb^{p38\delta KO}$ mice, without differences in C_{20}-CoA and C_{22}-CoA (Figure 10C). Therefore, it seems that $Alb^{p38\delta KO}$ mice augmented hepatic accumulation of LCCoA (C_{13}-C_{21}), mainly of stearoyl-CoA (C_{18}-CoA); without differences in very LCCoA (C_{22}-CoA) accumulation. Although, no

differences were found in ^{14}C-palmitate β-oxidation in hepatic extracts, what suggest that mitochondrial lipid β-oxidation is not impaired in Alb$^{p38\delta KO}$ mice, these mice presented decreased DAG *de novo* synthesis (Figure 10A and 10B respectively). Considering that C_{16} and C_{18}–CoA are the main acyl-CoA pool involved in the fatty acid β-oxidation, but also in DNL; hepatic DAG synthesis might be impaired in Alb$^{p38\delta KO}$ mice, and could explain the accumulation of LCCoA in the livers of these mice. Since DAG has been implicated as the main causative metabolite in fat-induced hepatic insulin resistance in the liver (Ginsberg, 2006, Alkhouri et al., 2009, Erion and Shulman, 2010); to inhibit DAG synthesis could be a protective mechanisms. However, acyl-CoA have also been identified as potential cause of lipotoxicity (Muoio and Newgard, 2008, Mitchell et al., 2008); and humans (Araya et al., 2004) and mice (Shimomura et al., 1998) with hepatic steatosis accumulate excess oleic acid ($C_{18:1}$), the end-product of *de novo* fatty acid synthesis. Therefore, further studies might clarify the potential protective role of decreasing DAG content, increasing LCCoA levels, as well as mechanisms and proteins involved. In agreement with this, when mitochondrial acyl-CoA: glycerol-sn-3-phosphate acyltransferase (mtGPAT)-deficient mice were placed on a HFD, they accumulated hepatic fatty acyl-CoA, but not hepatic DAG and triglyceride and they were protected against lipid-induced hepatic insulin resistance (Neschen et al., 2005).

We did not find differences in the ^{14}C-palmitate β-oxidation in CD-fed Alb$^{p38\delta KO}$ mice (Figure 10A); however, CS activity, one of the main proteins involved in the Krebs cycle, measured by PINTA was reduced (Figure 9G). We have to consider that acetyl-CoA is the molecule that is oxidized via Krebs cycle. In PINTA, (3-^{13}C)-lactate is used as tracer; therefore, the involved enzymes between the conversion of lactate to acetyl-CoA and the conversion of ^{14}C-palmitate to acetyl-CoA are different. Particularly, palmitate is converted to acetyl-CoA through 4 steps, in which acyl-CoA dehydrogenase (ACAD) and the MTP are involved; whereas lactate is first converted to pyruvate through LDH, and finally the pyruvate dehydrogenase complex (PDH) catalyzes the conversion of pyruvate into acetyl-CoA. Therefore, this suggests that the normal fatty acid β-oxidation that involves mitochondrial Krebs cycle would not be altered in CD-fed Alb$^{p38\delta KO}$ mice; however, the Krebs cycle might be impaired from pyruvate carboxylation and/or at the LDH level. Since we saw impaired glycolysis in HFD-fed Alb$^{p38\delta KO}$ mice, glycolytic flux could be also reduced in chow fed animals, limiting carbohydrate-dependent Krebs cycle; although, the low blood glucose levels that these mice showed could be the limiting factor per se. Moreover, since glucose metabolism is reduced, it makes sense do not decrease lipid fatty acid β-oxidation to guarantee mice survival. However, surprisingly, although RQ was lower in Alb$^{p38\delta KO}$ than in control mice (Figure 14B), RQ close to 0.8 means mixed diet (carbohydrates, lipids and proteins).

Moreover, high 3HB plasma levels were found in CD- fed Alb$^{p38\delta KO}$ mice (Figure 12A), suggesting increased hepatic KG. Ketone bodies are vital alternative metabolic fuel source for extrahepatic tissues, mainly the brain, during fasting and starvation periods; but they are also important in neonatal stage, post-exercise, during pregnancy and low-carbohydrate diets. Therefore, since CD-fed Alb$^{p38\delta KO}$ mice presented reduced fasting blood glucose levels (Figure 8B), it is normal that they increased the KG pathway to get energy. Ketone bodies are mainly produced by liver, because only hepatocytes and gut epithelial cells express the mitochondrial isoform of 3-hydroxymethylglutaryl- CoA synthase 2 (HMGCS2), which is the enzyme that catalyzes the first reaction of the KG (Puchalska and Crawford, 2017). Classically KG is considered a spillover pathway, when the acetyl-CoA levels from fatty acid oxidation exceed the CS activity and/or OAA availability for condensation to form citrate. Since we have not found differences in hepatic acetyl-CoA levels (Figure 9E); CD-fed Alb$^{p38\delta KO}$ mice might increase KG, driving acetyl-CoA to this pathway, due to low OAA availability for the Krebs cycle. Probably, because OAA is used in the GNG pathway, to try to increase the low fasting blood glucose levels that Alb$^{p38\delta KO}$ mice have. Interestingly, although it seems KG was increased and there was no differences in lipid β-oxidation in CD-fed Alb$^{p38\delta KO}$ mice, fasting FGF21 plasma levels were reduced is these mice (Figure 10E), contrary to previous works that define FGF21 as central driver of lipid oxidation and KG (Vernia et al., 2014, Badman et al., 2007, Inagaki et al., 2007). This data suggest that p38δ MAPK might be involved in FGF21 regulation and further studies might clarify involved mechanisms.

2.1 Lack of p38δ MAPK in hepatocytes protects against obesity-induced NAFLD. Involved mechanisms

We have found that the lack of p38δ MAPK in hepatocytes protects against HFD-induced NAFLD; actually, this is the first *in vivo* work which shows that one of the p38 MAPK member is involved in NAFLD pathophysiology. Previously works only suggested that p38 may be involved in hepatic steatosis (Zhang et al., 2016, Sun et al., 2016); particularly, p38α/β have been shown to be downregulated in obesity (Lee et al., 2011, Lawan and Bennett, 2017) and it seems that their inactivation, mediated by MKP-1, promotes hepatic steatosis (Flach et al., 2011, Wu et al., 2006, Lawan et al., 2015). By contrast, the role of hepatic JNK in NAFLD is more stablished. What is described is that hepatocyte-specific simultaneous knockout of JNK1 and JNK2 protects against HFD-induced hepatic steatosis (Vernia et al., 2014). Contrary to hepatic specific JNK1 ablation, that promotes hepatic steatosis (Sabio et al., 2009). Other work also points out that both JNK1 and 2 are required to protect from acute and chronic toxic liver injury (Cubero et al., 2016).

Therefore, Alb$^{p38\delta KO}$ mice were protected against HFD-induced NAFLD (Figure 6A). Interestingly, control mice showed huge mixed steatosis, mainly microvesicular steatosis, characterized by small lipid droplets, but also with some macrovesicles, which is the most frequently observed steatosis pattern (Thoolen et al., 2010). On the contrary, Alb$^{p38\delta KO}$ mice had reduced NAFLD with few large lipid droplets, more similar to macrovesicular steatosis, which have been previously related with lipid and cytoplasmic glycogen changes (Thoolen et al., 2010), in agreement with our data. Whereas microvesicular steatosis, usually known as hepatocellular ballooning, is the major feature of disease progression and sever dysfunction (Brunt et al., 2004, Matteoni et al., 1999, Yeh and Brunt, 2007, Greaves, 2012), macrovesicular steatosis is considered to have a good long-term prognosis with rare progression to fibrosis and cirrhosis (Tandra et al., 2011). Additionally, microvesicular steatosis is generally attributed to severe genetic or acquired defects in mitochondrial β-oxidation (Fromenty et al., 1997, Fromenty and Pessayre, 1997). However, HFD-fed Alb$^{p38\delta KO}$ mice that showed larger vesicles instead of microvesicles presented only increased the incomplete fatty acid β-oxidation (Figure 11C), which might suggest a mitochondrial function impairment. There is accumulating evidence that mitochondrial dysfunction, and therefore insufficient fatty acid oxidation plays a key role in NAFLD/NASH by impairing fat homeostasis. Moreover, incomplete FAO as is the case of mice lacking long-chain Acyl-CoA dehydrogenase promotes insulin resistance (Zhang et al., 2007). However, other studies have shown that the β-oxidation system can be either increased or fully activated in fatty liver. In this way, excessive mitochondrial Krebs cycle has also been related with pathological condition, being related with NAFLD development (Sunny et al., 2011, Satapati et al., 2012). What is clear is that in both circumstances, generation of ROS by the damaged respiratory chain are augmented (Begriche et al., 2006). Since mitochondrial healthy depends on multiple factors including the integrity of the mitochondrial DNA, the composition of cellular lipids, lipoprotein trafficking, the balance of pro- and antioxidant factors, and the metabolic demands placed on the liver (Caldwell et al., 2004); to better define specific mitochondrial alterations and altered proteins in NAFLD/NASH and in our case, the molecular mechanisms that promotes only an incomplete lipid β-oxidation in Alb$^{p38\delta KO}$ mice would help to better understand the role of mitochondria and fatty acid oxidation in NAFLD pathophysiology. What is clear, as our data show, is that complete hepatic lipid β-oxidation is not required to protect against NAFLD and insulin resistance.

The upregulation in the PPARα pathway, a master regulator of fatty acid metabolism in the liver (Pawlak et al., 2015) that Alb$^{p38\delta KO}$ mice showed (Figure 12A), agrees with the protection against NAFLD that these mice presented, in agreement with previous works (Hashimoto et al., 2000, Montagner et al., 2016). However, the use of PPARα agonist in humans have been shown weak potency or no effect in the NAFLD/NASH

treatment; although a new PPARα modulator (K-877) seems to be a promising agent for its treatment. By contrary, the use of a dual PPARα/δ agonist have also shown to improve NAFLD in mouse (Staels et al., 2013) and it seems to be a better treatment in humans; currently being in a phase 3 clinical trial study (Sumida and Yoneda, 2018). Since we also found that PPARδ pathway was upregulated in $Alb^{p38\delta KO}$ mice (Figure 12A), this suggests that the protection against NAFLD in $Alb^{p38\delta KO}$ mice may be mediated via PPARα/δ pathway upregulation.

It is known that PPARα induces FGF21 expression (Inagaki et al., 2007, Badman et al., 2007, Lundasen et al., 2007). FGF21 circulates in blood and it is mainly secreted by the liver during fasting (Markan et al., 2014). FGF21 is a potent regulator of metabolism (Owen et al., 2015, Potthoff et al., 2012, Fisher and Maratos-Flier, 2016), which has been also related with protection against hepatic steatosis and insulin resistance (Xu et al., 2009a, Berglund et al., 2009, Xu et al., 2009b); actually FGF21 has been suggested as therapy for obesity, insulin resistance and T2D (Jimenez et al., 2018, Gaich et al., 2013, Zhao et al., 2012). However, it has been also observed that obesity is a FGF21-resistant state, since FGF21 levels have been found increased in obesity (Dushay et al., 2010, Zhang et al., 2008) although the mediator of this insulin resistance remains unknown (Fisher et al., 2010). Moreover, even in obese mice which have already increased levels of FGF21, chronic administration of FGF21 reverses hepatic steatosis and improves insulin sensitivity (Xu et al., 2009a, Camporez et al., 2013). Since we found the most significant change in FGF21 plasma levels in HFD-fed $Alb^{p38\delta KO}$ mice after feeding, when FGF21 was dramatically inhibited, but only a slight FGF21 increase during fasting (Figure 12B); and considering that $Alb^{p38\delta KO}$ mice were protected against NAFLD and insulin resistance; our data point out to decrease FGF21 levels during postprandial state might be also important to protect against obesity-induced NAFLD and insulin resistance. However, this is contrary to a previous study that indicates FGF21 levels during feeding are also required to decrease insulin resistance. In this study specific FGF21 ablation in hepatocytes promotes hepatic steatosis and insulin resistance in HFD-fed mice (Markan et al., 2014). But, it is important to consider that mechanisms related to FGF21 are poorly understood; in fact, it has been shown that FGF21 can be also increased in a weaker way, by feeding stimuli, such as glucagon or ChREBP (Uebanso et al., 2011). This indicates that FGF21 levels might increase in such abnormal physiological conditions (starving or overfeeding); actually, serum FGF21 levels of healthy subjects show no major changes related to feeding and fasting over the course of a day (Galman et al., 2008). Therefore, to keep the correct FGF21 balance might be the clue. Further studies might clarify the role of FGF21 in the protection that $Alb^{p38\delta KO}$ mice showed and the regulation done by p38δ.

Additionally, further studies might determine whether p38δ MAPK can directly regulate PPARα expression, through direct phosphorylation as it has been previously shown in an *in vitro* kinase assay for p38α (Barger

et al., 2001) or whether p38δ controls the PPARα co-repressors, NCoR1 and NRIP1, as it is the case of JNK (Vernia et al., 2014). Moreover, further studies might also clarify whether p38δ-mediated FGF21 regulation is PPARα dependent, since PPARα KO mice is still able to increase Fgf21 levels upon fasting (Inagaki et al., 2007), it might be alternative mechanisms. Once more, this fact points out the importance of the p38δ MAPK isoform in the liver metabolism, regulating other important metabolic nodes, PPARα and FGF21. Interestingly, whereas $Alb^{p38\delta KO}$ mice showed incomplete FAO, the double $Alb^{p38\delta/FGF21KO}$ mice showed complete FAO (Figure 12C). This suggests FGF21 might impair complete mitochondrial FAO in HFD-fed mice lacking p38δ in hepatocytes. FGF21 has been related with KG (Vernia et al., 2014, Badman et al., 2007, Inagaki et al., 2007), peroxisomal oxidation (Badman et al., 2007, Vernia et al., 2014), mitochondrial fatty acid β-oxidation (Vernia et al., 2014, Badman et al., 2007, Inagaki et al., 2007), mainly at OXPHOS level (Vernia et al., 2014), and even with microsomal ω-oxidation (Vernia et al., 2014); however there are not studies which explore specific molecular mechanism by which FGF21 control the different kind of lipid oxidation. Therefore, our mouse models could help to better explore this.

Since $Alb^{p38\delta KO}$ mice showed increased incomplete FAO, but they were still protected against NAFLD, they might be used alternative non-mitochondrial lipid oxidation pathways to avoid intrahepatic lipid accumulation. Further studies might clarify this; however, since RNAseq and proteomics analysis in livers from $Alb^{p38\delta KO}$ mice showed slight upregulation of the ACOX1 signaling (data not shown), peroxisomal β-oxidation could be increased. The incomplete FAO as mechanisms to protect against NAFLD might have a temporal effectivity, because lipids partially oxidized will be finally accumulated in the hepatocytes; actually, $Alb^{p38\delta KO}$ mice showed some macrovesicles in liver (Figure 11A). However, $Alb^{p38\delta KO}$ mice could solve this problem increasing the Acyl-CoA hydrolysis pathway, where the main involved enzymes are the ACOT. These proteins hydrolyze acyl-CoA to the FFA and CoA. These enzymes have emerged as important lipid metabolism regulators because they control the level of FFA and acyl-CoA, which are involved in the activation or inhibition of many processes (Hunt et al., 2006, Tillander et al., 2017). Particularly, ACOT1 and 2 were found upregulated in livers from mice lacking p38δ (Figure 12A). ACOT1 and 2 have preference for long chain fatty acyl-CoA (Tillander et al., 2017); however, contrary to our data, the overexpression of ACOT2 in mouse livers enhances mitochondrial FAO (Moffat et al., 2014). Further studies using different approaches, as well as other FA as substrates (here only palmitate was used), may clarify peroxisome, mitochondria and ACOT role in lipid oxidation. Particularly 3 issues might be explored: 1) since ATP production was only altered in $Alb^{p38\delta KO}$ mice when ^{14}C-palmitoyl was used as substrate (Figure 11D), mitochondrial respiration might be further explored to see whether there is really mitochondrial dysfunction and to definitively confirm whether TCA is not functional. Moreover, the possible mitochondrial uncoupling that we observed

in livers from Alb$^{p38\delta KO}$ mice is agree with previous studies which have proposed to uncouple ATP production in the OXPHOS to treat T2D and NAFLD/NASH (Perry et al., 2015, Tao et al., 2014, Abulizi et al., 2017). 2) In case Alb$^{p38\delta KO}$ mice used peroxisome instead mitochondria for lipid β-oxidation, possible ROS accumulation, antioxidant systems and final implications might be explored. 3) An increase in the acyl-CoA hydrolysis would promote hepatic FA accumulation, which it is has been described is one of the main drivers of lipotoxicity; therefore possible consequences might be also explored.

Alb$^{p38\delta KO}$ mice showed decreased DNL (Figure 11B), accordingly with the protection against NAFLD that they showed. Cholesterol and mainly DAG have been clearly related with lipotoxicity and insulin resistance development (Ginsberg, 2006, Alkhouri et al., 2009, Erion and Shulman, 2010). Hepatic DAG content has been related with increased translocation of the primary novel protein kinase C (PKC) isoform ε in hepatocytes, to the plasma membrane, where binds and inhibits the activity of the intracellular kinase domain of the insulin receptor and consequently inhibits AKT phosphorylation (Dries et al., 2007, Samuel et al., 2007). Moreover, it has been shown that DAG concentration is readout of hepatic insulin resistance in obese humans (Magkos et al., 2012, Kumashiro et al., 2011). Additionally, the accumulation of cholesterol in mitochondria drives the liver mediated TNFα-mediated liver damage and ROS formation (Mari et al., 2006).

Since insulin signaling did not change in livers of Alb$^{p38\delta KO}$ mice (Figure 5A), reduced hepatic lipid content might be directly driving the protection against insulin resistance observed in these mice through alternative pathways (Figure 3C and 4A). Future studies might define particular mechanisms and lipids involve in the protection against insulin resistance in Alb$^{p38\delta KO}$ mice. Therefore this work, in agreement with recent literature, points out that to study individual lipid species role in metabolism and signaling is required for looking for possible therapeutic targets, especially in the liver, where these mechanisms have received less attention and basically it is only recognized the DAG/PKCε/INSR axis (Petersen and Shulman, 2018).

Lastly, it is important to consider that studies in mice lacking AKT1, AKT2 and insulin receptor together with ablation of Foxo1, one of the main transcription factor that promotes GNG, protects against insulin resistance (Lu et al., 2012, Titchenell et al., 2015), suggesting alternative unrecognized mechanism through which the liver responds to nutrients and insulin signaling. Moreover, current high-throughput techniques are reveling new proteins as parts of the insulin signaling network (Monetti et al., 2011). Therefore, Alb$^{p38\delta KO}$ mice could be also a new mouse model to find alternative pathways involve in insulin signaling and insulin resistance.

To summarize, CD-fed $Alb^{p38\delta KO}$ mice develop mild hypoglycemia, due to a glycogen storage reduction as a consequence of GYS2 activity impairment. Consequently, KG is increased. Moreover, $Alb^{p38\delta KO}$ mice hepatic DAG is decreased, which could be a preventive protective mechanism.
HFD-fed $Alb^{p38\delta KO}$ mice were protected against T2D and NAFLD. In one hand, GYS2 activity impairment and reduced glycogenesis and glycogen content reduced hyperglycemia. On the contrary, reduced DNL in HFD-fed $Alb^{p38\delta KO}$ mice as a consequence of decreased glycolytic flux, protected them against NAFLD. Since they showed diminished lipotoxicity, mice were protected against insulin resistance. Therefore, p38δ is a promising target to treat obesity-related T2D and NAFLD.

In this Thesis we have shown for the first time that hepatic p38δ MAPK is a key metabolic regulator, basically controlling glucose metabolism, but also with clear role in lipid metabolism. p38δ directly controls glycolysis, targeting PFKFB3 and glycogenesis, targeting GYS2. Additionally, p38δ is involved in the regulation of PPARα and FGF21; probably modulating the kind of lipid oxidation and accumulation depending of the nutrient state.

Therefore, in this work definitively we show that hepatic p38δ is a novel and central regulator of the liver metabolism and whole-body homeostasis. To decrease p38δ MAPK levels reduces liver energy state, which protects against high nutrient input; however, in normal conditions, it could be the cause of hypoglycemic-related diseases.

Conclusions

1. Chow diet-fed Alb$^{p38\delta KO}$ mice show mild hypoglycemia.

2. High fat diet-fed Alb$^{p38\delta KO}$ mice are protected against obesity-induced hyperglycemia, insulin resistance and NAFLD.

3. The overexpression of active p38δ MAPK in hepatocytes promotes hyperglycemia and insulin resistance.

4. Alb$^{p38\delta KO}$ mice have reduced glycogenesis, hepatic glycogen content, and consequently blood glucose levels.

5. Hepatic p38δ MAPK controls hepatic glucose metabolism through direct phosphorylation and regulation of GYS2 and PFKFB3 activity.

6. The lack of p38δ MAPK in hepatocytes decreases glycolytic flux that contributes to *de novo* lipogenesis, protecting HFD-fed mice against NAFLD and insulin resistance.

7. Hepatic p38δ MAPK might be a key factor controlling different lipid oxidation pathways, to protect against lipotoxicity and cell injury in HFD conditions.

8. Chow diet-fed Alb$^{p38\delta KO}$ mice accumulate C_{18}-CoA in the liver, decreasing DAG content.

9. p38δ MAPK might be a novel FGF21 regulator, a central hepatokine that controls whole body homeostasis.

10.Deletion of hepatic p38δ MAPK in obese mice protects against T2D and NAFLD.

Conclusiones

1. Los ratones Alb$^{p38\delta KO}$ alimentados con una dieta normal presentan hipoglucemia leve.

2. Los ratones Alb$^{p38\delta KO}$ alimentados con una dieta alta en grasa y colesterol están protegidos de hiperglucemia, resistencia a insulina e hígado graso no alcohólico asociados a la obesidad.

3. La sobreexpresión de la forma activa de p38δ en hepatocitos lleva al desarrollo de hiperglucemia y resistencia a insulina.

4. Los ratones Alb$^{p38\delta KO}$ presentan reducción de la glucogénesis hepática, del contenido hepático de glucógeno y como consecuencia disminución de los niveles de glucosa en sangre.

5. La estrés quinasa p38δ de los hepatocitos controla el metabolismo hepático glucídico a través de fosforilación y regulación directa de la actividad de las proteínas GYS2 y PFKFB3.

6. La carencia de p38δ en hepatocitos disminuye el flujo glucolítico, disminuyendo así la síntesis de lípidos *de novo* y protegiendo frente al desarrollo de hígado graso no alcohólico a ratones alimentados con una dieta alta en grasa y colesterol.

7. La estrés quinasa hepática p38δ parece ser un factor clave controlando diferentes vías de oxidación lipídica, para proteger frente a la acumulación intrahepática de lípidos y el daño celular en situaciones de dieta altas en grasa.

8. Los ratones Alb$^{p38\delta KO}$ alimentados con una dieta normal presentan acumulación de acil-CoA de C_{18} en hígado, disminuyendo el contenido de diacilglicéridos.

9. p38δ MAPK podría ser un nuevo regulador de FGF21, hepatoquina que controla la homeostasis global del organismo.

10. La deleción de p38δ en hepatocitos de ratones obesos protege frente a diabetes tipo 2 e hígado graso no alcohólico.

Bibliography

ABULIZI, A., PERRY, R. J., CAMPOREZ, J. P. G., JURCZAK, M. J., PETERSEN, K. F., ASPICHUETA, P. & SHULMAN, G. I. 2017. A controlled-release mitochondrial protonophore reverses hypertriglyceridemia, nonalcoholic steatohepatitis, and diabetes in lipodystrophic mice. *FASEB J,* 31**,** 2916-2924.

ACIN-PEREZ, R. & ENRIQUEZ, J. A. 2014. The function of the respiratory supercomplexes: the plasticity model. *Biochim Biophys Acta,* 1837**,** 444-50.

ADA. 2013. Available: http://www.diabetes.org/diabetes-basics/type-2/facts-about-type-2.html [Accessed 2019].

AGIUS, L. 2010. Physiological control of liver glycogen metabolism: lessons from novel glycogen phosphorylase inhibitors. *Mini Rev Med Chem,* 10**,** 1175-87.

AGUIRRE, V., WERNER, E. D., GIRAUD, J., LEE, Y. H., SHOELSON, S. E. & WHITE, M. F. 2002. Phosphorylation of Ser307 in insulin receptor substrate-1 blocks interactions with the insulin receptor and inhibits insulin action. *J Biol Chem,* 277**,** 1531-7.

ALEVY, Y. G., PATEL, A. C., ROMERO, A. G., PATEL, D. A., TUCKER, J., ROSWIT, W. T., MILLER, C. A., HEIER, R. F., BYERS, D. E., BRETT, T. J. & HOLTZMAN, M. J. 2012. IL-13-induced airway mucus production is attenuated by MAPK13 inhibition. *J Clin Invest,* 122**,** 4555-68.

ALKHOURI, N., DIXON, L. J. & FELDSTEIN, A. E. 2009. Lipotoxicity in nonalcoholic fatty liver disease: not all lipids are created equal. *Expert Rev Gastroenterol Hepatol,* 3**,** 445-51.

ALSINA-BEAUCHAMP, D., ESCOS, A., FAJARDO, P., GONZALEZ-ROMERO, D., DIAZ-MORA, E., RISCO, A., MARTIN-SERRANO, M. A., DEL FRESNO, C., DOMINGUEZ-ANDRES, J., APARICIO, N., ZUR, R., SHPIRO, N., BROWN, G. D., ARDAVIN, C., NETEA, M. G., ALEMANY, S., SANZ-EZQUERRO, J. J. & CUENDA, A. 2018. Myeloid cell deficiency of p38gamma/p38delta protects against candidiasis and regulates antifungal immunity. *EMBO Mol Med,* 10.

ANGULO, P. 2002. Nonalcoholic fatty liver disease. *N Engl J Med,* 346**,** 1221-31.

ANGULO, P. & LINDOR, K. D. 2002. Non-alcoholic fatty liver disease. *J Gastroenterol Hepatol,* 17 Suppl**,** S186-90.

ANTONIEWICZ, M. R., KELLEHER, J. K. & STEPHANOPOULOS, G. 2011. Measuring deuterium enrichment of glucose hydrogen atoms by gas chromatography/mass spectrometry. *Anal Chem,* 83**,** 3211-6.

ARAYA, J., RODRIGO, R., VIDELA, L. A., THIELEMANN, L., ORELLANA, M., PETTINELLI, P. & PONIACHIK, J. 2004. Increase in long-chain polyunsaturated fatty acid n - 6/n - 3 ratio in relation to hepatic steatosis in patients with non-alcoholic fatty liver disease. *Clin Sci (Lond),* 106**,** 635-43.

ARTHUR, J. S. & LEY, S. C. 2013. Mitogen-activated protein kinases in innate immunity. *Nat Rev Immunol,* 13**,** 679-92.

ASPICHUETA, P., PEREZ, S., OCHOA, B. & FRESNEDO, O. 2005. Endotoxin promotes preferential periportal upregulation of VLDL secretion in the rat liver. *J Lipid Res,* 46**,** 1017-26.

ATLAS, T. *PFKFB1* [Online]. Available: https://www.proteinatlas.org/ENSG00000158571-PFKFB1/tissue [Accessed 2019].

ATLAS, T. *PFKFB3* [Online]. Available: https://www.proteinatlas.org/ENSG00000170525-PFKFB3/tissue [Accessed 2019].

ATSHAVES, B. P., MARTIN, G. G., HOSTETLER, H. A., MCINTOSH, A. L., KIER, A. B. & SCHROEDER, F. 2010. Liver fatty acid-binding protein and obesity. *J Nutr Biochem,* 21**,** 1015-32.

AYALA, J. E., BRACY, D. P., MCGUINNESS, O. P. & WASSERMAN, D. H. 2006. Considerations in the design of hyperinsulinemic-euglycemic clamps in the conscious mouse. *Diabetes,* 55**,** 390-7.

AYALA, J. E., SAMUEL, V. T., MORTON, G. J., OBICI, S., CRONIGER, C. M., SHULMAN, G. I., WASSERMAN, D. H., MCGUINNESS, O. P. & CONSORTIUM, N. I. H. M. M. P. C. 2010. Standard operating procedures for describing and performing metabolic tests of glucose homeostasis in mice. *Dis Model Mech,* 3**,** 525-34.

AZPIAZU, I., MANCHESTER, J., SKURAT, A. V., ROACH, P. J. & LAWRENCE, J. C., JR. 2000. Control of glycogen synthesis is shared between glucose transport and glycogen synthase in skeletal muscle fibers. *Am J Physiol Endocrinol Metab,* 278**,** E234-43.

BADMAN, M. K., KOESTER, A., FLIER, J. S., KHARITONENKOV, A. & MARATOS-FLIER, E. 2009. Fibroblast growth factor 21-deficient mice demonstrate impaired adaptation to ketosis. *Endocrinology,* 150**,** 4931-40.

BADMAN, M. K., PISSIOS, P., KENNEDY, A. R., KOUKOS, G., FLIER, J. S. & MARATOS-FLIER, E. 2007. Hepatic fibroblast growth factor 21 is regulated by PPARalpha and is a key mediator of hepatic lipid metabolism in ketotic states. *Cell Metab,* 5**,** 426-37.

BALASUBRAMANIAN, S., EFIMOVA, T. & ECKERT, R. L. 2002. Green tea polyphenol stimulates a Ras, MEKK1, MEK3, and p38 cascade to increase activator protein 1 factor-dependent involucrin gene expression in normal human keratinocytes. *J Biol Chem,* 277**,** 1828-36.

BANDSMA, R. H., PRINSEN, B. H., VAN DER VELDEN MDE, S., RAKE, J. P., BOER, T., SMIT, G. P., REIJNGOUD, D. J. & KUIPERS, F. 2008. Increased de novo lipogenesis and delayed conversion of large VLDL into intermediate density lipoprotein particles contribute to hyperlipidemia in glycogen storage disease type 1a. *Pediatr Res,* 63**,** 702-7.

BARGER, P. M., BROWNING, A. C., GARNER, A. N. & KELLY, D. P. 2001. p38 mitogen-activated protein kinase activates peroxisome proliferator-activated receptor alpha: a potential role in the cardiac metabolic stress response. *J Biol Chem,* 276**,** 44495-501.

BARTELS, H., VOGT, B. & JUNGERMANN, K. 1987. Glycogen synthesis from pyruvate in the periportal and from glucose in the perivenous zone in perfused livers from fasted rats. *FEBS Lett,* 221**,** 277-83.

BASARANOGLU, M., BASARANOGLU, G. & SENTURK, H. 2013. From fatty liver to fibrosis: a tale of "second hit". *World J Gastroenterol,* 19**,** 1158-65.

BEARDMORE, V. A., HINTON, H. J., EFTYCHI, C., APOSTOLAKI, M., ARMAKA, M., DARRAGH, J., MCILRATH, J., CARR, J. M., ARMIT, L. J., CLACHER, C., MALONE, L., KOLLIAS, G. & ARTHUR, J. S. 2005. Generation and characterization of p38beta (MAPK11) gene-targeted mice. *Mol Cell Biol,* 25**,** 10454-64.

BEGRICHE, K., IGOUDJIL, A., PESSAYRE, D. & FROMENTY, B. 2006. Mitochondrial dysfunction in NASH: causes, consequences and possible means to prevent it. *Mitochondrion,* 6**,** 1-28.

BERG JM, T. J., STRYER L, CLARKE ND 2002. *Biochemistry*, W. H. Freeman and Company.

BERGLUND, E. D., LI, C. Y., BINA, H. A., LYNES, S. E., MICHAEL, M. D., SHANAFELT, A. B., KHARITONENKOV, A. & WASSERMAN, D. H. 2009. Fibroblast growth factor 21 controls glycemia via regulation of hepatic glucose flux and insulin sensitivity. *Endocrinology,* 150**,** 4084-93.

BHATT, H. B. & SMITH, R. J. 2015. Fatty liver disease in diabetes mellitus. *Hepatobiliary Surg Nutr,* 4**,** 101-8.

BIRKENFELD, A. L. & SHULMAN, G. I. 2014. Nonalcoholic fatty liver disease, hepatic insulin resistance, and type 2 diabetes. *Hepatology,* 59**,** 713-23.

BOJIC, L. A., TELFORD, D. E., FULLERTON, M. D., FORD, R. J., SUTHERLAND, B. G., EDWARDS, J. Y., SAWYEZ, C. G., GROS, R., KEMP, B. E., STEINBERG, G. R. & HUFF, M. W. 2014. PPARdelta activation attenuates hepatic steatosis in Ldlr-/- mice by enhanced fat oxidation, reduced lipogenesis, and improved insulin sensitivity. *J Lipid Res,* 55**,** 1254-66.

BOLANOS, J. P. 2013. Adapting glycolysis to cancer cell proliferation: the MAPK pathway focuses on PFKFB3. *Biochem J,* 452**,** e7-9.

BOLLEN, M. 2001. Combinatorial control of protein phosphatase-1. *Trends Biochem Sci,* 26**,** 426-31.

BOLLEN, M., KEPPENS, S. & STALMANS, W. 1998. Specific features of glycogen metabolism in the liver. *Biochem J,* 336 (Pt 1)**,** 19-31.

BONZON-KULICHENKO, E., GARCIA-MARQUES, F., TREVISAN-HERRAZ, M. & VAZQUEZ, J. 2015. Revisiting peptide identification by high-accuracy mass spectrometry: problems associated with the use of narrow mass precursor windows. *J Proteome Res,* 14**,** 700-10.

BRACONI QUINTAJE, S. & ORCHARD, S. 2008. The annotation of both human and mouse kinomes in UniProtKB/Swiss-Prot: one small step in manual annotation, one giant leap for full comprehension of genomes. *Mol Cell Proteomics,* 7**,** 1409-19.

BRAMBLETT, G. T., GOEDERT, M., JAKES, R., MERRICK, S. E., TROJANOWSKI, J. Q. & LEE, V. M. 1993. Abnormal tau phosphorylation at Ser396 in Alzheimer's disease recapitulates development and contributes to reduced microtubule binding. *Neuron,* 10**,** 1089-99.

BROWN, M. S. & GOLDSTEIN, J. L. 2008. Selective versus total insulin resistance: a pathogenic paradox. *Cell Metab,* 7**,** 95-6.

BROWNER, M. F., NAKANO, K., BANG, A. G. & FLETTERICK, R. J. 1989. Human muscle glycogen synthase cDNA sequence: a negatively charged protein with an asymmetric charge distribution. *Proc Natl Acad Sci U S A,* 86**,** 1443-7.

BROWNING, J. D. & HORTON, J. D. 2004. Molecular mediators of hepatic steatosis and liver injury. *J Clin Invest,* 114**,** 147-52.

BRUNT, E. M., NEUSCHWANDER-TETRI, B. A., OLIVER, D., WEHMEIER, K. R. & BACON, B. R. 2004. Nonalcoholic steatohepatitis: histologic features and clinical correlations with 30 blinded biopsy specimens. *Hum Pathol,* 35**,** 1070-82.

BUEE-SCHERRER, V. & GOEDERT, M. 2002. Phosphorylation of microtubule-associated protein tau by stress-activated protein kinases in intact cells. *FEBS Lett,* 515**,** 151-4.

BULTOT, L., GUIGAS, B., VON WILAMOWITZ-MOELLENDORFF, A., MAISIN, L., VERTOMMEN, D., HUSSAIN, N., BEULLENS, M., GUINOVART, J. J., FORETZ, M., VIOLLET, B., SAKAMOTO, K., HUE, L. & RIDER, M. H. 2012. AMP-activated protein kinase phosphorylates and inactivates liver glycogen synthase. *Biochem J,* 443**,** 193-203.

BUZZETTI, E., PINZANI, M. & TSOCHATZIS, E. A. 2016. The multiple-hit pathogenesis of non-alcoholic fatty liver disease (NAFLD). *Metabolism,* 65**,** 1038-48.

CALDWELL, S. H., CHANG, C. Y., NAKAMOTO, R. K. & KRUGNER-HIGBY, L. 2004. Mitochondria in nonalcoholic fatty liver disease. *Clin Liver Dis,* 8**,** 595-617, x.

CAMPOREZ, J. P., JORNAYVAZ, F. R., PETERSEN, M. C., PESTA, D., GUIGNI, B. A., SERR, J., ZHANG, D., KAHN, M., SAMUEL, V. T., JURCZAK, M. J. & SHULMAN, G. I. 2013. Cellular mechanisms by which FGF21 improves insulin sensitivity in male mice. *Endocrinology,* 154**,** 3099-109.

CANTLEY, J. L., YOSHIMURA, T., CAMPOREZ, J. P., ZHANG, D., JORNAYVAZ, F. R., KUMASHIRO, N., GUEBRE-EGZIABHER, F., JURCZAK, M. J., KAHN, M., GUIGNI, B. A., SERR, J., HANKIN, J., MURPHY, R. C., CLINE, G. W., BHANOT, S., MANCHEM, V. P., BROWN, J. M., SAMUEL, V. T. & SHULMAN, G. I. 2013. CGI-58 knockdown sequesters diacylglycerols in lipid droplets/ER-preventing diacylglycerol-mediated hepatic insulin resistance. *Proc Natl Acad Sci U S A,* 110**,** 1869-74.

CAO, W., COLLINS, Q. F., BECKER, T. C., ROBIDOUX, J., LUPO, E. G., JR., XIONG, Y., DANIEL, K. W., FLOERING, L. & COLLINS, S. 2005. p38 Mitogen-activated protein kinase plays a stimulatory role in hepatic gluconeogenesis. *J Biol Chem,* 280**,** 42731-7.

CARABAZA, A., CIUDAD, C. J., BAQUE, S. & GUINOVART, J. J. 1992. Glucose has to be phosphorylated to activate glycogen synthase, but not to inactivate glycogen phosphorylase in hepatocytes. *FEBS Lett,* 296**,** 211-4.

CARDELL, R. R., JR., MICHAELS, J. E., HUNG, J. T. & CARDELL, E. L. 1985. SERGE, the subcellular site of initial hepatic glycogen deposition in the rat: a radioautographic and cytochemical study. *J Cell Biol,* 101**,** 201-6.

CARR, R. M. & AHIMA, R. S. 2016. Pathophysiology of lipid droplet proteins in liver diseases. *Exp Cell Res,* 340**,** 187-92.

CEREZO-GUISADO, M. I., DEL REINO, P., REMY, G., KUMA, Y., ARTHUR, J. S., GALLEGO-ORTEGA, D. & CUENDA, A. 2011. Evidence of p38gamma and p38delta involvement in cell transformation processes. *Carcinogenesis,* 32**,** 1093-9.

CEULEMANS, H. & BOLLEN, M. 2004. Functional diversity of protein phosphatase-1, a cellular economizer and reset button. *Physiol Rev,* 84**,** 1-39.

CHADT, A., SCHERNECK, S., JOOST, H. G. & AL-HASANI, H. 2000. Molecular links between Obesity and Diabetes: "Diabesity". *In:* DE GROOT, L. J., CHROUSOS, G., DUNGAN, K., FEINGOLD, K. R., GROSSMAN, A., HERSHMAN, J. M., KOCH, C., KORBONITS, M., MCLACHLAN, R., NEW, M., PURNELL, J., REBAR, R., SINGER, F. & VINIK, A. (eds.) *Endotext.* South Dartmouth (MA).

CHAKRAVARTHY, M. V., PAN, Z., ZHU, Y., TORDJMAN, K., SCHNEIDER, J. G., COLEMAN, T., TURK, J. & SEMENKOVICH, C. F. 2005. "New" hepatic fat activates PPARalpha to maintain glucose, lipid, and cholesterol homeostasis. *Cell Metab,* 1**,** 309-22.

CHANG-CHEN, K. J., MULLUR, R. & BERNAL-MIZRACHI, E. 2008. Beta-cell failure as a complication of diabetes. *Rev Endocr Metab Disord,* 9**,** 329-43.

CHAVEZ, J. A. & SUMMERS, S. A. 2012. A ceramide-centric view of insulin resistance. *Cell Metab,* 15**,** 585-94.

CHEN, G., LIANG, G., OU, J., GOLDSTEIN, J. L. & BROWN, M. S. 2004. Central role for liver X receptor in insulin-mediated activation of Srebp-1c transcription and stimulation of fatty acid synthesis in liver. *Proc Natl Acad Sci U S A,* 101**,** 11245-50.

CHEUNG, O. & SANYAL, A. J. 2008. Abnormalities of lipid metabolism in nonalcoholic fatty liver disease. *Semin Liver Dis,* 28**,** 351-9.

CHUNG, S. T., CHACKO, S. K., SUNEHAG, A. L. & HAYMOND, M. W. 2015. Measurements of Gluconeogenesis and Glycogenolysis: A Methodological Review. *Diabetes,* 64**,** 3996-4010.

CLEMENTI, A. H., GAUDY, A. M., VAN ROOIJEN, N., PIERCE, R. H. & MOONEY, R. A. 2009. Loss of Kupffer cells in diet-induced obesity is associated with increased hepatic steatosis, STAT3 signaling, and further decreases in insulin signaling. *Biochim Biophys Acta,* 1792**,** 1062-72.

CLINE, G. W., JOHNSON, K., REGITTNIG, W., PERRET, P., TOZZO, E., XIAO, L., DAMICO, C. & SHULMAN, G. I. 2002. Effects of a novel glycogen synthase kinase-3 inhibitor on insulin-stimulated glucose metabolism in Zucker diabetic fatty (fa/fa) rats. *Diabetes,* 51**,** 2903-10.

COELHO, M., OLIVEIRA, T. & FERNANDES, R. 2013. Biochemistry of adipose tissue: an endocrine organ. *Arch Med Sci,* 9**,** 191-200.

COGHLAN, M. P., CULBERT, A. A., CROSS, D. A., CORCORAN, S. L., YATES, J. W., PEARCE, N. J., RAUSCH, O. L., MURPHY, G. J., CARTER, P. S., ROXBEE COX, L., MILLS, D., BROWN, M. J., HAIGH, D., WARD, R. W., SMITH, D. G., MURRAY, K. J., REITH, A. D. & HOLDER, J. C. 2000. Selective small molecule inhibitors of glycogen synthase kinase-3 modulate glycogen metabolism and gene transcription. *Chem Biol,* 7**,** 793-803.

COHEN, J. C., HORTON, J. D. & HOBBS, H. H. 2011. Human fatty liver disease: old questions and new insights. *Science,* 332**,** 1519-23.

COLLABORATORS, G. B. D. O., AFSHIN, A., FOROUZANFAR, M. H., REITSMA, M. B., SUR, P., ESTEP, K., LEE, A., MARCZAK, L., MOKDAD, A. H., MORADI-LAKEH, M., NAGHAVI, M., SALAMA, J. S., VOS, T., ABATE, K. H., ABBAFATI, C., AHMED, M. B., AL-ALY, Z., ALKERWI, A., AL-RADDADI, R., AMARE, A. T., AMBERBIR, A., AMEGAH, A. K., AMINI, E., AMROCK, S. M., ANJANA, R. M., ARNLOV, J., ASAYESH, H., BANERJEE, A., BARAC, A., BAYE, E., BENNETT, D. A., BEYENE, A. S., BIADGILIGN, S., BIRYUKOV, S., BJERTNESS, E., BONEYA, D. J., CAMPOS-NONATO, I., CARRERO, J. J., CECILIO, P., CERCY, K., CIOBANU, L. G., CORNABY, L., DAMTEW, S. A., DANDONA, L., DANDONA, R., DHARMARATNE, S. D., DUNCAN, B. B., ESHRATI, B., ESTEGHAMATI, A., FEIGIN, V. L., FERNANDES, J. C., FURST, T., GEBREHIWOT, T. T., GOLD, A., GONA, P. N., GOTO, A., HABTEWOLD, T. D., HADUSH, K. T., HAFEZI-NEJAD, N., HAY, S. I., HORINO, M., ISLAMI, F., KAMAL, R., KASAEIAN, A., KATIKIREDDI, S. V., KENGNE, A. P., KESAVACHANDRAN, C. N., KHADER, Y. S., KHANG, Y. H., KHUBCHANDANI, J., KIM, D., KIM, Y. J., KINFU, Y., KOSEN, S., KU, T., DEFO, B. K., KUMAR, G. A., LARSON, H. J., LEINSALU, M., LIANG, X., LIM, S. S., LIU, P., LOPEZ, A. D., LOZANO, R., MAJEED, A.,

MALEKZADEH, R., MALTA, D. C., MAZIDI, M., MCALINDEN, C., MCGARVEY, S. T., MENGISTU, D. T., MENSAH, G. A., MENSINK, G. B. M., MEZGEBE, H. B., MIRRAKHIMOV, E. M., MUELLER, U. O., NOUBIAP, J. J., OBERMEYER, C. M., OGBO, F. A., OWOLABI, M. O., et al. 2017. Health Effects of Overweight and Obesity in 195 Countries over 25 Years. *N Engl J Med,* 377**,** 13-27.

CORTEZ-PINTO, H., DE MOURA, M. C. & DAY, C. P. 2006. Non-alcoholic steatohepatitis: from cell biology to clinical practice. *J Hepatol,* 44**,** 197-208.

COSKUN, T., BINA, H. A., SCHNEIDER, M. A., DUNBAR, J. D., HU, C. C., CHEN, Y., MOLLER, D. E. & KHARITONENKOV, A. 2008. Fibroblast growth factor 21 corrects obesity in mice. *Endocrinology,* 149**,** 6018-27.

COUGHLAN, M. T., YAP, F. Y., TONG, D. C., ANDRIKOPOULOS, S., GASSER, A., THALLAS-BONKE, V., WEBSTER, D. E., MIYAZAKI, J., KAY, T. W., SLATTERY, R. M., KAYE, D. M., DREW, B. G., KINGWELL, B. A., FOURLANOS, S., GROOP, P. H., HARRISON, L. C., KNIP, M. & FORBES, J. M. 2011. Advanced glycation end products are direct modulators of beta-cell function. *Diabetes,* 60**,** 2523-32.

COULTHARD, L. R., WHITE, D. E., JONES, D. L., MCDERMOTT, M. F. & BURCHILL, S. A. 2009. p38(MAPK): stress responses from molecular mechanisms to therapeutics. *Trends Mol Med,* 15**,** 369-79.

CRIADO, G., RISCO, A., ALSINA-BEAUCHAMP, D., PEREZ-LORENZO, M. J., ESCOS, A. & CUENDA, A. 2014. Alternative p38 MAPKs are essential for collagen-induced arthritis. *Arthritis Rheumatol,* 66**,** 1208-17.

CUADRADO, A. & NEBREDA, A. R. 2010. Mechanisms and functions of p38 MAPK signalling. *Biochem J,* 429**,** 403-17.

CUBERO, F. J., ZOUBEK, M. E., HU, W., PENG, J., ZHAO, G., NEVZOROVA, Y. A., AL MASAOUDI, M., BECHMANN, L. P., BOEKSCHOTEN, M. V., MULLER, M., PREISINGER, C., GASSLER, N., CANBAY, A. E., LUEDDE, T., DAVIS, R. J., LIEDTKE, C. & TRAUTWEIN, C. 2016. Combined Activities of JNK1 and JNK2 in Hepatocytes Protect Against Toxic Liver Injury. *Gastroenterology,* 150**,** 968-81.

CUENDA, A. & ROUSSEAU, S. 2007. p38 MAP-kinases pathway regulation, function and role in human diseases. *Biochim Biophys Acta,* 1773**,** 1358-75.

CUEVAS, B. D., ABELL, A. N. & JOHNSON, G. L. 2007. Role of mitogen-activated protein kinase kinase kinases in signal integration. *Oncogene,* 26**,** 3159-71.

CUSI, K. 2009. Role of insulin resistance and lipotoxicity in non-alcoholic steatohepatitis. *Clin Liver Dis,* 13**,** 545-63.

CZAJA, M. J. 2016. Function of Autophagy in Nonalcoholic Fatty Liver Disease. *Dig Dis Sci,* 61**,** 1304-13.

CZYZYK, T. A., ROMERO-PICO, A., PINTAR, J., MCKINZIE, J. H., TSCHOP, M. H., STATNICK, M. A. & NOGUEIRAS, R. 2012. Mice lacking delta-opioid receptors resist the development of diet-induced obesity. *FASEB J,* 26**,** 3483-92.

DASHTI, S. R., EFIMOVA, T. & ECKERT, R. L. 2001. MEK6 regulates human involucrin gene expression via a p38alpha - and p38delta -dependent mechanism. *J Biol Chem,* 276**,** 27214-20.

DAVIS, R. J. 2000. Signal transduction by the JNK group of MAP kinases. *Cell,* 103**,** 239-52.

DAY, C. P. & JAMES, O. F. 1998. Steatohepatitis: a tale of two "hits"? *Gastroenterology,* 114**,** 842-5.

DE LA IGLESIA, N., MUKHTAR, M., SEOANE, J., GUINOVART, J. J. & AGIUS, L. 2000. The role of the regulatory protein of glucokinase in the glucose sensory mechanism of the hepatocyte. *J Biol Chem,* 275**,** 10597-603.

DEFRONZO, R. A. 2004. Pathogenesis of type 2 diabetes mellitus. *Med Clin North Am,* 88**,** 787-835, ix.

DEL REINO, P., ALSINA-BEAUCHAMP, D., ESCOS, A., CEREZO-GUISADO, M. I., RISCO, A., APARICIO, N., ZUR, R., FERNANDEZ-ESTEVEZ, M., COLLANTES, E., MONTANS, J. & CUENDA, A. 2014. Pro-oncogenic role of alternative p38 mitogen-activated protein kinases p38gamma and p38delta, linking inflammation and cancer in colitis-associated colon cancer. *Cancer Res,* 74**,** 6150-60.

DEMARQUOY, J. & LE BORGNE, F. 2015. Crosstalk between mitochondria and peroxisomes. *World J Biol Chem,* 6**,** 301-9.

DENG, H., YU, F., CHEN, J., ZHAO, Y., XIANG, J. & LIN, A. 2008. Phosphorylation of Bad at Thr-201 by JNK1 promotes glycolysis through activation of phosphofructokinase-1. *J Biol Chem,* 283**,** 20754-60.

DESIDERI, E., VEGLIANTE, R., CARDACI, S., NEPRAVISHTA, R., PACI, M. & CIRIOLO, M. R. 2014. MAPK14/p38alpha-dependent modulation of glucose metabolism affects ROS levels and autophagy during starvation. *Autophagy,* 10**,** 1652-65.

DEUTSCH, J., GRANGE, E., RAPOPORT, S. I. & PURDON, A. D. 1994. Isolation and quantitation of long-chain acyl-coenzyme A esters in brain tissue by solid-phase extraction. *Anal Biochem,* 220**,** 321-3.

DHANASEKARAN, D. N., KASHEF, K., LEE, C. M., XU, H. & REDDY, E. P. 2007. Scaffold proteins of MAP-kinase modules. *Oncogene,* 26**,** 3185-202.

DING, C., LI, Y., GUO, F., JIANG, Y., YING, W., LI, D., YANG, D., XIA, X., LIU, W., ZHAO, Y., HE, Y., LI, X., SUN, W., LIU, Q., SONG, L., ZHEN, B., ZHANG, P., QIAN, X., QIN, J. & HE, F. 2016. A Cell-type-resolved Liver Proteome. *Mol Cell Proteomics,* 15**,** 3190-3202.

DOEGE, H., GRIMM, D., FALCON, A., TSANG, B., STORM, T. A., XU, H., ORTEGON, A. M., KAZANTZIS, M., KAY, M. A. & STAHL, A. 2008. Silencing of hepatic fatty acid transporter protein 5 in vivo reverses diet-induced non-alcoholic fatty liver disease and improves hyperglycemia. *J Biol Chem,* 283**,** 22186-92.

DOHERTY, M. J., MOORHEAD, G., MORRICE, N., COHEN, P. & COHEN, P. T. 1995. Amino acid sequence and expression of the hepatic glycogen-binding (GL)-subunit of protein phosphatase-1. *FEBS Lett,* 375**,** 294-8.

DONNELLY, K. L., SMITH, C. I., SCHWARZENBERG, S. J., JESSURUN, J., BOLDT, M. D. & PARKS, E. J. 2005. Sources of fatty acids stored in liver and secreted via lipoproteins in patients with nonalcoholic fatty liver disease. *J Clin Invest,* 115**,** 1343-51.

DRIES, D. R., GALLEGOS, L. L. & NEWTON, A. C. 2007. A single residue in the C1 domain sensitizes novel protein kinase C isoforms to cellular diacylglycerol production. *J Biol Chem,* 282**,** 826-30.

DU PLESSIS, J., VAN PELT, J., KORF, H., MATHIEU, C., VAN DER SCHUEREN, B., LANNOO, M., OYEN, T., TOPAL, B., FETTER, G., NAYLER, S., VAN DER MERWE, T., WINDMOLDERS, P., VAN GAAL, L., VERRIJKEN, A., HUBENS, G., GERICKE, M., CASSIMAN, D., FRANCQUE, S., NEVENS, F. & VAN DER MERWE, S. 2015. Association of Adipose Tissue Inflammation With Histologic Severity of Nonalcoholic Fatty Liver Disease. *Gastroenterology,* 149**,** 635-48 e14.

DURAN, J., OBACH, M., NAVARRO-SABATE, A., MANZANO, A., GOMEZ, M., ROSA, J. L., VENTURA, F., PERALES, J. C. & BARTRONS, R. 2009. Pfkfb3 is transcriptionally upregulated in diabetic mouse liver through proliferative signals. *FEBS J,* 276**,** 4555-68.

DUSHAY, J., CHUI, P. C., GOPALAKRISHNAN, G. S., VARELA-REY, M., CRAWLEY, M., FISHER, F. M., BADMAN, M. K., MARTINEZ-CHANTAR, M. L. & MARATOS-FLIER, E. 2010. Increased fibroblast growth factor 21 in obesity and nonalcoholic fatty liver disease. *Gastroenterology,* 139**,** 456-63.

ECKEL, R. H., KAHN, S. E., FERRANNINI, E., GOLDFINE, A. B., NATHAN, D. M., SCHWARTZ, M. W., SMITH, R. J. & SMITH, S. R. 2011. Obesity and type 2 diabetes: what can be unified and what needs to be individualized? *J Clin Endocrinol Metab,* 96**,** 1654-63.

EFIMOVA, T., BROOME, A. M. & ECKERT, R. L. 2003. A regulatory role for p38 delta MAPK in keratinocyte differentiation. Evidence for p38 delta-ERK1/2 complex formation. *J Biol Chem,* 278**,** 34277-85.

EFIMOVA, T., BROOME, A. M. & ECKERT, R. L. 2004. Protein kinase Cdelta regulates keratinocyte death and survival by regulating activity and subcellular localization of a p38delta-extracellular signal-regulated kinase 1/2 complex. *Mol Cell Biol,* 24**,** 8167-83.

EKBERG, K., LANDAU, B. R., WAJNGOT, A., CHANDRAMOULI, V., EFENDIC, S., BRUNENGRABER, H. & WAHREN, J. 1999. Contributions by kidney and liver to glucose production in the postabsorptive state and after 60 h of fasting. *Diabetes,* 48**,** 292-8.

ERION, D. M. & SHULMAN, G. I. 2010. Diacylglycerol-mediated insulin resistance. *Nat Med,* 16**,** 400-2.

EVANS, R. M., BARISH, G. D. & WANG, Y. X. 2004. PPARs and the complex journey to obesity. *Nat Med,* 10**,** 355-61.

EYERS, P. A., CRAXTON, M., MORRICE, N., COHEN, P. & GOEDERT, M. 1998. Conversion of SB 203580-insensitive MAP kinase family members to drug-sensitive forms by a single amino-acid substitution. *Chem Biol,* 5**,** 321-8.

FALCON, A., DOEGE, H., FLUITT, A., TSANG, B., WATSON, N., KAY, M. A. & STAHL, A. 2010. FATP2 is a hepatic fatty acid transporter and peroxisomal very long-chain acyl-CoA synthetase. *Am J Physiol Endocrinol Metab,* 299**,** E384-93.

FAN, C. Y., PAN, J., USUDA, N., YELDANDI, A. V., RAO, M. S. & REDDY, J. K. 1998. Steatohepatitis, spontaneous peroxisome proliferation and liver tumors in mice lacking peroxisomal fatty acyl-CoA oxidase. Implications for peroxisome proliferator-activated receptor alpha natural ligand metabolism. *J Biol Chem,* 273**,** 15639-45.

FARESE, R. V., JR., ZECHNER, R., NEWGARD, C. B. & WALTHER, T. C. 2012. The problem of establishing relationships between hepatic steatosis and hepatic insulin resistance. *Cell Metab,* 15**,** 570-3.

FELBER, J. P. & GOLAY, A. 2002. Pathways from obesity to diabetes. *Int J Obes Relat Metab Disord,* 26 Suppl 2**,** S39-45.

FELDSTEIN, A. E., CANBAY, A., ANGULO, P., TANIAI, M., BURGART, L. J., LINDOR, K. D. & GORES, G. J. 2003. Hepatocyte apoptosis and fas expression are prominent features of human nonalcoholic steatohepatitis. *Gastroenterology,* 125**,** 437-43.

FELIG, P. 1973. The glucose-alanine cycle. *Metabolism,* 22**,** 179-207.

FENG, B., JIAO, P., HELOU, Y., LI, Y., HE, Q., WALTERS, M. S., SALOMON, A. & XU, H. 2014. Mitogen-activated protein kinase phosphatase 3 (MKP-3)-deficient mice are resistant to diet-induced obesity. *Diabetes,* 63**,** 2924-34.

FERNANDEZ-NOVELL, J. M., BELLIDO, D., VILARO, S. & GUINOVART, J. J. 1997. Glucose induces the translocation of glycogen synthase to the cell cortex in rat hepatocytes. *Biochem J,* 321 (Pt 1)**,** 227-31.

FERNANDEZ-NOVELL, J. M., LOPEZ-IGLESIAS, C., FERRER, J. C. & GUINOVART, J. J. 2002. Zonal distribution of glycogen synthesis in isolated rat hepatocytes. *FEBS Lett,* 531**,** 222-8.

FERRER, J. C., FAVRE, C., GOMIS, R. R., FERNANDEZ-NOVELL, J. M., GARCIA-ROCHA, M., DE LA IGLESIA, N., CID, E. & GUINOVART, J. J. 2003. Control of glycogen deposition. *FEBS Lett,* 546**,** 127-32.

FIOL, C. J., MAHRENHOLZ, A. M., WANG, Y., ROESKE, R. W. & ROACH, P. J. 1987. Formation of protein kinase recognition sites by covalent modification of the substrate. Molecular mechanism for the synergistic action of casein kinase II and glycogen synthase kinase 3. *J Biol Chem,* 262**,** 14042-8.

FIRNEISZ, G. 2014. Non-alcoholic fatty liver disease and type 2 diabetes mellitus: the liver disease of our age? *World J Gastroenterol,* 20**,** 9072-89.

FISHER, F. M., CHUI, P. C., ANTONELLIS, P. J., BINA, H. A., KHARITONENKOV, A., FLIER, J. S. & MARATOS-FLIER, E. 2010. Obesity is a fibroblast growth factor 21 (FGF21)-resistant state. *Diabetes,* 59**,** 2781-9.

FISHER, F. M. & MARATOS-FLIER, E. 2016. Understanding the Physiology of FGF21. *Annu Rev Physiol,* 78**,** 223-41.

FLACH, R. J., QIN, H., ZHANG, L. & BENNETT, A. M. 2011. Loss of mitogen-activated protein kinase phosphatase-1 protects from hepatic steatosis by repression of cell death-inducing DNA fragmentation factor A (DFFA)-like effector C (CIDEC)/fat-specific protein 27. *J Biol Chem,* 286**,** 22195-202.

FOLCH, J., LEES, M. & SLOANE STANLEY, G. H. 1957. A simple method for the isolation and purification of total lipides from animal tissues. *J Biol Chem,* 226**,** 497-509.

FRANKLIN, C. C. & KRAFT, A. S. 1997. Conditional expression of the mitogen-activated protein kinase (MAPK) phosphatase MKP-1 preferentially inhibits p38 MAPK and stress-activated protein kinase in U937 cells. *J Biol Chem,* 272**,** 16917-23.

FRANSEN, M., LISMONT, C. & WALTON, P. 2017. The Peroxisome-Mitochondria Connection: How and Why? *Int J Mol Sci,* 18.

FREZZA, C., CIPOLAT, S. & SCORRANO, L. 2007. Organelle isolation: functional mitochondria from mouse liver, muscle and cultured fibroblasts. *Nat Protoc,* 2**,** 287-95.

FRIEDMAN, S. L. 2008. Mechanisms of hepatic fibrogenesis. *Gastroenterology,* 134**,** 1655-69.

FROMENTY, B., BERSON, A. & PESSAYRE, D. 1997. Microvesicular steatosis and steatohepatitis: role of mitochondrial dysfunction and lipid peroxidation. *J Hepatol,* 26 Suppl 1**,** 13-22.

FROMENTY, B. & PESSAYRE, D. 1997. Impaired mitochondrial function in microvesicular steatosis. Effects of drugs, ethanol, hormones and cytokines. *J Hepatol,* 26 Suppl 2**,** 43-53.

FURUHASHI, M. & HOTAMISLIGIL, G. S. 2008. Fatty acid-binding proteins: role in metabolic diseases and potential as drug targets. *Nat Rev Drug Discov,* 7**,** 489-503.

GAESTEL, M., KOTLYAROV, A. & KRACHT, M. 2009. Targeting innate immunity protein kinase signalling in inflammation. *Nat Rev Drug Discov,* 8**,** 480-99.

GAICH, G., CHIEN, J. Y., FU, H., GLASS, L. C., DEEG, M. A., HOLLAND, W. L., KHARITONENKOV, A., BUMOL, T., SCHILSKE, H. K. & MOLLER, D. E. 2013. The effects of LY2405319, an FGF21 analog, in obese human subjects with type 2 diabetes. *Cell Metab,* 18**,** 333-40.

GALMAN, C., LUNDASEN, T., KHARITONENKOV, A., BINA, H. A., ERIKSSON, M., HAFSTROM, I., DAHLIN, M., AMARK, P., ANGELIN, B. & RUDLING, M. 2008. The circulating metabolic regulator FGF21 is induced by prolonged fasting and PPARalpha activation in man. *Cell Metab,* 8**,** 169-74.

GANTKE, T., SRISKANTHARAJAH, S. & LEY, S. C. 2011. Regulation and function of TPL-2, an IkappaB kinase-regulated MAP kinase kinase kinase. *Cell Res,* 21**,** 131-45.

GAO, L., SMIT, M. A., VAN DEN OORD, J. J., GOEMAN, J. J., VERDEGAAL, E. M., VAN DER BURG, S. H., STAS, M., BECK, S., GRUIS, N. A., TENSEN, C. P., WILLEMZE, R., PEEPER, D. S. & VAN DOORN, R. 2013. Genome-wide promoter methylation analysis identifies epigenetic silencing of MAPK13 in primary cutaneous melanoma. *Pigment Cell Melanoma Res,* 26**,** 542-54.

GAO, X., VAN DER VEEN, J. N., HERMANSSON, M., ORDONEZ, M., GOMEZ-MUNOZ, A., VANCE, D. E. & JACOBS, R. L. 2015. Decreased lipogenesis in white adipose tissue contributes to the resistance to high fat diet-induced obesity in phosphatidylethanolamine N-methyltransferase-deficient mice. *Biochim Biophys Acta,* 1851**,** 152-62.

GAO, Z., HWANG, D., BATAILLE, F., LEFEVRE, M., YORK, D., QUON, M. J. & YE, J. 2002. Serine phosphorylation of insulin receptor substrate 1 by inhibitor kappa B kinase complex. *J Biol Chem,* 277**,** 48115-21.

GARCIA-MARQUES, F., TREVISAN-HERRAZ, M., MARTINEZ-MARTINEZ, S., CAMAFEITA, E., JORGE, I., LOPEZ, J. A., MENDEZ-BARBERO, N., MENDEZ-FERRER, S., DEL POZO, M. A., IBANEZ, B., ANDRES, V., SANCHEZ-MADRID, F., REDONDO, J. M., BONZON-KULICHENKO, E. & VAZQUEZ, J. 2016. A Novel Systems-Biology Algorithm for the Analysis of Coordinated Protein Responses Using Quantitative Proteomics. *Mol Cell Proteomics,* 15**,** 1740-60.

GARCIA-MONZON, C., MARTIN-PEREZ, E., IACONO, O. L., FERNANDEZ-BERMEJO, M., MAJANO, P. L., APOLINARIO, A., LARRANAGA, E. & MORENO-OTERO, R. 2000. Characterization of pathogenic and prognostic factors of nonalcoholic steatohepatitis associated with obesity. *J Hepatol,* 33**,** 716-24.

GARCIA-ROCHA, M., ROCA, A., DE LA IGLESIA, N., BABA, O., FERNANDEZ-NOVELL, J. M., FERRER, J. C. & GUINOVART, J. J. 2001. Intracellular distribution of glycogen synthase and glycogen in primary cultured rat hepatocytes. *Biochem J,* 357**,** 17-24.

GEHART, H., KUMPF, S., ITTNER, A. & RICCI, R. 2010. MAPK signalling in cellular metabolism: stress or wellness? *EMBO Rep,* 11**,** 834-40.

GHATAK, S., BISWAS, A., DHALI, G. K., CHOWDHURY, A., BOYER, J. L. & SANTRA, A. 2011. Oxidative stress and hepatic stellate cell activation are key events in arsenic induced liver fibrosis in mice. *Toxicol Appl Pharmacol,* 251**,** 59-69.

GINSBERG, H. N. 2006. Is the slippery slope from steatosis to steatohepatitis paved with triglyceride or cholesterol? *Cell Metab,* 4**,** 179-81.

GOEDERT, M. 2001. The significance of tau and alpha-synuclein inclusions in neurodegenerative diseases. *Curr Opin Genet Dev,* 11**,** 343-51.

GOEDERT, M., HASEGAWA, M., JAKES, R., LAWLER, S., CUENDA, A. & COHEN, P. 1997. Phosphorylation of microtubule-associated protein tau by stress-activated protein kinases. *FEBS Lett,* 409**,** 57-62.

GONZALEZ-TERAN, B., CORTES, J. R., MANIERI, E., MATESANZ, N., VERDUGO, A., RODRIGUEZ, M. E., GONZALEZ-RODRIGUEZ, A., VALVERDE, A. M., MARTIN, P., DAVIS, R. J. & SABIO, G. 2013. Eukaryotic elongation factor 2 controls TNF-alpha translation in LPS-induced hepatitis. *J Clin Invest,* 123**,** 164-78.

GONZALEZ-TERAN, B., LOPEZ, J. A., RODRIGUEZ, E., LEIVA, L., MARTINEZ-MARTINEZ, S., BERNAL, J. A., JIMENEZ-BORREGUERO, L. J., REDONDO, J. M., VAZQUEZ, J. & SABIO, G. 2016a. p38gamma and delta promote heart hypertrophy by targeting the mTOR-inhibitory protein DEPTOR for degradation. *Nat Commun,* 7**,** 10477.

GONZALEZ-TERAN, B., MATESANZ, N., NIKOLIC, I., VERDUGO, M. A., SREERAMKUMAR, V., HERNANDEZ-COSIDO, L., MORA, A., CRAINICIUC, G., SAIZ, M. L., BERNARDO, E., LEIVA-VEGA, L., RODRIGUEZ, E., BONDIA, V., TORRES, J. L., PEREZ-SIEIRA, S., ORTEGA, L., CUENDA, A., SANCHEZ-MADRID, F., NOGUEIRAS, R., HIDALGO, A., MARCOS, M. & SABIO, G. 2016b. p38gamma and p38delta reprogram liver metabolism by modulating neutrophil infiltration. *Embo j,* 35**,** 536-52.

GOOD, M. C., ZALATAN, J. G. & LIM, W. A. 2011. Scaffold proteins: hubs for controlling the flow of cellular information. *Science,* 332**,** 680-6.

GORSKI, K., CARNEIRO, M. & SCHIBLER, U. 1986. Tissue-specific in vitro transcription from the mouse albumin promoter. *Cell,* 47**,** 767-76.

GOTO, Y., SHINJO, K., KONDO, Y., SHEN, L., TOYOTA, M., SUZUKI, H., GAO, W., AN, B., FUJII, M., MURAKAMI, H., OSADA, H., TANIGUCHI, T., USAMI, N., KONDO, M., HASEGAWA, Y., SHIMOKATA, K., MATSUO, K., HIDA, T., FUJIMOTO, N., KISHIMOTO, T., ISSA, J. P. & SEKIDO, Y. 2009. Epigenetic profiles distinguish malignant pleural mesothelioma from lung adenocarcinoma. *Cancer Res,* 69**,** 9073-82.

GRABACKA, M., PIERZCHALSKA, M., DEAN, M. & REISS, K. 2016. Regulation of Ketone Body Metabolism and the Role of PPARalpha. *Int J Mol Sci,* 17.

GREAVES, P. 2012. *Histopathology of Preclinical Toxicity Studies*, Academic Press.

GREFHORST, A., ELZINGA, B. M., VOSHOL, P. J., PLOSCH, T., KOK, T., BLOKS, V. W., VAN DER SLUIJS, F. H., HAVEKES, L. M., ROMIJN, J. A., VERKADE, H. J. & KUIPERS, F. 2002. Stimulation of lipogenesis by pharmacological activation of the liver X receptor leads to production of large, triglyceride-rich very low density lipoprotein particles. *J Biol Chem,* 277**,** 34182-90.

GRUBEN, N., SHIRI-SVERDLOV, R., KOONEN, D. P. & HOFKER, M. H. 2014. Nonalcoholic fatty liver disease: A main driver of insulin resistance or a dangerous liaison? *Biochim Biophys Acta,* 1842**,** 2329-2343.

GU, K., COWIE, C. C. & HARRIS, M. I. 1999. Diabetes and decline in heart disease mortality in US adults. *JAMA,* 281**,** 1291-7.

GUM, R. J., MCLAUGHLIN, M. M., KUMAR, S., WANG, Z., BOWER, M. J., LEE, J. C., ADAMS, J. L., LIVI, G. P., GOLDSMITH, E. J. & YOUNG, P. R. 1998. Acquisition of sensitivity of stress-activated protein kinases to the p38 inhibitor, SB 203580, by alteration of one or more amino acids within the ATP binding pocket. *J Biol Chem,* 273**,** 15605-10.

HAIDER, A. S., PETERS, S. B., KAPORIS, H., CARDINALE, I., FEI, J., OTT, J., BLUMENBERG, M., BOWCOCK, A. M., KRUEGER, J. G. & CARUCCI, J. A. 2006. Genomic analysis defines a cancer-specific gene expression

signature for human squamous cell carcinoma and distinguishes malignant hyperproliferation from benign hyperplasia. *J Invest Dermatol,* 126**,** 869-81.

HALE, K. K., TROLLINGER, D., RIHANEK, M. & MANTHEY, C. L. 1999. Differential expression and activation of p38 mitogen-activated protein kinase alpha, beta, gamma, and delta in inflammatory cell lineages. *J Immunol,* 162**,** 4246-52.

HAMMAM, O., MAHMOUD, O., ZAHRAN, M., ALY, S., HOSNY, K., HELMY, A. & ANAS, A. 2012. The role of fas/fas ligand system in the pathogenesis of liver cirrhosis and hepatocellular carcinoma. *Hepat Mon,* 12**,** e6132.

HAMMEL, P., COUVELARD, A., O'TOOLE, D., RATOUIS, A., SAUVANET, A., FLEJOU, J. F., DEGOTT, C., BELGHITI, J., BERNADES, P., VALLA, D., RUSZNIEWSKI, P. & LEVY, P. 2001. Regression of liver fibrosis after biliary drainage in patients with chronic pancreatitis and stenosis of the common bile duct. *N Engl J Med,* 344**,** 418-23.

HAN, H. S., KANG, G., KIM, J. S., CHOI, B. H. & KOO, S. H. 2016. Regulation of glucose metabolism from a liver-centric perspective. *Exp Mol Med,* 48**,** e218.

HAN, J., RICHTER, B., LI, Z., KRAVCHENKO, V. & ULEVITCH, R. J. 1995. Molecular cloning of human p38 MAP kinase. *Biochim Biophys Acta,* 1265**,** 224-7.

HAN, M. S., JUNG, D. Y., MOREL, C., LAKHANI, S. A., KIM, J. K., FLAVELL, R. A. & DAVIS, R. J. 2013. JNK expression by macrophages promotes obesity-induced insulin resistance and inflammation. *Science,* 339**,** 218-22.

HANASHIRO, I. & ROACH, P. J. 2002. Mutations of muscle glycogen synthase that disable activation by glucose 6-phosphate. *Arch Biochem Biophys,* 397**,** 286-92.

HASEMANN, C. A., ISTVAN, E. S., UYEDA, K. & DEISENHOFER, J. 1996. The crystal structure of the bifunctional enzyme 6-phosphofructo-2-kinase/fructose-2,6-bisphosphatase reveals distinct domain homologies. *Structure,* 4**,** 1017-29.

HASHIMOTO, T., COOK, W. S., QI, C., YELDANDI, A. V., REDDY, J. K. & RAO, M. S. 2000. Defect in peroxisome proliferator-activated receptor alpha-inducible fatty acid oxidation determines the severity of hepatic steatosis in response to fasting. *J Biol Chem,* 275**,** 28918-28.

HAYHURST, G. P., LEE, Y. H., LAMBERT, G., WARD, J. M. & GONZALEZ, F. J. 2001. Hepatocyte nuclear factor 4alpha (nuclear receptor 2A1) is essential for maintenance of hepatic gene expression and lipid homeostasis. *Mol Cell Biol,* 21**,** 1393-403.

HAZLEHURST, J. M., WOODS, C., MARJOT, T., COBBOLD, J. F. & TOMLINSON, J. W. 2016. Non-alcoholic fatty liver disease and diabetes. *Metabolism,* 65**,** 1096-108.

HELLERSTEIN, M. K., NEESE, R. A., LINFOOT, P., CHRISTIANSEN, M., TURNER, S. & LETSCHER, A. 1997. Hepatic gluconeogenic fluxes and glycogen turnover during fasting in humans. A stable isotope study. *J Clin Invest,* 100**,** 1305-19.

HENKEL, J., GARTNER, D., DORN, C., HELLERBRAND, C., SCHANZE, N., ELZ, S. R. & PUSCHEL, G. P. 2011. Oncostatin M produced in Kupffer cells in response to PGE2: possible contributor to hepatic insulin resistance and steatosis. *Lab Invest,* 91**,** 1107-17.

HERRERO-MENDEZ, A., ALMEIDA, A., FERNANDEZ, E., MAESTRE, C., MONCADA, S. & BOLANOS, J. P. 2009. The bioenergetic and antioxidant status of neurons is controlled by continuous degradation of a key glycolytic enzyme by APC/C-Cdh1. *Nat Cell Biol,* 11**,** 747-52.

HIROSUMI, J., TUNCMAN, G., CHANG, L., GORGUN, C. Z., UYSAL, K. T., MAEDA, K., KARIN, M. & HOTAMISLIGIL, G. S. 2002. A central role for JNK in obesity and insulin resistance. *Nature,* 420**,** 333-6.

HIRSCHEY, M. D., SHIMAZU, T., GOETZMAN, E., JING, E., SCHWER, B., LOMBARD, D. B., GRUETER, C. A., HARRIS, C., BIDDINGER, S., ILKAYEVA, O. R., STEVENS, R. D., LI, Y., SAHA, A. K., RUDERMAN, N. B., BAIN, J. R., NEWGARD, C. B., FARESE, R. V., JR., ALT, F. W., KAHN, C. R. & VERDIN, E. 2010. SIRT3 regulates mitochondrial fatty-acid oxidation by reversible enzyme deacetylation. *Nature,* 464**,** 121-5.

HOJLUND, K., BIRK, J. B., KLEIN, D. K., LEVIN, K., ROSE, A. J., HANSEN, B. F., NIELSEN, J. N., BECK-NIELSEN, H. & WOJTASZEWSKI, J. F. 2009. Dysregulation of glycogen synthase COOH- and NH2-terminal phosphorylation by insulin in obesity and type 2 diabetes mellitus. *J Clin Endocrinol Metab,* 94**,** 4547-56.

HOLLAND, W. L., ADAMS, A. C., BROZINICK, J. T., BUI, H. H., MIYAUCHI, Y., KUSMINSKI, C. M., BAUER, S. M., WADE, M., SINGHAL, E., CHENG, C. C., VOLK, K., KUO, M. S., GORDILLO, R., KHARITONENKOV, A. & SCHERER, P. E. 2013. An FGF21-adiponectin-ceramide axis controls energy expenditure and insulin action in mice. *Cell Metab,* 17**,** 790-7.

HOOPER, A. J., ADAMS, L. A. & BURNETT, J. R. 2011. Genetic determinants of hepatic steatosis in man. *J Lipid Res,* 52**,** 593-617.

HORTON, J. D., GOLDSTEIN, J. L. & BROWN, M. S. 2002. SREBPs: activators of the complete program of cholesterol and fatty acid synthesis in the liver. *J Clin Invest,* 109**,** 1125-31.

HOSSAIN, P., KAWAR, B. & EL NAHAS, M. 2007. Obesity and diabetes in the developing world--a growing challenge. *N Engl J Med,* 356**,** 213-5.

HOTAMISLIGIL, G. S. 2006. Inflammation and metabolic disorders. *Nature,* 444**,** 860-7.

HUA, J., MA, X., WEBB, T., POTTER, J. J., OELKE, M. & LI, Z. 2010. Dietary fatty acids modulate antigen presentation to hepatic NKT cells in nonalcoholic fatty liver disease. *J Lipid Res,* 51**,** 1696-703.

HUANG, H., DAI, H. P., KANG, J., CHEN, B. Y., SUN, T. Y. & XU, Z. J. 2015. Double-Blind Randomized Trial of Pirfenidone in Chinese Idiopathic Pulmonary Fibrosis Patients. *Medicine (Baltimore),* 94**,** e1600.

HUANG, W., METLAKUNTA, A., DEDOUSIS, N., ZHANG, P., SIPULA, I., DUBE, J. J., SCOTT, D. K. & O'DOHERTY, R. M. 2010. Depletion of liver Kupffer cells prevents the development of diet-induced hepatic steatosis and insulin resistance. *Diabetes,* 59**,** 347-57.

HUNT, M. C., RAUTANEN, A., WESTIN, M. A., SVENSSON, L. T. & ALEXSON, S. E. 2006. Analysis of the mouse and human acyl-CoA thioesterase (ACOT) gene clusters shows that convergent, functional evolution results in a reduced number of human peroxisomal ACOTs. *FASEB J,* 20**,** 1855-64.

HUYNH, F. K., GREEN, M. F., KOVES, T. R. & HIRSCHEY, M. D. 2014. Measurement of fatty acid oxidation rates in animal tissues and cell lines. *Methods Enzymol,* 542**,** 391-405.

IDF 2017. *International Diabetes Federation.*

INAGAKI, T., DUTCHAK, P., ZHAO, G., DING, X., GAUTRON, L., PARAMESWARA, V., LI, Y., GOETZ, R., MOHAMMADI, M., ESSER, V., ELMQUIST, J. K., GERARD, R. D., BURGESS, S. C., HAMMER, R. E., MANGELSDORF, D. J. & KLIEWER, S. A. 2007. Endocrine regulation of the fasting response by PPARalpha-mediated induction of fibroblast growth factor 21. *Cell Metab,* 5**,** 415-25.

IRIMIA, J. M., MEYER, C. M., PEPER, C. L., ZHAI, L., BOCK, C. B., PREVIS, S. F., MCGUINNESS, O. P., DEPAOLI-ROACH, A. & ROACH, P. J. 2010. Impaired glucose tolerance and predisposition to the fasted state in liver glycogen synthase knock-out mice. *J Biol Chem,* 285**,** 12851-61.

IRIMIA, J. M., MEYER, C. M., SEGVICH, D. M., SURENDRAN, S., DEPAOLI-ROACH, A. A., MORRAL, N. & ROACH, P. J. 2017. Lack of liver glycogen causes hepatic insulin resistance and steatosis in mice. *J Biol Chem,* 292**,** 10455-10464.

ITOH, M., ADACHI, M., YASUI, H., TAKEKAWA, M., TANAKA, H. & IMAI, K. 2002. Nuclear export of glucocorticoid receptor is enhanced by c-Jun N-terminal kinase-mediated phosphorylation. *Mol Endocrinol,* 16**,** 2382-92.

ITTNER, A., BLOCK, H., REICHEL, C. A., VARJOSALO, M., GEHART, H., SUMARA, G., GSTAIGER, M., KROMBACH, F., ZARBOCK, A. & RICCI, R. 2012. Regulation of PTEN activity by p38delta-PKD1 signaling in neutrophils confers inflammatory responses in the lung. *J Exp Med,* 209**,** 2229-46.

IZBAN, M. G. & PAPACONSTANTINOU, J. 1989. Cell-specific expression of mouse albumin promoter. Evidence for cell-specific DNA elements within the proximal promoter region and cis-acting DNA elements upstream of -160. *J Biol Chem,* 264**,** 9171-9.

JAESCHKE, A. & DAVIS, R. J. 2007. Metabolic stress signaling mediated by mixed-lineage kinases. *Mol Cell,* 27**,** 498-508.

JELEN, S., GENA, P., LEBECK, J., ROJEK, A., PRAETORIUS, J., FROKIAER, J., FENTON, R. A., NIELSEN, S., CALAMITA, G. & RUTZLER, M. 2012. Aquaporin-9 and urea transporter-A gene deletions affect urea transmembrane passage in murine hepatocytes. *Am J Physiol Gastrointest Liver Physiol,* 303**,** G1279-87.

JENSEN, J., TANTIWONG, P., STUENAES, J. T., MOLINA-CARRION, M., DEFRONZO, R. A., SAKAMOTO, K. & MUSI, N. 2012. Effect of acute exercise on glycogen synthase in muscle from obese and diabetic subjects. *Am J Physiol Endocrinol Metab,* 303**,** E82-9.

JIANG, Y., GRAM, H., ZHAO, M., NEW, L., GU, J., FENG, L., DI PADOVA, F., ULEVITCH, R. J. & HAN, J. 1997. Characterization of the structure and function of the fourth member of p38 group mitogen-activated protein kinases, p38delta. *J Biol Chem,* 272**,** 30122-8.

JIAO, P., FENG, B. & XU, H. 2012. Mapping MKP-3/FOXO1 interaction and evaluating the effect on gluconeogenesis. *PLoS One,* 7**,** e41168.

JIMENEZ, V., JAMBRINA, C., CASANA, E., SACRISTAN, V., MUNOZ, S., DARRIBA, S., RODO, J., MALLOL, C., GARCIA, M., LEON, X., MARCO, S., RIBERA, A., ELIAS, I., CASELLAS, A., GRASS, I., ELIAS, G., FERRE, T., MOTAS, S., FRANCKHAUSER, S., MULERO, F., NAVARRO, M., HAURIGOT, V., RUBERTE, J. & BOSCH, F. 2018. FGF21 gene therapy as treatment for obesity and insulin resistance. *EMBO Mol Med,* 10.

JING XU, D. J. L., CLARENCE HALE, SHANAKA STANISLAUS, MICHELLE CHEN, GLENN SIVITS, STEVEN VONDERFECHT, RANDY HECHT, YUE-SHENG LI, RICHARD A. LINDBERG, JIN-LONG CHEN, DAE YOUNG JUNG, ZHIYOU ZHANG, HWI-JIN KO, JASON K. KIM, MURIELLE M. VÉNIANT 2009. Fibroblast Growth Factor 21 Reverses Hepatic Steatosis, Increases Energy Expenditure, and Improves Insulin Sensitivity in Diet-Induced Obese Mice. *Diabetes,* 58(1)**,** 250-259.

JING, Y., LIU, W., CAO, H., ZHANG, D., YAO, X., ZHANG, S., XIA, H., LI, D., WANG, Y. C., YAN, J., HUI, L. & YING, H. 2015. Hepatic p38alpha regulates gluconeogenesis by suppressing AMPK. *J Hepatol,* 62**,** 1319-27.

JITRAPAKDEE, S., ST MAURICE, M., RAYMENT, I., CLELAND, W. W., WALLACE, J. C. & ATTWOOD, P. V. 2008. Structure, mechanism and regulation of pyruvate carboxylase. *Biochem J,* 413**,** 369-87.

JORNAYVAZ, F. R. & SHULMAN, G. I. 2012. Diacylglycerol activation of protein kinase Cepsilon and hepatic insulin resistance. *Cell Metab,* 15**,** 574-84.

JUGE-AUBRY, C. E., HAMMAR, E., SIEGRIST-KAISER, C., PERNIN, A., TAKESHITA, A., CHIN, W. W., BURGER, A. G. & MEIER, C. A. 1999. Regulation of the transcriptional activity of the peroxisome proliferator-activated receptor alpha by phosphorylation of a ligand-independent trans-activating domain. *J Biol Chem,* 274**,** 10505-10.

JUNTTILA, M. R., ALA-AHO, R., JOKILEHTO, T., PELTONEN, J., KALLAJOKI, M., GRENMAN, R., JAAKKOLA, P., WESTERMARCK, J. & KAHARI, V. M. 2007. p38alpha and p38delta mitogen-activated protein kinase isoforms regulate invasion and growth of head and neck squamous carcinoma cells. *Oncogene,* 26**,** 5267-79.

JURCZAK, M. J., LEE, A. H., JORNAYVAZ, F. R., LEE, H. Y., BIRKENFELD, A. L., GUIGNI, B. A., KAHN, M., SAMUEL, V. T., GLIMCHER, L. H. & SHULMAN, G. I. 2012. Dissociation of inositol-requiring enzyme (IRE1alpha)-

mediated c-Jun N-terminal kinase activation from hepatic insulin resistance in conditional X-box-binding protein-1 (XBP1) knock-out mice. *J Biol Chem,* 287**,** 2558-67.

KANT, S., BARRETT, T., VERTII, A., NOH, Y. H., JUNG, D. Y., KIM, J. K. & DAVIS, R. J. 2013. Role of the mixed-lineage protein kinase pathway in the metabolic stress response to obesity. *Cell Rep,* 4**,** 681-8.

KELSALL, I. R., MUNRO, S., HALLYBURTON, I., TREADWAY, J. L. & COHEN, P. T. 2007. The hepatic PP1 glycogen-targeting subunit interaction with phosphorylase a can be blocked by C-terminal tyrosine deletion or an indole drug. *FEBS Lett,* 581**,** 4749-53.

KERSTEN, S., SEYDOUX, J., PETERS, J. M., GONZALEZ, F. J., DESVERGNE, B. & WAHLI, W. 1999. Peroxisome proliferator-activated receptor alpha mediates the adaptive response to fasting. *J Clin Invest,* 103**,** 1489-98.

KEYSE, S. M. 2000. Protein phosphatases and the regulation of mitogen-activated protein kinase signalling. *Curr Opin Cell Biol,* 12**,** 186-92.

KHARITONENKOV, A., SHIYANOVA, T. L., KOESTER, A., FORD, A. M., MICANOVIC, R., GALBREATH, E. J., SANDUSKY, G. E., HAMMOND, L. J., MOYERS, J. S., OWENS, R. A., GROMADA, J., BROZINICK, J. T., HAWKINS, E. D., WROBLEWSKI, V. J., LI, D. S., MEHRBOD, F., JASKUNAS, S. R. & SHANAFELT, A. B. 2005. FGF-21 as a novel metabolic regulator. *J Clin Invest,* 115**,** 1627-35.

KITATANI, K., SHELDON, K., ANELLI, V., JENKINS, R. W., SUN, Y., GRABOWSKI, G. A., OBEID, L. M. & HANNUN, Y. A. 2009. Acid beta-glucosidase 1 counteracts p38delta-dependent induction of interleukin-6: possible role for ceramide as an anti-inflammatory lipid. *J Biol Chem,* 284**,** 12979-88.

KLARER, A. C., O'NEAL, J., IMBERT-FERNANDEZ, Y., CLEM, A., ELLIS, S. R., CLARK, J., CLEM, B., CHESNEY, J. & TELANG, S. 2014. Inhibition of 6-phosphofructo-2-kinase (PFKFB3) induces autophagy as a survival mechanism. *Cancer Metab,* 2**,** 2.

KOMATSU, M., YAZAKI, M., TANAKA, N., SANO, K., HASHIMOTO, E., TAKEI, Y., SONG, Y. Z., TANAKA, E., KIYOSAWA, K., SAHEKI, T., AOYAMA, T. & KOBAYASHI, K. 2008. Citrin deficiency as a cause of chronic liver disorder mimicking non-alcoholic fatty liver disease. *J Hepatol,* 49**,** 810-20.

KRAFT, C. A., EFIMOVA, T. & ECKERT, R. L. 2007. Activation of PKCdelta and p38delta MAPK during okadaic acid dependent keratinocyte apoptosis. *Arch Dermatol Res,* 299**,** 71-83.

KRISMAN, C. R. & BARENGO, R. 1975. A precursor of glycogen biosynthesis: alpha-1,4-glucan-protein. *Eur J Biochem,* 52**,** 117-23.

KRSSAK, M., BREHM, A., BERNROIDER, E., ANDERWALD, C., NOWOTNY, P., DALLA MAN, C., COBELLI, C., CLINE, G. W., SHULMAN, G. I., WALDHAUSL, W. & RODEN, M. 2004. Alterations in postprandial hepatic glycogen metabolism in type 2 diabetes. *Diabetes,* 53**,** 3048-56.

KUJIRAOKA, T., SATOH, Y., AYAORI, M., SHIRAISHI, Y., ARAI-NAKAYA, Y., HAKUNO, D., YADA, H., KUWADA, N., ENDO, S., ISODA, K. & ADACHI, T. 2013. Hepatic extracellular signal-regulated kinase 2 suppresses endoplasmic reticulum stress and protects from oxidative stress and endothelial dysfunction. *J Am Heart Assoc,* 2**,** e000361.

KUMA, Y., CAMPBELL, D. G. & CUENDA, A. 2004. Identification of glycogen synthase as a new substrate for stress-activated protein kinase 2b/p38beta. *Biochem J,* 379**,** 133-9.

KUMA, Y., SABIO, G., BAIN, J., SHPIRO, N., MARQUEZ, R. & CUENDA, A. 2005. BIRB796 inhibits all p38 MAPK isoforms in vitro and in vivo. *J Biol Chem,* 280**,** 19472-9.

KUMASHIRO, N., ERION, D. M., ZHANG, D., KAHN, M., BEDDOW, S. A., CHU, X., STILL, C. D., GERHARD, G. S., HAN, X., DZIURA, J., PETERSEN, K. F., SAMUEL, V. T. & SHULMAN, G. I. 2011. Cellular mechanism of insulin resistance in nonalcoholic fatty liver disease. *Proc Natl Acad Sci U S A,* 108**,** 16381-5.

KURLAND, I. J., EL-MAGHRABI, M. R., CORREIA, J. J. & PILKIS, S. J. 1992. Rat liver 6-phosphofructo-2-kinase/fructose-2,6-bisphosphatase. Properties of phospho- and dephospho- forms and of two mutants in which Ser32 has been changed by site-directed mutagenesis. *J Biol Chem,* 267**,** 4416-23.

LANCASTER, L., ALBERA, C., BRADFORD, W. Z., COSTABEL, U., DU BOIS, R. M., FAGAN, E. A., FISHMAN, R. S., GLASPOLE, I., GLASSBERG, M. K., KING, T. E., JR., LEDERER, D. J., LIN, Z., NATHAN, S. D., PEREIRA, C. A., SWIGRIS, J. J., VALEYRE, D. & NOBLE, P. W. 2016. Safety of pirfenidone in patients with idiopathic pulmonary fibrosis: integrated analysis of cumulative data from 5 clinical trials. *BMJ Open Respir Res,* 3**,** e000105.

LAWAN, A. & BENNETT, A. M. 2017. Mitogen-Activated Protein Kinase Regulation in Hepatic Metabolism. *Trends Endocrinol Metab,* 28**,** 868-878.

LAWAN, A., ZHANG, L., GATZKE, F., MIN, K., JURCZAK, M. J., AL-MUTAIRI, M., RICHTER, P., CAMPOREZ, J. P., COUVILLON, A., PESTA, D., ROTH FLACH, R. J., SHULMAN, G. I. & BENNETT, A. M. 2015. Hepatic mitogen-activated protein kinase phosphatase 1 selectively regulates glucose metabolism and energy homeostasis. *Mol Cell Biol,* 35**,** 26-40.

LEE, J., SUN, C., ZHOU, Y., LEE, J., GOKALP, D., HERREMA, H., PARK, S. W., DAVIS, R. J. & OZCAN, U. 2011. p38 MAPK-mediated regulation of Xbp1s is crucial for glucose homeostasis. *Nat Med,* 17**,** 1251-60.

LEE, V. M., GOEDERT, M. & TROJANOWSKI, J. Q. 2001. Neurodegenerative tauopathies. *Annu Rev Neurosci,* 24**,** 1121-59.

LEONE, T. C., WEINHEIMER, C. J. & KELLY, D. P. 1999. A critical role for the peroxisome proliferator-activated receptor alpha (PPARalpha) in the cellular fasting response: the PPARalpha-null mouse as a model of fatty acid oxidation disorders. *Proc Natl Acad Sci U S A,* 96**,** 7473-8.

LEWIS, G. F., CARPENTIER, A., ADELI, K. & GIACCA, A. 2002. Disordered fat storage and mobilization in the pathogenesis of insulin resistance and type 2 diabetes. *Endocr Rev,* 23**,** 201-29.

LI, S., BROWN, M. S. & GOLDSTEIN, J. L. 2010. Bifurcation of insulin signaling pathway in rat liver: mTORC1 required for stimulation of lipogenesis, but not inhibition of gluconeogenesis. *Proc Natl Acad Sci U S A,* 107**,** 3441-6.

LI, Z., JIANG, Y., ULEVITCH, R. J. & HAN, J. 1996. The primary structure of p38 gamma: a new member of p38 group of MAP kinases. *Biochem Biophys Res Commun,* 228**,** 334-40.

LINARES, J. F., DURAN, A., REINA-CAMPOS, M., AZA-BLANC, P., CAMPOS, A., MOSCAT, J. & DIAZ-MECO, M. T. 2015. Amino Acid Activation of mTORC1 by a PB1-Domain-Driven Kinase Complex Cascade. *Cell Rep,* 12**,** 1339-52.

LISTENBERGER, L. L., HAN, X., LEWIS, S. E., CASES, S., FARESE, R. V., JR., ORY, D. S. & SCHAFFER, J. E. 2003. Triglyceride accumulation protects against fatty acid-induced lipotoxicity. *Proc Natl Acad Sci U S A,* 100**,** 3077-82.

LOIS, K. & KUMAR, S. 2009. Obesity and diabetes. *Endocrinol Nutr,* 56 Suppl 4**,** 38-42.

LOMAKO, J., LOMAKO, W. M. & WHELAN, W. J. 1988. A self-glucosylating protein is the primer for rabbit muscle glycogen biosynthesis. *FASEB J,* 2**,** 3097-103.

LU, L., CHEN, Y. & ZHU, Y. 2017. The molecular basis of targeting PFKFB3 as a therapeutic strategy against cancer. *Oncotarget,* 8**,** 62793-62802.

LU, M., WAN, M., LEAVENS, K. F., CHU, Q., MONKS, B. R., FERNANDEZ, S., AHIMA, R. S., UEKI, K., KAHN, C. R. & BIRNBAUM, M. J. 2012. Insulin regulates liver metabolism in vivo in the absence of hepatic Akt and Foxo1. *Nat Med,* 18**,** 388-95.

LUNDASEN, T., HUNT, M. C., NILSSON, L. M., SANYAL, S., ANGELIN, B., ALEXSON, S. E. & RUDLING, M. 2007. PPARalpha is a key regulator of hepatic FGF21. *Biochem Biophys Res Commun,* 360**,** 437-40.

LYU, K., ZHANG, D., NOZAKI, Y., ZHANG, Y., BHANOT, S., CLINE, G., SAMUEL, V. AND SHULMAN, GI. 2018. Membrane sn-1,2 Diacylglycerol Mediates Lipid-Induced Hepatic Insulin Resistance In Vivo. *Diabetes,* 67.

MACAULAY, K., DOBLE, B. W., PATEL, S., HANSOTIA, T., SINCLAIR, E. M., DRUCKER, D. J., NAGY, A. & WOODGETT, J. R. 2007. Glycogen synthase kinase 3alpha-specific regulation of murine hepatic glycogen metabolism. *Cell Metab,* 6**,** 329-37.

MAGKOS, F., SU, X., BRADLEY, D., FABBRINI, E., CONTE, C., EAGON, J. C., VARELA, J. E., BRUNT, E. M., PATTERSON, B. W. & KLEIN, S. 2012. Intrahepatic diacylglycerol content is associated with hepatic insulin resistance in obese subjects. *Gastroenterology,* 142**,** 1444-6 e2.

MAGNUSSON, I., ROTHMAN, D. L., KATZ, L. D., SHULMAN, R. G. & SHULMAN, G. I. 1992. Increased rate of gluconeogenesis in type II diabetes mellitus. A 13C nuclear magnetic resonance study. *J Clin Invest,* 90**,** 1323-7.

MAKRIDAKIS, M. & VLAHOU, A. 2010. Secretome proteomics for discovery of cancer biomarkers. *J Proteomics,* 73**,** 2291-305.

MANIERI, E. & SABIO, G. 2015. Stress kinases in the modulation of metabolism and energy balance. *J Mol Endocrinol,* 55**,** R11-22.

MARI, M., CABALLERO, F., COLELL, A., MORALES, A., CABALLERIA, J., FERNANDEZ, A., ENRICH, C., FERNANDEZ-CHECA, J. C. & GARCIA-RUIZ, C. 2006. Mitochondrial free cholesterol loading sensitizes to TNF- and Fas-mediated steatohepatitis. *Cell Metab,* 4**,** 185-98.

MARIN-PENALVER, J. J., MARTIN-TIMON, I., SEVILLANO-COLLANTES, C. & DEL CANIZO-GOMEZ, F. J. 2016. Update on the treatment of type 2 diabetes mellitus. *World J Diabetes,* 7**,** 354-95.

MARKAN, K. R., NABER, M. C., AMEKA, M. K., ANDEREGG, M. D., MANGELSDORF, D. J., KLIEWER, S. A., MOHAMMADI, M. & POTTHOFF, M. J. 2014. Circulating FGF21 is liver derived and enhances glucose uptake during refeeding and overfeeding. *Diabetes,* 63**,** 4057-63.

MARTIN-MURPHY, B. V., YOU, Q., WANG, H., DE LA HOUSSAYE, B. A., REILLY, T. P., FRIEDMAN, J. E. & JU, C. 2014. Mice lacking natural killer T cells are more susceptible to metabolic alterations following high fat diet feeding. *PLoS One,* 9**,** e80949.

MARTINEZ-BARTOLOME, S., NAVARRO, P., MARTIN-MAROTO, F., LOPEZ-FERRER, D., RAMOS-FERNANDEZ, A., VILLAR, M., GARCIA-RUIZ, J. P. & VAZQUEZ, J. 2008. Properties of average score distributions of SEQUEST: the probability ratio method. *Mol Cell Proteomics,* 7**,** 1135-45.

MATESANZ, N., NIKOLIC, I., LEIVA, M., PULGARIN-ALFARO, M., SANTAMANS, A. M., BERNARDO, E., MORA, A., HERRERA-MELLE, L., RODRIGUEZ, E., BEIROA, D., CABALLERO, A., MARTIN-GARCIA, E., ACIN-PEREZ, R., HERNANDEZ-COSIDO, L., LEIVA-VEGA, L., TORRES, J. L., CENTENO, F., NEBREDA, A. R., ENRIQUEZ, J. A., NOGUEIRAS, R., MARCOS, M. & SABIO, G. 2018. p38alpha blocks brown adipose tissue thermogenesis through p38delta inhibition. *PLoS Biol,* 16**,** e2004455.

MATSUZAKA, T. & SHIMANO, H. 2011. Molecular mechanisms involved in hepatic steatosis and insulin resistance. *J Diabetes Investig,* 2**,** 170-5.

MATTEONI, C. A., YOUNOSSI, Z. M., GRAMLICH, T., BOPARAI, N., LIU, Y. C. & MCCULLOUGH, A. J. 1999. Nonalcoholic fatty liver disease: a spectrum of clinical and pathological severity. *Gastroenterology,* 116**,** 1413-9.

MCCLAIN, C. J., BARVE, S. & DEACIUC, I. 2007. Good fat/bad fat. *Hepatology,* 45**,** 1343-6.

MCINTYRE, T. M., PONTSLER, A. V., SILVA, A. R., ST HILAIRE, A., XU, Y., HINSHAW, J. C., ZIMMERMAN, G. A., HAMA, K., AOKI, J., ARAI, H. & PRESTWICH, G. D. 2003. Identification of an intracellular receptor for lysophosphatidic acid (LPA): LPA is a transcellular PPARgamma agonist. *Proc Natl Acad Sci U S A,* 100**,** 131-6.

MIAO, C. H., NAKAI, H., THOMPSON, A. R., STORM, T. A., CHIU, W., SNYDER, R. O. & KAY, M. A. 2000. Nonrandom transduction of recombinant adeno-associated virus vectors in mouse hepatocytes in vivo: cell cycling does not influence hepatocyte transduction. *J Virol,* 74**,** 3793-803.

MICHAEL, M. D., KULKARNI, R. N., POSTIC, C., PREVIS, S. F., SHULMAN, G. I., MAGNUSON, M. A. & KAHN, C. R. 2000. Loss of insulin signaling in hepatocytes leads to severe insulin resistance and progressive hepatic dysfunction. *Mol Cell,* 6**,** 87-97.

MILLER, A. L., WEBB, M. S., COPIK, A. J., WANG, Y., JOHNSON, B. H., KUMAR, R. & THOMPSON, E. B. 2005. p38 Mitogen-activated protein kinase (MAPK) is a key mediator in glucocorticoid-induced apoptosis of lymphoid cells: correlation between p38 MAPK activation and site-specific phosphorylation of the human glucocorticoid receptor at serine 211. *Mol Endocrinol,* 19**,** 1569-83.

MILLER, R. A. & BIRNBAUM, M. J. 2010. An energetic tale of AMPK-independent effects of metformin. *J Clin Invest,* 120**,** 2267-70.

MINEHIRA, K., YOUNG, S. G., VILLANUEVA, C. J., YETUKURI, L., ORESIC, M., HELLERSTEIN, M. K., FARESE, R. V., JR., HORTON, J. D., PREITNER, F., THORENS, B. & TAPPY, L. 2008. Blocking VLDL secretion causes hepatic steatosis but does not affect peripheral lipid stores or insulin sensitivity in mice. *J Lipid Res,* 49**,** 2038-44.

MITCHELL, G. A., GAUTHIER, N., LESIMPLE, A., WANG, S. P., MAMER, O. & QURESHI, I. 2008. Hereditary and acquired diseases of acyl-coenzyme A metabolism. *Mol Genet Metab,* 94**,** 4-15.

MITRO, N., MAK, P. A., VARGAS, L., GODIO, C., HAMPTON, E., MOLTENI, V., KREUSCH, A. & SAEZ, E. 2007. The nuclear receptor LXR is a glucose sensor. *Nature,* 445**,** 219-23.

MOFFAT, C., BHATIA, L., NGUYEN, T., LYNCH, P., WANG, M., WANG, D., ILKAYEVA, O. R., HAN, X., HIRSCHEY, M. D., CLAYPOOL, S. M. & SEIFERT, E. L. 2014. Acyl-CoA thioesterase-2 facilitates mitochondrial fatty acid oxidation in the liver. *J Lipid Res,* 55**,** 2458-70.

MONETTI, M., LEVIN, M. C., WATT, M. J., SAJAN, M. P., MARMOR, S., HUBBARD, B. K., STEVENS, R. D., BAIN, J. R., NEWGARD, C. B., FARESE, R. V., SR., HEVENER, A. L. & FARESE, R. V., JR. 2007. Dissociation of hepatic steatosis and insulin resistance in mice overexpressing DGAT in the liver. *Cell Metab,* 6**,** 69-78.

MONETTI, M., NAGARAJ, N., SHARMA, K. & MANN, M. 2011. Large-scale phosphosite quantification in tissues by a spike-in SILAC method. *Nat Methods,* 8**,** 655-8.

MONSENEGO, J., MANSOURI, A., AKKAOUI, M., LENOIR, V., ESNOUS, C., FAUVEAU, V., TAVERNIER, V., GIRARD, J. & PRIP-BUUS, C. 2012. Enhancing liver mitochondrial fatty acid oxidation capacity in obese mice improves insulin sensitivity independently of hepatic steatosis. *J Hepatol,* 56**,** 632-9.

MONTAGNER, A., POLIZZI, A., FOUCHE, E., DUCHEIX, S., LIPPI, Y., LASSERRE, F., BARQUISSAU, V., REGNIER, M., LUKOWICZ, C., BENHAMED, F., IROZ, A., BERTRAND-MICHEL, J., AL SAATI, T., CANO, P., MSELLI-LAKHAL, L., MITHIEUX, G., RAJAS, F., LAGARRIGUE, S., PINEAU, T., LOISEAU, N., POSTIC, C., LANGIN, D., WAHLI, W. & GUILLOU, H. 2016. Liver PPARalpha is crucial for whole-body fatty acid homeostasis and is protective against NAFLD. *Gut,* 65**,** 1202-14.

MOORHEAD, G., MACKINTOSH, C., MORRICE, N. & COHEN, P. 1995. Purification of the hepatic glycogen-associated form of protein phosphatase-1 by microcystin-Sepharose affinity chromatography. *FEBS Lett,* 362**,** 101-5.

MORA, A., SAKAMOTO, K., MCMANUS, E. J. & ALESSI, D. R. 2005. Role of the PDK1-PKB-GSK3 pathway in regulating glycogen synthase and glucose uptake in the heart. *FEBS Lett,* 579**,** 3632-8.

MOURI MI, B. M. 2019. *Hyperglycemia*, StatPearls

MOXHAM, C. M., TABRIZCHI, A., DAVIS, R. J. & MALBON, C. C. 1996. Jun N-terminal kinase mediates activation of skeletal muscle glycogen synthase by insulin in vivo. *J Biol Chem,* 271**,** 30765-73.

MRACEK, T., DRAHOTA, Z. & HOUSTEK, J. 2013. The function and the role of the mitochondrial glycerol-3-phosphate dehydrogenase in mammalian tissues. *Biochim Biophys Acta,* 1827**,** 401-10.

MUKAI, T., EGAWA, M., TAKEUCHI, T., YAMASHITA, H. & KUSUDO, T. 2017. Silencing of FABP1 ameliorates hepatic steatosis, inflammation, and oxidative stress in mice with nonalcoholic fatty liver disease. *FEBS Open Bio,* 7**,** 1009-1016.

MUOIO, D. M. & NEWGARD, C. B. 2008. Mechanisms of disease:Molecular and metabolic mechanisms of insulin resistance and beta-cell failure in type 2 diabetes. *Nat Rev Mol Cell Biol,* 9**,** 193-205.

NAGASAWA, T., INADA, Y., NAKANO, S., TAMURA, T., TAKAHASHI, T., MARUYAMA, K., YAMAZAKI, Y., KURODA, J. & SHIBATA, N. 2006. Effects of bezafibrate, PPAR pan-agonist, and GW501516, PPARdelta agonist, on development of steatohepatitis in mice fed a methionine- and choline-deficient diet. *Eur J Pharmacol,* 536**,** 182-91.

NAGLE, C. A., KLETT, E. L. & COLEMAN, R. A. 2009. Hepatic triacylglycerol accumulation and insulin resistance. *J Lipid Res,* 50 Suppl**,** S74-9.

NAM, H. J., LANE, M. D., PADRON, E., GURDA, B., MCKENNA, R., KOHLBRENNER, E., ASLANIDI, G., BYRNE, B., MUZYCZKA, N., ZOLOTUKHIN, S. & AGBANDJE-MCKENNA, M. 2007. Structure of adeno-associated virus serotype 8, a gene therapy vector. *J Virol,* 81**,** 12260-71.

NASSIR, F., ADEWOLE, O. L., BRUNT, E. M. & ABUMRAD, N. A. 2013. CD36 deletion reduces VLDL secretion, modulates liver prostaglandins, and exacerbates hepatic steatosis in ob/ob mice. *J Lipid Res,* 54**,** 2988-97.

NASSIR, F. & IBDAH, J. A. 2014. Role of mitochondria in alcoholic liver disease. *World J Gastroenterol,* 20**,** 2136-42.

NASSIR, F., RECTOR, R. S., HAMMOUD, G. M. & IBDAH, J. A. 2015. Pathogenesis and Prevention of Hepatic Steatosis. *Gastroenterol Hepatol (N Y),* 11**,** 167-75.

NAVARRO, P., TREVISAN-HERRAZ, M., BONZON-KULICHENKO, E., NUNEZ, E., MARTINEZ-ACEDO, P., PEREZ-HERNANDEZ, D., JORGE, I., MESA, R., CALVO, E., CARRASCAL, M., HERNAEZ, M. L., GARCIA, F., BARCENA, J. A., ASHMAN, K., ABIAN, J., GIL, C., REDONDO, J. M. & VAZQUEZ, J. 2014. General statistical framework for quantitative proteomics by stable isotope labeling. *J Proteome Res,* 13**,** 1234-47.

NAVARRO, P. & VAZQUEZ, J. 2009. A refined method to calculate false discovery rates for peptide identification using decoy databases. *J Proteome Res,* 8**,** 1792-6.

NESCHEN, S., MORINO, K., HAMMOND, L. E., ZHANG, D., LIU, Z. X., ROMANELLI, A. J., CLINE, G. W., PONGRATZ, R. L., ZHANG, X. M., CHOI, C. S., COLEMAN, R. A. & SHULMAN, G. I. 2005. Prevention of hepatic steatosis

and hepatic insulin resistance in mitochondrial acyl-CoA:glycerol-sn-3-phosphate acyltransferase 1 knockout mice. *Cell Metab,* 2**,** 55-65.

NISHIMURA, M., FEDOROV, S. & UYEDA, K. 1994. Glucose-stimulated synthesis of fructose 2,6-bisphosphate in rat liver. Dephosphorylation of fructose 6-phosphate, 2-kinase:fructose 2,6-bisphosphatase and activation by a sugar phosphate. *J Biol Chem,* 269**,** 26100-6.

NOGUEIRAS, R., PEREZ-TILVE, D., VEYRAT-DUREBEX, C., MORGAN, D. A., VARELA, L., HAYNES, W. G., PATTERSON, J. T., DISSE, E., PFLUGER, P. T., LOPEZ, M., WOODS, S. C., DIMARCHI, R., DIEGUEZ, C., RAHMOUNI, K., ROHNER-JEANRENAUD, F. & TSCHOP, M. H. 2009. Direct control of peripheral lipid deposition by CNS GLP-1 receptor signaling is mediated by the sympathetic nervous system and blunted in diet-induced obesity. *J Neurosci,* 29**,** 5916-25.

NOVELLASDEMUNT, L., BULTOT, L., MANZANO, A., VENTURA, F., ROSA, J. L., VERTOMMEN, D., RIDER, M. H., NAVARRO-SABATE, A. & BARTRONS, R. 2013. PFKFB3 activation in cancer cells by the p38/MK2 pathway in response to stress stimuli. *Biochem J,* 452**,** 531-43.

NUTTALL, F. Q., GANNON, M. C., BAI, G. & LEE, E. Y. 1994. Primary structure of human liver glycogen synthase deduced by cDNA cloning. *Arch Biochem Biophys,* 311**,** 443-9.

O'CALLAGHAN, C., FANNING, L. J. & BARRY, O. P. 2014. p38delta MAPK: Emerging Roles of a Neglected Isoform. *Int J Cell Biol,* 2014**,** 272689.

O'CALLAGHAN, C., FANNING, L. J., HOUSTON, A. & BARRY, O. P. 2013. Loss of p38delta mitogen-activated protein kinase expression promotes oesophageal squamous cell carcinoma proliferation, migration and anchorage-independent growth. *Int J Oncol,* 43**,** 405-15.

OH, K. J., HAN, H. S., KIM, M. J. & KOO, S. H. 2013. CREB and FoxO1: two transcription factors for the regulation of hepatic gluconeogenesis. *BMB Rep,* 46**,** 567-74.

OHKUMA, T., PETERS, S. A. E. & WOODWARD, M. 2018. Sex differences in the association between diabetes and cancer: a systematic review and meta-analysis of 121 cohorts including 20 million individuals and one million events. *Diabetologia,* 61**,** 2140-2154.

OKU, H., SHIMIZU, T., KAWABATA, T., NAGIRA, M., HIKITA, I., UEYAMA, A., MATSUSHIMA, S., TORII, M. & ARIMURA, A. 2008. Antifibrotic action of pirfenidone and prednisolone: different effects on pulmonary cytokines and growth factors in bleomycin-induced murine pulmonary fibrosis. *Eur J Pharmacol,* 590**,** 400-8.

ORELLANA-GAVALDA, J. M., HERRERO, L., MALANDRINO, M. I., PANEDA, A., SOL RODRIGUEZ-PENA, M., PETRY, H., ASINS, G., VAN DEVENTER, S., HEGARDT, F. G. & SERRA, D. 2011. Molecular therapy for obesity and diabetes based on a long-term increase in hepatic fatty-acid oxidation. *Hepatology,* 53**,** 821-32.

OWEN, B. M., MANGELSDORF, D. J. & KLIEWER, S. A. 2015. Tissue-specific actions of the metabolic hormones FGF15/19 and FGF21. *Trends Endocrinol Metab,* 26**,** 22-9.

PAL, M., FEBBRAIO, M. A. & LANCASTER, G. I. 2016. The roles of c-Jun NH2-terminal kinases (JNKs) in obesity and insulin resistance. *J Physiol,* 594**,** 267-79.

PAPACKOVA, Z., PALENICKOVA, E., DANKOVA, H., ZDYCHOVA, J., SKOP, V., KAZDOVA, L. & CAHOVA, M. 2012. Kupffer cells ameliorate hepatic insulin resistance induced by high-fat diet rich in monounsaturated fatty acids: the evidence for the involvement of alternatively activated macrophages. *Nutr Metab (Lond),* 9**,** 22.

PARGELLIS, C., TONG, L., CHURCHILL, L., CIRILLO, P. F., GILMORE, T., GRAHAM, A. G., GROB, P. M., HICKEY, E. R., MOSS, N., PAV, S. & REGAN, J. 2002. Inhibition of p38 MAP kinase by utilizing a novel allosteric binding site. *Nat Struct Biol,* 9**,** 268-72.

PARKER, G. J., LUND, K. C., TAYLOR, R. P. & MCCLAIN, D. A. 2003. Insulin resistance of glycogen synthase mediated by o-linked N-acetylglucosamine. *J Biol Chem,* 278**,** 10022-7.

PATEL, S. S. & SIDDIQUI, M. S. 2019. Current and Emerging Therapies for Non-alcoholic Fatty Liver Disease. *Drugs,* 79**,** 75-84.

PAWLAK, M., LEFEBVRE, P. & STAELS, B. 2015. Molecular mechanism of PPARalpha action and its impact on lipid metabolism, inflammation and fibrosis in non-alcoholic fatty liver disease. *J Hepatol,* 62**,** 720-33.

PEDERSON, B. A., COPE, C. R., SCHROEDER, J. M., SMITH, M. W., IRIMIA, J. M., THURBERG, B. L., DEPAOLI-ROACH, A. A. & ROACH, P. J. 2005a. Exercise capacity of mice genetically lacking muscle glycogen synthase: in mice, muscle glycogen is not essential for exercise. *J Biol Chem,* 280**,** 17260-5.

PEDERSON, B. A., SCHROEDER, J. M., PARKER, G. E., SMITH, M. W., DEPAOLI-ROACH, A. A. & ROACH, P. J. 2005b. Glucose metabolism in mice lacking muscle glycogen synthase. *Diabetes,* 54**,** 3466-73.

PEREIRA, S., YU, W. Q., MOORE, J., MORI, Y., TSIANI, E. & GIACCA, A. 2016. Effect of a p38 MAPK inhibitor on FFA-induced hepatic insulin resistance in vivo. *Nutr Diabetes,* 6**,** e210.

PERRY, R. J., BORDERS, C. B., CLINE, G. W., ZHANG, X. M., ALVES, T. C., PETERSEN, K. F., ROTHMAN, D. L., KIBBEY, R. G. & SHULMAN, G. I. 2016. Propionate Increases Hepatic Pyruvate Cycling and Anaplerosis and Alters Mitochondrial Metabolism. *J Biol Chem,* 291**,** 12161-70.

PERRY, R. J., PENG, L., CLINE, G. W., BUTRICO, G. M., WANG, Y., ZHANG, X. M., ROTHMAN, D. L., PETERSEN, K. F. & SHULMAN, G. I. 2017. Non-invasive assessment of hepatic mitochondrial metabolism by positional isotopomer NMR tracer analysis (PINTA). *Nat Commun,* 8**,** 798.

PERRY, R. J., PENG, L., CLINE, G. W., WANG, Y., RABIN-COURT, A., SONG, J. D., ZHANG, D., ZHANG, X. M., NOZAKI, Y., DUFOUR, S., PETERSEN, K. F. & SHULMAN, G. I. 2018. Mechanisms by which a Very-Low-Calorie Diet Reverses Hyperglycemia in a Rat Model of Type 2 Diabetes. *Cell Metab,* 27**,** 210-217 e3.

PERRY, R. J., ZHANG, D., ZHANG, X. M., BOYER, J. L. & SHULMAN, G. I. 2015. Controlled-release mitochondrial protonophore reverses diabetes and steatohepatitis in rats. *Science,* 347**,** 1253-6.

PETERSEN, K. F., BEFROY, D. E., DUFOUR, S., ROTHMAN, D. L. & SHULMAN, G. I. 2016a. Assessment of Hepatic Mitochondrial Oxidation and Pyruvate Cycling in NAFLD by (13)C Magnetic Resonance Spectroscopy. *Cell Metab,* 24**,** 167-71.

PETERSEN, M. C., MADIRAJU, A. K., GASSAWAY, B. M., MARCEL, M., NASIRI, A. R., BUTRICO, G., MARCUCCI, M. J., ZHANG, D., ABULIZI, A., ZHANG, X. M., PHILBRICK, W., HUBBARD, S. R., JURCZAK, M. J., SAMUEL, V. T., RINEHART, J. & SHULMAN, G. I. 2016b. Insulin receptor Thr1160 phosphorylation mediates lipid-induced hepatic insulin resistance. *J Clin Invest,* 126**,** 4361-4371.

PETERSEN, M. C. & SHULMAN, G. I. 2017. Roles of Diacylglycerols and Ceramides in Hepatic Insulin Resistance. *Trends Pharmacol Sci,* 38**,** 649-665.

PETERSEN, M. C. & SHULMAN, G. I. 2018. Mechanisms of Insulin Action and Insulin Resistance. *Physiol Rev,* 98**,** 2133-2223.

PETERSEN, M. C., VATNER, D. F. & SHULMAN, G. I. 2017. Regulation of hepatic glucose metabolism in health and disease. *Nat Rev Endocrinol,* 13**,** 572-587.

PIETROCOLA, F., GALLUZZI, L., BRAVO-SAN PEDRO, J. M., MADEO, F. & KROEMER, G. 2015. Acetyl coenzyme A: a central metabolite and second messenger. *Cell Metab,* 21**,** 805-21.

PITCHER, J., SMYTHE, C., CAMPBELL, D. G. & COHEN, P. 1987. Identification of the 38-kDa subunit of rabbit skeletal muscle glycogen synthase as glycogenin. *Eur J Biochem,* 169**,** 497-502.

POSTIC, C., DENTIN, R. & GIRARD, J. 2004. Role of the liver in the control of carbohydrate and lipid homeostasis. *Diabetes Metab,* 30**,** 398-408.

POSTIC, C. & MAGNUSON, M. A. 2000. DNA excision in liver by an albumin-Cre transgene occurs progressively with age. *Genesis,* 26**,** 149-50.

POSTIC, C., SHIOTA, M., NISWENDER, K. D., JETTON, T. L., CHEN, Y., MOATES, J. M., SHELTON, K. D., LINDNER, J., CHERRINGTON, A. D. & MAGNUSON, M. A. 1999. Dual roles for glucokinase in glucose homeostasis as determined by liver and pancreatic beta cell-specific gene knock-outs using Cre recombinase. *J Biol Chem,* 274**,** 305-15.

POTTHOFF, M. J., KLIEWER, S. A. & MANGELSDORF, D. J. 2012. Endocrine fibroblast growth factors 15/19 and 21: from feast to famine. *Genes Dev,* 26**,** 312-24.

POWELL, D. J., FRIEDMAN, J. M., OULETTE, A. J., KRAUTER, K. S. & DARNELL, J. E., JR. 1984. Transcriptional and post-transcriptional control of specific messenger RNAs in adult and embryonic liver. *J Mol Biol,* 179**,** 21-35.

PUCHALSKA, P. & CRAWFORD, P. A. 2017. Multi-dimensional Roles of Ketone Bodies in Fuel Metabolism, Signaling, and Therapeutics. *Cell Metab,* 25**,** 262-284.

PUIGSERVER, P., RHEE, J., LIN, J., WU, Z., YOON, J. C., ZHANG, C. Y., KRAUSS, S., MOOTHA, V. K., LOWELL, B. B. & SPIEGELMAN, B. M. 2001. Cytokine stimulation of energy expenditure through p38 MAP kinase activation of PPARgamma coactivator-1. *Mol Cell,* 8**,** 971-82.

PURI, P., BAILLIE, R. A., WIEST, M. M., MIRSHAHI, F., CHOUDHURY, J., CHEUNG, O., SARGEANT, C., CONTOS, M. J. & SANYAL, A. J. 2007. A lipidomic analysis of nonalcoholic fatty liver disease. *Hepatology,* 46**,** 1081-90.

PYPER, S. R., VISWAKARMA, N., YU, S. & REDDY, J. K. 2010. PPARalpha: energy combustion, hypolipidemia, inflammation and cancer. *Nucl Recept Signal,* 8**,** e002.

QIAO, L., MACDOUGALD, O. A. & SHAO, J. 2006. CCAAT/enhancer-binding protein alpha mediates induction of hepatic phosphoenolpyruvate carboxykinase by p38 mitogen-activated protein kinase. *J Biol Chem,* 281**,** 24390-7.

RACANELLI, V. & REHERMANN, B. 2006. The liver as an immunological organ. *Hepatology,* 43**,** S54-62.

RAJAMAKI, K., MAYRANPAA, M. I., RISCO, A., TUIMALA, J., NURMI, K., CUENDA, A., EKLUND, K. K., OORNI, K. & KOVANEN, P. T. 2016. p38delta MAPK: A Novel Regulator of NLRP3 Inflammasome Activation With Increased Expression in Coronary Atherogenesis. *Arterioscler Thromb Vasc Biol,* 36**,** 1937-46.

RATZIU, V., GOODMAN, Z. & SANYAL, A. 2015. Current efforts and trends in the treatment of NASH. *J Hepatol,* 62**,** S65-75.

RINES, A. K., SHARABI, K., TAVARES, C. D. & PUIGSERVER, P. 2016. Targeting hepatic glucose metabolism in the treatment of type 2 diabetes. *Nat Rev Drug Discov,* 15**,** 786-804.

RISCO, A., DEL FRESNO, C., MAMBOL, A., ALSINA-BEAUCHAMP, D., MACKENZIE, K. F., YANG, H. T., BARBER, D. F., MORCELLE, C., ARTHUR, J. S., LEY, S. C., ARDAVIN, C. & CUENDA, A. 2012. p38gamma and p38delta kinases regulate the Toll-like receptor 4 (TLR4)-induced cytokine production by controlling ERK1/2 protein kinase pathway activation. *Proc Natl Acad Sci U S A,* 109**,** 11200-5.

RISCO, A., MARTIN-SERRANO, M. A., BARBER, D. F. & CUENDA, A. 2018. p38gamma and p38delta Are Involved in T Lymphocyte Development. *Front Immunol,* 9**,** 65.

ROACH, P. J. 2002. Glycogen and its metabolism. *Curr Mol Med,* 2**,** 101-20.

ROBLES, M. S., HUMPHREY, S. J. & MANN, M. 2017. Phosphorylation Is a Central Mechanism for Circadian Control of Metabolism and Physiology. *Cell Metab,* 25**,** 118-127.

ROMEO, S., KOZLITINA, J., XING, C., PERTSEMLIDIS, A., COX, D., PENNACCHIO, L. A., BOERWINKLE, E., COHEN, J. C. & HOBBS, H. H. 2008. Genetic variation in PNPLA3 confers susceptibility to nonalcoholic fatty liver disease. *Nat Genet,* 40**,** 1461-5.

ROS, S., GARCIA-ROCHA, M., DOMINGUEZ, J., FERRER, J. C. & GUINOVART, J. J. 2009. Control of liver glycogen synthase activity and intracellular distribution by phosphorylation. *J Biol Chem,* 284**,** 6370-8.

ROS, S., ZAFRA, D., VALLES-ORTEGA, J., GARCIA-ROCHA, M., FORROW, S., DOMINGUEZ, J., CALBO, J. & GUINOVART, J. J. 2010. Hepatic overexpression of a constitutively active form of liver glycogen synthase improves glucose homeostasis. *J Biol Chem,* 285**,** 37170-7.

ROTH, R. J., LE, A. M., ZHANG, L., KAHN, M., SAMUEL, V. T., SHULMAN, G. I. & BENNETT, A. M. 2009. MAPK phosphatase-1 facilitates the loss of oxidative myofibers associated with obesity in mice. *J Clin Invest,* 119**,** 3817-29.

ROTHMAN, D. L., MAGNUSSON, I., KATZ, L. D., SHULMAN, R. G. & SHULMAN, G. I. 1991. Quantitation of hepatic glycogenolysis and gluconeogenesis in fasting humans with 13C NMR. *Science,* 254**,** 573-6.

RUI, L. 2014. Energy metabolism in the liver. *Compr Physiol,* 4**,** 177-97.

RUIZ, J. I. & OCHOA, B. 1997. Quantification in the subnanomolar range of phospholipids and neutral lipids by monodimensional thin-layer chromatography and image analysis. *J Lipid Res,* 38**,** 1482-9.

SABIO, G., CAVANAGH-KYROS, J., KO, H. J., JUNG, D. Y., GRAY, S., JUN, J. Y., BARRETT, T., MORA, A., KIM, J. K. & DAVIS, R. J. 2009. Prevention of steatosis by hepatic JNK1. *Cell Metab,* 10**,** 491-8.

SABIO, G., DAS, M., MORA, A., ZHANG, Z., JUN, J. Y., KO, H. J., BARRETT, T., KIM, J. K. & DAVIS, R. J. 2008. A stress signaling pathway in adipose tissue regulates hepatic insulin resistance. *Science,* 322**,** 1539-43.

SABIO, G. & DAVIS, R. J. 2010. cJun NH2-terminal kinase 1 (JNK1): roles in metabolic regulation of insulin resistance. *Trends Biochem Sci,* 35**,** 490-6.

SABIO, G. & DAVIS, R. J. 2014. TNF and MAP kinase signalling pathways. *Semin Immunol,* 26**,** 237-45.

SABIO, G., KENNEDY, N. J., CAVANAGH-KYROS, J., JUNG, D. Y., KO, H. J., ONG, H., BARRETT, T., KIM, J. K. & DAVIS, R. J. 2010. Role of muscle c-Jun NH2-terminal kinase 1 in obesity-induced insulin resistance. *Mol Cell Biol,* 30**,** 106-15.

SABIO, G., REUVER, S., FEIJOO, C., HASEGAWA, M., THOMAS, G. M., CENTENO, F., KUHLENDAHL, S., LEAL-ORTIZ, S., GOEDERT, M., GARNER, C. & CUENDA, A. 2004. Stress- and mitogen-induced phosphorylation of the synapse-associated protein SAP90/PSD-95 by activation of SAPK3/p38gamma and ERK1/ERK2. *Biochem J,* 380**,** 19-30.

SAMUEL, V. T., LIU, Z. X., WANG, A., BEDDOW, S. A., GEISLER, J. G., KAHN, M., ZHANG, X. M., MONIA, B. P., BHANOT, S. & SHULMAN, G. I. 2007. Inhibition of protein kinase Cepsilon prevents hepatic insulin resistance in nonalcoholic fatty liver disease. *J Clin Invest,* 117**,** 739-45.

SAMUEL, V. T., PETERSEN, K. F. & SHULMAN, G. I. 2010. Lipid-induced insulin resistance: unravelling the mechanism. *Lancet,* 375**,** 2267-77.

SAMUEL, V. T. & SHULMAN, G. I. 2012. Mechanisms for insulin resistance: common threads and missing links. *Cell,* 148**,** 852-71.

SATAPATI, S., SUNNY, N. E., KUCEJOVA, B., FU, X., HE, T. T., MENDEZ-LUCAS, A., SHELTON, J. M., PERALES, J. C., BROWNING, J. D. & BURGESS, S. C. 2012. Elevated TCA cycle function in the pathology of diet-induced hepatic insulin resistance and fatty liver. *J Lipid Res,* 53**,** 1080-92.

SAVAGE, D. B., CHOI, C. S., SAMUEL, V. T., LIU, Z. X., ZHANG, D., WANG, A., ZHANG, X. M., CLINE, G. W., YU, X. X., GEISLER, J. G., BHANOT, S., MONIA, B. P. & SHULMAN, G. I. 2006. Reversal of diet-induced hepatic steatosis and hepatic insulin resistance by antisense oligonucleotide inhibitors of acetyl-CoA carboxylases 1 and 2. *J Clin Invest,* 116**,** 817-24.

SCHINDLER, E. M., HINDES, A., GRIBBEN, E. L., BURNS, C. J., YIN, Y., LIN, M. H., OWEN, R. J., LONGMORE, G. D., KISSLING, G. E., ARTHUR, J. S. & EFIMOVA, T. 2009. p38delta Mitogen-activated protein kinase is essential for skin tumor development in mice. *Cancer Res,* 69**,** 4648-55.

SCHONFELD, P. & WOJTCZAK, L. 2016. Short- and medium-chain fatty acids in energy metabolism: the cellular perspective. *J Lipid Res,* 57**,** 943-54.

SCHRADER, M. & FAHIMI, H. D. 2006. Peroxisomes and oxidative stress. *Biochim Biophys Acta,* 1763**,** 1755-66.

SCHUPPAN, D., SURABATTULA, R. & WANG, X. Y. 2018. Determinants of fibrosis progression and regression in NASH. *J Hepatol,* 68**,** 238-250.

SCHWARZ, J. M., LINFOOT, P., DARE, D. & AGHAJANIAN, K. 2003. Hepatic de novo lipogenesis in normoinsulinemic and hyperinsulinemic subjects consuming high-fat, low-carbohydrate and low-fat, high-carbohydrate isoenergetic diets. *Am J Clin Nutr,* 77**,** 43-50.

SHARABI, K., TAVARES, C. D., RINES, A. K. & PUIGSERVER, P. 2015. Molecular pathophysiology of hepatic glucose production. *Mol Aspects Med,* 46**,** 21-33.

SHI, H., KOKOEVA, M. V., INOUYE, K., TZAMELI, I., YIN, H. & FLIER, J. S. 2006. TLR4 links innate immunity and fatty acid-induced insulin resistance. *J Clin Invest,* 116**,** 3015-25.

SHIMOMURA, I., SHIMANO, H., KORN, B. S., BASHMAKOV, Y. & HORTON, J. D. 1998. Nuclear sterol regulatory element-binding proteins activate genes responsible for the entire program of unsaturated fatty acid biosynthesis in transgenic mouse liver. *J Biol Chem,* 273**,** 35299-306.

SHINDO, N., FUJISAWA, T., SUGIMOTO, K., NOJIMA, K., OZE-FUKAI, A., YOSHIKAWA, Y., WANG, X., YASUDA, O., IKEGAMI, H. & RAKUGI, H. 2010. Involvement of microsomal triglyceride transfer protein in nonalcoholic steatohepatitis in novel spontaneous mouse model. *J Hepatol,* 52**,** 903-12.

SHOELSON, S. E., LEE, J. & GOLDFINE, A. B. 2006. Inflammation and insulin resistance. *J Clin Invest,* 116**,** 1793-801.

SHOELSON, S. E., LEE, J. & YUAN, M. 2003. Inflammation and the IKK beta/I kappa B/NF-kappa B axis in obesity- and diet-induced insulin resistance. *Int J Obes Relat Metab Disord,* 27 Suppl 3**,** S49-52.

SHULMAN, G. I., ROTHMAN, D. L., JUE, T., STEIN, P., DEFRONZO, R. A. & SHULMAN, R. G. 1990. Quantitation of muscle glycogen synthesis in normal subjects and subjects with non-insulin-dependent diabetes by 13C nuclear magnetic resonance spectroscopy. *N Engl J Med,* 322**,** 223-8.

SICA, A., INVERNIZZI, P. & MANTOVANI, A. 2014. Macrophage plasticity and polarization in liver homeostasis and pathology. *Hepatology,* 59**,** 2034-42.

SILJAMAKI, E., RAIKO, L., TORISEVA, M., NISSINEN, L., NAREOJA, T., PELTONEN, J., KAHARI, V. M. & PELTONEN, S. 2014. p38delta mitogen-activated protein kinase regulates the expression of tight junction protein ZO-1 in differentiating human epidermal keratinocytes. *Arch Dermatol Res,* 306**,** 131-41.

SILVA, F. M., DA SILVA, M. H., BRACHT, A., ELLER, G. J., CONSTANTIN, R. P. & YAMAMOTO, N. S. 2010. Effects of metformin on glucose metabolism of perfused rat livers. *Mol Cell Biochem,* 340**,** 283-9.

SINGH, R., KAUSHIK, S., WANG, Y., XIANG, Y., NOVAK, I., KOMATSU, M., TANAKA, K., CUERVO, A. M. & CZAJA, M. J. 2009. Autophagy regulates lipid metabolism. *Nature,* 458**,** 1131-5.

SOLINAS, G. & BECATTINI, B. 2017. JNK at the crossroad of obesity, insulin resistance, and cell stress response. *Mol Metab,* 6**,** 174-184.

SOUTHAMPTON-UNIVERSITY. 2017. *How the body produces glucose when we are fasting* [Online]. Available: https://www.futurelearn.com/courses/understanding-insulin/0/steps/22456 [Accessed].

STAELS, B., RUBENSTRUNK, A., NOEL, B., RIGOU, G., DELATAILLE, P., MILLATT, L. J., BARON, M., LUCAS, A., TAILLEUX, A., HUM, D. W., RATZIU, V., CARIOU, B. & HANF, R. 2013. Hepatoprotective effects of the dual peroxisome proliferator-activated receptor alpha/delta agonist, GFT505, in rodent models of nonalcoholic fatty liver disease/nonalcoholic steatohepatitis. *Hepatology,* 58**,** 1941-52.

STEFAN, N., SCHICK, F. & HARING, H. U. 2017. Causes, Characteristics, and Consequences of Metabolically Unhealthy Normal Weight in Humans. *Cell Metab,* 26**,** 292-300.

STRAUB, B. K., STOEFFEL, P., HEID, H., ZIMBELMANN, R. & SCHIRMACHER, P. 2008. Differential pattern of lipid droplet-associated proteins and de novo perilipin expression in hepatocyte steatogenesis. *Hepatology,* 47**,** 1936-46.

SUMARA, G., FORMENTINI, I., COLLINS, S., SUMARA, I., WINDAK, R., BODENMILLER, B., RAMRACHEYA, R., CAILLE, D., JIANG, H., PLATT, K. A., MEDA, P., AEBERSOLD, R., RORSMAN, P. & RICCI, R. 2009. Regulation of PKD by the MAPK p38delta in insulin secretion and glucose homeostasis. *Cell,* 136**,** 235-48.

SUMIDA, Y. & YONEDA, M. 2018. Current and future pharmacological therapies for NAFLD/NASH. *J Gastroenterol,* 53**,** 362-376.

SUN, H., WANG, X., CHEN, J., SONG, K., GUSDON, A. M., LI, L., BU, L. & QU, S. 2016. Melatonin improves non-alcoholic fatty liver disease via MAPK-JNK/P38 signaling in high-fat-diet-induced obese mice. *Lipids Health Dis,* 15**,** 202.

SUNNY, N. E., PARKS, E. J., BROWNING, J. D. & BURGESS, S. C. 2011. Excessive hepatic mitochondrial TCA cycle and gluconeogenesis in humans with nonalcoholic fatty liver disease. *Cell Metab,* 14**,** 804-10.

SZCZEPANIAK, L. S., NURENBERG, P., LEONARD, D., BROWNING, J. D., REINGOLD, J. S., GRUNDY, S., HOBBS, H. H. & DOBBINS, R. L. 2005. Magnetic resonance spectroscopy to measure hepatic triglyceride content: prevalence of hepatic steatosis in the general population. *Am J Physiol Endocrinol Metab,* 288**,** E462-8.

TAK, P. P. & FIRESTEIN, G. S. 2001. NF-kappaB: a key role in inflammatory diseases. *J Clin Invest,* 107**,** 7-11.

TAKEKAWA, M., ADACHI, M., NAKAHATA, A., NAKAYAMA, I., ITOH, F., TSUKUDA, H., TAYA, Y. & IMAI, K. 2000. p53-inducible wip1 phosphatase mediates a negative feedback regulation of p38 MAPK-p53 signaling in response to UV radiation. *EMBO J,* 19**,** 6517-26.

TAKEKAWA, M., MAEDA, T. & SAITO, H. 1998. Protein phosphatase 2Calpha inhibits the human stress-responsive p38 and JNK MAPK pathways. *EMBO J,* 17**,** 4744-52.

TALUKDAR, S., OH, D. Y., BANDYOPADHYAY, G., LI, D., XU, J., MCNELIS, J., LU, M., LI, P., YAN, Q., ZHU, Y., OFRECIO, J., LIN, M., BRENNER, M. B. & OLEFSKY, J. M. 2012. Neutrophils mediate insulin resistance in mice fed a high-fat diet through secreted elastase. *Nat Med,* 18**,** 1407-12.

TAN, F. L., OOI, A., HUANG, D., WONG, J. C., QIAN, C. N., CHAO, C., OOI, L., TAN, Y. M., CHUNG, A., CHEOW, P. C., ZHANG, Z., PETILLO, D., YANG, X. J. & TEH, B. T. 2010. p38delta/MAPK13 as a diagnostic marker for cholangiocarcinoma and its involvement in cell motility and invasion. *Int J Cancer,* 126**,** 2353-61.

TANDRA, S., YEH, M. M., BRUNT, E. M., VUPPALANCHI, R., CUMMINGS, O. W., UNALP-ARIDA, A., WILSON, L. A. & CHALASANI, N. 2011. Presence and significance of microvesicular steatosis in nonalcoholic fatty liver disease. *J Hepatol,* 55**,** 654-659.

TANOLI, T., YUE, P., YABLONSKIY, D. & SCHONFELD, G. 2004. Fatty liver in familial hypobetalipoproteinemia: roles of the APOB defects, intra-abdominal adipose tissue, and insulin sensitivity. *J Lipid Res,* 45**,** 941-7.

TANOUE, T. & NISHIDA, E. 2003. Molecular recognitions in the MAP kinase cascades. *Cell Signal,* 15**,** 455-62.

TANOUE, T., YAMAMOTO, T., MAEDA, R. & NISHIDA, E. 2001. A Novel MAPK phosphatase MKP-7 acts preferentially on JNK/SAPK and p38 alpha and beta MAPKs. *J Biol Chem,* 276**,** 26629-39.

TAO, H., ZHANG, Y., ZENG, X., SHULMAN, G. I. & JIN, S. 2014. Niclosamide ethanolamine-induced mild mitochondrial uncoupling improves diabetic symptoms in mice. *Nat Med,* 20**,** 1263-9.

THIERBACH, R., SCHULZ, T. J., ISKEN, F., VOIGT, A., MIETZNER, B., DREWES, G., VON KLEIST-RETZOW, J. C., WIESNER, R. J., MAGNUSON, M. A., PUCCIO, H., PFEIFFER, A. F., STEINBERG, P. & RISTOW, M. 2005. Targeted disruption of hepatic frataxin expression causes impaired mitochondrial function, decreased life span and tumor growth in mice. *Hum Mol Genet,* 14**,** 3857-64.

THOMAS, J. A., SCHLENDER, K. K. & LARNER, J. 1968. A rapid filter paper assay for UDPglucose-glycogen glucosyltransferase, including an improved biosynthesis of UDP-14C-glucose. *Anal Biochem,* 25**,** 486-99.

THOOLEN, B., MARONPOT, R. R., HARADA, T., NYSKA, A., ROUSSEAUX, C., NOLTE, T., MALARKEY, D. E., KAUFMANN, W., KUTTLER, K., DESCHL, U., NAKAE, D., GREGSON, R., VINLOVE, M. P., BRIX, A. E., SINGH, B., BELPOGGI, F. & WARD, J. M. 2010. Proliferative and nonproliferative lesions of the rat and mouse hepatobiliary system. *Toxicol Pathol,* 38**,** 5S-81S.

THORENS, B. & MUECKLER, M. 2010. Glucose transporters in the 21st Century. *Am J Physiol Endocrinol Metab,* 298**,** E141-5.

TILG, H. & MOSCHEN, A. R. 2010. Evolution of inflammation in nonalcoholic fatty liver disease: the multiple parallel hits hypothesis. *Hepatology,* 52**,** 1836-46.

TILLANDER, V., ALEXSON, S. E. H. & COHEN, D. E. 2017. Deactivating Fatty Acids: Acyl-CoA Thioesterase-Mediated Control of Lipid Metabolism. *Trends Endocrinol Metab,* 28**,** 473-484.

TITCHENELL, P. M., CHU, Q., MONKS, B. R. & BIRNBAUM, M. J. 2015. Hepatic insulin signalling is dispensable for suppression of glucose output by insulin in vivo. *Nat Commun,* 6**,** 7078.

TOMAS-LOBA, A., MANIERI, E., GONZALEZ-TERAN, B., MORA, A., LEIVA-VEGA, L., SANTAMANS, A. M., ROMERO-BECERRA, R., RODRIGUEZ, E., PINTOR-CHOCANO, A., FEIXAS, F., LOPEZ, J. A., CABALLERO, B., TRAKALA, M., BLANCO, O., TORRES, J. L., HERNANDEZ-COSIDO, L., MONTALVO-ROMERAL, V., MATESANZ, N., ROCHE-MOLINA, M., BERNAL, J. A., MISCHO, H., LEON, M., CABALLERO, A., MIRANDA-SAAVEDRA, D.,

RUIZ-CABELLO, J., NEVZOROVA, Y. A., CUBERO, F. J., BRAVO, J., VAZQUEZ, J., MALUMBRES, M., MARCOS, M., OSUNA, S. & SABIO, G. 2019. p38gamma is essential for cell cycle progression and liver tumorigenesis. *Nature,* 568**,** 557-560.

TORRES, T. P., CATLIN, R. L., CHAN, R., FUJIMOTO, Y., SASAKI, N., PRINTZ, R. L., NEWGARD, C. B. & SHIOTA, M. 2009. Restoration of hepatic glucokinase expression corrects hepatic glucose flux and normalizes plasma glucose in zucker diabetic fatty rats. *Diabetes,* 58**,** 78-86.

TREMMEL, M., GERDTHAM, U. G., NILSSON, P. M. & SAHA, S. 2017. Economic Burden of Obesity: A Systematic Literature Review. *Int J Environ Res Public Health,* 14.

UEBANSO, T., TAKETANI, Y., YAMAMOTO, H., AMO, K., OMINAMI, H., ARAI, H., TAKEI, Y., MASUDA, M., TANIMURA, A., HARADA, N., YAMANAKA-OKUMURA, H. & TAKEDA, E. 2011. Paradoxical regulation of human FGF21 by both fasting and feeding signals: is FGF21 a nutritional adaptation factor? *PLoS One,* 6**,** e22976.

VAN SCHAFTINGEN, E. & HERS, H. G. 1986. Purification and properties of phosphofructokinase 2/fructose 2,6-bisphosphatase from chicken liver and from pigeon muscle. *Eur J Biochem,* 159**,** 359-65.

VAN SCHAFTINGEN, E., VEIGA-DA-CUNHA, M. & NICULESCU, L. 1997. The regulatory protein of glucokinase. *Biochem Soc Trans,* 25**,** 136-40.

VERMA, S. & HUSSAIN, M. E. 2017. Obesity and diabetes: An update. *Diabetes Metab Syndr,* 11**,** 73-79.

VERNIA, S., CAVANAGH-KYROS, J., GARCIA-HARO, L., SABIO, G., BARRETT, T., JUNG, D. Y., KIM, J. K., XU, J., SHULHA, H. P., GARBER, M., GAO, G. & DAVIS, R. J. 2014. The PPARalpha-FGF21 hormone axis contributes to metabolic regulation by the hepatic JNK signaling pathway. *Cell Metab,* 20**,** 512-25.

VIJAYVARGIA, R., MANN, K., WEISS, H. R., POWNALL, H. J. & RUAN, H. 2010. JNK deficiency enhances fatty acid utilization and diverts glucose from oxidation to glycogen storage in cultured myotubes. *Obesity (Silver Spring),* 18**,** 1701-9.

VILLANUEVA, A., NEWELL, P., CHIANG, D. Y., FRIEDMAN, S. L. & LLOVET, J. M. 2007. Genomics and signaling pathways in hepatocellular carcinoma. *Semin Liver Dis,* 27**,** 55-76.

VIVES-BAUZA, C., YANG, L. & MANFREDI, G. 2007. Assay of mitochondrial ATP synthesis in animal cells and tissues. *Methods Cell Biol,* 80**,** 155-71.

VON WILAMOWITZ-MOELLENDORFF, A., HUNTER, R. W., GARCIA-ROCHA, M., KANG, L., LOPEZ-SOLDADO, I., LANTIER, L., PATEL, K., PEGGIE, M. W., MARTINEZ-PONS, C., VOSS, M., CALBO, J., COHEN, P. T., WASSERMAN, D. H., GUINOVART, J. J. & SAKAMOTO, K. 2013. Glucose-6-phosphate-mediated activation of liver glycogen synthase plays a key role in hepatic glycogen synthesis. *Diabetes,* 62**,** 4070-82.

WADA, M., CANALS, D., ADADA, M., COANT, N., SALAMA, M. F., HELKE, K. L., ARTHUR, J. S., SHROYER, K. R., KITATANI, K., OBEID, L. M. & HANNUN, Y. A. 2017. P38 delta MAPK promotes breast cancer progression and lung metastasis by enhancing cell proliferation and cell detachment. *Oncogene,* 36**,** 6649-6657.

WAINWRIGHT, P., SCORLETTI, E. & BYRNE, C. D. 2017. Type 2 Diabetes and Hepatocellular Carcinoma: Risk Factors and Pathogenesis. *Curr Diab Rep,* 17**,** 20.

WANG, L., MA, R., FLAVELL, R. A. & CHOI, M. E. 2002. Requirement of mitogen-activated protein kinase kinase 3 (MKK3) for activation of p38alpha and p38delta MAPK isoforms by TGF-beta 1 in murine mesangial cells. *J Biol Chem,* 277**,** 47257-62.

WANG, X., DEVAIAH, S. P., ZHANG, W. & WELTI, R. 2006. Signaling functions of phosphatidic acid. *Prog Lipid Res,* 45**,** 250-78.

WEI, Y., RECTOR, R. S., THYFAULT, J. P. & IBDAH, J. A. 2008. Nonalcoholic fatty liver disease and mitochondrial dysfunction. *World J Gastroenterol,* 14**,** 193-9.

WEINSTEIN, D. A., CORREIA, C. E., SAUNDERS, A. C. & WOLFSDORF, J. I. 2006. Hepatic glycogen synthase deficiency: an infrequently recognized cause of ketotic hypoglycemia. *Mol Genet Metab,* 87**,** 284-8.

WESTON, C. R. & DAVIS, R. J. 2007. The JNK signal transduction pathway. *Curr Opin Cell Biol,* 19**,** 142-9.

WHITE, M. F. 2003. Insulin signaling in health and disease. *Science,* 302**,** 1710-1.

WHO. 16 February 2018 *Obesity and overweight* [Online]. Available: https://www.who.int/en/news-room/fact-sheets/detail/obesity-and-overweight [Accessed].

WILLIAMSON, R. M., PRICE, J. F., GLANCY, S., PERRY, E., NEE, L. D., HAYES, P. C., FRIER, B. M., VAN LOOK, L. A., JOHNSTON, G. I., REYNOLDS, R. M., STRACHAN, M. W. & EDINBURGH TYPE 2 DIABETES STUDY, I. 2011. Prevalence of and risk factors for hepatic steatosis and nonalcoholic Fatty liver disease in people with type 2 diabetes: the Edinburgh Type 2 Diabetes Study. *Diabetes Care,* 34**,** 1139-44.

WILSON, K. P., MCCAFFREY, P. G., HSIAO, K., PAZHANISAMY, S., GALULLO, V., BEMIS, G. W., FITZGIBBON, M. J., CARON, P. R., MURCKO, M. A. & SU, M. S. 1997. The structural basis for the specificity of pyridinylimidazole inhibitors of p38 MAP kinase. *Chem Biol,* 4**,** 423-31.

WINAU, F., QUACK, C., DARMOISE, A. & KAUFMANN, S. H. 2008. Starring stellate cells in liver immunology. *Curr Opin Immunol,* 20**,** 68-74.

WISNIEWSKI, J. R., ZOUGMAN, A., NAGARAJ, N. & MANN, M. 2009. Universal sample preparation method for proteome analysis. *Nat Methods,* 6**,** 359-62.

WONG, V. W., WONG, G. L., CHOI, P. C., CHAN, A. W., LI, M. K., CHAN, H. Y., CHIM, A. M., YU, J., SUNG, J. J. & CHAN, H. L. 2010. Disease progression of non-alcoholic fatty liver disease: a prospective study with paired liver biopsies at 3 years. *Gut,* 59**,** 969-74.

WU, C., OKAR, D. A., NEWGARD, C. B. & LANGE, A. J. 2001. Overexpression of 6-phosphofructo-2-kinase/fructose-2, 6-bisphosphatase in mouse liver lowers blood glucose by suppressing hepatic glucose production. *J Clin Invest,* 107**,** 91-8.

WU, C., OKAR, D. A., NEWGARD, C. B. & LANGE, A. J. 2002. Increasing fructose 2,6-bisphosphate overcomes hepatic insulin resistance of type 2 diabetes. *Am J Physiol Endocrinol Metab,* 282**,** E38-45.

WU, H. T., CHEN, C. T., CHENG, K. C., LI, Y. X., YEH, C. H. & CHENG, J. T. 2011. Pharmacological activation of peroxisome proliferator-activated receptor delta improves insulin resistance and hepatic steatosis in high fat diet-induced diabetic mice. *Horm Metab Res,* 43**,** 631-5.

WU, J. J., ROTH, R. J., ANDERSON, E. J., HONG, E. G., LEE, M. K., CHOI, C. S., NEUFER, P. D., SHULMAN, G. I., KIM, J. K. & BENNETT, A. M. 2006. Mice lacking MAP kinase phosphatase-1 have enhanced MAP kinase activity and resistance to diet-induced obesity. *Cell Metab,* 4**,** 61-73.

WU, X. & WILLIAMS, K. J. 2012. NOX4 pathway as a source of selective insulin resistance and responsiveness. *Arterioscler Thromb Vasc Biol,* 32**,** 1236-45.

WU, Z., JIAO, P., HUANG, X., FENG, B., FENG, Y., YANG, S., HWANG, P., DU, J., NIE, Y., XIAO, G. & XU, H. 2010. MAPK phosphatase-3 promotes hepatic gluconeogenesis through dephosphorylation of forkhead box O1 in mice. *J Clin Invest,* 120**,** 3901-11.

XIONG, Y., COLLINS, Q. F., AN, J., LUPO, E., JR., LIU, H. Y., LIU, D., ROBIDOUX, J., LIU, Z. & CAO, W. 2007. p38 mitogen-activated protein kinase plays an inhibitory role in hepatic lipogenesis. *J Biol Chem,* 282**,** 4975-82.

XU, J., LLOYD, D. J., HALE, C., STANISLAUS, S., CHEN, M., SIVITS, G., VONDERFECHT, S., HECHT, R., LI, Y. S., LINDBERG, R. A., CHEN, J. L., JUNG, D. Y., ZHANG, Z., KO, H. J., KIM, J. K. & VENIANT, M. M. 2009a. Fibroblast growth factor 21 reverses hepatic steatosis, increases energy expenditure, and improves insulin sensitivity in diet-induced obese mice. *Diabetes,* 58**,** 250-9.

XU, J., STANISLAUS, S., CHINOOKOSWONG, N., LAU, Y. Y., HAGER, T., PATEL, J., GE, H., WEISZMANN, J., LU, S. C., GRAHAM, M., BUSBY, J., HECHT, R., LI, Y. S., LI, Y., LINDBERG, R. & VENIANT, M. M. 2009b. Acute glucose-lowering and insulin-sensitizing action of FGF21 in insulin-resistant mouse models--association with liver and adipose tissue effects. *Am J Physiol Endocrinol Metab,* 297**,** E1105-14.

YAMAGUCHI, K., YANG, L., MCCALL, S., HUANG, J., YU, X. X., PANDEY, S. K., BHANOT, S., MONIA, B. P., LI, Y. X. & DIEHL, A. M. 2007. Inhibiting triglyceride synthesis improves hepatic steatosis but exacerbates liver damage and fibrosis in obese mice with nonalcoholic steatohepatitis. *Hepatology,* 45**,** 1366-74.

YANG, Z., FUJII, H., MOHAN, S. V., GORONZY, J. J. & WEYAND, C. M. 2013. Phosphofructokinase deficiency impairs ATP generation, autophagy, and redox balance in rheumatoid arthritis T cells. *J Exp Med,* 210**,** 2119-34.

YANG, Z., GORONZY, J. J. & WEYAND, C. M. 2014. The glycolytic enzyme PFKFB3/phosphofructokinase regulates autophagy. *Autophagy,* 10**,** 382-3.

YEH, M. M. & BRUNT, E. M. 2007. Pathology of nonalcoholic fatty liver disease. *Am J Clin Pathol,* 128**,** 837-47.

YILMAZ, Y. 2012a. Review article: is non-alcoholic fatty liver disease a spectrum, or are steatosis and non-alcoholic steatohepatitis distinct conditions? *Aliment Pharmacol Ther,* 36**,** 815-23.

YILMAZ, Y. 2012b. Review article: non-alcoholic fatty liver disease and osteoporosis--clinical and molecular crosstalk. *Aliment Pharmacol Ther,* 36**,** 345-52.

YOUN, J. H. & BUCHANAN, T. A. 1993. Fasting does not impair insulin-stimulated glucose uptake but alters intracellular glucose metabolism in conscious rats. *Diabetes,* 42**,** 757-63.

YOUNG, P. R., MCLAUGHLIN, M. M., KUMAR, S., KASSIS, S., DOYLE, M. L., MCNULTY, D., GALLAGHER, T. F., FISHER, S., MCDONNELL, P. C., CARR, S. A., HUDDLESTON, M. J., SEIBEL, G., PORTER, T. G., LIVI, G. P., ADAMS, J. L. & LEE, J. C. 1997. Pyridinyl imidazole inhibitors of p38 mitogen-activated protein kinase bind in the ATP site. *J Biol Chem,* 272**,** 12116-21.

YU, S., MATSUSUE, K., KASHIREDDY, P., CAO, W. Q., YELDANDI, V., YELDANDI, A. V., RAO, M. S., GONZALEZ, F. J. & REDDY, J. K. 2003. Adipocyte-specific gene expression and adipogenic steatosis in the mouse liver due to peroxisome proliferator-activated receptor gamma1 (PPARgamma1) overexpression. *J Biol Chem,* 278**,** 498-505.

ZHANG, C., GAO, J., LI, M., DENG, Y. & JIANG, C. 2018. p38delta MAPK regulates aggresome biogenesis by phosphorylating SQSTM1 in response to proteasomal stress. *J Cell Sci,* 131.

ZHANG, D., LIU, Z. X., CHOI, C. S., TIAN, L., KIBBEY, R., DONG, J., CLINE, G. W., WOOD, P. A. & SHULMAN, G. I. 2007. Mitochondrial dysfunction due to long-chain Acyl-CoA dehydrogenase deficiency causes hepatic steatosis and hepatic insulin resistance. *Proc Natl Acad Sci U S A,* 104**,** 17075-80.

ZHANG, H. A., YANG, X. Y. & XIAO, Y. F. 2016. AMPKalpha1 overexpression alleviates the hepatocyte model of nonalcoholic fatty liver disease via inactivating p38MAPK pathway. *Biochem Biophys Res Commun,* 474**,** 364-370.

ZHANG, W., DEPAOLI-ROACH, A. A. & ROACH, P. J. 1993. Mechanisms of multisite phosphorylation and inactivation of rabbit muscle glycogen synthase. *Arch Biochem Biophys,* 304**,** 219-25.

ZHANG, X., YEUNG, D. C., KARPISEK, M., STEJSKAL, D., ZHOU, Z. G., LIU, F., WONG, R. L., CHOW, W. S., TSO, A. W., LAM, K. S. & XU, A. 2008. Serum FGF21 levels are increased in obesity and are independently associated with the metabolic syndrome in humans. *Diabetes,* 57**,** 1246-53.

ZHANG, Y., LEI, T., HUANG, J. F., WANG, S. B., ZHOU, L. L., YANG, Z. Q. & CHEN, X. D. 2011. The link between fibroblast growth factor 21 and sterol regulatory element binding protein 1c during lipogenesis in hepatocytes. *Mol Cell Endocrinol,* 342**,** 41-7.

ZHANG, Y. L., HERNANDEZ-ONO, A., SIRI, P., WEISBERG, S., CONLON, D., GRAHAM, M. J., CROOKE, R. M., HUANG, L. S. & GINSBERG, H. N. 2006. Aberrant hepatic expression of PPARgamma2 stimulates hepatic lipogenesis in a mouse model of obesity, insulin resistance, dyslipidemia, and hepatic steatosis. *J Biol Chem,* 281**,** 37603-15.

ZHAO, Y., DUNBAR, J. D. & KHARITONENKOV, A. 2012. FGF21 as a therapeutic reagent. *Adv Exp Med Biol,* 728**,** 214-28.

ZHOU, X., FERRARIS, J. D., DMITRIEVA, N. I., LIU, Y. & BURG, M. B. 2008. MKP-1 inhibits high NaCl-induced activation of p38 but does not inhibit the activation of TonEBP/OREBP: opposite roles of p38alpha and p38delta. *Proc Natl Acad Sci U S A,* 105**,** 5620-5.

ZUR, R., GARCIA-IBANEZ, L., NUNEZ-BUIZA, A., APARICIO, N., LIAPPAS, G., ESCOS, A., RISCO, A., PAGE, A., SAIZ-LADERA, C., ALSINA-BEAUCHAMP, D., MONTANS, J., PARAMIO, J. M. & CUENDA, A. 2015. Combined deletion of p38gamma and p38delta reduces skin inflammation and protects from carcinogenesis. *Oncotarget,* 6**,** 12920-35.

Acknowledgements

Por fiiin!!!, por fin llega el momento de dar las gracias y sobre todo de cerrar etapa. Si dijera que fue fácil, mentiría. Eso sí, mereció la pena, por todo lo que he vivido, madurado y aprendido. Me siento feliz, orgullosa y llena de ganas y curiosidad por lo que vendrá ahora.

Como son tantas personas con las que te cruzas, para bien o para mal, tanto lo que cada una te enseña; ya que no hay suficiente espacio, y aunque lo hubiera mi memoria me traicionaría, quiero empezar dando un GRACIAS general a todo el que ha compartido algún momento de esta etapa conmigo, también a todas las personas que con su mayor o menor granito de arena han contribuido al desarrollo de este trabajo. Gracias a mis amigos, a los nuevos y a los de siempre; sobre todo, Jessi, sé que podré contar siempre contigo y tú conmigo.

Lo siguiente, por supuesto, dar las gracias a Guadalupe Sabio, mi directora de tesis, por haberme dado la oportunidad de entrar en el CNIC, por volvérmela a dar por segunda vez en un momento bastante complicado, para mí, permitiéndome realizar esta tesis, con la que he aprendido tanto, en uno de los mejores sitios en los que podría haberla hecho…me considero muy afortunada por ello. Pero gracias también por permitirme vivir dos fantásticas experiencias, en todos los niveles, durante las dos estancias de investigación. De corazón, muchísima suerte y GRACIAS por todo!!

Toñiiii, co-directora, toca decirte cenquiuuus!! Por la ayuda sobre todo en la recta final, pero principalmente mil GRACIAS por confiar y creer en mí…no sabes el valor que tiene un ánimo!! o un tú puedes!!! En un día en el que realmente sientes que no puedes más…de corazón también, muchísima suerte…que nada, ni nadie te apague nunca.

Toca agradecer a la gente del antiguo Sabio´s Lab…Elena, Nuria, Bárbara, Luis, Edgar y mi Eli. Gracias por acogerme y hacerme sentir una más desde el primer día. Luis, cuánto coñazo te he dado a veces…sólo decirte que nunca te había visto tan feliz como ahora, y espero que sea así siempre. Edgarcinooooo, cuántas risas, cuánto te he echado de menos!!! Y también cuánto he echado de menos a mí Eli, tus consejos, tu ayuda, tu sonrisa…me acuerdo un montón de nuestros cortitos momentos en USA, qué suerte haber compartido también esa experiencia contigo!!! Barbis, gracias por enseñarme tanto…Sin duda, que os fuérais, marcó un antes y un después en el labo.

Gracias también a la gente del Sabio´s Lab de ahora, gracias por en mayor o menor medida ayudarme y aguantarme….Alfonso, Leti, Magda, gracias también por tus consejos; Rafa, que no Fran, gracias por sufrirme tan bien; Ivana, mi Serbia preferida, no cambies, porque tú sí que sabes vivir la vida; mi pequeña Cris, mi versión mejorada…lucha siempre por lo que quieres y búscame siempre que lo necesites….mil millones de gracias por tu ayuda y estoy segura que hagas lo que hagas te irá genial. Arancha, eres auténtica, gracias por llegar al labo y

por tu ayuda, no cambies nunca. Aye, ánimo!! Estoy segura que todo te irá genial, tú sabes cómo conseguirlo. María…vive así de feliz cada día y no pierdas nunca ese entusiasmo y esas ganas con las que cada día vas al labo…gracias por transmitirme esa energía. Pequeña Ainoa, gracias por aparecer y dar tanta alegría y buenos momentos al labo. Gracias también al resto de gente del CNIC, que nos facilitan tanto la vida…sobre todo gracias a Marta (animalario), Laura y Almudena.

Retrocediendo en el tiempo, vuelvo a la carrera y al máster…madre mía, que de ilusiones y sueños por cumplir…a veces me gustaría recuperar un poco esa inocencia. Gracias a todos los profesores y compañeros de la UAM y sobre todo Marta, gracias por seguir ahí. ¡¡Tú puedes con todo, sólo tienes que creérlo!! Y pensando en carrera y máster, esto no hubiera sido posible sin mis tíos y primos…chacha (Mª Cruz), Javi, Inés y Javier…siempre os estaré agradecida por acogerme durante 6 años, que se dice pronto. Gracias por hacerme sentir una más de la familia y nunca pedir nada a cambio. Inés, somos las power girls de la familia y para mí, eres como una hermana. No quiero dejar de decir también gracias a mis otros tíos y primos, chache (Pedro), Mª Jose, Ismael, Pedro y Mario que siempre me habéis tratado con cariño y bonitas palabras.

Siguiendo adelante…llega mi etapa Urjc…que complicada, pero que divertida a la vez…como me gustaba eso de dar clases!! Gracias por el apoyo a aquellos que me lo dieron…especialmente gracias Dani y Patriiiiiiii…sin tu amistad no hubiera sobrevivido allí…y ánimo que tampoco te queda nada!!!

Palacios, si hablo de Urjc, te toca. Qué bonita casualidad encontrarte!! Gracias por enseñarme y ayudarme tanto, soy mejor persona gracias a ti. Sin duda eres la persona que más ha marcado esta etapa…siempre serás especial, pero porque tú eres especial, sabes que te admiro. Espero que pronto nuestros caminos se junten del todo de nuevo. Iloveu.

No puedo dejar de dar las gracias a la gente del labo de París, donde realicé mi primera estancia. Merci beaucoup pour l'accueil chaleureux. Même si mon séjour à Paris a été court, cela m'a permis d'avoir une bouffée d'air frais et j'en avais vraiment besoin. J'aimerai particulièrement remercier Serge Luque qui a cru en moi sans me connaître, merci également pour les discussions scientifiques très intéressantes. Thanks a lot to Ewaut too.

Por supuesto, también gracias a la gente del labo de USA, donde hice mi segunda estancia. Thanks a lot to my laboratory at Yale! Firstly, thanks to Dr. Shulman for allowing me to join your knowledge, to learn so much…I have been very lucky to meet you, because I love the science that you do…I admire you. Thanks to everybody, specially to Mario, Ali and Rachel…I felt I was at home! And Leigh, you are amazing…thanks a lot for your help…you have here a friend forever.

Talking about my USA experience…of course Nicole and Stefanie, both of you were very special for me. Thanks for your friendship that I hope it will be forever…we need to live much more adventures together.

El final de estos agradecimientos, como no podía ser de otra manera, son para mi familia…la mejor que me podía haber tocado, os quiero y daría lo que fuera por vosotros, y porque siempre seáis así de felices. A mis hermanos, Carlos, Raúl y Víctor; gracias por cuidarme, con vosotros sé que nunca estaré sola. Lo mejor de ser la mayor, es que no me perderé ninguno de vuestros logros, éxitos, penas y alegrías. Estoy orgullosa de vosotros y siempre, siempre, siempre estaré para lo que necesitéis. Yaya, eres mi primer ejemplo de mujer luchadora a seguir…gracias por tanto…quédate mucho más con nosotros. A mis padres, me quedaría sin páginas al daros las gracias por tanto…soy lo que soy gracias a vosotros. Gracias por la educación, por enseñarme a luchar siempre por lo que quiero, a no rendirme, a no tener miedo, ni vergüenza…gracias por enseñarme a vivir, a aprender de lo bueno y de lo malo, a sonreír a la vida…gracias por ayudarme y apoyarme siempre. Sé que estáis orgullosos de mí, lo que seguramente no sepáis, es que yo estoy mucho más de vosotros; porque sois ejemplo de perseverancia, trabajo y buen corazón. Os debo todo!! Os quiero!!

Simplemente acabaré diciendo a todo aquel que siga en este fascinante mundo de la ciencia, que lo cuide, respete y no pierda la curiosidad de conocer. Para mí, posiblemente esto acabe aquí, pero espero haber contribuido con mi granito de arena….al menos, di todo lo mejor de mí.

Appendix

Publications derived from the training period at UAM:

Matesanz N, Bernardo E, Acín-Pérez R, Manieri E, Pérez-Sieira S, Hernández-Cosido L, **Montalvo-Romeral V**, Mora A, Rodríguez MA, Leiva-Vega L, Lechuga AV, Ruiz-Cabello J, Torres JL, Crespo-Ruiz M, Centeno F, Álvarez CV, Marcos M, Enríquez JA, Nogueiras R y Sabio G.*"MKK6 controls T3-mediated browning of white adipose tissue".* Nat Commun. 2017 11;8(1):856.

Tomás-Loba A, Manieri E, González-Terán B, Mora A, Leiva-Vega L , Santamans AM, Romero-Becerra R, Rodríguez E, Pintor-Chocano A, Feixas F, López JA, Caballero B, Trakala M, Blanco O, Torres JL, Hernández-Cosido L, **Montalvo-Romeral V**, Matesanz N, Roche-Molina M, Bernal JA, Mischo H, León M, Caballero A, Miranda-Saavedra D, Jesús Ruiz-Cabello J , Nevzorova YA, Cubero FJ, Bravo J, Vázquez J, Malumbres M, Marcos M, Osuna S, Sabio G. *"p38γ is essential for cell cycle progression and liver tumorigenesis"*. Nature 2019 568(7753):557-560.

nature COMMUNICATIONS

ARTICLE

DOI: 10.1038/s41467-017-00948-z OPEN

MKK6 controls T3-mediated browning of white adipose tissue

Nuria Matesanz[1], Edgar Bernardo[1], Rebeca Acín-Pérez[1], Elisa Manieri[1,2], Sonia Pérez-Sieira[3,4], Lourdes Hernández-Cosido[5], Valle Montalvo-Romeral[1], Alfonso Mora[1], Elena Rodríguez[1], Luis Leiva-Vega[1], Ana Victoria Lechuga-Vieco[1,6], Jesús Ruiz-Cabello[1,6,7], Jorge L. Torres[8], Maria Crespo-Ruiz[1], Francisco Centeno[9], Clara V. Álvarez[3], Miguel Marcos[8], Jose Antonio Enríquez[1,10], Ruben Nogueiras[3,4] & Guadalupe Sabio[1]

Increasing the thermogenic capacity of adipose tissue to enhance organismal energy expenditure is considered a promising therapeutic strategy to combat obesity. Here, we report that expression of the p38 MAPK activator MKK6 is elevated in white adipose tissue of obese individuals. Using knockout animals and shRNA, we show that *Mkk6* deletion increases energy expenditure and thermogenic capacity of white adipose tissue, protecting mice against diet-induced obesity and the development of diabetes. Deletion of *Mkk6* increases T3-stimulated UCP1 expression in adipocytes, thereby increasing their thermogenic capacity. Mechanistically, we demonstrate that, in white adipose tissue, p38 is activated by an alternative pathway involving AMPK, TAK, and TAB. Our results identify MKK6 in adipocytes as a potential therapeutic target to reduce obesity.

[1] Fundación Centro Nacional de Investigaciones Cardiovasculares Carlos III, Calle Melchor Fernández Almagro, 3, 28029 Madrid, Spain. [2] Centro Nacional de Biotecnología, CSIC, Calle Darwin, 3, 28049 Madrid, Spain. [3] Department of Physiology, CIMUS, University of Santiago de Compostela-Instituto de Investigación Sanitaria, Avda. Barcelona, 15782 Santiago de Compostela, Spain. [4] CIBER Fisiopatología de la Obesidad y Nutrición (CIBERobn), Travesía da Choupana, 15706 Santiago de Compostela, Spain. [5] Department of General Surgery, Bariatric Surgery Unit, University of Salamanca, Paseo de San Vicente, 58, 37007 Salamanca, Spain. [6] CIBER Enfermedades respiratorias (CIBERES), Calle Monforte de Lemos, 3-5, 28029 Madrid, Spain. [7] Universidad Complutense de Madrid, Av. Séneca, 2, 28040 Madrid, Spain. [8] Department of Internal Medicine, University Hospital of Salamanca-IBSAL, Paseo de San Vicente, 58, 37007 Salamanca, Spain. [9] Facultad de Ciencias, University of Extremadura, Grupo GIEN (Grupo de Investigación en Enfermedades Neurodegenerativas), Avda. de Elvas, s/n, 06071 Badajoz, Spain. [10] CIBER Fragilidad y Envejecimiento Saludable (CIBERFES), Calle Monforte de Lemos, 3-5, 28029 Madrid, Spain. Correspondence and requests for materials should be addressed to G.S. (email: gsabio@cnic.es)

The incidence of obesity and associated diseases is increasing worldwide. Defined as an exacerbated increase in body weight associated with fat accumulation, obesity is the consequence of a sustained positive energy balance that occurs when energy intake is higher than energy expenditure. Some pharmacological drugs specifically designed to treat obesity have focussed on reducing mainly food intake; however, this approach has had limited efficacy and is associated with undesired secondary effects. Therefore, new strategies are needed to treat obesity and diabetes[1].

Brown adipose tissue (BAT) is specialized in the dissipation of energy as heat to protect against hypothermia, in a process known as non-shivering thermogenesis[2, 3]. BAT was thought to disappear shortly after birth; however, positron emission tomography identified metabolically active BAT in adults in defined regions, and scattered within white adipose tissue (WAT), suggesting a possible influence on whole-body energy homeostasis[4–6]. The ability to generate heat (thermogenic capacity) depends on uncoupling protein 1 (UCP1)[7]. UCP1 forms a pore in the inner mitochondrial membrane, through which protons can leak, dissipating the electrochemical proton gradient required for ATP synthesis in the mitochondrial matrix. As a result, ATP synthesis is blunted and the energy is released as heat. Brown adipocyte function is regulated in part by thyroid hormones (TH). T3 promotes mitochondrial biogenesis, induces the expression of UCP1, and increases the activity of brown adipocytes[8, 9]. T3 has also been implicated in the induction of the browning of WAT in humans[10]. Increased UCP1 expression in WAT has been suggested as a mechanism for the prevention of obesity[11]. However, little is known about the molecular mechanism controlling this browning process in WAT.

p38α is activated by low temperatures[12]. Moreover, cell-culture studies with p38 inhibitors have identified p38 kinase as a possible mediator of UCP1 expression in the browning[12, 13]. Besides, the p38 downstream target activating transcription factor 2 (ATF2) induces the expression of peroxisome proliferator-activated receptor gamma (PPARγ) co-activator 1α (PGC-1α), and these two nuclear transcription factors together control the expression of UCP1[12]. The stress-activated protein kinase (SAPK) pathway is composed by two main branches: p38 kinases and the c-Jun N-terminal protein kinases (JNK). There are four p38 isoforms (α, β, γ, and δ) and three JNK isoforms (JNK1, 2, and 3)[14]. The JNK pathway has been extensively studied and is implicated in the development of obesity and insulin resistance[15]. In contrast, the role of p38 kinases in this context has received less attention, and their physiological role remains poorly understood.

In this study, we investigated the role of the upstream p38 activator MAPK kinase 6 (MKK6) during obesity induced by a high-fat diet (HFD). Lack of MKK6 increases the basal expression of UCP1 and promotes T3-mediated induction of UCP1 expression in WAT. Moreover, the browning of WAT and subsequent increased energy expenditure in mice lacking MKK6 protects these animals against HFD-induced obesity. This phenotype depends on T3 signaling: the lack of MKK6 increases the sensitivity of adipose tissue to T3-mediated browning. These results indicate that MKK6 is a central regulator of WAT browning and is a possible target for obesity treatment.

Results

Lack of MKK6 induces resistance to diet-induced obesity. MKKs are the activators of the MAPK family members and control multiple cell responses to diverse stimuli[16]. Although certain MKKs and their downstream pathways are known to be activated in human adipose tissue during obesity[17], the role of MKK6 is still unknown. Analysis of protein levels of MKK6 in fat of lean and obese mice (fed a HFD for 8 weeks) revealed markedly higher levels of MKK6 in epididymal white fat (eWAT) and subcutaneous fat (sWAT) than mice fed a standard chow diet, indicating a possible role of MKK6 in WAT metabolism (Fig. 1a and Supplementary Fig. 1a). No differences were observed in muscle and liver, while BAT presented a reduction in MKK6 expression after HFD (Supplementary Fig. 1a).

To explore this further, we fed HFD to mice lacking MKK6 (*Mkk6*$^{-/-}$). Compared with wild-type (WT) controls, *Mkk6*$^{-/-}$ mice were protected against HFD-induced obesity (Fig. 1b). The lower body weight in *Mkk6*$^{-/-}$ mice correlated with a lower fat mass detected by nuclear magnetic resonance (NMR) (Fig. 1c). Further analysis showed that the weight of liver, eWAT, sWAT, and BAT was lower in *Mkk6*$^{-/-}$ mice (Supplementary Fig. 1b). These differences were associated with smaller adipocytes and lipid droplets (Supplementary Fig. 1c, d) and a protection against liver steatosis (Supplementary Fig. 1c, e).

***Mkk6*$^{-/-}$ mice are protected against diabetes**. The reduced fat accumulation in *Mkk6*$^{-/-}$ mice prompted us to investigate whether these mice were protected against HFD-induced diabetes. *Mkk6*$^{-/-}$ mice had significantly lower levels of HFD-induced hyperglycemia and hyperinsulinemia than WT mice, presenting lower insulin resistance (Fig. 1d–f). Moreover, HFD-fed *Mkk6*$^{-/-}$ mice showed enhanced glucose tolerance (Fig. 1g) and insulin sensitivity (Fig. 1h). The greater glucose tolerance in *Mkk6*$^{-/-}$ mice was matched by a higher glucose-induced blood insulin concentration (Fig. 1i). These data indicate that MKK6 deficiency protects against HFD-induced insulin resistance. Western blot analysis showed that suppression of insulin-stimulated AKT activation as a result of HFD was substantially prevented in eWAT from *Mkk6*$^{-/-}$ mice with liver and skeletal muscle also partially protected (Fig. 1j and Supplementary Fig. 1f). These results confirm that HFD-fed *Mkk6*$^{-/-}$ mice have higher systemic insulin sensitivity than WT mice.

Higher energy expenditure and WAT browning in *Mkk6*$^{-/-}$ mice. Indirect calorimetry analysis demonstrated that HFD-*Mkk6*$^{-/-}$ mice had higher energy expenditure (EE) that WT independently of its correction or not by lean mass (Fig. 2a) without significant differences in O_2/CO_2 gas exchange, locomotor activity, or food intake (Supplementary Fig. 2a). The increased EE by MKK6 deficiency was likely to be a major determinant of MKK6-regulated obesity and prompted us to examine thermogenesis. When maintained at room temperature (23 °C), the core body temperature of HFD-fed *Mkk6*$^{-/-}$ mice was higher than their WT counterparts (Fig. 2b). Since BAT is the main regulator of body temperature in mice, we asked whether the lower lipid content in BAT of *Mkk6*$^{-/-}$ mice was caused by thermogenesis due to higher BAT activity. However, analysis with an infrared (IR) camera showed no differences in BAT temperature between genotypes (Supplementary Fig. 2b). Moreover, there were no differences in RNA or protein expression of UCP1, the main enzyme responsible for mitochondria thermogenesis in BAT (Supplementary Fig. 2c). Messenger RNA (mRNA) levels of other genes associated with BAT activity were also unaltered in *Mkk6*$^{-/-}$ mice, including the transcriptional coactivators *Ppargc1a*, *Ppargc1b*, *Cidea*, and the metabolic enzymes *Accb* and *Ldhb* (Supplementary Fig. 2d, e).

Recent reports show that specific stimuli can induce thermogenic capability to WAT in a process called “WAT browning”, in which the adipocytes activate typical genes of BAT[18–20]. Analysis of BAT-associated genes in epididymal and subcutaneous white fat revealed that WAT from *Mkk6*$^{-/-}$ mice expressed elevated mRNA levels of the browning and mitochondrial biogenesis

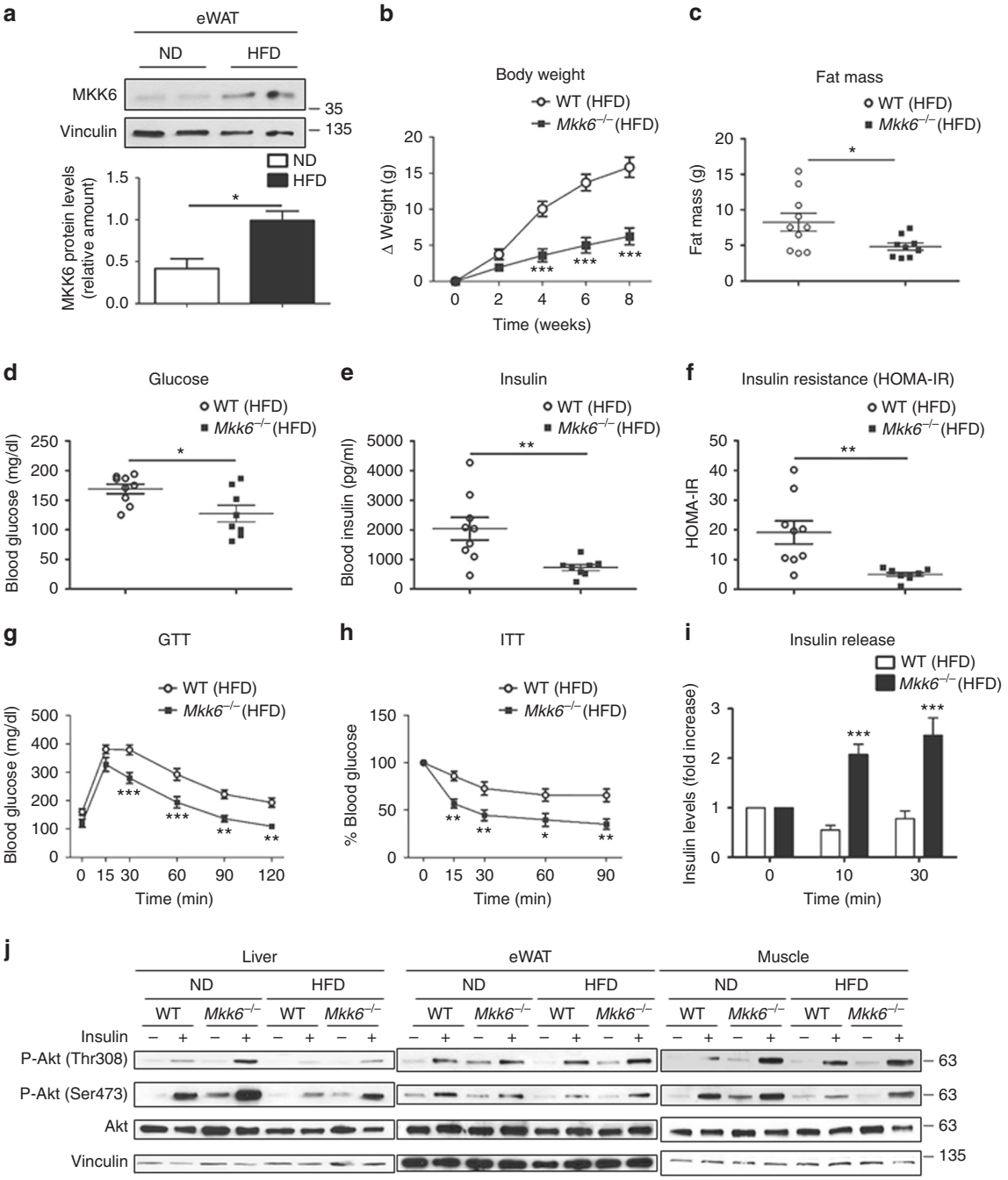

Fig. 1 *Mkk6*$^{-/-}$ mice are protected against diet-induced obesity and hyperglycemia **a** Western blot showing elevated MKK6 expression in epididymal white fat (eWAT) from WT mice fed a HFD for 8 weeks. A representative blot from three technical replications (top) and quantification (bottom) are shown (mean ± SEM; *$p < 0.05$, ND vs HFD *t* test, $n = 4$ mice). **b** Body weight time course in WT and *Mkk6*$^{-/-}$ male mice (8–10 weeks old) fed a HFD over 8 weeks. Data are presented as the increase above initial weight. HFD-induced weight gain was significantly higher in WT than *Mkk6*$^{-/-}$ mice (mean ± SEM, WT $n = 10$ mice; *Mkk6*$^{-/-}$ $n = 7$ mice). **c** Fat mass in *Mkk6*$^{-/-}$ and WT mice after 8 weeks of HFD (mean ± SEM, WT $n = 10$ mice; *Mkk6*$^{-/-}$ $n = 9$ mice). **d**, **e** Fasting blood glucose and insulin in *Mkk6*$^{-/-}$ and WT mice fed the HFD (8 weeks) (mean ± SEM, WT $n = 9$ mice; *Mkk6*$^{-/-}$ $n = 8$ mice). **f** Insulin resistance rate in WT and *Mkk6*$^{-/-}$ mice calculated as homeostasis model assessment (HOMA-IR) ratio (mean ± SEM, WT $n = 9$ mice; *Mkk6*$^{-/-}$ $n = 8$ mice). **g**, **h** Glucose tolerance test (GTT), and insulin tolerance test (ITT) in WT and *Mkk6*$^{-/-}$ mice fed the HFD (8 weeks). Blood glucose concentration was measured in mice given intraperitoneal injections of glucose (1 g/kg) or insulin (0.75 IU/kg) (mean ± SEM, WT $n = 10$ mice; *Mkk6*$^{-/-}$ $n = 7$ mice). **i** Insulin release test in HFD-fed WT and *Mkk6*$^{-/-}$ mice. Mice received i.p. glucose (2 g/kg) after overnight fasting (mean ± SEM, WT $n = 9$ mice; *Mkk6*$^{-/-}$ $n = 6$ mice). **j** Western blot analysis of Akt activation in liver, epididymal white adipose tissue (eWAT), and skeletal muscle from mice fed normal chow diet (ND) or high-fat diet (HFD). Mice were treated without or with insulin (1.5 IU/kg) for 15 min after overnight fasting. Each line represents a pool of tissue from 4 mice.*$p < 0.05$, **$p < 0.01$, ***$p < 0.001$ WT vs *Mkk6*$^{-/-}$ (two-way ANOVA coupled to Bonferroni's post-tests or *t* test or Welch's test when variances were different)

markers as *Cidea*[21], and *Cpt1b*, *Cpt2*, and *Cox8b* (Fig. 2c, d and Supplementary Fig. 2g). Moreover eWAT and iWAT showed increased UCP1 at mRNA and protein levels (Fig. 2d, e and Supplementary Fig. 2f). Proton NMR spectroscopy (^{1}H-MRS) analysis of the eWAT tissue from HFD-*Mkk6*$^{-/-}$ mice identified a BAT-like spectrum profile (Fig. 2f), with water signal and six fat peaks resolvable in spectroscopy[22] as is characteristic of BAT (Supplementary Fig. 2h) and different from WAT. Furthermore, in vivo phosphorus NMR spectroscopy (^{31}P-MRS) also indicated a lower total ATP content with respect to total free inorganic phosphate (Pi) in *Mkk6*$^{-/-}$ eWAT pointing out to a reduced ATP synthesis (Fig. 2f). On the basis of these observations, we hypothesized that the increased energy metabolism in *Mkk6*$^{-/-}$ mice might be a consequence of increased non-shivering thermogenesis in WAT. To test this, we housed animals at different temperatures. Under thermoneutral conditions (30 °C), when adaptive thermogenesis is not required, weight gain was similar between HFD-fed WT and *Mkk6*$^{-/-}$ mice (Fig. 2g). Besides, HFD-*Mkk6*$^{-/-}$ mice are more resistant to cold exposure (4 °C) (Fig. 2h), and after this browning stimulus, *Mkk6*$^{-/-}$ mice

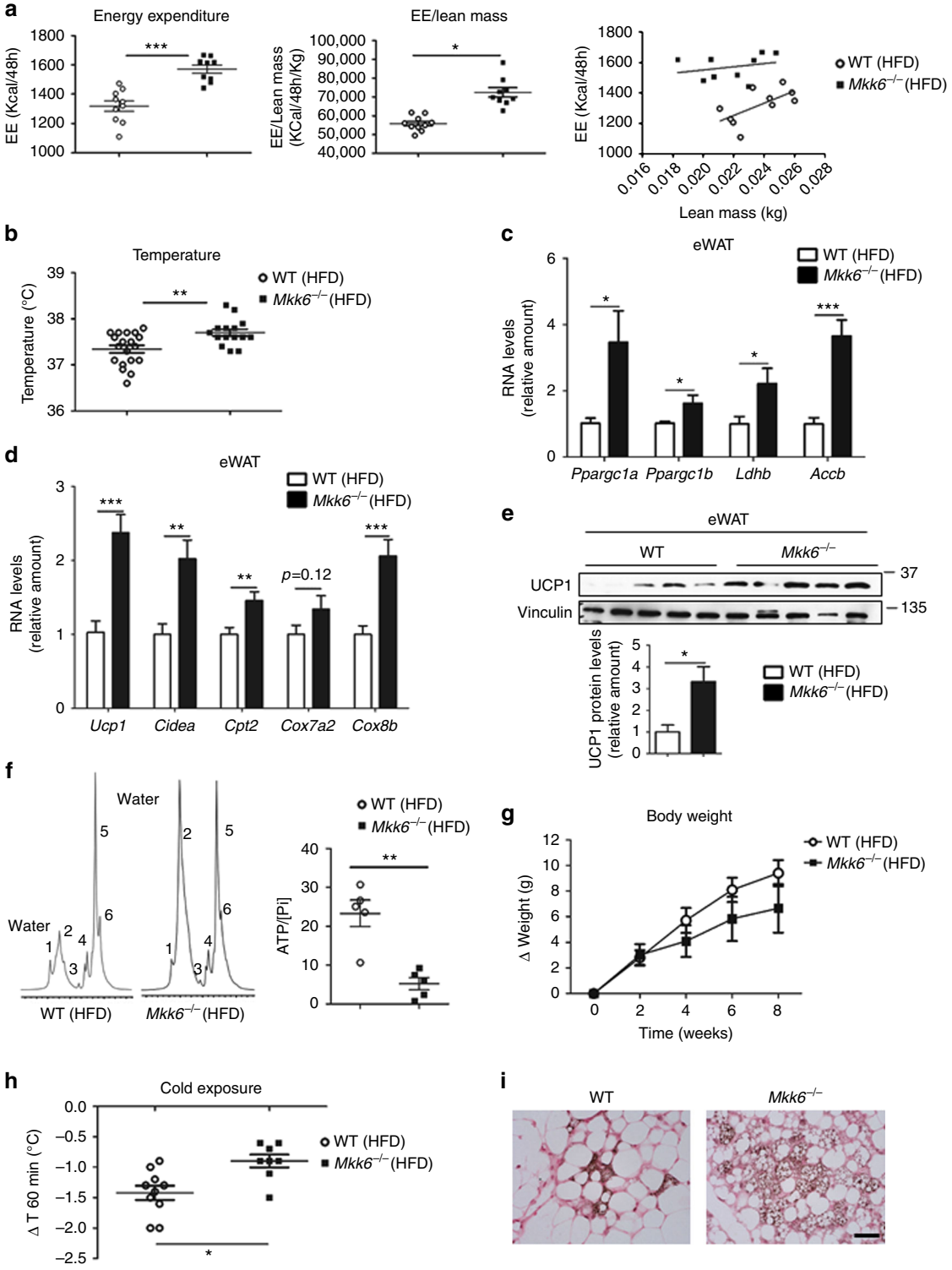

expressed higher UCP1 levels in subcutaneous white fat than their WT counterparts (Fig. 2i). Taken together, these data indicate that the low-weight gain in HFD-fed *Mkk6*$^{-/-}$ mice is due to WAT browning and the associated increase in thermogenesis.

VMH deletion of *Mkk6* does not affect systemic metabolism. The central nervous system is a key regulator of whole-body metabolism and can control weight gain through several mechanisms including browning[17, 23]. The ventromedial hypothalamus (VMH) is a region that controls feeding and thermoregulation[24]. Thereby, we assessed the metabolic phenotype after the stereotaxic injection of lentivirus containing MKK6 short hairpin RNA (shRNA; sh*Mkk6*) into the VMH. After the injection, mice were fed a HFD for 8 weeks and the levels of MKK6 in the whole hypothalamus were assessed (Supplementary Fig. 3a). Mice treated with sh*MKK6* showed no differences in body weight, body composition, or food intake compared with mice injected with lentivirus containing scramble control shRNA (Supplementary Fig. 3b–e). Furthermore, sh*Mkk6*-treated mice were not protected against HFD-induced glucose intolerance (Supplementary Fig. 3f).

Peripheral suppression of MKK6 protects against obesity. The above results might suggest that obesity protection in *Mkk6*$^{-/-}$ mice is mediated by a peripheral mechanism, independent of MKK6 signaling in the brain. To investigate this possibility, we administered sh*Mkk6* lentivirus intravenously. Western blot analysis confirmed reduced MKK6 expression in adipose tissue and liver (Supplementary Fig. 4a, b). Intravenous sh*Mkk6* protected mice against HFD-induced obesity (Supplementary Fig. 4c), decreased weight of eWAT, BAT, and liver, but not skeletal muscle (Supplementary Fig. 4d), and gave partial protection against liver steatosis (Supplementary Fig. 4e). In addition, sh*Mkk6*-treated mice had lower fasting serum glucose levels, showing protection against hyperglycemia (Supplementary Fig. 4f). These results thus confirm that the phenotype of *Mkk6*$^{-/-}$ mice has a peripheral origin. To discard a possible role of MKK6 in HFD-induced obesity in muscle and liver, we generated conditional mice of *Mkk6* (Supplementary Fig. 4g). Analysis of mice lacking MKK6 in liver or muscle discarded a role of these organs in the phenotype and suggested a cell autonomus role of MKK6 in WAT (Supplementary Fig. 4i, j).

p38 activation through the AMPK/TAK/TAB pathway in *Mkk6*$^{-/-}$. BAT expression of UCP1 and PGC1α is believed to be regulated by p38 kinases through activation of the transcription factors ATF2 and CREB[25]. Western blot analysis of WAT from HFD-fed mice demonstrated enhanced activation of p38, ATF2, and CREB in *Mkk6*$^{-/-}$ animals (Fig. 3a). These results are unexpected because MKK6 is a canonical p38 activator. In BAT, GADD45γ induces thermogenic gene expression through activation of p38 after norepinephrin stimulous[26]. To study if lack of MKK6 could affect GADD45γ expression, we performed real-time quantitative reverse transcription PCR (qRT-PCR) analysis of *Gadd45g* expression in eWAT. No differences were found between WT and *Mkk6*$^{-/-}$ animals (Supplementary Fig. 5a). It has been postulated that in absence of the canonical activation, p38 can be triggered by an alternative pathway involving AMPK and TAB1/TAK1 complex[27]. In agreement with this hypothesis, AMPK was hyperactivated in WAT from HFD-fed *Mkk6*$^{-/-}$ mice as judged by phosphorylation levels of AMPK and its substrate ACC (Fig. 3a). Moreover, p38 and AMPK were also hyperactivated in adipocytes derived from *Mkk6*$^{-/-}$ animals as shown by ATF2 and ACC phosphorylation (Fig. 3b). To assess whether AMPK/TAB/TAK1 was involved in p38 hyperactivation, we infected *Mkk6*$^{-/-}$ pre-adipocytes with lentiviral vectors containing shRNA against AMPK, TAB1, and TAK1. Reduction of AMPK, TAK1, or TAB1 protein levels resulted in lower p38 phosphorylation and activation as it is shown by ATF2 phosphorylation (Fig. 3c). These results indicate that in absence of MKK6, adipocytes spontaneously engaged the metabolic master regulator AMPK to trigger p38 activation.

***Mkk6* deficiency increases adipocyte sensitivity to the T3.** Next, we addressed whether the effect of MKK6 on WAT function was cell-autonomous using adipocytes from WT and *Mkk6*$^{-/-}$ mice. First, we analyzed whether MKK6 was required to suppress UCP1 expression. In correlation with the increased ATF2 phosphorylation, we found intensified UCP1 levels in *Mkk6*$^{-/-}$ adipocytes (Fig. 3d). These data indicate that lack of MKK6 increased UCP1 expression in adipocytes in a cell-autonomous manner. To asses p38α implication in the increased UCP1 levels detected in *Mkk6*$^{-/-}$ adipocytes, *Mkk6*$^{-/-}$ pre-adipocytes infected with lentiviral vectors containing shRNA against p38α were differentiated to adipocytes and UCP1 levels quantified. Decrease of p38α resulted in a reduction of UCP1 protein levels (Fig. 4e), showing that p38α activation observed in *Mkk6*$^{-/-}$ adipocytes participates in the enhanced UPC1 expression. The higher WAT UCP1 content in *Mkk6*$^{-/-}$ could corroborate substantial mitochondrial proton leak as a mechanism to dissipate energy as heat. To test this possibility, we measured the respiratory capacity of white adipocytes. In concordance with higher UCP1 expression, *Mkk6*$^{-/-}$ adipocytes had a lower spare respiratory capacity than WT adipocytes regardless of the source of the nutrient (glucose or fatty acid) (Fig. 3f). Moreover, transmission electron microscopy analysis of mitochondria from eWAT showed clear differences in mitochondria with higher mitochondria electrodensity observed in the *Mkk6*$^{-/-}$ indicating that this

Fig. 2 *Mkk6*$^{-/-}$ mice have higher energy expenditure by increased thermogenesis. **a** Comparison of energy balance between HFD-fed WT and *Mkk6*$^{-/-}$ mice. Mice were fed the HFD for 8 weeks and examined in a metabolic cage over a 2-day period to measure energy expenditure (EE). EE levels non-corrected (left), corrected by lean mass (centre), or an ANCOVA analysis (right) are shown (mean ± SEM, WT $n = 10$ mice; *Mkk6*$^{-/-}$ $n = 9$ mice). **b** Body temperature of HFD-fed WT and *Mkk6*$^{-/-}$ mice (mean ± SEM, WT $n = 19$ mice; *Mkk6*$^{-/-}$ $n = 15$ mice). **c**, **d** qRT-PCR analysis of thyroid-hormone-responsive genes and browning-associated genes in epididymal fat (eWAT). Data were normalized to the expression of *Gapdh* mRNA in each sample, and are presented as mean ± SEM (WT $n = 7$–23 mice, *Mkk6*$^{-/-}$ $n = 5$–19 mice). **e** Western blot analysis of uncoupling protein 1 (UCP1) in epididymal (eWAT) of WT and *Mkk6*$^{-/-}$ mice. Quantification of eWAT UCP1 protein levels is also shown (mean ± SEM, $n = 5$ mice). **f** Representative white adipose tissue MR spectrum (from 5 mice) from WT (left) and *Mkk6*$^{-/-}$ (right) mice fed the 8-week HFD. WAT from *Mkk6*$^{-/-}$ shows a BAT-like pattern with two large peaks of emission corresponding to water peak (peak 2 at 4.8 p.p.m.) and lipid component (peak 5 at 1.6–1.3 p.p.m.). Also showed quantification of ATP cellular content respect total (cytosolic and mitochondrial) free inorganic phosphate (Pi) (peak at 5.3–5 p.p.m.) in eWAT (mean ± SEM, $n = 5$ mice). **g** Body weight changes in WT and *Mkk6*$^{-/-}$ mice during the 8-week HFD period; mice were housed at 30 °C. (mean ± SEM, WT $n = 10$ mice; *Mkk6*$^{-/-}$ $n = 7$ mice). **h** Effect of cold exposure (4 °C, 60 min) on body temperature in WT and *Mkk6*$^{-/-}$ mice fed the 8-week HFD (mean ± SEM, WT $n = 10$ mice; *Mkk6*$^{-/-}$ $n = 8$ mice). **i** Staining of UCP1 after 1 week of cold exposure in sWAT. Scale bar: 50 μm. Statistically significant differences between *Mkk6*$^{-/-}$ mice and WT mice are indicated: $^{*}p < 0.05$; $^{**}p < 0.01$; $^{***}p < 0.001$ (*t* test or Welch's test when variances were different)

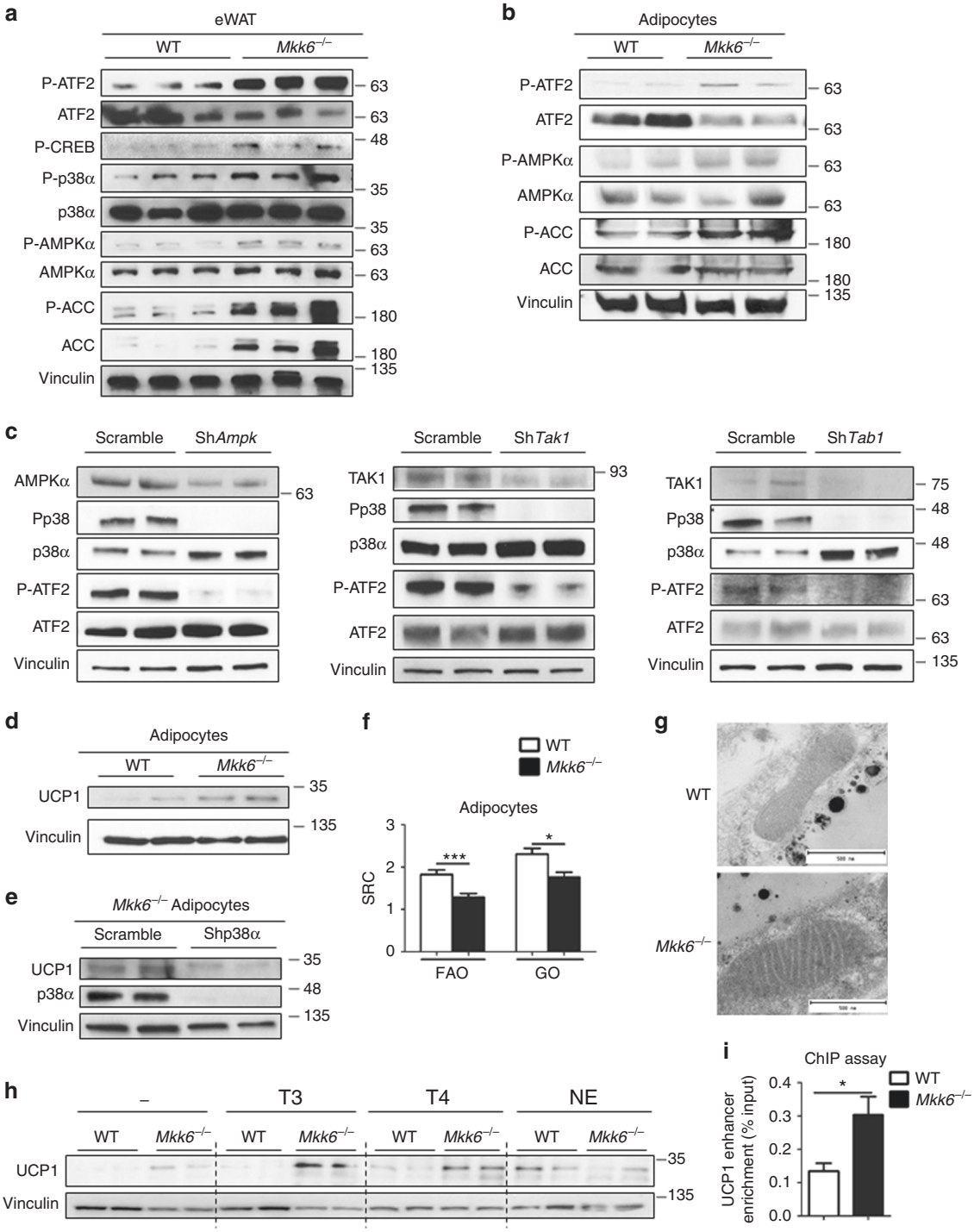

Fig. 3 *Mkk6*$^{-/-}$ white adipose tissue is predisposed to T3-induced browning. **a** Activation of p38 and AMPK pathways in epididymal white fat from HFD-fed WT and *Mkk6*$^{-/-}$ mice. Immunoblot analysis with the indicated antibodies was performed in extracts from mice starved overnight. **b** Immunoblot analysis of in vitro differentiated WT and *Mkk6*$^{-/-}$ adipocytes. Representative from three different experiments done by duplicate. **c** *Mkk6*$^{-/-}$ pre-adipocytes were infected with shRNA against AMPK, TAK1, TAB1, or scramble as a control. Activation of p38 was assayed by immunoblot of p38 and ATF2 phosphorylation. Representative from three different experiments. **d** UCP1 protein expression in in vitro differentiated WT and *Mkk6*$^{-/-}$ adipocytes. Representative from three different experiments done by duplicate. **e** *Mkk6*$^{-/-}$ pre-adipocytes were infected with shRNA against p38α or scramble as a control, and then differentiated to adipocytes. UCP1 levels were assayed by immunoblot $n = 4$. **f** Mitochondrial spare respiratory capacity (SRC) was assessed by Seahorse assay in primary WT and *Mkk6*$^{-/-}$ adipocytes incubated with glucose oxidation (GO) or fatty acid oxidation (FAO) medium (mean ± SEM, WT $n = 22$ WT or 24 *Mkk6*$^{-/-}$ wells from three mice cultured independently). **g** Representative transmission electronic microscopy images of mitochondria in eWAT from WT and *Mkk6*$^{-/-}$ HFD-fed mice ($n = 3$ mice). Scale bar: 500 nm. **h** Immunoblot analysis of UCP1 protein in in vitro differentiated WT and *Mkk6*$^{-/-}$ adipocytes stimulated for 48 h with T3, T4, or norepinephrine (NE). Representative from three different experiments done by duplicate. **i** Analysis of UCP1 enhancer enrichment in differentiated WAT from WT and *Mkk6*$^{-/-}$ mice after chromatin immunoprecipitation with thyroid hormone receptor α/β antibody. Results are expressed as mean ± SEM ($n = 12$ from three different sets).*$p < 0.05$, **$p < 0.01$, ***$p < 0.001$ WT vs *Mkk6*$^{-/-}$ (*t* test or Welch's test when variances were different)

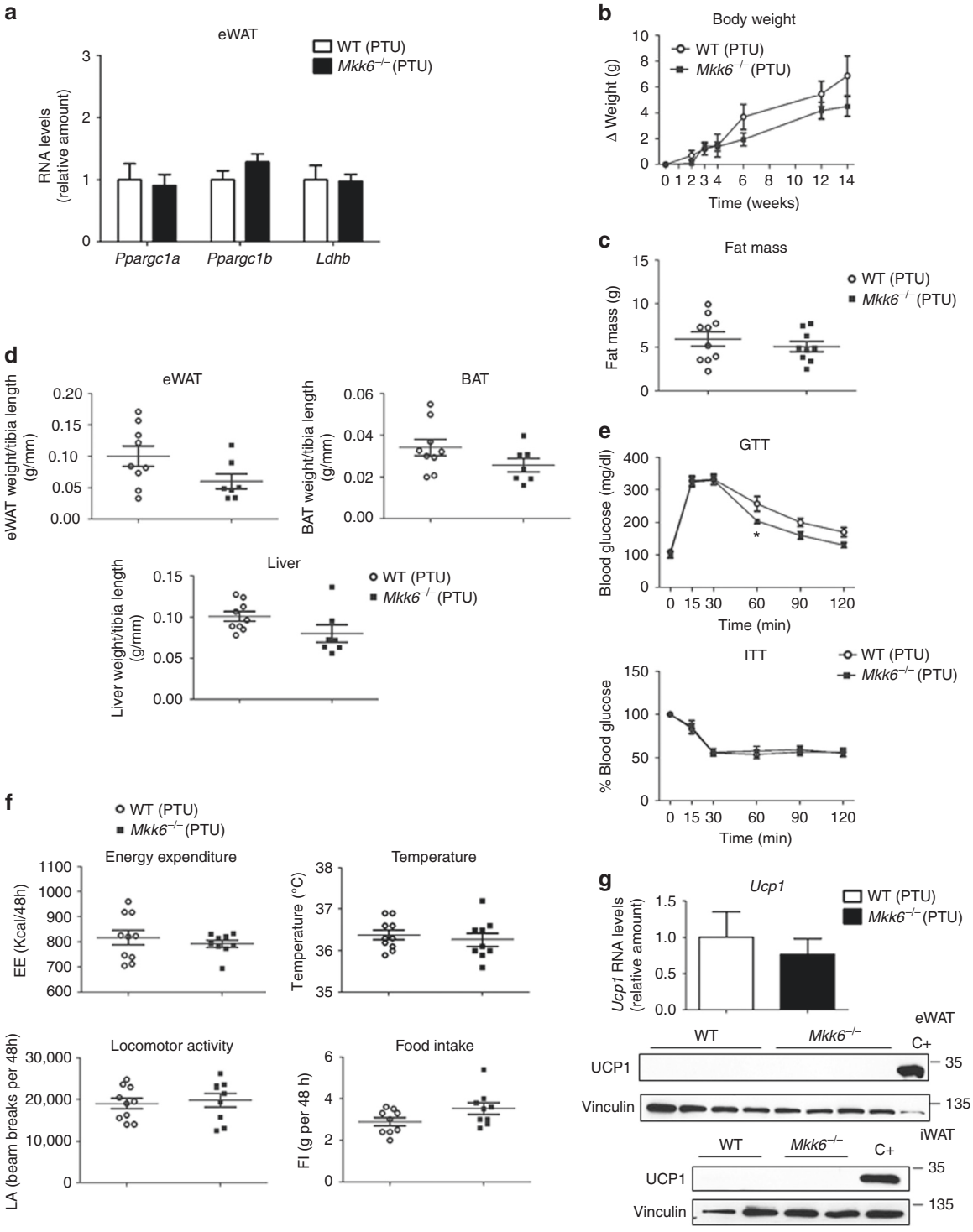

Fig. 4 Thyroid hormones participate in the *Mkk6*$^{-/-}$ phenotype. WT and *Mkk6*$^{-/-}$ mice were treated with propylthiouracil (PTU, 1.2 mM), an inhibitor of thyroid hormone synthesis, during the 8-week HFD period. **a** qRT-PCR analysis of genes associated with BAT activity in eWAT. mRNA expression was normalized to the amount of *Gapdh* mRNA (WT $n = 10$ mice; *Mkk6*$^{-/-}$ $n = 9$ mice). **b** Body weight changes in *Mkk6*$^{-/-}$ and WT mice treated with HFD and PTU (WT $n = 10$ mice; *Mkk6*$^{-/-}$ $n = 9$ mice). **c** Fat mass in *Mkk6*$^{-/-}$ and WT mice at the end of the 8-week HFD and PTU treatment (WT $n = 10$ mice; *Mkk6*$^{-/-}$ $n = 9$ mice). **d** Weight of epididymal white fat (eWAT), brown fat (BAT), and liver relative to tibia length in WT and *Mkk6*$^{-/-}$ mice. (WT $n = 9$ mice; *Mkk6*$^{-/-}$ $n = 7$ mice) **e** Glucose tolerance test (GTT), and insulin tolerance test (ITT) performed in WT and *Mkk6*$^{-/-}$ mice. Overnight or 1-h-starved mice were given an intraperitoneal injection of glucose (1 g/kg) or insulin (0.75 IU/kg), respectively (WT $n = 9$ mice; *Mkk6*$^{-/-}$ $n = 8$ mice). **f** Energy balance at the end of the treatment period, measured in WT and *Mkk6*$^{-/-}$ mice housed in a metabolic cage over 2 days; PTU abolished the enhancement of energy expenditure and body temperature in *Mkk6*$^{-/-}$ mice without changing locomotor activity or food intake. (WT $n = 10$ mice; *Mkk6*$^{-/-}$ $n = 9$ mice except food intake $n = 9$ mice). **g** qRT-PCR analysis of *Ucp1* mRNA (upper panel) and immunoblot analysis of UCP1 protein (lower panels) in eWAT and iWAT. mRNA expression was normalized to the amount of *Gapdh* mRNA (WT $n = 10$ mice; *Mkk6*$^{-/-}$ $n = 9$ mice). Results are expressed as mean ± SEM. *$p < 0.05$ (two-way ANOVA coupled to Bonferroni's post-tests or Welch's test when variances were different)

mitochondria are more active than the ones from WT (Fig. 3g). To investigate whether *Mkk6*$^{-/-}$ white pre-adipocytes were more prompted to differentiate to brown adipocytes than WT, white pre-adipocytes were differentiated using a white adipocyte differentiation protocol (WAT) or a brown adipocyte differentiation protocol (WAT + BAT). Only *Mkk6*$^{-/-}$ WAT adipocytes differentiated by the BAT protocol enhanced the oxygen consumption in response to norepinephrine, a characteristic of brown adipocytes, supporting a browning phenotype of *Mkk6*$^{-/-}$ WAT (Supplementary Fig. 5b).

WAT browning in vivo is mediated through a cascade involving β3-adrenergic receptor activation and TH signaling. To investigate which factors contribute to the WAT browning observed in *Mkk6*$^{-/-}$ mice, we monitored UCP1 expression in immortalized *Mkk6*$^{-/-}$ and WT white adipocytes stimulated with T3, T4, and norepinephrine (Fig. 3h). Importantly, adipocytes from *Mkk6*$^{-/-}$ mice were more sensitive to TH stimulation, expressing higher levels of UCP1 than WT cells (Fig. 3h and Supplementary Fig. 5c). *Ucp1* expression is regulated by a highly conserved enhancer element with binding sites for nuclear receptors and bZIP transcriptional factors[28]. Then, we used a chromatin immunoprecipitation (ChIP) assay to analyze the binding of TH receptors (THRs) to the UCP1 enhancer in differentiated WAT from WT and *Mkk6*$^{-/-}$ mice. We observed a significant enrichment in UCP1 enhancer in *Mkk6*$^{-/-}$ adipocytes after ChIP with THRα/β antibody (Fig. 3i) indicating higher sensibility to TH and explaining the increased UCP1 expression. Since our data indicated that p38 activation in WAT was mediated by AMPK, which enhanced UCP1, we evaluated whether T3 could trigger AMPK activation. T3 treatment increased AMPK phosphorylation and activation that correlated with higher levels of UCP1 (Supplementary Fig. 5d).

To determine the relationship between MKK6 loss and T3-induced mitochondrial reorganization, adipocytes were co-stained with the fluorescent dyes Bodipy (which selectively binds to accumulated neutral lipids) and Mitotracker (selective for intracellular mitochondria) (Supplementary Fig. 5e). Lipid droplets looked smaller in *Mkk6*$^{-/-}$ where T3 stimulation seemed to promote lipid droplet breakage that was absent in the WT. The staining correlates with the mitochondrial distribution in T3-treated *Mkk6*$^{-/-}$ indicating enhanced metabolic activity. Together, these data indicate that in *Mkk6*$^{-/-}$ adipocytes T3 promotes a fast lipid utilization by mitochondria in parallel to the increase in UCP1, ultimately leading to the browning of white adipocytes.

TH contribute to the metabolic actions of MKK6. We next examined the potential causal link thyroid hormone inducing WAT browning and the prevention of HFD-induced weight gain in *Mkk6*$^{-/-}$ mice. Treatment of mice with propylthiouracil (PTU), an inhibitor of thyroid hormone production[29], suppressed the effects of thyroid hormone-responsive genes in the WAT of *Mkk6*$^{-/-}$ mice (Fig. 4a compared to Fig. 2c, d), the differences in weight and fat mass (Fig. 4b–d), and the changes in glucose and insulin tolerance tests (Fig. 4e) between genotypes. After PTU treatment, EE and body temperature in *Mkk6*$^{-/-}$ mice were similar to readings in WT counterpart, with no changes in locomotor activity or food intake (Fig. 4f). Suppression of TH production also eliminated the increased *Ucp1* expression in WAT (Fig. 4g), while levels in BAT were unaltered (Supplementary Fig. 6a, b). Correct TH inhibition by PTU was assayed by the thyroid expression of genes controlled by TH (Supplementary Fig. 6c). These results indicate that the metabolic phenotype of *Mkk6*$^{-/-}$ mice involves an elevated responsiveness of WAT to TH.

To rule out that part of the effects in vivo were due to changes in the serum TH levels in *Mkk6*$^{-/-}$ mice, we evaluated circulating T3 and T4, and thyroid-stimulating hormone (TSH) levels. While no differences were observed in T3 or T4, serum TSH and pituitary expression of *Tshb* were significantly reduced in *Mkk6*$^{-/-}$ mice (Supplementary Fig. 7a, b) correlating with an increased sensitivity to T3. Although we did not find any change in total hypothalamic content of *Trh* (thyrotropin-releasing hormone) mRNA, or *Ttf1*, *Tshr*, or *Tpo* mRNA in the thyroid gland, we found a substantial repression of thyroglobulin and pendrin (Pds/Slc26A4, the basal iodine transporter), two essential genes in the hormone synthesis pathway in the thyroid, that indicated a physiological extreme downregulation due to T3 hypersensitivity (Supplementary Fig. 7c, d).

We also examined mRNA expression of deiodinases (Dio1, 2, 3) and α and β THRs in eWAT, BAT, and liver. As shown in the Supplementary Fig. 8, the only consistent change in all tissues studied is a reduction in Dio2 expression (the key enzyme converting inactive T4 into active T3) being statistically significant only in BAT. This reduced Dio2 expression would reflect again and a cellular hypersensibility to otherwise normal serum levels of T3.

To further investigate TH responsiveness in more detail, we first suppressed endogenous TH production by administering PTU to WT and *Mkk6*$^{-/-}$ mice fed a HFD for 2 weeks, and then treated all animals with T3. Both genotypes showed similar weight gain after treatment with PTU initially (Fig. 5a); however, after addition of exogenous T3 weight gain in *Mkk6*$^{-/-}$ mice decreased with respect to WT mice (Fig. 5a). After 8 weeks of T3 treatment, *Mkk6*$^{-/-}$ mice had lower fat mass and fat accumulation in several tissues than WT mice, (Fig. 5b, c) and improved fed glucose levels (Fig. 5d). T3 treatment also increased EE in *Mkk6*$^{-/-}$ mice (Fig. 5e), correlating with activation of TH-controlled genes in WAT (Fig. 5f, g) with no differences in liver and only increase of *Ppargc1a* in BAT (Supplementary Fig. 9). These results confirm that lack of MKK6 increases the sensitivity of WAT to TH in vivo, resulting in a browning effect in WAT.

Knocking down *Mkk6* reduces HFD-induced metabolic syndrome. To test whether depletion of MKK6 has potential as a treatment for obesity, we fed a HFD to WT mice for 8 weeks and then injected them i.v. with lentivirus expressing a scrambled sequence or a shRNA targeting MKK6 (Fig. 6a) that we had already known that reduced MKK6 in adipose tissue (Supplementary Fig. 4a). Mice injected with sh*Mkk6* gained less body mass after lentiviral administration (Fig. 6b) and were protected against HFD-induced hyperinsulinemia and hyperglycemia (Fig. 6c, d). These results indicate that inhibition of MKK6 in peripheral tissues, and particularly in WAT, could have potential in humans as a treatment for obesity and the associated diabetes.

To further study whether these effects observed in mice would be transferable to humans, MKK6 expression in visceral fat from obese and lean individuals was investigated. Analysis of MKK6 protein levels in visceral fat revealed markedly higher levels of MKK6 in obese patients (Fig. 6e).

In conclusion, our data demonstrate that the expression of MKK6 in WAT is important to establish the obese phenotype and resistance to TH. Moreover, its ablation allows WAT UCP1 expression and browning mediated by normal levels of T3 with the consequent increase in EE ameliorating obesity and diabetes (Fig. 7).

Discussion

In this report, we show that the activity of the mitogen protein kinase MKK6 prevents the browning of WAT. Thus, the WAT of

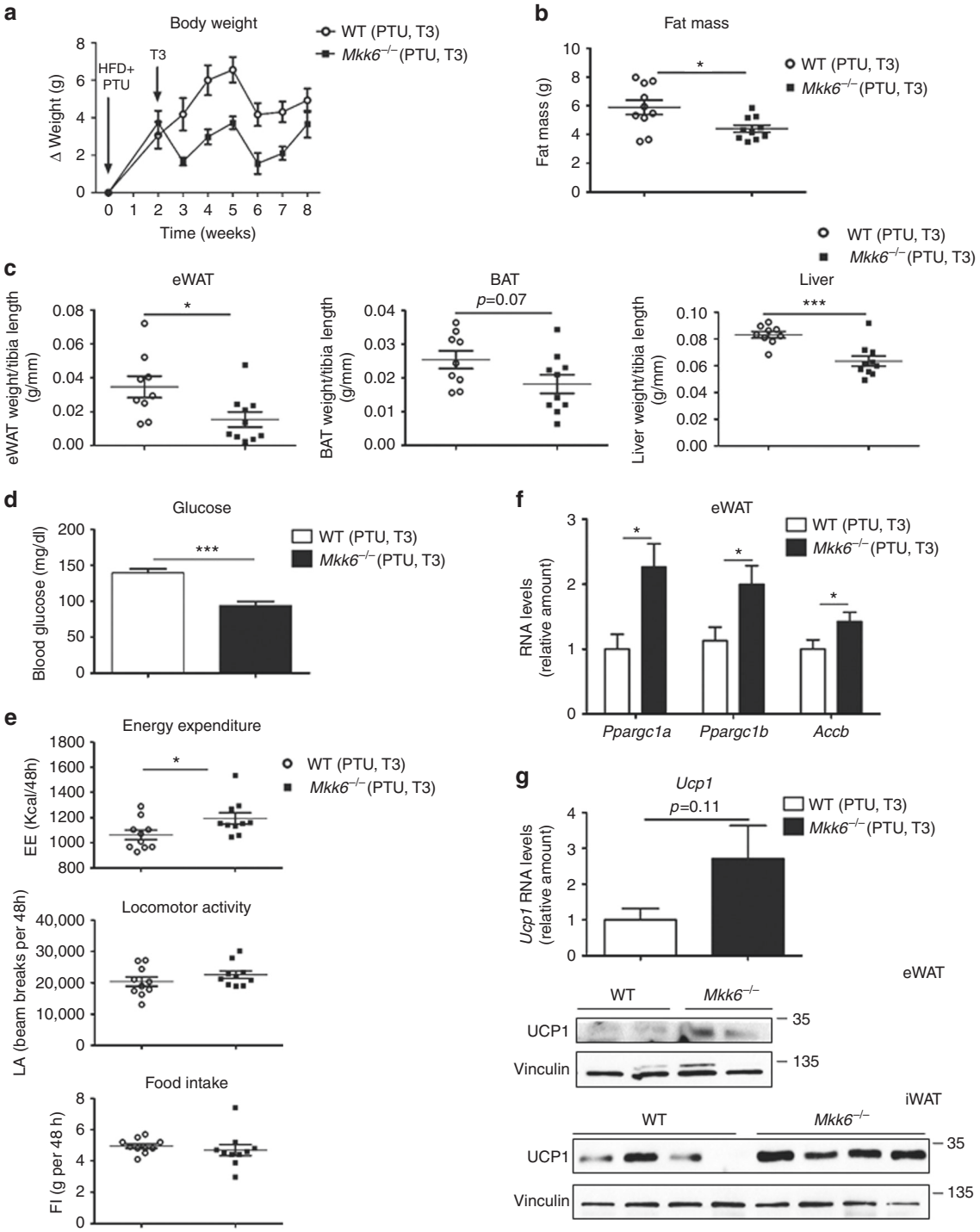

Fig. 5 Lack of MKK6 increases peripheral TH sensitivity. WT and *Mkk6*$^{-/-}$ mice were treated with 1.2 mM PTU during the 8-week HFD period. After the first 2 weeks of treatment, mice received daily i.p. injections with T3 (3 µg/100 g in 0.2% BSA-PBS). **a** Effect of T3 on body weight in *Mkk6*$^{-/-}$ and WT mice during the treatment period ($p < 0.0001$ WT vs *Mkk6*$^{-/-}$ two-way ANOVA). **b** Fat mass in *Mkk6*$^{-/-}$ and WT mice at the end of the treatment period. **c** Weight of epididymal white fat (eWAT), brown fat (BAT), and liver relative to tibia length (WT $n = 9$ mice; *Mkk6*$^{-/-}$ $n = 10$ mice). **d** Blood glucose concentration was quantified in mice. **e** Energy expenditure, locomotor activity and food intake determined using metabolic cages. **f** qRT-PCR analysis of genes associated with BAT activity in total RNA extracted from eWAT. mRNA expression was normalized to the amount of *Gapdh* mRNA. **g** qRT-PCR analysis of *Ucp1* mRNA (left) and immunoblot analysis of UCP1 protein (right) in eWAT and iWAT. mRNA expression was normalized to the amount of *Gapdh* mRNA (WT $n = 9$ mice; *Mkk6*$^{-/-}$ $n = 10$ mice except *Ppargc1b* WT $n = 8$ mice, *Mkk6*$^{-/-}$ $n = 9$ mice). Results are expressed as mean ± SEM ($n = 10$ mice, except when is indicated). $^{*}p < 0.05$, $^{***}p < 0.001$ WT vs *Mkk6*$^{-/-}$ (*t* test or Welch's test when variances were different)

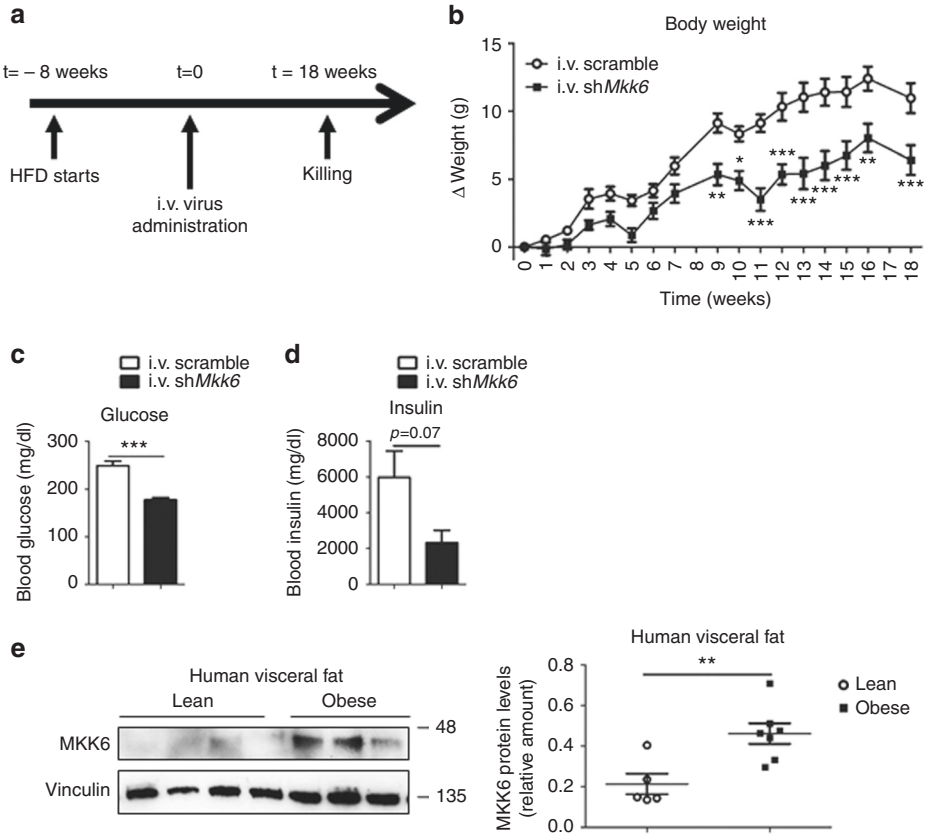

Fig. 6 MKK6 depletion has potential as an obesity treatment. **a** WT mice fed a HFD for 8 weeks were injected i.v. with lentivirus containing shRNA against MKK6 or a scramble sequence. **b** Body weight progression in WT mice after injecting lentivirus. Blood glucose (**c**) and insulin (**d**) in scramble or sh*Mkk6*-injected WT mice. Results are expressed as mean ± SEM ($n = 5$ mice). $^{**}p < 0.01$, $^{***}p < 0.0001$ i.v. scramble vs i.v. sh*Mkk6* (two-way ANOVA coupled to Bonferroni's post-tests or *t* test). **e** Western blot analysis showing elevated MKK6 levels in visceral fat from obese subjects vs controls. Results are expressed as mean ± SEM. $^{**}p < 0.01$ (lean $n = 5$, obese $n = 7$) A representative blot from three technical replicates (left) and quantification (right) are shown

mice lacking this kinase have elevated expression of UCP1, the landmark of browing, as well as other important regulators of this process, such as CIDEA, PGC1α, and PGC1β. Our results demonstrate the physiological relevance of this effect in controlling whole-body metabolism and obesity. Lack of MKK6 increases EE and body temperature, protecting animals from HFD-induced obesity and diet-induced diabetes. WAT browning is required for efficient protection, given that the phenotype is attenuated when animals are kept under thermoneutral conditions, indicating that manifestation of the phenotype requires active thermogenesis. The browning of WAT and the protection against HFD are dependent on the increased sensitivity of *Mkk6*$^{-/-}$ white adipocytes to T3, as they are ablated by inhibition of T3 production with PTU treatment and restored by retreatment with exogenous T3. The role of MKK6 in controlling browning is reinforced by the observation that T3 induces higher levels of UCP1 expression in differentiated *Mkk6*$^{-/-}$ adipocytes than in WT counterparts. Importantly, the results obtained in animal models seem to have clinical relevance, since higher levels of MKK6 were found in the fat of obese patients.

BAT is central in thermogenesis for cold adaptation and energy balance, and depends on the action of UCP1[30]. UCP1 expression is regulated by the sympathetic nervous system, mainly through norepinephrine and thyroid hormone[31]. T3 potentiates the effect of norepinephrine and is essential for the action of UCP1 in cold adaptation[32]. Our observation extends the role of T3 to the control of browning of WAT and the implication of MKK6/p38 in this signaling. Importantly, these effects could be only found in WAT, since the lack of MKK6 in other tissues such as liver or muscle did not cause any relevant metabolic change.

Mkk6$^{-/-}$ mice present normal T4 with reduced TSH levels, a whole mark of subclinical hyperthyroidism status[33]. Through different subsets of experiments, we have discarded diferent causes for subclinical hypertiroidism. Our data indicated that hypothalamus was not implicated in the phenotype (Supplementary Figs. 4 and 6). Serum T3 strongly reflects liver production by DIO2[34, 35]. Higher T3 conversion from T4 through increased expression of DIO2 was also discarded (Supplementary Fig. 8). In the other hand, we have obtained relevant data indicating a cellular T3 hypersensitivity in the *Mkk6*$^{-/-}$ mice mainly affecting WAT (Fig. 3). Furthermore, T3 induces stronger UCP1 expression in *Mkk6*$^{-/-}$ adipocytes than in WT (Fig. 3 and Supplementary Fig. 5). In addition, injection of a fixed dose of T3 in PTU hypothyroid mice fed with a HFD recover the lean phenotype (less weight, less hyperglycemia, less fat, and increased browning) only in *Mkk6*$^{-/-}$ mice but not in the WT (Fig. 5). Overall, we have found a positive modulator of T3 action at the white adipocyte cellular level in MKK6 with potential clinical relevance (Fig. 7). Although the implication of TH in metabolic and cellular actions on fat and other tissues including browning have been reported[36, 37], our data present for the first time an "intracellular modulation of the T3 activity" independently of the THRs, Trh, Tsh, or T4, and with normal levels of T3. These regulation might allow the modulation of T3 action specifically in WAT through MKK6 antagonists, which would prevent the

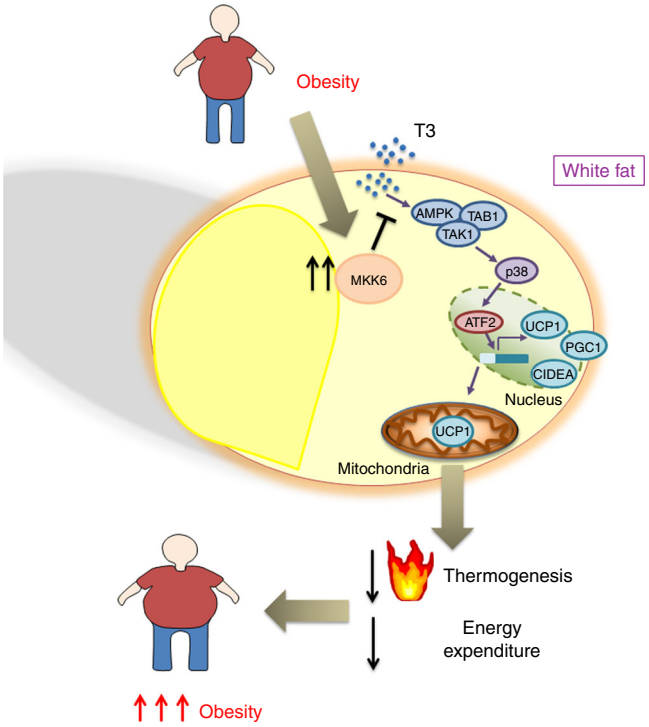

Fig. 7 MKK6 is an important regulator of browning. In obesity, high MKK6 levels block UCP1 induction by T3. Reduction in UCP1 levels decreases thermogenesis and energy expenditure. MKK6 could be a therapeutic target to reduce overweight

appearance of TH-associated off-target effects in other tissues. These findings have translational relevance because of high proportion of WAT in obese humans and the fact that human beige/brite adipocytes seem to be functional.

We also demonstrate that in WAT, the activation of p38 could be mediated by the alternative mechanism involving AMPK/TAK/TAB. The regulation of p38 activation by AMPK and its interaction with the scaffold protein TAB1 has been shown previously in cardiomiocytes and T cells[27, 38]. However, it was thought that this alternative activation was specific of these tissues. Here, for the first time we show that AMPK/TAB1 pathway controls p38 MAPK activation in white adipocytes. These results have important clinical relevance because activators of AMPK could be used to activate the p38 pathway in adipocytes, and increase browning of WAT through the ATF2 phosphorylation and UCP1 transcription.

In summary, as in obese individuals, the ability to induce browning is reduced[6, 39], our results have potential clinical significance. In humans, it has highlighted the role of beige/brite fat as opposed to real BAT, hence the increase of MKK6 levels in obese individuals suggest that impaired brite function activation may be in part mediated by this excess of MKK6 in adipose tissue. The higher action of MKK6 axes in visceral fat of obese individuals might contribute to make their adipose tissue resistant to T3, what would underlie the observed resistance to WAT browning. This also agrees with the observation that obese patients have significantly elevated TSH with lower T4 levels, as found not only in a population study with >4600 individuals[40], but also in a smaller but well-controlled study in 581 obese patients excluding diabetes, thyroid, and other endocrine diseases[41]. The high-TSH/low-T4 profile could be due to a peripheral resistance against T3 induced by obesity[42] and is also significantly correlated with insulin resistance[40].

In addition, since it has been recently shown that the expression of browning genes in human WAT correlates with serum T4[4], our findings suggest that the levels of MKK6 in adipose tissue may be of relevance for the weight gain and weight loss seen in hypo and hyperthyroid patients, respectively. However, further studies should assess this aspect in the appropriate cohort of patients.

Our findings establish a role for MKK6 in the regulation of body energy balance through the modulation of WAT browning, with potential implications for the treatment of obesity.

Methods

Study population and sample collection. The study population included 58 adults with body mass index (BMI) ≥35 who underwent elective bariatric surgery at the University Hospital of Salamanca. Patients were excluded if they had a history of alcohol abuse or excessive alcohol consumption (>30 g per day in men and >20 g per day in women), chronic hepatitis C or B. Control subjects ($n = 13$) were recruited among patients who underwent laparoscopic cholecystectomy for gallstone disease. The study was approved by the Ethics Committee of the University Hospital of Salamanca and all subjects provided written informed consent to undergo visceral fat biopsy under direct vision during surgery.

Data were collected on demographic information (age, sex, and ethnicity), anthropomorphic measurements (BMI), smoking and alcohol history, coexisting medical conditions, and medication use. Before surgery, fasting venous blood samples were collected for measuring complete cell blood count, total bilirubin, aspartate aminotransferase (AST), alanine AST (ALT), total cholesterol, high-density lipoprotein, low-density lipoprotein, triglycerides, creatinine, glucose, and albumin (Supplementary Table 1).

Animal models. The use and generation of C57Bl6J WT mice and knockout mice lacking MKK6 kinase in homozygosis (*Mkk6*$^{-/-}$, B6.129-*Map2k6*^{tm1Flv}) was previously described[43]. All the animals were maintained on a C57BL/6J background (back-crossed 10 generations). Mice with a germ-line mutation in the *Map2k6* gene and LoxP elements inserted into two introns (Map2k6LoxP) were generated after homologous recombination in ES cells. ES cells were electroporated with this vector (Supplementary Fig. 4g) and selected with 200 µg/ml G418 and 2 µM gangcyclovir. Several correctly targeted ES cell clones were identified by southern blot and PCR. These ES cell clones were injected into C57BL/6J blastocysts to create chimeric mice that transmitted the mutated Map2k6 allele through the germ line. The Flp NeoR cassette was excised by crossing these mice with ACTB:FLPe B6;SJL mice, which express a FLP1 recombinase gene under the direction of the human ACTB promoter. These animals were crossed with FVB-Tg (Ckmm-cre)5Khn/J line on the C57BL/6J background (Jackson Laboratory) to generate mice lacking MKK6 in muscle and with B6.Cg-Tg(Alb-cre)21Mgn/J for deletion in hepatocytes. Genotype was confirmed by PCR analysis of genomic DNA. Male mice were fed with a normal chow diet or a HFD (Research Diets Inc.) for 8 weeks ad libidum. PTU treatment was administrated for 8 weeks in the drinking water at 1.2 mM together with Kool Aid™ to improve the taste. In some experiments, T3 (3 µg/100 g in 0.2% BSA–PBS) was injected i.p. daily. For temperature experiments, mice were housed at 30 °C for 8 weeks while feeding a HFD in case of thermoneutral analysis, and exposed to 4 °C for 1 h or 1 week after HFD treatment in case of cold adaptation studies. All animal procedures conformed to EU Directive 86/609/EEC and Recommendation 2007/526/EC regarding the protection of animals used for experimental and other scientific purposes, enacted under Spanish law 1201/2005. The procedures have been reviewed by the Institutional Animal Care and Use Committee (IACUC) of Centro Nacional de Investigaciones Cardiovasculares, and approved by Consejeria de Medio Ambiente, Administración Local y Ordenación del Territorio of Comunidad de Madrid.

Lentiviral vector production and mice infection. Lentiviruses were produced as described[44]. Briefly, transient calcium phosphate cotransfection of HEK-293 cells was done with the pGIZP empty, pGIZP.sh*Mkk6*, pGIZP.sh*Ampk*, pGIZP.sh*Tak1*, pGIZP.sh*Tab1*, or pGIZT.sh*Mapk14* vectors from Thermo scientific together with pΔ8.9 and pVSV-G. The supernatants containing the LV particles were collected 48 and 72 h after removal of the calcium phosphate precipitate, and were centrifuged at 700 × g, 4 °C for 10 min, and concentrated (165×) by ultracentrifugation for 2 h at 121986 g at 4 °C (Ultraclear Tubes, SW28 rotor and Optima L-100 XP Ultracentrifuge; Beckman). Viruses were collected by adding cold sterile PBS and were titrated by quantitative PCR.

Mice were injected in VMH or tail vein with lentiviral particles suspended in PBS. Seven days after infection, mice were fed a HFD diet.

Cell culture. For obtaining white pre-adipocites, WT and *Mkk6*$^{-/-}$ inguinal fat were mechanically and enzymatically disaggregated using type-A collagenase (2 mg/ml collagenase type-A, Roche) at 37 °C. Cell suspension passed through a 70 µm cell strainer (Falcon) to eliminate stroma and debris, and centrifuged at 400 × g for 8 min at RT. Pellet was collected and cells were counted using a CasyTon cell counter. Pre-adipocytes were inmortalized by infection with SV40T-pBABE-neo virus. Cells were differentiated to adipocytes for 9 days in 8% FCS medium supplemented with 5 µg/ml insulin, 25 µg/ml IBMX, 1 µg/ml dexamethasone, and 1 µM troglitazone. Then cultures were incubated with 100 nM T3, 100 nM T4, and 1 µM norepinephrine for 48 h before extraction. Alternatively, pre-adipocytes were differentiated to adipocytes using brown adipocyte differentiation protocol in which cells were induced to brown fat with 20 nM insulin, 1 nM T3, 125 µM indomethacin, 2 µg/ml dexamethasone, and 50 mM IBMX for 48 h, and maintained with 20 nM of insulin, and 1 nM of T3 for 8 days. In some experiments, white pre-adipocytes were infected with lentivirus containing shRNA targeting AMPK, TAK1, TAB1, p38α, or a scrambled sequence, and selected by resistance to puromycin.

Cell cultures used in this paper were tested for mycoplasma infection.

Analysis of mitochondrial function. Pre-dipocytes were plated and differentiated in gelatin (0.1%)-coated 96 seahorse plates. T3 stimulation was performed 48 h prior to the oxygen consumption analysis. MitoStress oxygen consumption rate (OCR) was assessed in XF medium containing either 25 mM glucose (glucose oxidation medium) or 1 mM palmitate, 2 mM L-glutamine, and 1 mM sodium pyruvate (fatty acid oxidation medium) using a XF-96 extracellular flux analyzers (Seahorse Bioscience, Agilent Technologies), and data normalized by cell number (CyQuant, Invitrogen). Spare respiration capacity (OCR carbonyl cyanide-4-(trifluoromethoxy)phenylhydrazone (FCCP)/OCR basal) and oxygen consumption in response to norepinephrine (NE) (fold increase (FI) NE/basal) was calculated.

Western blot. Samples were lysated with RIPA buffer containing protease and phosphatase inhibitors (Tris-Hcl 50 mM, pH 7,5; Triton X-100 1%; EDTA 1 mM, pH 8; EGTA 1 mM; NaF 50 mM; β-glycerophosphate-Na 1 mM; sodium pirophosphate 5 mM; orthovanadate-Na 1 mM; sucrose 0.27 M; PMSF 0.1 mM, β-mercaptoethanol 1 mM, aprotinin 10 µg/ml, and leupectin 5 µg/ml). Lysates were separated by SDS-PAGE and incubated in a 1/1000 dilution with antibodies against phospho-Akt (Thr308) antibody (Cell Signalling Technology cat# 9275s), phospho-Akt (Ser473) antibody (Cell Signalling Technology cat# 9271s), Akt antibody (Cell Signalling Technology cat# 9272s), phospho-ATF2 (Thr69/71) antibody (Cell Signalling Technology cat# 9225s), ATF2 (20F1) antibody (Cell Signalling Technology cat# 9226s), phospho-CREB (Ser133) (87G3) antibody (Cell Signalling Technology cat# 9198), phospho-p38 (Thr180/Tyr182) antibody (Cell Signalling Technology cat# 9211s), phospho-AMPKalpha (Thr172) antibody (Cell Signalling Technology cat# 2531s), AMPKalpha (23A3) antibody (Cell Signalling Technology cat# 2603s), phospho-acetyl-CoA carboxylase (Ser79) antibody (Cell Signalling Technology cat# 3661s), acetyl-CoA carboxylase (C83B10) antibody (Cell Signalling Technology cat# 3676s), TAK1 (D94D7) antibody (Cell Signalling Technology cat# 5206s), TAB1 antibody (C-20) (Santa Cruz Biotechnology cat# sc-6053), p38alpha antibody (C-20) (Santa Cruz Biotechnology cat# sc-535), monoclonal anti-vinculin (clone hVIN-1) antibody (Sigma-Aldrich cat# V9131), MKK6 polyclonal antibody (Stressgen Biotechnologies cat# ADI-KAP-MA014-E), or anti-UCP1 antibody (Abcam cat# AB10983) all used at 1:1000, followed by an incubation with a secondary antibody conjugated with horseradish peroxidase (HRP) (1:5000). Reactive bands were detected by chemioluminiscence and quantified by Image J software. Uncropped western blot images are shown in Supplementary Fig. 10.

Histology staining. Fresh liver, white fat, and brown fat were fixed with formalin 10%, included in paraffin, and cut in 5-mm slides followed by a hematoxylin and eosin staining. Adipocyte size was quantified using Image J software.

Fat droplets were detected by oil red staining (0.7% in propylenglycol) in 8-mm slides included in OCT compound (Tissue-Tek©).

Glucose tolerance test. Starved overnight mice were injected i.p. with 1 g/kg of glucose and blood glucose levels quantified by an Ascensia Breeze 2 glucose meter at 0, 15, 30, 60, 90, and 120 min post injection.

Insulin tolerance test. Insulin tolerance test was performed injecting i.p. 0.75 IU/kg of insulin at mice starved 1 h and detecting blood glucose levels by a glucometer at different time points post injection (0, 15, 30, 60, 90, and 120) as indicated in the figure.

Insulin release and measurement. Mice were injected with 2 g/kg of glucose and blood collected by submaxilar puncture at 0, 10, and 30 min after injection. Insulin was quantified in serum by a multiplexed ELISA with a Luminex 200 analyser (Bio-Rad) following manufacture instructions.

Indirect calorimetry system. EE, respiratory exchange, locomotor activity, and food intake were quantified using the indirect calorimetry system (TSE LabMaster, TSE Systems, Germany) during 2 days.

Temperature. Body temperature was detected by a rectal thermometer (AZ 8851K/J/T Handheld Digital Thermometer-Single, AZ Instruments Corp., Taiwan).

BAT-adjacent interscapular temperature was quantified by thermographic images using a FLIR® T430sc Infrared Camera (FLIR Systems, Inc., Wilsonville, Oregon) and analyzed through FlirIR software.

Magnetic resonance imaging and NMR spectroscopy analysis. Fat mass was analyzed by magnetic resonance imaging (whole body composition analyzer; EchoMRI, Houston, TX, USA).

Spectroscopy examinations of WAT were performed in vivo on a 7T preclinical system (Agilent Varian, Palo Alto, USA) equipped with a DD2 console and an active shielded 205/120 gradient insert coil with 130 mT/m maximum strength. Double-tuned circular transmit/receive coil were used for phosphorus/proton (20 mm), placed over the epididymal fat and BAT (Rapid Biomedical GmBH, Rimpar Germany).

Proton NMR spectra were acquired by 128 transients with 2048 complex points with a spectral bandwidth of 10 kHz and a repetition time of 1.2 ms. Spectra were acquired with adiabatic radiofrequency pulses to improve sensitivity and minimize spectral distortions with an Ernst flip angle. Chemical shifts were expressed relative to the water signal (4.7–4.8 p.p.m.) in ^{1}H-MRS and phosphocreatine (0 p.p.m.) in ^{31}P-MRS. Signals in NMR spectra were determined quantitatively by integration after automatic or manual baseline correction, with fitting of each peak of the spectrum (after phase and baseline correction) to a Lorentzian function using the Mestrenova program (Mestrelab Research, Santiago de Compostea, Spain; released 2015-02-04 version:10.0.1-14719) on a Macintosh computer. An exponential line broadening (3 Hz for proton) was applied before Fourier transformation.

qRT-PCR. RNA of 1 mg extracted with RNeasy Plus Mini kit (Quiagen©) following manufacture instructions, was transcribed to complementary DNA and qRT-PCR performed using Fast Sybr Green probe (Applied Biosystems) and the appropriated primers in the 7900 Fast Real Time thermocycler (Applied Biosystems). Relative mRNA expression was normalized to *Gapdh* mRNA measured in each sample. Alternatively, RT-PCR was performed using Fast TaqMan probe (Applied Biosystems) and the appropriate TaqMan Assay (Applied Biosystems) in the 7900 Fast Real Time thermocycler. Relative mRNA expression was normalized to 18s mRNA measured in each sample or to *Hprt* mRNA in thyroid analysis. Primers and TaqMan Assays used are specified in Supplementary Table 2.

UCP1 immunostaining and confocal analysis. For UCP1 immunostaining, fresh fat depots were fixed with formalin 10%, included in paraffin, cut in 5-mm slides, and sequentially stained with a UCP1 antibody (1/500, Abcam cat# AB10983), a biotinylated goat anti-rabbit secondary antibody (1/500, Jackson Immuno Research Laboratories), a streptavidin-conjugated ABC complex, and the substrate 3,3′-diaminobenzidene conjugated with horseradish peroxidase (Vector Laboratories cat# PK-6100), followed by brief counterstaining with Nuclear Fast Red hematoxylin (Sigma).

Alternatively, adipocytes were stained with UCP1 primary antibody (1/500, Abcam cat# AB10983) together with a fluorescent goat anti-rabbit secondary antibody (Invitrogen), Bodipy (Invitrogen), and Dapi (Invitrogen) to study UCP1 expression. Images were captured using a Leica SPE confocal microscope (Leica Microsystems, Wetzlar, Germany).

To analyze mitochondria organization, adipocytes were stained with Mito Tracker Deep Red (Invitrogen) and Bodipy (Invitrogen).

Mitochondria morphology analysis. Fresh fat depots of 1 mm^2 were fixed with a mix of paraformaldheyde 4% and glutaraldheyde 2% in 0.4 M hepes buffer for 4 h at 4 °C. Once fixed, samples were washed with 0.4 M hepes buffer and analyzed in a transmission electronic microscope (JEOL 1230) associated to a TVIPS CMOS 4K camera. Pictures were obtained at 80 kV.

Chromatin immunoprecipitation assay. Immortalized white pre-adipocytes from WT and *Mkk6*$^{-/-}$ mice were differentiated to adipocytes for 9 days and processed to extract chromatin according to SimpleChIP® Plus Kit from Cell Signalling. Chromatin was immunoprecipitated with a THRα/THRβ antibody (C3) (ThermoScientific cat# MA1-215), and, after elution and purification, DNA analyzed by qRT-PCR using UCP1 enhancer primers (fw: TCTACAGCGTCACAGAGGGT, rv: TGATTTCTGCTCTTCTGGCA) and control primers against RPL30 intron 2 supplied by SimpleChIP® Plus Kit. Results are expressed as % of input.

Hormone circulating levels measurement. T3, T4, and TSH were quantified in serum by a multiplexed ELISA with a Luminex 200 analyser (Bio-Rad) following manufacture instructions.

Statistical analysis. Results are expressed as mean ± SEM. Statistical analysis was evaluated by Student's *t* test and two-way ANOVA with values of $p < 0.05$ considered significant.

Data availability. The authors declare that all the data supporting the findings of this study are available within the paper and its Supplementary Information Files, or available from the authors upon reasonable request.

Received: 5 April 2017 Accepted: 8 August 2017
Published online: 11 October 2017

References

1. Muller, T. D. et al. p62 links beta-adrenergic input to mitochondrial function and thermogenesis. *J. Clin. Invest.* **123**, 469–478 (2013).
2. Lowell, B. B. et al. Development of obesity in transgenic mice after genetic ablation of brown adipose tissue. *Nature* **366**, 740–742 (1993).
3. Cederberg, A. et al. FOXC2 is a winged helix gene that counteracts obesity, hypertriglyceridemia, and diet-induced insulin resistance. *Cell* **106**, 563–573 (2001).
4. Cypess, A. M. et al. Identification and importance of brown adipose tissue in adult humans. *N. Engl. J. Med.* **360**, 1509–1517 (2009).
5. Nedergaard, J., Bengtsson, T. & Cannon, B. Unexpected evidence for active brown adipose tissue in adult humans. *Am. J. Physiol. Endocrinol. Metab.* **293**, E444–E452 (2007).
6. van Marken Lichtenbelt, W. D. et al. Cold-activated brown adipose tissue in healthy men. *N. Engl. J. Med.* **360**, 1500–1508 (2009).
7. Kozak, L. P. & Harper, M. E. Mitochondrial uncoupling proteins in energy expenditure. *Annu. Rev. Nutr.* **20**, 339–363 (2000).
8. Golozoubova, V. et al. Depressed thermogenesis but competent brown adipose tissue recruitment in mice devoid of all hormone-binding thyroid hormone receptors. *Mol. Endocrinol.* **18**, 384–401 (2004).
9. Silva, J. E. Thermogenic mechanisms and their hormonal regulation. *Physiol. Rev.* **86**, 435–464 (2006).
10. Lee, J. Y. et al. Triiodothyronine induces UCP-1 expression and mitochondrial biogenesis in human adipocytes. *Am. J. Physiol. Cell Physiol.* **302**, C463–C472 (2012).
11. Guerra, C., Koza, R. A., Yamashita, H., Walsh, K. & Kozak, L. P. Emergence of brown adipocytes in white fat in mice is under genetic control. Effects on body weight and adiposity. *J. Clin. Invest.* **102**, 412–420 (1998).
12. Cao, W. et al. p38 mitogen-activated protein kinase is the central regulator of cyclic AMP-dependent transcription of the brown fat uncoupling protein 1 gene. *Mol. Cell. Biol.* **24**, 3057–3067 (2004).
13. Zhang, Y. et al. Irisin stimulates browning of white adipocytes through mitogen-activated protein kinase p38 MAP kinase and ERK MAP kinase signaling. *Diabetes* **63**, 514–525 (2014).
14. Paul, A. et al. Stress-activated protein kinases: activation, regulation and function. *Cell. Signal.* **9**, 403–410 (1997).
15. Sabio, G. & Davis, R. J. cJun NH2-terminal kinase 1 (JNK1): roles in metabolic regulation of insulin resistance. *Trends Biochem. Sci.* **35**, 490–496 (2010).
16. Sabio, G. & Davis, R. J. TNF and MAP kinase signalling pathways. *Semin. Immunol.* **26**, 237–245 (2014).
17. Manieri, E. & Sabio, G. Stress kinases in the modulation of metabolism and energy balance. *J. Mol. Endocrinol.* **55**, R11–R22 (2015).
18. Barbatelli, G. et al. The emergence of cold-induced brown adipocytes in mouse white fat depots is determined predominantly by white to brown adipocyte transdifferentiation. *Am. J. Physiol. Endocrinol. Metab.* **298**, E1244–E1253 (2010).
19. Ghorbani, M. & Himms-Hagen, J. Appearance of brown adipocytes in white adipose tissue during CL 316,243-induced reversal of obesity and diabetes in Zucker fa/fa rats. *Int. J. Obes. Relat. Metab. Disord.* **21**, 465–475 (1997).
20. Cousin, B. et al. Occurrence of brown adipocytes in rat white adipose tissue: molecular and morphological characterization. *J. Cell Sci.* **103**, 931–942 (1992).
21. Fisher, F. M. et al. FGF21 regulates PGC-1alpha and browning of white adipose tissues in adaptive thermogenesis. *Genes Dev.* **26**, 271–281 (2012).
22. Hamilton, G., Smith, D. L. Jr., Bydder, M., Nayak, K. S. & Hu, H. H. MR properties of brown and white adipose tissues. *J. Magn. Reson. Imaging* **34**, 468–473 (2011).
23. Contreras, C. et al. The brain and brown fat. *Ann. Med.* **47**, 150–168 (2015).
24. Beiroa, D. et al. GLP-1 agonism stimulates brown adipose tissue thermogenesis and browning through hypothalamic AMPK. *Diabetes* **63**, 3346–3358 (2014).
25. Bordicchia, M. et al. Cardiac natriuretic peptides act via p38 MAPK to induce the brown fat thermogenic program in mouse and human adipocytes. *J. Clin. Invest.* **122**, 1022–1036 (2012).
26. Gantner, M. L., Hazen, B. C., Conkright, J. & Kralli, A. GADD45gamma regulates the thermogenic capacity of brown adipose tissue. *Proc. Natl Acad. Sci. USA* **111**, 11870–11875 (2014).
27. Lanna, A., Henson, S. M., Escors, D. & Akbar, A. N. The kinase p38 activated by the metabolic regulator AMPK and scaffold TAB1 drives the senescence of human T cells. *Nat. Immunol.* **15**, 965–972 (2014).
28. Rim, J. S. & Kozak, L. P. Regulatory motifs for CREB-binding protein and Nfe2l2 transcription factors in the upstream enhancer of the mitochondrial uncoupling protein 1 gene. *J. Biol. Chem.* **277**, 34589–34600 (2002).
29. Sabio, G. et al. Role of the hypothalamic-pituitary-thyroid axis in metabolic regulation by JNK1. *Genes Dev.* **24**, 256–264 (2010).
30. Nedergaard, J. et al. UCP1: the only protein able to mediate adaptive non-shivering thermogenesis and metabolic inefficiency. *Biochim. Biophys. Acta* **1504**, 82–106 (2001).
31. Rabelo, R., Schifman, A., Rubio, A., Sheng, X. & Silva, J. E. Delineation of thyroid hormone-responsive sequences within a critical enhancer in the rat uncoupling protein gene. *Endocrinology* **136**, 1003–1013 (1995).
32. Ribeiro, M. O. et al. Thyroid hormone--sympathetic interaction and adaptive thermogenesis are thyroid hormone receptor isoform--specific. *J. Clin. Invest.* **108**, 97–105 (2001).
33. Franklyn, J. A. The thyroid--too much and too little across the ages. The consequences of subclinical thyroid dysfunction. *Clin. Endocrinol.* **78**, 1–8 (2013).
34. Marsili, A., Zavacki, A. M., Harney, J. W. & Larsen, P. R. Physiological role and regulation of iodothyronine deiodinases: a 2011 update. *J. Endocrinol. Invest.* **34**, 395–407 (2011).
35. Schneider, M. J. et al. Targeted disruption of the type 2 selenodeiodinase gene (DIO2) results in a phenotype of pituitary resistance to T4. *Mol. Endocrinol.* **15**, 2137–2148 (2001).
36. Lahesmaa, M. et al. Hyperthyroidism increases brown fat metabolism in humans. *J. Clin. Endocrinol. Metab.* **99**, E28–E35 (2014).
37. Skarulis, M. C. et al. Thyroid hormone induced brown adipose tissue and amelioration of diabetes in a patient with extreme insulin resistance. *J. Clin. Endocrinol. Metab.* **95**, 256–262 (2010).
38. Ge, B. et al. MAPKK-independent activation of p38alpha mediated by TAB1-dependent autophosphorylation of p38alpha. *Science* **295**, 1291–1294 (2002).
39. Saito, M. et al. High incidence of metabolically active brown adipose tissue in healthy adult humans: effects of cold exposure and adiposity. *Diabetes* **58**, 1526–1531 (2009).
40. Knudsen, N. et al. Small differences in thyroid function may be important for body mass index and the occurrence of obesity in the population. *J. Clin. Endocrinol. Metab.* **90**, 4019–4024 (2005).
41. Ambrosi, B. et al. Relationship of thyroid function with body mass index and insulin-resistance in euthyroid obese subjects. *J. Endocrinol. Invest.* **33**, 640–643 (2010).
42. Vella, K. R. et al. Thyroid hormone signaling in vivo requires a balance between coactivators and corepressors. *Mol. Cell. Biol.* **34**, 1564–1575 (2014).
43. Tanaka, N. et al. Differential involvement of p38 mitogen-activated protein kinase kinases MKK3 and MKK6 in T-cell apoptosis. *EMBO Rep.* **3**, 785–791 (2002).
44. Urso, K. et al. NFATc3 regulates the transcription of genes involved in T-cell activation and angiogenesis. *Blood* **118**, 795–803 (2011).

Acknowledgements

We thank S. Bartlett for English editing. We are grateful to R.J. Davis for critical reading of the manuscript and R. González-Sarmiento for help with clinical study design. We thank the staff at the CNIC Animal facility and S. Pérez-Romero for technical assistance. G.S. and R.A.-P. are investigators of the Ramón y Cajal Program. E.M. was a Caixa fellow, and V.M.-R. and E.B. were FPI (FPI BES-2014-069332 and FPI BES-2011-043428, respectively). This work was funded by the following grants supported in part by funds from European Regional Development Fund (ERDF-FEDER): to G.S.: funding from the European Union's Seventh Framework Programme (FP7/2007-2013) under grant agreement no. ERC 260464, EFSD/Lilly, MINECO-FEDER SAF2016-79126-R, and Comunidad de Madrid S2010/BMD-2326; to M.M.: ISCIII and FEDER, PI10/01692, and I3SNS-INT12/049; to L.H.-C.: Junta de Castilla y León GRS 681/A/11; to R.N.: MINECO BFU2015-70664-R, Xunta de Galicia 2015-CP080 and PIE13/00024, and ERC281408; European grants UE0/MCA1108 and UE0/MCA1201; and the Comunidad de Madrid CAM/API1009; to F.C.: Junta de Extremadura-FEDER BR15164; to C.V.A. BFU2013-46109-R. The CNIC is supported by the Ministry of Economy, Industry and Competitiveness (MEIC) and the Pro CNIC Foundation, and is a Severo Ochoa Center of Excellence (SEV-2015-0505).

Author contributions

Conceptualization, N.M. and G.S.; methodology, N.M., E.B., R.A.-P., E.M., S.P.-S., V.M.-R., A.M., E.R., L.L.-V., A.V.L.-V., C.V.A., J.R.-C., F.C., J.A.E., R.N., and G.S.;

investigation, N.M., E.B., R.A.-P., E.M., S.P.-S., L.H.-C., V.M.-R., A.M., E.R., L.L.-V., A.V.L.-V., M.C.-R., C.V.A., J.R.-C., J.L.T., F.C., M.M., J.A.E., R.N., and G.S.; writing—original draft, N.M. and G.S.; writing—review and editing, N.M., E.B., R.A.-P., E.M., S.P.-S., L.H.-C., V.M.-R., A.M., E.R., L.L.-V., A.V.L.-V., C.V.A., J.R.-C., J.L.T., F.C., M.M., J.A.E., R.N., and G.S.; funding acquisition, G.S.; resources,. M.M., L.H.-C., J.L.T.; supervision, G.S.

Additional information

Supplementary Information accompanies this paper at doi:10.1038/s41467-017-00948-z.

Competing interests: The authors declare no competing financial interests.

Reprints and permission information is available online at http://npg.nature.com/reprintsandpermissions/

Publisher's note: Springer Nature remains neutral with regard to jurisdictional claims in published maps and institutional affiliations.

LETTER

https://doi.org/10.1038/s41586-019-1112-8

p38γ is essential for cell cycle progression and liver tumorigenesis

Antonia Tomás-Loba[1], Elisa Manieri[1,2,19], Bárbara González-Terán[1,19], Alfonso Mora[1], Luis Leiva-Vega[1], Ayelén M. Santamans[1], Rafael Romero-Becerra[1], Elena Rodríguez[1], Aránzazu Pintor-Chocano[1], Ferran Feixas[3], Juan Antonio López[1], Beatriz Caballero[1], Marianna Trakala[4], Óscar Blanco[5], Jorge L. Torres[5], Lourdes Hernández-Cosido[5], Valle Montalvo-Romeral[1], Nuria Matesanz[1], Marta Roche-Molina[1], Juan Antonio Bernal[1], Hannah Mischo[6], Marta León[1], Ainoa Caballero[1], Diego Miranda-Saavedra[7,8], Jesús Ruiz-Cabello[1,9,10,11,13], Yulia A. Nevzorova[12,13], Francisco Javier Cubero[14,15], Jerónimo Bravo[16], Jesús Vázquez[1,17], Marcos Malumbres[4], Miguel Marcos[5], Sílvia Osuna[3,18] & Guadalupe Sabio[1]*

The cell cycle is a tightly regulated process that is controlled by the conserved cyclin-dependent kinase (CDK)–cyclin protein complex[1]. However, control of the G0-to-G1 transition is not completely understood. Here we demonstrate that p38 MAPK gamma (p38γ) acts as a CDK-like kinase and thus cooperates with CDKs, regulating entry into the cell cycle. p38γ shares high sequence homology, inhibition sensitivity and substrate specificity with CDK family members. In mouse hepatocytes, p38γ induces proliferation after partial hepatectomy by promoting the phosphorylation of retinoblastoma tumour suppressor protein at known CDK target residues. Lack of p38γ or treatment with the p38γ inhibitor pirfenidone protects against the chemically induced formation of liver tumours. Furthermore, biopsies of human hepatocellular carcinoma show high expression of p38γ, suggesting that p38γ could be a therapeutic target in the treatment of this disease.

Despite the identified role of CDKs in cell cycle progression, the precise molecular mechanisms that trigger initiation of the cell cycle are unknown in most cell types. The p38 MAPKs (p38α, p38β, p38γ and p38δ) and the CDKs belong to the CMGC protein kinase superfamily[2]. Sequence analysis of the catalytic domains of proteins from this superfamily showed that the p38 MAPKs form a sister group within the CDK family (Extended Data Fig. 1a). A heuristic three-dimensional (3D) search of active CDK1 and CDK2 revealed a higher degree of structural similarity with p38γ than with other stress kinases (Supplementary Table 1). Molecular dynamics simulations showed that the CDK1 inhibitor RO3306 has a similar affinity for the ATP-binding site of p38γ as it does for CDK1; it has weaker affinities for CDK2 and p38δ, and no affinity towards p38α. This suggests that p38γ and CDK1 have similar inhibition mechanisms (Extended Data Fig. 1b–e, Supplementary Videos 1, 2).

To test whether p38γ and CDKs share common substrates, we studied retinoblastoma tumour suppressor protein (Rb). Rb remains hypophosphorylated and active in G0, but during cell cycle progression it is sequentially phosphorylated by CDKs; its subsequent inactivation promotes entry into the cell cycle and proliferation[3]. In vitro kinase assays revealed that p38γ equally phosphorylated Rb at 12 CDK target residues[3] (Extended Data Figs. 1f, 2a). Moreover, we detected Rb in immunoprecipitates of p38γ from liver lysates (Fig. 1a). p38γ-mediated Rb phosphorylation in vivo was confirmed in livers from p38γ-knockout (*Mapk12*$^{-/-}$) mice that were infected with liver-specific adeno-associated viruses expressing a constitutively active form of p38γ (AAVp38γ*) (Fig. 1b). These data indicate that p38γ has

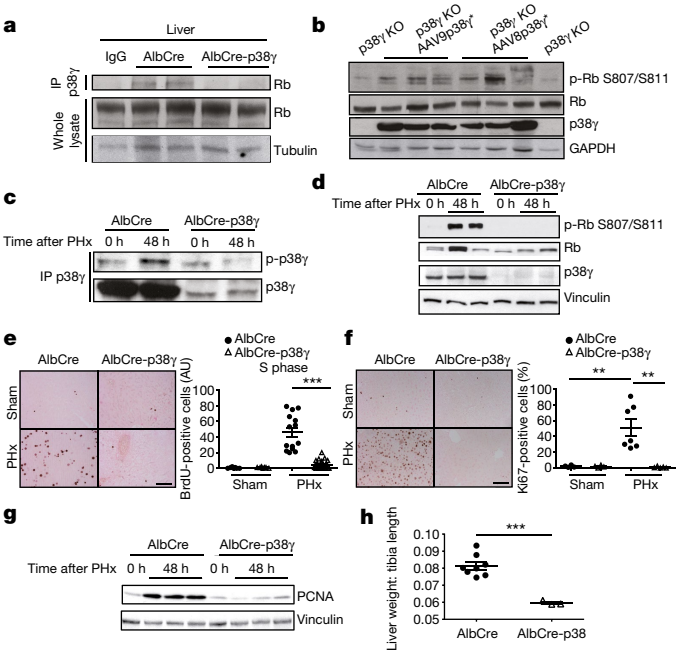

Fig. 1 | p38γ phosphorylates Rb and promotes liver proliferation after PHx. a, Immunoprecipitation from control livers (AlbCre mice, using IgG) and from livers in which p38γ was specifically knocked out (AlbCre-p38γ mice, using anti-p38γ), after treatment with DEN for 48 h. **b**, Immunoblots from livers of p38γ-knockout (p38γ KO) mice injected with adeno-associated virus (AAV8 or AAV9) expressing active p38γ (p38γ*). The prefix 'p-' indicates phosphorylation. **c**–**g**, Analysis of livers from AlbCre and AlbCre-p38γ mice 48 h after PHx or sham procedure. **c**, **d**, Liver immunoblot. **e**, BrdU immunostaining. Left, representative images; right, quantification of BrdU-positive cells. $n = 3$–7. **f**, Ki67 immunostaining. Left, representative images; right, quantification of Ki67-positive cells. $n = 4$–6. **g**, Proliferating cell nuclear antigen (PCNA) immunoblot. **h**, Ratio of liver weight (g) to tibia length (mm), 15 days after surgery. $n = 3$–8. All quantifications are shown as mean ± s.e.m. Comparisons were made by one-way analysis of variance (ANOVA) coupled to Bonferroni's post-test (**e**, **f**) or two-sided Student's *t*-test (**h**); $^{**}P < 0.01$; $^{***}P < 0.001$. Scale bars, 100 μm.

[1]Centro Nacional de Investigaciones Cardiovasculares (CNIC), Madrid, Spain. [2]Centro Nacional de Biotecnología, CSIC, Madrid, Spain. [3]Departament de Química and Institut de Química Computacional i Catàlisi, Universitat de Girona, Girona, Spain. [4]Centro Nacional de Investigaciones Oncológicas (CNIO), Madrid, Spain. [5]University of Salamanca, University Hospital of Salamanca-IBSAL, Salamanca, Spain. [6]Sir William Dunn School of Pathology, Oxford University, Oxford, UK. [7]Centro de Biología Molecular Severo Ochoa, CSIC/Universidad Autónoma de Madrid, Madrid, Spain. [8]University of Oxford Wolfson Building, Oxford, UK. [9]CIC biomaGUNE, 2014, Donostia-San Sebastián, Spain. [10]IKERBASQUE, Basque Foundation for Science, Bilbao, Spain. [11]Ciber de Enfermedades Respiratorias (CIBERES), Madrid, Spain. [12]University Hospital RWTH Aachen, Aachen, Germany. [13]Faculty of Biology, Complutense University, Madrid, Spain. [14]Complutense University School of Medicine, Madrid, Spain. [15]12 de Octubre Health Research Institute (imas12), Madrid, Spain. [16]Instituto de Biomedicina de Valencia, IBV-CSIC, Valencia, Spain. [17]CIBER Enfermedades Cardiovasculares (CIBERCV), Madrid, Spain. [18]ICREA, Barcelona, Spain. [19]These authors contributed equally: Elisa Manieri, Bárbara González-Terán. *e-mail: gsabio@cnic.es

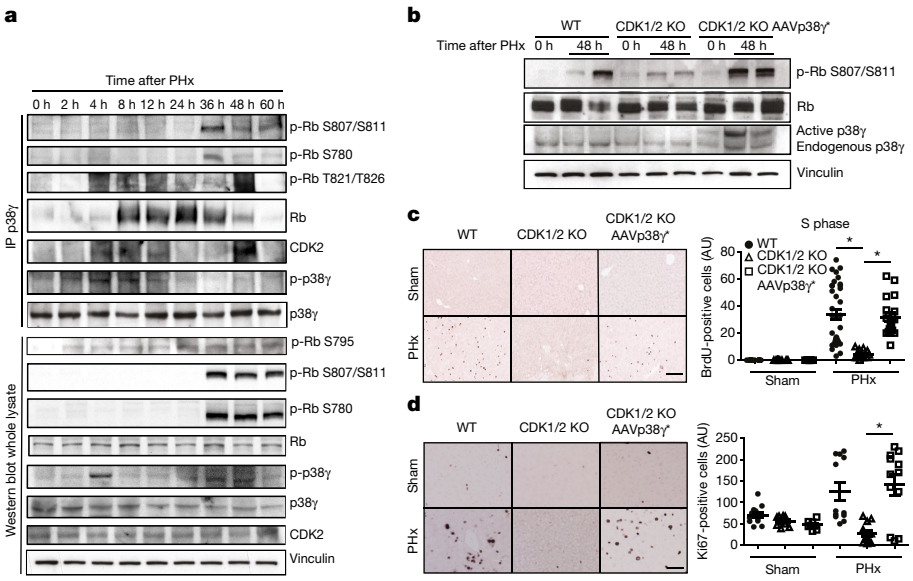

Fig. 2 | p38γ compensates for the loss of CDK1 or CDK2. a, Immunoprecipitation (using anti-p38γ) from liver lysates of wild-type mice that were euthanized at the indicated time points after PHx. **b**–**d**, Analysis of livers from wild-type mice (WT), CDK1/2 knockout (AAV2/8-Cre) mice (CDK1/2 KO) and CDK1/2 knockout mice infected with active p38γ (CDK1/2 KO AAVp38γ*) after PHx or sham procedure. **b**, Liver immunoblot. **c**, BrdU immunostaining. Left, representative images; right, quantification of BrdU-positive cells. AU, arbitrary units. $n = 4$–7. **d**, Ki67 immunostaining. Left, representative images; right, quantification of Ki67-positive cells. One-way ANOVA coupled to Kruskal–Wallis post-tests (**c**, **d**); $^*P < 0.05$. Scale bars, 500 μm. All quantifications are shown as mean ± s.e.m.

similarities with CDKs: it shares structural homology, comparable binding dynamics for RO3306 in the ATP-binding site and a similar substrate specificity.

Phosphorylation-induced Rb inactivation in hepatocytes is sufficient to promote the G0-to-G1 transition[4,5]. After partial hepatectomy (PHx)—a well-established model of hepatocyte proliferation—p38γ was phosphorylated and activated (Fig. 1c). To address the physiological effect of p38γ-mediated Rb phosphorylation after PHx, we compared hepatocyte proliferation in mice that lacked p38γ in hepatocytes (AlbCre-p38γ) and in control AlbCre mice (AlbCre$^{+/-}$). Whereas PHx induced the phosphorylation of Rb in control mice, this effect was abolished in AlbCre-p38γ mice (Fig. 1d) without changes in CDK expression (Extended Data Fig. 2b). Loss of Rb phosphorylation in AlbCre-p38γ mice correlated with reduced induction of cyclin E and A (Extended Data Fig. 2b). Compared with AlbCre mice, AlbCre-p38γ mice also showed markedly reduced hepatic DNA synthesis and hepatocyte proliferation—as measured by bromodeoxyuridine (BrdU) incorporation, Ki67 immunostaining and proliferating cell nuclear antigen expression (Fig. 1e–g). The reduced hepatocyte proliferation in AlbCre-p38γ mice was reflected in a reduced extent of liver regeneration (Fig. 1h, Extended Data Fig. 3a). Together, these results indicate that p38γ is required in hepatocytes for Rb phosphorylation and liver regeneration.

To corroborate these results and avoid the effects of unspecific deletion of p38γ, we infected AlbCre-p38γ mice with AAVp38γ*. The hepatocyte-specific expression of active p38γ recovered hepatocyte proliferation, Rb phosphorylation and liver regeneration (Extended Data Fig. 3b–f). It is known that N-terminal Rb phosphorylation by p38α delays cell cycle progression, rendering Rb insensitive to regulation by CDKs[6]. However, unlike hepatocyte-specific active p38α, active p38γ promoted phosphorylation of the Rb C terminus and hepatocyte proliferation (Extended Data Fig. 3g, h).

Lack of p38γ was found to impair liver regeneration, although it did not affect survival (Extended Data Fig. 4a). This is consistent with peak Rb phosphorylation and hepatocyte proliferation, which occurred at 60 h after PHx (Extended Data Fig. 4b, f). p38δ—the p38 isoform that is most closely related to p38γ—can compensate for the lack of p38γ and can phosphorylate its substrates[7–9]. The expression of p38δ

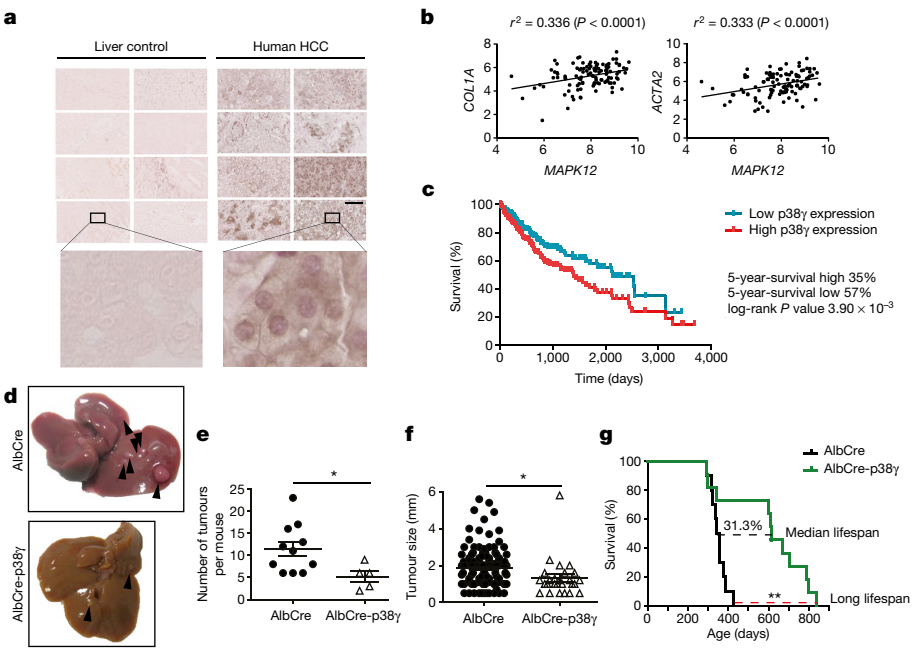

Fig. 3 | p38γ drives the development of HCC. a, p38γ immunostaining in human HCC and healthy liver control. Scale bar, 500 μm. **b**, Pearson's correlation of mRNA levels in human livers, comparing expression levels of *MAPK12* with those of *COL1A* (encoding collagen, left) and *ACTA2* (encoding actin, right). $n = 107$. **c**, Kaplan–Meier survival curves of patients stratified by p38γ expression. $n = 372$. **d**–**f**, Analysis of DEN-induced HCC in six-month-old AlbCre and AlbCre-p38γ mice. **d**, Photographs of livers from an AlbCre mouse (top) and an AlbCre-p38γ mouse (bottom). Arrows mark tumours. **e**, **f**, Number of tumours (**e**) and tumour size (**f**) in AlbCre and AlbCre-p38γ mice. $n = 5$–11. $^*P < 0.05$. **g**, Kaplan–Meier analysis of survival. $n = 10, 11$. $^{**}P < 0.01$. Scale bar, 100 μm. 31.3% is the difference in median lifespan between AlbCre and AlbCre-p38γ mice. All quantifications are shown as mean ± s.e.m. Comparisons were performed using a Mantel–Cox log-rank test (**c**, **g**); Mann–Whitney *U*-test (**e**); or two-sided Student's *t*-test (**f**).

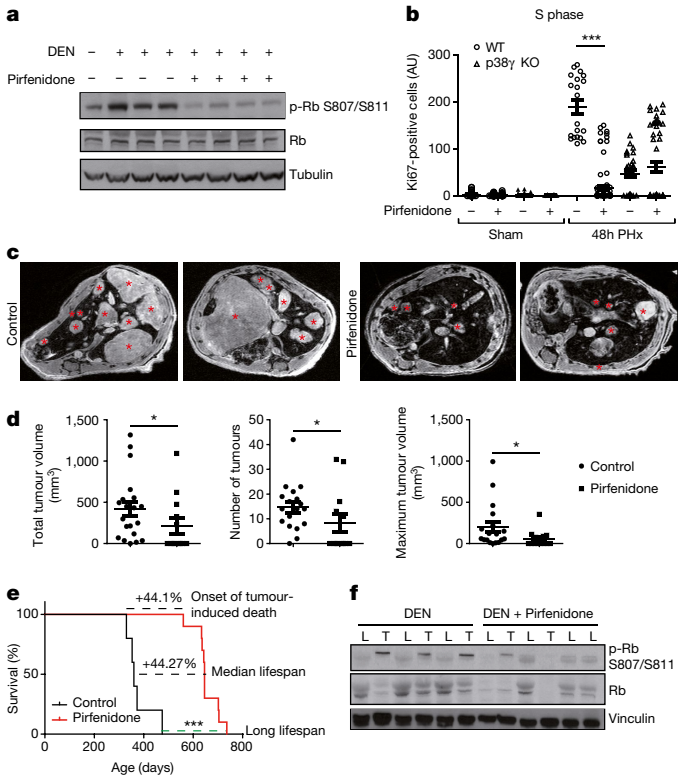

Fig. 4 | Pirfenidone inhibits p38γ activity and protects against DEN-induced HCC. a, Immunoblot of mouse liver 2 weeks after acute treatment with DEN. **b**, Ki67 immunohistochemistry in pirfenidone-treated mice before PHx. $n = 5$–17. One-way ANOVA; $^{***}P < 0.001$. **c**–**e**, Livers were imaged 11 months after DEN injection, with or without pirfenidone treatment. **c**, MRI scans of control and pirfenidone-treated livers. **d**, Number of tumours, maximum tumour volume and total tumour volume per mouse ($n = 20$–13), analysed from magnetic resonance images using OsiriX software; Mann–Whitney *U*-test; $^{*}P < 0.05$. **e**, Kaplan–Meier analysis of survival. The percentages are the differences in onset of tumour-induced death and median lifespan between control and pifenidone-treated mice. $n = 9$–6. Mantel–Cox log-rank test; $^{***}P < 0.001$. **f**, Immunoblot analysis in hepatic tumours (T) and lesion-free peritumour zones (L) in mice treated as in **d**–**f**. All data are mean ± s.e.m.

in AlbCre-p38γ mice increased after PHx (Extended Data Fig. 4c), and in hepatocytes that lacked both kinases (AlbCre-p38γδ), Rb phosphorylation was abolished and hepatocyte proliferation was significantly delayed (Extended Data Fig. 4d–h). Furthermore, stress-activated p38γ-mediated cell cycle regulation is not restricted to hepatocytes, because p38γ was also found to phosphorylate Rb in gut epithelial cells that were treated with dextran sodium sulfate (Extended Data Fig. 5).

The precise mechanism by which Rb is phosphorylated in vivo remains unclear, because single genetic ablation of CDK2 or CDK1 does not block hepatocyte DNA replication during liver regeneration[10,11]. In vitro kinase assays with CDK2 and p38γ* showed that a greater number of Rb residues were phosphorylated when both kinases were used, which suggests that these kinases work together to control Rb phosphorylation (Extended Data Fig. 6a). Immunoprecipitation analysis confirmed a binding interaction between p38γ and CDK2 in hepatocytes (Extended Data Fig. 6b, c). To explore the cooperation between p38γ and CDK2, we examined the activation of these kinases after PHx by western blot. p38γ was activated just 4 h after PHx, as evidenced by its increased binding of Rb and by Rb phosphorylation at Ser795, Ser821 and Ser826. Moreover, a second p38γ activation peak was detected at 24 h—corresponding to the phosphorylation of Rb on residues Ser807, Ser811 and Ser780—followed by hepatocyte proliferation as detected by BrdU incorporation (Fig. 2a, Extended Data Fig. 6d). Interaction between CDK2 and p38γ increased during these two p38γ activation peaks (Fig. 2a). These results correlate with a stronger interaction between CDK2 and Rb when p38γ is present (Extended Data Fig. 6e), whereas p38γ binding to Rb was shown to be independent of CDK1 and CDK2 (Extended Data Fig. 6c). Moreover, studies with a nonphosphorylatable Rb mutant[12] indicated that the phosphorylation of Rb is required in order for it to bind to CDK2 (Extended Data Fig. 6f).

In addition, p38γ was able to compensate for the loss of CDK1 or CDK2. Infection with AAVp38γ* rescued Rb phosphorylation after silencing or ablation of the genes that encode CDK1 or CDK2, and fully preserved hepatocyte proliferation and hepatic DNA synthesis in the livers of CDK1- or CDK2-depleted mice (Fig. 2b–d, Extended Data Fig. 6g–i). Collectively, these results suggest that p38γ controls hepatocyte proliferation through the regulation of Rb phosphorylation, and probably induces proliferation through cooperation with classical CDKs. Moreover, infection with AAVp38γ* rescued Rb phosphorylation and proliferation after silencing of the genes that encode CDK4 and CDK6 (Extended Data Fig. 6j–m); this confirms the ability of p38γ to phosphorylate Rb in the absence of these CDKs.

CDK1 ablation is known to protect against liver tumorigenesis[13]. Notably, the mutation rates of CDK1 and p38γ in human hepatocellular carcinoma (HCC) samples are similar (Extended Data Fig. 7a), and the mutations located in the L16 loop of p38γ induce its activation[14]. p38γ expression was also found to be higher in human HCC cell lines than in primary hepatocytes (Extended Data Fig. 7b), and p38γ was activated in livers from genetically engineered HCC mouse models (Extended Data Fig. 7c). Furthermore, p38γ staining was far stronger in human HCC biopsies than in non-tumour tissues (Fig. 3a, Extended Data Fig. 7d). *MAPK12* expression directly correlated with the expression of *ACTA2* and *COL1A*; these genes encode actin and collagen, respectively, which are markers of fibrosis that usually precede the development of liver cancer (Fig. 3b, Supplementary Table 2). Moreover, high p38γ expression was associated with a poorer outcome in cases of liver cancer (Fig. 3c), and p38γ knockdown attenuated proliferation and colony formation in HCC cell lines (Extended Data Fig. 8). These findings may indicate an involvement of p38γ in the development of human liver tumours.

In agreement, p38γ was activated after the injection of diethylnitrosamine (DEN), and p38γ deficiency markedly attenuated DEN-induced Rb phosphorylation and compensatory proliferation, correlating with reduced expression of proliferating cell nuclear antigen and reduced proliferation of hepatocytes (Extended Data Fig. 9a–c). Moreover, HCC was strongly suppressed in AlbCre-p38γ mice, which had smaller and fewer tumours and improved survival times compared with AlbCre mice (Fig. 3d–g).

AlbCre-p38γ mice were also protected against liver cancer induced by carbon tetrachloride or by in combination with a high-fat diet (Extended Data Fig. 9d–g). We next evaluated the effect of p38γ inactivation on liver tumorigenesis. The inhibitor pirfenidone bound to and inhibited p38γ without affecting CDK2 activity (Fig. 4a, Extended Data Fig. 10a, b), and reduced hepatic DNA synthesis in wild-type mice but not in AlbCre-p38γ mice, indicating a p38γ-mediated effect (Fig. 4b). Pirfenidone reduced the number and size of liver tumours in DEN-treated mice and improved their survival, without evident secondary effects (Fig. 4c–e, Extended Data Fig. 10c). Moreover, the therapeutic effects of p38γ inhibition were confirmed by the specific ablation of p38γ using AAV2/8-CAG-Cre once the tumours were already established (Extended Data Fig. 10d–g). Notably, the tumours that grew in the pirfenidone-treated mice lost Rb expression (Fig. 4f); this suggests that, upon pirfenidone treatment, only tumours that lack Rb are able to proliferate. These data are consistent with the inactivation of tumour suppressors such as Rb through chromosomal mutations during tumour development[15], thus indicating that pirfenidone could be effective against HCC tumours that maintain Rb expression.

Our results show that p38γ functions in collaboration with CDK; this is similar to the role of MAPK in CDK signalling that has recently been established in yeast[16]. Members of the p38 MAPK protein family

can be grouped into two classes, with p38α and p38β in one class, and p38γ and p38δ in the other[17]. All members of this family share the same mechanism of activation by upstream MAPK kinases; however, the two classes do not share substrate specificity or inhibitor selectivity. p38α increases cell survival by N-terminal phosphorylation of Rb, which renders Rb insensitive to inactivation by CDKs[6]. Consequently, the knockdown of p38α in hepatocytes results in increased development of HCC[18]. These results reinforce the idea that different p38 isoforms can have opposing functions[19].

We have demonstrated that p38γ is sufficient to induce entry into the cell cycle even when the expression of CDKs is downregulated. This might allow for a cell cycle regulation that is different from the canonical mitogenic signal and CDK activation pathway, and instead functions via stress damage and p38γ activation, thereby exerting a tight regulation on the cell cycle.

This study suggests that a non-classical CDK could initiate the cell cycle in a cyclin-independent manner in quiescence, when CDK–cyclin complexes are less abundant. p38γ may represent a unique type of kinase that enables cells to escape from quiescence in response to stress stimuli. The confirmation that p38γ is essential for Rb-dependent cell cycle progression and liver tumorigenesis strongly supports the potential of p38γ as a therapeutic target in HCC, and could provide a new approach towards the treatment of this disease.

Online content

Any methods, additional references, Nature Research reporting summaries, source data, statements of data availability and associated accession codes are available at https://doi.org/10.1038/s41586-019-1112-8.

Received: 11 October 2017; Accepted: 7 March 2019;
Published online: 10 April 2019

1. Malumbres, M. Cyclin-dependent kinases. *Genome Biol.* **15**, 122 (2014).
2. Varjosalo, M. et al. The protein interaction landscape of the human CMGC kinase group. *Cell Rep.* **3**, 1306–1320 (2013).
3. Malumbres, M. & Barbacid, M. Cell cycle, CDKs and cancer: a changing paradigm. *Nat. Rev. Cancer* **9**, 153–166 (2009).
4. Canhoto, A. J., Chestukhin, A., Litovchick, L. & DeCaprio, J. A. Phosphorylation of the retinoblastoma-related protein p130 in growth-arrested cells. *Oncogene* **19**, 5116–5122 (2000).
5. Mayhew, C. N. et al. Liver-specific pRB loss results in ectopic cell cycle entry and aberrant ploidy. *Cancer Res.* **65**, 4568–4577 (2005).
6. Gubern, A. et al. The N-terminal phosphorylation of RB by p38 bypasses its inactivation by CDKs and prevents proliferation in cancer cells. *Mol. Cell* **64**, 25–36 (2016).
7. Sabio, G. et al. p38γ regulates the localisation of SAP97 in the cytoskeleton by modulating its interaction with GKAP. *EMBO J.* **24**, 1134–1145 (2005).
8. González-Terán, B. et al. p38γ and δ promote heart hypertrophy by targeting the mTOR-inhibitory protein DEPTOR for degradation. *Nat. Commun.* **7**, 10477 (2016).
9. González-Terán, B. et al. Eukaryotic elongation factor 2 controls TNF-α translation in LPS-induced hepatitis. *J. Clin. Invest.* **123**, 164–178 (2013).
10. Lundberg, A. S. & Weinberg, R. A. Functional inactivation of the retinoblastoma protein requires sequential modification by at least two distinct cyclin-cdk complexes. *Mol. Cell. Biol.* **18**, 753–761 (1998).
11. Hu, W. et al. Concurrent deletion of cyclin E1 and cyclin-dependent kinase 2 in hepatocytes inhibits DNA replication and liver regeneration in mice. *Hepatology* **59**, 651–660 (2014).
12. Narasimha, A. M. et al. Cyclin D activates the Rb tumor suppressor by mono-phosphorylation. *eLife* **3**, e02872 (2014).
13. Diril, M. K. et al. Cyclin-dependent kinase 1 (Cdk1) is essential for cell division and suppression of DNA re-replication but not for liver regeneration. *Proc. Natl Acad. Sci. USA* **109**, 3826–3831 (2012).
14. Diskin, R., Askari, N., Capone, R., Engelberg, D. & Livnah, O. Active mutants of the human p38α mitogen-activated protein kinase. *J. Biol. Chem.* **279**, 47040–47049 (2004).
15. Giacinti, C. & Giordano, A. RB and cell cycle progression. *Oncogene* **25**, 5220–5227 (2006).
16. Repetto, M. V. et al. CDK and MAPK synergistically regulate signaling dynamics via a shared multi-site phosphorylation region on the scaffold protein Ste5. *Mol. Cell* **69**, 938–952.e6 (2018).
17. Manieri, E. & Sabio, G. Stress kinases in the modulation of metabolism and energy balance. *J. Mol. Endocrinol.* **55**, R11–R22 (2015).
18. Hui, L. et al. p38α suppresses normal and cancer cell proliferation by antagonizing the JNK-c-Jun pathway. *Nat. Genet.* **39**, 741–749 (2007).
19. Matesanz, N. et al. p38α blocks brown adipose tissue thermogenesis through p38δ inhibition. *PLoS Biol.* **16**, e2004455 (2018).

Acknowledgements We thank S. Bartlett for English editing, D. Engelberg for the constitutively active mutants, the Division of Signal Transduction Therapy for recombinant proteins, and CNIC Advanced Imaging and Vector Units for technical support. G.S. (RYC-2009-04972), F.J.C. (RYC-2014-15242), and Y.A.N. (RYC-2015-17438) are investigators of the Ramón y Cajal Program. E.M. and M.T. were awarded La Caixa fellowships and R.R.-B. was a fellow of the Fundación Ramón Areces-UAM and FPU. B.G.-T. is a fellow of the FPI Severo Ochoa CNIC program (SVP-2013-067639). F.J.C. is a Gilead Liver Research Scholar. This work was funded by grants supported in part by funds from the European Regional Development Fund: the European Union's Seventh Framework Programme (FP7/2007-2013) ERC 260464, EFSD/Lilly European Diabetes Research Programme Dr Sabio, 2017 Leonardo Grant for Researchers and Cultural Creators, BBVA Foundation (Investigadores-BBVA-2017) IN[17]_BBM_BAS_0066, MINECO-FEDER SAF2016-79126-R, and Comunidad de Madrid IMMUNOTHERCAN-CM S2010/BMD-2326 and B2017/BMD-3733 to G.S.; Juan de la Cierva and MINECO SAF2014-61233-JIN to A.T.-L.; the European Community for MSCA-IF-2014-EF-661160-MetAccembly grant to F.F.; Spanish MINECO CTQ2014-59212-P, European Community for CIG project (PCIG14-GA-2013-630978), and European Research Council (ERC) under the European Union's Horizon 2020 (ERC-2015-StG-679001-NetMoDEzyme) to S.O.; the German Research Foundation (SFB/TRR57/P04 and DFG NE 2128/2-1) and MINECO SAF2017-87919R to Y.A.N.; EXOHEP-CM S2017/BMD-3727 and the COST Action CA17112, MINECO SAF2016-78711, and the AMMF Cholangiocarcinoma Charity 2018/117 to F.J.C.; MINECO (SAF2015-69920-R co-funded by ERDF-EU), the Consolider-Ingenio 2010 Programme (SAF2014-57791-REDC), Excellence Network CellSYS (BFU2014-52125-REDT), and the iLUNG Programme (B2017/BMD-3884) from the Comunidad de Madrid to M. Malumbres; MINECO SAF2015-67077-R and SAF2017-89901-R to J.B.; MINECO (BIO2015-67580-P), Carlos III Institute of Health-Fondo de Investigación Sanitaria (ProteoRed PRB3, IPT17/0019 - ISCIII-SGEFI/ERDF), Fundación La Marató and 'La Caixa' Banking Foundation (HR17-00247) to J.V.; ISCIII and FEDER PI16/01548 and Junta de Castilla y León GRS 1362/A/16 and INT/M/17/17 to M. Marcos; Junta de Castilla y León GRS 1356/A/16 and GRS 1587/A/17 to J.L.-T.; and MCNU (SAF2017-84494-C2-1-R) to J.R.-C. The CNIC is supported by the Ministerio de Ciencia, Innovación y Universidades (MCNU) and the Pro CNIC Foundation, and is a Severo Ochoa Center of Excellence (SEV-2015-0505).

Author contributions G.S. conceived and supervised this project. G.S. and A.T.-L. designed and developed the hypothesis. E.M., L.L.-V., M.L. and A.T.-L. performed experiments using DEN, carbon tetrachloride, streptozotocin and dextran sodium sulfate, and A.T.-L. analysed the data. B.G.-T., A.T.-L. and A.M. performed partial hepatectomies. A.M., A.M.S., R.R.-B. and A.T.-L. prepared Fig. 2a. A.T.-L., H.M. and B.C. performed cell experiments. A.P.-C. performed S10b. E.R., A.P.-C. and A.C. carried out immunostaining experiments and A.T.-L. analysed the data. M. Malumbres, M.T., A.M., A.M.S., V.M.-R. and A.T.-L. performed CDK1/2 knockout experiments and immunohistochemistry. M. Marcos, L.H.-C., O.B., J.L.T. and N.M. performed the analysis of human samples. Y.A.N., F.J.C. and R.R.-B. developed genetic HCC models. S.O. and F.F. carried out molecular dynamics simulations. J.A.B. and M.R.-M. generated the AAVs. J.B. performed heuristic three-dimensional analysis. J.A.L. and J.V. performed and analysed the proteomic experiments. J.R.-C. carried out MRI experiments and A.T.-L. analysed the data. D.M.-S. generated the phylogenetic tree. A.T.-L. performed the remainder of the experiments. A.T.-L. and G.S. wrote the manuscript with input from all authors.

Competing interests The authors declare no competing interests.

Additional information
Extended data is available for this paper at https://doi.org/10.1038/s41586-019-1112-8.
Supplementary information is available for this paper at https://doi.org/10.1038/s41586-019-1112-8.
Reprints and permissions information is available at http://www.nature.com/reprints.
Correspondence and requests for materials should be addressed to G.S.
Publisher's note: Springer Nature remains neutral with regard to jurisdictional claims in published maps and institutional affiliations.

METHODS

Study population and sample collection. Immunohistochemical staining of p38γ was performed in liver samples from 46 patients (86.1% male, mean age 69.2 years, standard deviation (s.d.) 22.6 years) and 11 controls (36.4% male, mean age 45.9 years, s.d. 14.7 years) recruited at the University Hospital of Salamanca, Spain. Patients were diagnosed with hepatocellular carcinoma by liver biopsy, and control individuals were recruited from patients who underwent laparoscopic cholecystectomy for gallstone disease and had no laboratory or histopathological evidence of other liver diseases. This study was approved by the Ethics Committee of the University Hospital of Salamanca. Need for informed consent for immunostaining analysis from stored tissue from patients with liver cancer was waived by the Ethical Committee. A portion of each liver biopsy was fixed in 10% formalin and stained with haematoxylin and eosin (H&E) and Masson's trichrome for standard histopathological interpretation. Immunostaining of p38γ was performed with an antibody from R&D (AF1347; 1:250).

For the analysis of liver mRNA levels, the study population included two groups. One group consisted of obese adult patients with body mass index (BMI) ≥ 35 kg m^{-2} and a liver biopsy compatible with non-alcoholic fatty liver disease who underwent elective bariatric surgery ($n = 79$). The second group consisted of individuals with BMI < 35 kg m^{-2} who underwent laparoscopic cholecystectomy for cholelithiasis ($n = 30$). Participants were excluded if they had a history of alcohol use disorders or excessive alcohol consumption (>30 g per day in men and >20 g per day in women), chronic hepatitis C or B, or if laboratory and/or histopathological data showed causes of liver disease other than non-alcoholic fatty liver disease. The study was approved by the Ethics Committee of the University Hospital of Salamanca and all subjects provided written informed consent to undergo liver biopsy under direct vision during surgery. All patients signed written informed consent for participation. Data were collected on demographic information (age, sex and ethnicity), anthropomorphic measurements (BMI), smoking and alcohol history, coexisting medical conditions and medication use. Before surgery, fasting venous blood samples were collected for determination of complete blood cell count, total bilirubin, aspartate aminotransferase, alanine aminotransferase, total cholesterol, high-density lipoprotein, low-density lipoprotein, triglycerides, creatinine, glucose and albumin. Baseline characteristics of these groups are listed in Supplementary Table 2. Kaplan–Meier survival curves of patients stratified by low or high expression of p38γ were obtained and plotted from the Human Protein Atlas database.

Animal maintenance and treatments. Mice were housed in a pathogen-free animal facility under a 12 h light/dark cycle at constant temperature and humidity, and fed standard rodent chow and water ad libitum. For all studies, we used p38γloxP (B6.129-Mapk12tm1), p38δloxP (B6.129-Mapk13tm1)[20], AlbCre (B6.Cg-Tg(Albcre)21Mgn/J)[21] and whole-body knockout mice for p38γ. Mice were backcrossed for at least 10 generations in C57BL/6. Cdk1-lox; Cdk2-knockout mice, cMYCtg and LIKKγ knockout were described previously[22–24]. Genotypes were determined by PCR. All experiments were performed with male mice. Experiments involving animals were conducted in accordance with the Guide for the Care and Use of Laboratory Animals and approved by the CNIC Animal Care and Use Committee. The maximum tumour size permitted was 15 mm.

For long-term studies of liver tumour development and Kaplan–Meier analysis different protocols were assessed: (i) 15-day-old mice received a single intraperitoneal (i.p.) injection of diethylnitrosamine (DEN; Sigma-Aldrich) dissolved in saline at a dose of 50 mg kg^{-1} body weight. Pirfenidone (CAS: 53179-13-8; eBioChem) was administrated in drinking water at 2 g l^{-1} starting at 7 months after DEN injection and continuing for 3 months. Mice in one randomly pre-assigned group were euthanized at 1 or 6 months after DEN administration for histological and biochemical analyses. Age-matched mice in a second group were used to assess mortality. For short-term studies evaluating DEN-induced hepatic injury and compensatory proliferation, adult mice were treated with DEN by a single i.p. injection at a dose of 100 mg kg^{-1} of body weight and euthanized 2 h later. (ii) Streptozotocin was administered by i.p. injection (60 mg g^{-1}) to mice at postnatal day (P)1.5. All mice were fed a high-fat diet after weaning and histopathological studies were assessed at 27 weeks of age. (iii) Carbon tetrachloride was administered to adult mice via i.p. injection 3 times per week for 16 weeks. After the treatment, mice were euthanized for histopathological and biochemical studies and tumour analysis.

For PHx, adult mice were anaesthetized using a mixture of isoflurane and oxygen. Seventy percent of the liver was excised, which involves removal of the medial and left lateral lobes (used for histological and biochemical analyses). Liver proliferation, regeneration and histological and biochemical analysis were performed at 48 h and 15 days after PHx.

Immunohistochemical analyses. Liver and tumour tissues were fixed with phosphate-buffered 10% formalin and embedded in paraffin. Sections of 5 μm were stained with H&E for histopathological examination. Cell proliferation was assessed by immunohistochemical staining for Ki67 (ab15580, 1:100; Abcam), BrdU (ab6326, 1:100; Abcam) and phospho-Rb (S795) (9301, 1:100; Cell Signaling Technology).

BrdU treatment. Forty-eight hours after PHx, hepatocytes were labelled with BrdU in vivo by i.p. injection of 2 mg BrdU. After 2 h, mice were euthanized and livers extracted.

Assessment of HCC by magnetic resonance imaging. Tumours were monitored by MRI using administered gadoxetate disodium (Primovist; Bayer Healthcare) administered intravenously as a contrast medium to enhance focal hepatic tumours. Tumour volume was measured using OsiriX software (Pixmeo). Three-dimensional gradient echovolumetric imaging with minimum repetition time and echo time (3 ms and 1.5 ms, respectively), 20° flip angle and isotropic 150 μm spatial resolution, totalling 6 min acquisition time, were acquired around 10 min after Primovist injection (2 mg kg^{-1} body weight) via the tail vein. Images were acquired on an actively shielded 7 T horizontal scanner (Agilent) equipped with MM2 electronics, a 115/60 gradient insert coil, and a ^{1}H circular-polarization, transmit–receive volume coil of 35 mm inner diameter and 30 mm active length, built by Neos Biotec. Before contrast injection, each mouse was anaesthetized by inhalation of a mixture of isoflurane and oxygen (2–4%) and its breathing rhythm and temperature were monitored (Model 1024, SA Instruments). Animals were positioned supine on a customized bed with a built-in nose cone supplying inhalatory anaesthesia (1–2%) and kept at 35–37 °C by warm airflow throughout the experiment. After euthanasia, livers were collected, weighed, and the number of visible tumours was counted macroscopically and measured with a calliper. The figure shows axial slices extracted from the 3D volume dataset. Tumours were collected and frozen for biochemical analyses. For liver analysis, the largest lobe was fixed in formalin and embedded in paraffin. Sections were stained with H&E and examined microscopically.

Biochemical analysis. Total hepatic proteins were extracted from 30 mg frozen liver or tumour tissue using 500 μl of lysis buffer containing 50 mM Tris-HCl pH 7.5, 1 mM EGTA, 1 mM EDTA, 50 mM NaF, 1 mM sodium glycerophosphate, 5 mM pyrophosphate, 0.27 M sucrose, 1% Triton X-100, 0.1 mM PMSF, 0.1% β-mercaptoethanol, 1 mM sodium orthovanadate, 1 μg ml^{-1} leupeptin and 1 μg ml^{-1} aprotinin. Proteins were separated by sodium dodecyl sulfate–polyacrylamide gel electrophoresis (SDS–PAGE) and transferred onto 0.2 μm nitrocellulose membranes (BioRad). Membranes were blotted with primary antibodies targeting p38 (9212, 1:1,000; Cell Signaling Technology), p38γ (2307, 1:5,000; Cell Signaling Technology), a previously described p38γ antibody used for IP[19], phospho-p38 T180/Y182 (921, 1:1,000; Cell Signaling Technology), Rb (9313, 1:1,000; Cell Signaling Technology), phospho-Rb Ser 807/811 (8516, 1:1,000; Cell Signaling Technology), CDK2 ((78B2) 2546, 1:1,000 Cell Signaling Technology), PCNA (ab1897, 1:1,000; Abcam), vinculin (V4505, 1:1,000; Sigma-Aldrich), and GAPDH (G9245, 1:1,000; Sigma-Aldrich). Membranes were incubated with an appropriate horseradish peroxidase-conjugated secondary antibody (GE Healthcare) and developed using an enhanced chemiluminescent substrate (GE Healthcare). In western blots, each lane corresponds to a different mouse.

Hepatic, cardiac and renal injury was assessed from the levels of serum alanine aminotransferase, aspartate aminotransferase, creatine kinase, creatinine, alkaline phosphatase, and total bilirubin; all measurements were performed at the CNIC Animal Facility Unit.

Kinase assay. For the competitive kinase assays to evaluate the cooperation between CDK2 and p38γ, we used 0.5 μg of total protein and 0.5 μg of each kinase per reaction (Rb only, Rb + p38γ, Rb + CDK2/cyclin A, Rb + p38γ + CDK2/cyclin A). We added 100 μM ATP to each reaction at 30 °C for 15 min. To find all the residues phosphorylated by CDK2 and p38γ, we used 2 μg of total protein and 1 μg of each kinase per reaction (Rb only, Rb + p38γ, Rb + CDK2/cyclin A, Rb + p38γ + CDK2/cyclin A). We added 100 μM ATP to each reaction at 30 °C for 60 min.

Reactions were run on ExpressPlus PAGE acrylamide gels from GenScript, stained, and bands corresponding to Rb were then excised and analysed by mass spectrometry (MS) to identify phosphopeptides[8].

RNA isolation and quantitative PCR analysis. Total RNA was isolated from liver and tumour tissue with the RNeasy Mini Kit (Qiagen) with on-column DNase I digestion. RNA was quantified using a NanoDrop spectrophotometer. Complementary DNA synthesis was carried out using the High-Capacity cDNA Reverse Transcription Kit (Applied Biosystems). Expression of the housekeeping genes *Rn18s* and *Gapdh* was used for normalization. Quantitative PCR (qPCR) was performed using Fast SYBR Green (Applied Biosystems) on a 7900HT Fast Real-time PCR system (Applied Biosystems). Primer sequences were as follows (F, forward; R, reverse):

Gapdh F: TGAAGCAGGCATCTGAGGG, *Gapdh* R: CGAAGGTGGAAG AGTGGGA; *Rn18s* F: CAGCTCCAAGCGTTCCTGG, *Rn18s* R: GGCCTTCAAT TACAGTCGTCTTC; *Ccnd1* F: GGTCCATAGTGACGGTCAGGT, *Ccnd1* R: GCGTACCCTGACACCAATCTC; *Ccne1* F: GCCTTCACCATTCATGTGGAT, *Ccne1* R: TTGCTGCGGGTAAAGAGACAG; *Ccna1* F: GTGGCTCC

GACCTTTCAGTC, *Ccna1* R: CACAGTCTTGTCAATCTTGGCA; *Rb1* F: CCGTTTTCATGCAGAGACTAAA, *Rb1* R: GAGGTATTGGTGACAAGG TAGGA; *Cdk1* F: AGAAGGTACTTACGGTGTGGT, *Cdk1* R: GAGAGA TTTCCCGAATTGCAGT; *Cdk2* F: CCTGCTCATTAATGCAGAGGG, *Cdk2* R: GTGCTGGGTACACACTAGGTG; *Cdk4* F: ATGGCTGCCACTCGATATGAA, *Cdk4* R: TCCTCCATTAGGAACTCTCACAC; human *COL1A* F: GAGGGCCAAG ACGAAGACATC, human *COL1A* R: CAGATCACGTCA TCGCACAAC; human *ACTA2* F: AAAAGACAGCTACGTGGGTGA, human *ACTA2* R: GCCATGTT CTATCGGGTACTTC.

Cell lines and proliferation and transfection assays. We used HCC cell lines derived from human patients (HepG2, Huh7, Snu354, Snu398 and Snu449, NCBI BioSample) and wild-type human hepatocytes (HepaRG from Life Technologies). We first studied p38γ expression in cells derived from patients with HCC to avoid the unjustified use of mice. Cell lines were tested for mycoplasma contamination by PCR. Cells were cultured in DMEM (Sigma-Aldrich, D5796) supplemented with 10% FBS (HyClone, SV30160.03), L-glutamine (Lonza, 20 mM in 0.85% NaCl) and penicillin/streptomycin (Lonza, DE17-602E; 10,000 units of each antibiotic).

HepG2 and Snu398 cells were used for knock-down assays. shRNAs against p38γ were purchased from Dharmacon (V3LHS_636283 and V3LHS_636282).

To measure proliferation, HepG2 and Snu398 cells treated with shp38γ or shScramble were seeded in 24-well plates at 15×10^4 cells per well at different FBS concentrations (0.1%, 0.2%, 2% and 20%). Cells were counted after 48 h of incubation.

For colony-formation assays, 2×10^3 HepG2 and Snu398 treated with shp38γ or shScramble were seeded in a p100 Petri dish. After 2 weeks (without changing the medium) the colonies were fixed and stained with 0.1% crystal violet.

For soft agar assays, HepG2 shp38γ and HepG2 shScramble cells (10^5) were seeded in a p100 Petri dish between a base agar layer (0.5% agar, 1 × DMEM and 10% FBS) and a top agarose solution (0.7% agar, 1 × DMEM and 20% FBS). The medium was replenished every 3 days. After 20 days, plates were stained with 0.5% crystal violet, and colonies were counted using a light microscope.

HA-Rb wild-type and HA-RbΔCDK plasmids (Addgene; 58905 and 58906, respectively) were transfected into HEK 293T cells using the calcium phosphate transfection method. Cells were lysed 36 h post-transfection, and immunoprecipitation assays were performed.

Lentivirus and adeno-associated virus production. Lentiviruses were produced as described[4]. Transient calcium phosphate co-transfection of HEK-293T cells was carried out with shCDK1 (RMM4532-EG12534), shCDK2 (RMM4532-EG12534), shCDK4 (RMM4532-EG12567) or CDK6 (RMM4532-EG12571) from Dharmacon, together with pΔ8.9 and pVSV-G packaging plasmids. Supernatants containing the lentiviral particles were collected 48 h and 72 h after removal of the calcium phosphate precipitate, centrifuged at 700*g* at 4 °C for 10 min, and concentrated (×165) by ultracentrifugation for 2 h at 121,986*g* at 4 °C (Ultraclear Tubes, SW28 rotor and Optima L-100 XP Ultracentrifuge; Beckman). Viruses were resuspended in cold sterile PBS and titrated by qPCR.

AAV plasmids were cloned and propagated in the Stbl3 *Escherichia coli* strain (Life Technologies). pCEFL Flag p38γ D129A and pCEFL-p38α-D176AF327S[25] were cloned into a liver-specific HRC-hAAT promoter plasmid[26] to generate pAAV-HRC-hAAT-p38γact (AAVp38γ*). AAV2/8-CAG-Cre-WPRE was obtained from Harvard University. These AAV plasmids were packaged into AAV-9 or AAV-8 capsids to specifically target the liver, produced by the Viral Vector Unit at CNIC as described[8]. Adeno-associated viruses (serotypes AAV8 and AAV9) were produced in HEK-293T cells and collected from the supernatant. Mice were injected in the tail vein with 1×10^{11} adenoviral particles suspended in PBS.

Molecular dynamics simulations. Molecular dynamics simulations were used to study the spontaneous binding of the inhibitor RO3306 to the ATP-binding sites of p38γ, CDK1, CDK2 and p38α. The spontaneous binding of the inhibitor pirfenidone to the p38γ ATP-binding site was also studied. The parameters for RO3306 and pirfenidone in the molecular dynamics simulations were generated within the ANTECHAMBER module of AMBER 16 (ref. [27]) using the general AMBER force field (GAFF), with partial charges set to fit the electrostatic potential generated at the HF/6-31G(d) level by the RESP model. The charges were calculated according to the Merz-Singh-Kollman scheme using Gaussian 09.

Many crystal structures are available for the homologues p38α and p38β. However, p38γ has been crystallized only in the phosphorylated state and in the presence of an ATP derivative in the ATP-binding site (Protein Data Bank (PDB) accession number 1CM8). In this crystal structure, the loops corresponding to residues 34–39, 316–321 and 330–334 were not resolved. For the molecular dynamics simulations, we generated two models of p38γ using the SwissModel homology model server and 1CM8 (phosphorylated and ATP-bound state p38γ) and 3GP0 (inhibitor-bound state of p38β) as templates. Molecular dynamics simulations of CDK1 were carried out using PDB 5HQ0 as a reference, removing the crystallized ligand that occupies the ATP-binding site. Molecular dynamics simulations of CDK2 were performed using PDB 3PXR, corresponding to the apo CDK2 state. For p38α, PDB 3GI3 was used as a reference for starting the molecular dynamics simulations, removing the crystallized ligand occupying the ATP-binding site. In all cases, we placed RO3306 or pirfenidone in an arbitrary position in the solvent region (more than 20 Å away from the ATP-binding site). From these coordinates, we began unrestrained conventional molecular dynamics (cMD) simulations (250 ns) followed by accelerated molecular dynamics (aMD) simulations (1,500 ns for p38γ with RO3306, 2,000 ns for CDK1 with RO3306, 2,250 ns for CDK2 with RO3306, 2,000 ns for p38α with RO3306 and 2,000 ns for p38γ with pirfenidone) to allow the inhibitor to diffuse freely until it spontaneously associated with the protein surface, and finally targeted the ATP-binding site. Inhibitor binding was monitored throughout the simulations by plotting a selected distance between the hydrogen-bond acceptor of the inhibitor and the backbone of a residue located at the ATP-binding site responsible for the recognition and stabilization of the inhibitor (Met112 for p38γ and Met109 for p38α, and Leu83 for CDK1 and CDK2; see Extended Data Figs. 1, 10). Short distances indicate binding of RO3306 in the ATP-binding site. Spontaneous binding to p38γ was observed in five out of ten simulations (light purple, light and dark blue, light red, and teal in Extended Data Fig. 1b); in the case of CDK1, spontaneous binding was observed in two out of ten simulations (light blue and light pink). When binding occurs, RO3306 remains in the ATP-binding pocket for the rest of the simulation, thus indicating the strong affinity of the inhibitor towards p38γ and CDK1. By contrast, spontaneous binding does not occur in p38α or in only 1 out of 10 simulations in CDK2 (see Extended Data Fig. 1c). Comparison of the spontaneous binding events for p38γ and p38δ that were observed in 500 ns of aMD simulation time indicate that RO3306 has a higher affinity towards p38γ (RO3306 is bound to p38γ and p38δ for 19.7% and 5.5% of the simulation time, respectively; see Extended Data Fig. 1d).

Each system was immersed in a pre-equilibrated truncated octahedral box of water molecules with an internal offset distance of 10 Å, using the LEAP module. All systems were neutralized with explicit counterions (Na^+ or Cl^-). A two-stage geometry optimization approach was performed. First, a short minimization was made of the positions of the water molecules, with positional restraints on the solute by a harmonic potential with a force constant of 500 kcal mol^{-1} $Å^{-2}$. The second stage was an unrestrained minimization of all the atoms in the simulation cell. The systems were then gently heated through six 50-ps steps, each increasing the temperature by 50 K (0–300 K) under constant volume and using periodic boundary conditions and the particle mesh Ewald approach to introduce long-range electrostatic effects. For these steps, an 8 Å cutoff was applied to Lennard-Jones and electrostatic interactions. Bonds involving hydrogen were constrained with the SHAKE algorithm. Harmonic restraints of 10 kcal mol^{-1} were applied to the solute, and the Langevin equilibration scheme was used to control and equalize the temperature. The time step was kept at 2 fs during the heating stages, allowing potential inhomogeneities to self-adjust. Each system was then equilibrated for 2 ns with a 2-fs time step at a constant pressure of 1 atm. Finally, a 250 ns conventional molecular dynamics trajectory at constant volume and temperature (300 K) was collected, followed by ten replicas of 1,500 ns of dual-boost aMD[28,29] for p38γ in the presence of RO3306, ten replicas of 2,000 ns of aMD for CDK1 in the presence of RO3306, ten replicas of 2,250 ns of aMD for CDK2 in the presence of RO3306, ten replicas of 2,000 ns of aMD for p38α in the presence of RO3306, and five replicas of 2,000 ns of aMD for p38γ in the presence of pirfenidone. In total, we gathered 15 μs of aMD for p38γ, 20 μs of aMD for CDK1, 22.5 μs of aMD for CDK2, and 20 μs of aMD for p38α, all of them with RO3306, and 10 μs of aMD for p38γ with pirfenidone. These long-timescale unconstrained aMD simulations were performed with the aim of capturing several spontaneous binding events. aMD enhances the conformational sampling of biomolecules by adding a non-negative boost potential to the system when the system potential is lower than a reference energy:

$$V^*(\mathrm{r}) = V(\mathrm{r}), \;\; V(\mathrm{r}) \geq E,$$

$$V^*(\mathrm{r}) = V(\mathrm{r}) + \Delta V(\mathrm{r}) \; V(\mathrm{r}) < E,$$

where $V(\mathrm{r})$ is the original potential, E is the reference energy, and $V^*(\mathrm{r})$ is the modified potential. In the simplest form, the boost potential is given by

$$\Delta V(\mathrm{r}) = (E - V(\mathrm{r}))^2 / (\alpha + E - V(\mathrm{r})),$$

where α is the acceleration factor. As the acceleration factor α decreases, the energy surface becomes more flattened and biomolecular transitions between the low-energy states are increased.

Here, a total boost potential is applied to all atoms in the system in addition to a more aggressive dihedral boost, that is, (E_{dihed}, α_{dihed}; E_{total}, α_{total}), within the

dual-boost aMD approach. The acceleration parameters used in this study are as follows:

$$E_{\mathrm{dihed}} = V_{\mathrm{dihed-avg}} + 3.5 \times N_{\mathrm{res}},\ \alpha_{\mathrm{dihed}} = 3.5 \times N_{\mathrm{res}}/5;$$

$$E_{\mathrm{total}} = V_{\mathrm{total-avg}} + 0.2 \times N_{\mathrm{atoms}},\ \alpha_{\mathrm{total}} = 0.2 \times N_{\mathrm{atoms}},$$

where N_{res} is the number of protein residues, N_{atoms} is the total number of atoms, and $V_{\mathrm{dihed\_avg}}$ and $V_{\mathrm{total\_avg}}$ are the average dihedral and total potential energies calculated from 250 ns cMD simulations, respectively.

Statistical analysis and reproducibility. Data are expressed as mean ± s.e.m. Differences were analysed by Student's *t*-test, with significance assigned at $P < 0.05$. Fisher's exact test was used to compare HCC incidence. The Wilcoxon–Mann–Whitney rank-sum test was used to calculate the statistical significance of the observed differences between groups with different variances. The log-rank test was used to assess significance in the Kaplan–Meier analysis. GraphPad Prism version 5 software was used for calculations.

Sample-size estimates for animal experiments were determined using power calculations. GraphPad Prism version 5 software was used for statistical analyses. Unpaired Student's *t*-tests were used to determine the power ($a = 0.05$, two-tailed). We observed many statistically significant effects in the data, indicating that the effective sample size was sufficient for studying the phenomena of interest. The experiments using mice were randomized. Mice were grouped based on gender (male), genotype, treatments, weight and age, and were randomly selected. We were blinded to allocation during experiments and outcome assessment. For in vivo experiments, an investigator treated the mice and collected the tissue samples. These samples were assigned code numbers. The analyses—including qPCR, immunohistochemistry staining and western blotting—were performed by another independent investigator. Experiments were repeated two or three times. All attempts at replication were successful.

Figure 1. **a**–**d**, Representative of at least three independent experiments. **e**, Data are mean ± s.e.m. $n = 3$–5 fields from AlbCre mice: 0 h, $n = 3$; 48 h, $n = 5$; AlbCre-p38γ mice: 0 h, $n = 5$; 48 h, $n = 7$ mice. $^{***}P < 0.001$. Comparisons were made by one-way ANOVA coupled to Bonferroni's post-test. **f**, Data are mean ± s.e.m. $n = 2$–5 fields from AlbCre mice: 0 h, $n = 4$; 48 h, $n = 7$; AlbCre-p38γ mice: 0 h, $n = 4$; 48 h, $n = 6$ mice. $^{**}P < 0.01$; $^{***}P < 0.001$. Comparisons were made by one-way ANOVA coupled to Bonferroni's post-test. **h**, Representative of at least three independent experiments. 1 h, data are mean ± s.e.m. AlbCre mice: $n = 3$; AlbCre-p38γ mice: $n = 8$. $^{***}P < 0.001$. Comparisons were performed using the two-sided Student's *t*-test.

Figure 2. **a**, **b**, Representative of at least three independent experiments. **c**, Data are mean ± s.e.m. $n = 4$–5 fields from AlbCre mice: 0 h, $n = 7$; 48 h, $n = 7$; CDK1/2 KO mice: 0 h, $n = 3$; 48 h, $n = 3$; CDK1/2 KO AAVp38γ* mice: 0 h, $n = 4$; 48 h, $n = 4$ mice. $^{*}P < 0.05$. Comparisons were made by one-way ANOVA coupled to Kruskal–Wallis post-tests. **d**, Data are mean ± s.e.m. $n = 3$–5 fields from AlbCre mice: 0 h, $n = 7$; 48 h, $n = 7$; AlbCre-p38γ mice: 0 h, $n = 3$; 48 h, $n = 3$; AlbCre-p38γ AAVp38γ* mice: 0 h, $n = 3$; 48 h, $n = 3$. $^{*}P < 0.05$. Comparisons were performed by a one-way ANOVA coupled to Kruskal–Wallis post-tests.

Figure 3. **a**, Immunohistochemistry was performed in two independent experiments. **b**, Linear relationships from $n = 107$ individuals tested by Pearson's correlation; $P < 0.001$. **c**, Kaplan–Meier survival curves of patients stratified by low or high expression of p38γ, $n = 372$ individuals; Mantel–Cox log-rank test. $P = 0.0039$. **e**, **f**, Data are mean ± s.e.m. Mann–Whitney *U*-test (**e**) and two-sided Student's *t*-test (**f**) in AlbCre mice: $n = 11$, AlbCre-p38γ mice: $n = 5$. **g**, Kaplan–Meier analysis of survival in DEN-treated AlbCre mice: $n = 10$ and AlbCre-p38γ mice: $n = 11$ mice. Mantel–Cox log-rank test; $^{**}P < 0.01$.

Figure 4. **a**, Representative of at least three independent experiments. **b**, Data are mean ± s.e.m. AlbCre untreated mice: 0 h, $n = 10$; 48 h, $n = 5$; AlbCre-p38γ untreated mice: 0 h, $n = 10$; 48 h, $n = 7$; AlbCre mice: 0 h, $n = 10$; 48 h, $n = 10$; AlbCre-p38γ mice: 0 h, $n = 17$; 48 h, $n = 10$ pirfenidone-treated mice. One-way ANOVA; $^{***}P < 0.001$. **c**, Representative of at least three independent experiments. **d**, Data are mean ± s.e.m. Tumour number: control, $n = 20$; pirfenidone, $n = 13$; total tumour volume: control, $n = 18$; Pirfenidone, $n = 13$; maximum tumour: control, $n = 18$; pirfenidone, $n = 13$ mice. Mann–Whitney *U*-test; $^{*}P < 0.05$. **e**, Kaplan–Meier analysis of survival. Mantel–Cox log-rank test; $^{***}P < 0.001$. Control, $n = 6$; Pirfenidone-treated, $n = 9$ mice. **f**, Representative of at least three independent experiments. Each lane corresponds to a different liver or tumour sample.

Reporting summary. Further information on research design is available in the Nature Research Reporting Summary linked to this paper.

Data availability

The datasets supporting the findings of this study are available within the paper and its Supplementary Information. Source Data (gels and graphs) for Figs. 1–4 and Extended Data Figs. 1–10 are provided with the online version of the paper. There is no restriction on data availability.

20. González-Terán, B. et al. p38γ and p38δ reprogram liver metabolism by modulating neutrophil infiltration. *EMBO J.* **35**, 536–552 (2016).
21. Postic, C. & Magnuson, M. A. DNA excision in liver by an albumin-Cre transgene occurs progressively with age. *Genesis* **26**, 149–150 (2000).
22. Trakala, M. et al. Functional reprogramming of polyploidization in megakaryocytes. *Dev. Cell* **32**, 155–167 (2015).
23. Cubero, F. J. et al. Haematopoietic cell-derived Jnk1 is crucial for chronic inflammation and carcinogenesis in an experimental model of liver injury. *J. Hepatol.* **62**, 140–149 (2015).
24. Zheng, K., Cubero, F. J. & Nevzorova, Y. A. c-MYC—making liver sick: role of c-MYC in hepatic cell function, homeostasis and disease. *Genes (Basel)* **8**, 123 (2017).
25. Askari, N. et al. Hyperactive variants of p38α induce, whereas hyperactive variants of p38γ suppress, activating protein 1-mediated transcription. *J. Biol. Chem.* **282**, 91–99 (2007).
26. Miao, C. H. et al. Inclusion of the hepatic locus control region, an intron, and untranslated region increases and stabilizes hepatic factor IX gene expression *in vivo* but not *in vitro*. *Mol. Ther.* **1**, 522–532, (2000).
27. Case, D. A. et al. *AMBER v.16* (University of California, San Francisco, 2017).
28. Hamelberg, D., Mongan, J. & McCammon, J. A. Accelerated molecular dynamics: a promising and efficient simulation method for biomolecules. *J. Chem. Phys.* **120**, 11919–11929 (2004).
29. Hamelberg, D., de Oliveira, C. A. & McCammon, J. A. Sampling of slow diffusive conformational transitions with accelerated molecular dynamics. *J. Chem. Phys.* **127**, 155102 (2007).

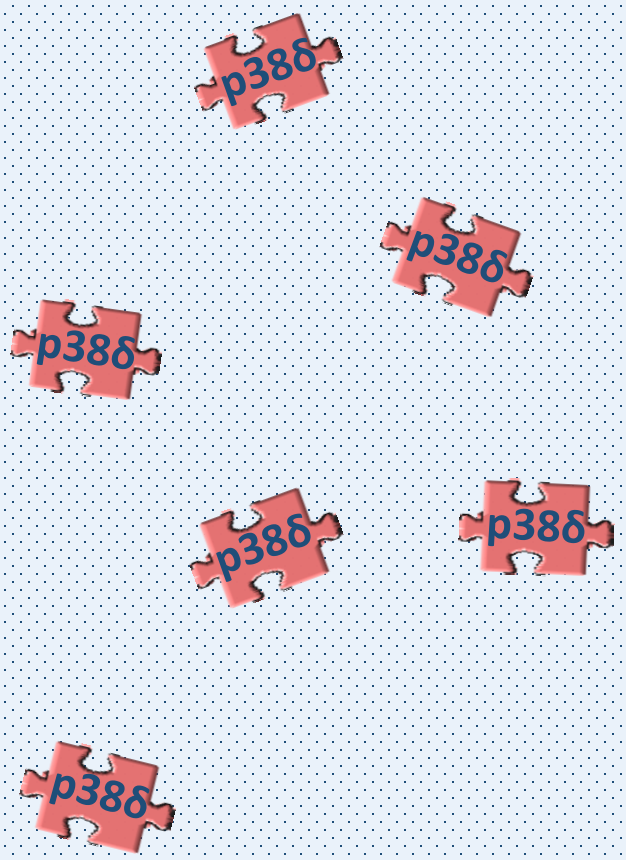

Universidad Autónoma de Madrid